OBJECT-BASED MAPPING OF TEMPERATE MARINE HABITATS FROM MULTI-RESOLUTION REMOTE SENSING DATA

Paula Lightfoot

Thesis submitted to Newcastle University for the degree of Doctor of Philosophy

School of Natural and Environmental Sciences

October 2018

Object-based mapping of temperate marine habitats from multi-resolution remote sensing data

Paula Lightfoot

Supervisors: Dr Clare Fitzsimmons, Prof. Nicholas V.C. Polunin and Dr Catherine L. Scott

Examiners: Dr Fleur Visser and Dr Heather Sugden

Abstract

Habitat maps are needed to inform marine spatial planning but current methods of field survey and data interpretation are time-consuming and subjective. Object-based image analysis (OBIA) and remote sensing could deliver objective, cost-effective solutions informed by ecological knowledge. OBIA enables development of automated workflows to segment imagery, creating ecologically meaningful objects which are then classified based on spectral or geometric properties, relationships to other objects and contextual data. Successfully applied to terrestrial and tropical marine habitats for over a decade, turbidity and lack of suitable remotely sensed data had limited OBIA's use in temperate seas to date. This thesis evaluates the potential of OBIA and remote sensing to inform designation, management and monitoring of temperate Marine Protected Areas (MPAs) through four studies conducted in English North Sea MPAs.

An initial study developed OBIA workflows to produce circalittoral habitat maps from acoustic data using sequential threshold-based and nearest neighbour classifications. These methods produced accurate substratum maps over large areas but could not reliably predict distribution of species communities from purely physical data under largely homogeneous environmental conditions.

OBIA methods were then tested in an intertidal MPA with fine-scale habitat heterogeneity using high resolution imagery collected by unmanned aerial vehicle. Topographic models were created from the imagery using photogrammetry. Validation of these models through comparison with ground truth measurements showed high vertical accuracy and the ability to detect decimetre-scale features.

The topographic and spectral layers were interpreted simultaneously using OBIA, producing habitat maps at two thematic scales. Classifier comparison showed that Random Forests

outperformed the nearest neighbour approach, while a knowledge-based rule set produced accurate results but requires further research to improve reproducibility.

The final study applied OBIA methods to aerial and LiDAR time-series, demonstrating that despite considerable variability in the data, pre- and post-classification change detection methods had sufficient accuracy to monitor deviation from a background level of natural environmental fluctuation.

This thesis demonstrates the potential of OBIA and remote sensing for large-scale rapid assessment, detailed surveillance and change detection, providing insight to inform choice of classifier, sampling protocol and thematic scale which should aid wider adoption of these methods in temperate MPAs.

Acknowledgements

This PhD was made possible by the vision of Dr Clare Fitzsimmons and Dr Catherine Scott and the financial support provided by the Natural Environment Research Council and Natural England. I am deeply grateful to them for offering me this wonderful opportunity and to all those whose help and support along the way enabled me to take full advantage of it.

First, my thanks go to my supervisors Dr Clare Fitzsimmons, Professor Nick Polunin and Dr Catherine Scott (Natural England) for their guidance in all aspects of the research and also for their encouragement and support to seize opportunities to disseminate our findings to a wide audience, ensuring practical outcomes from our work.

Many people and organisations helped me to collect and collate the data used in this thesis. The UAV surveys were made possible by the North and East Yorkshire Ecological Data Centre, who not only supplied and flew the UAV and but also taught me how to use specialist software to plan flights and process imagery, so a big thank you to Simon Pickles, Mark Wills, Clare Langrick and Wendy Bostock (and of course to "Desmond" the drone!). Sincere thanks are also due to Newcastle University's School of Civil Engineering and Geosciences for the generous loan of GNSS equipment, and to Martin Robertson in particular for the even more generous gift of his time in teaching me how to use the equipment and post-process the data. I am grateful to Cat Logan, Bex Lynam, John Hume, Helen Percival, Jane Pottas and Sarah Paton for their help with fieldwork, from providing ground support for UAV flights to counting seaweeds in quadrats…and for putting up with that very long walk over very large boulders!

Neil McLachlan, Senior Coastal Engineer at East Riding of Yorkshire Council, was a great help as I was collating the aerial and LiDAR data for Flamborough Head, always responding extremely promptly and helpfully to my many questions. Special thanks must go to Markus Diesing and the staff at Cefas for the opportunity to create habitat maps for two recommended Marine Conservation Zones, providing access to high quality data and the benefit of their considerable expertise and knowledge. I am so pleased to have been able to contribute in some way to the development of the UK's Marine Protected Area network.

Katie Medcalf and the staff at Environment Systems provided invaluable support while I was getting to grips with eCognition software and were a great source of inspiration in showing

how remote sensing and GIS can be used on a daily basis to support nature conservation. Thank you for your wonderful hospitality, I thoroughly enjoyed all my visits to Aberystwyth!

I am grateful to the British Ecological Society, Natural Environment Research Council, Remote Sensing and Photogrammetry Society and the GeoHab Student Awards Committee who all provided grants which enabled me to take advantage of valuable training opportunities and to present my research at international conferences.

I would also like to thank the staff and students in our research group and particularly everyone at the Dove Marine Laboratory – it has been a huge pleasure and privilege to work in this wonderful place!

Finally and most importantly, my heartfelt thanks go to my husband, Phil. I suspect I was more of a distraction than a help while you were doing your PhD over twenty years ago, but now the roles are reversed you have been a constant source of encouragement and support to me. Thank you for your patience during my long time away from our home, for your help and companionship with fieldwork and for all your extremely useful and kind advice from the perspective of someone who's been through it all before. There is not enough ice cream in the world to express how truly grateful I am!

Table of Contents

List of Figures

List of Tables

List of Acronyms

BPI	Bathymetric Position Index
CASI	Compact Airborne Spectrographic Imager
Cefas	Centre for Environment, Fisheries and Aquaculture Science
Defra	Department for Environment, Food and Rural Affairs
EUNIS	European Nature Information System
GCP	Ground Control Point
GNSS	Global Navigation Satellite System
JNCC	Joint Nature Conservation Committee
LiDAR	Light Detection and Ranging
MBES	Multibeam Echo Sounder
MCZ	Marine Conservation Zone
MF	Membership Function
MMO	Marine Management Organisation
MPA	Marine Protected Area
NDVI	Normalised Difference Vegetation Index
NTZ	No Take Zone
OBIA	Object-based image analysis
PSA	Particle Size Analysis
RF	Random Forests
RGB	Red, Green, Blue
rMCZ	Recommended Marine Conservation Zone
SACFOR	Superabundant, Abundant, Common, Frequent, Occasional, Rare
SNN	Standard Nearest Neighbour
UAV	Unmanned Aerial Vehicle
VLOS	Visual Line of Sight

Chapter 1: Introduction

1.1 The need for marine and coastal habitat maps

Marine and coastal ecosystems provide multiple goods and services upon which human lives and livelihoods depend (Barbier, 2012), but this environment is under increasing anthropogenic pressure. Direct and indirect results of human activities in the marine environment include overexploitation of resources, coastal modification, pollution, introduction of non-native species, ocean acidification and climate change, resulting in habitat degradation, biodiversity loss and decline in ecosystem services (Worm *et al.*, 2006; Airoldi *et al.*, 2008; Brander *et al.*, 2010). Globally, over 40% of the ocean is strongly affected by human activities, with no area being completely free from human influence (Halpern *et al.*, 2008), and the cumulative impact of human activities is increasing in 66% of the ocean (Halpern *et al.*, 2015). The coastal zone is particularly heavily used, accounting for just 4% of the earth's land area but containing over a third of the world's population (Millenium Ecosystem Assessment, 2005). Less than 15% of Europe's coastline is considered to be in 'good' condition (Airoldi and Beck, 2007).

Global and regional conventions have recognised the need to reduce pressure on marine ecosystems, resolve conflicts between users and ensure sustainable use of resources through integrated ecosystem-based management of activities (United Nations, 1982; OSPAR, 1992; United Nations, 1992). Marine spatial planning (MSP) has been identified as an effective tool for delivering ecosystem-based management (Ehler and Douvere, 2007; Ehler and Douvere, 2009), and over the past decade it has started to be implemented in many countries through national policy or legislation (Fletcher *et al.*, 2014; Portman, 2016).

Knowledge of the extent and distribution of marine and coastal habitats is a fundamental requirement of MSP (Crowder and Norse, 2008; Cogan *et al.*, 2009; Baker and Harris, 2012). Because sensitivity to pressure from human activities varies with habitat type, seabed habitat maps and pressure-feature-sensitivity matrices can inform the spatial zoning of activities (Zacharias and Gregr, 2005; Foden *et al.*, 2011; Williams *et al.*, 2011; Caldow *et al.*, 2015). In particular, habitat maps are needed to inform the establishment of a representative and ecologically coherent network of Marine Protected Areas (MPAs), which is a core element of marine spatial planning (Jordan *et al.*, 2005; Stevens and Connolly, 2005; Evans *et al.*, 2015). Furthermore, the extent and quality of habitats must be monitored to

evaluate the success of MSP measures and meet requirements for reporting under conservation legislation, for example the EU Habitats Directive (EC, 1992) and Marine Strategy Framework Directive (EC, 2008).

However, due to the high cost of conducting surveys in the marine environment, it is estimated that only 5-10% of the seabed has been mapped with a resolution comparable to the terrestrial environment (Wright and Heyman, 2008). In the absence of survey data, large scale seabed habitat maps have been produced by 'top down' predictive modelling from multiple environmental variables; this is a cost-effective way of covering a large area, but the spatial and thematic resolution of the maps are low as they are limited by the resolution of the input data (Cameron, 2011; Huang *et al.*, 2011; McBreen, 2011; Robinson *et al.*, 2011; Vasquez *et al.*, 2014).

More robust solutions may be provided by remote sensing and object-based image analysis (OBIA), which have considerably progressed habitat mapping for conservation management in both terrestrial and tropical marine environments (Corbane *et al.*, 2015; Medcalf *et al.*, 2015; Hedley *et al.*, 2016). Temperate marine ecosystems present particular challenges and opportunities, and applications of remote sensing and OBIA in this environment are just beginning to be explored, drawing on knowledge gained from terrestrial remote sensing (Diesing *et al.*, 2016). Progress in this area is urgently needed, because lack of detailed knowledge of the seabed and lack of confidence in modelled habitat maps can hinder the planning and designation of MPAs (Caveen *et al.*, 2014; Levin *et al.*, 2014).

This introductory chapter synthesises current knowledge on the use of remote sensing and OBIA for habitat mapping, identifies gaps in understanding to be addressed by this study and outlines the objectives and structure of the thesis.

1.2 Remote sensing

Remote sensing is "the science and art of obtaining information about an object, area, or phenomenon through the analysis of data acquired by a device that is not in contact with the object, area, or phenomenon under investigation" (Lillesand *et al.*, 2015). Passive remote sensors measure energy radiated or reflected from the Earth's surface, while active remote sensors emit a pulse of laser, sonar or radar and measure the energy returned to the detector (Turner *et al.*, 2003). Both active and passive remote sensors have a range of applications in the marine environment. Satellite ocean colour imagery enables

measurement of primary productivity (Vargas *et al.*, 2009) and suspended particulate matter (Loisel *et al.*, 2014). High resolution visible and infrared imagery can be used to indicate illegal fishing activity (Elvidge *et al.*, 2015) and monitor megafauna (Fretwell *et al.*, 2014). Microwave radiometry and infrared imagery can map sea surface temperature (Prigent *et al.*, 2013; Kilpatrick *et al.*, 2015). Synthetic aperture radar (SAR) imagery can be used to detect oil spills (Xu *et al.*, 2014), record wave height and direction (Stopa and Mouche, 2017) and monitor sea ice (Geldsetzer *et al.*, 2015). Bathymetry can be measured using sonar or, in shallow water, LiDAR, satellite imagery or hyperspectral aerial imagery (Gao, 2009; Klemas, 2011).

One of the most important contributions of remote sensing to terrestrial ecology is the production of land cover, land use and habitat maps and their interpretation to detect environmental change (Kerr and Ostrovsky, 2003), yet this application of remote sensing has been relatively limited in the marine environment to date. Research into remote sensing for benthic mapping has been dominated by studies of shallow tropical habitats such as coral reefs, mangroves and seagrass beds, due partly to the ecological importance and vulnerability of these habitats and partly to the ability to detect these habitats using optical sensors (Kuenzer *et al.*, 2011; Goodman *et al.*, 2013; Lyons *et al.*, 2013; Roelfsema *et al.*, 2013a; Hedley *et al.*, 2016). Optical sensors cannot provide imagery of the seabed in deep water or turbid shallow water, but recent developments in sonar technology, data processing and georeferencing have enabled the generation of seabed images by remote sensing in this environment based on measurements of depth, hardness and roughness (Mayer, 2006). These developments have led to a growing number of studies evaluating acoustic systems and data interpretation methods for benthic mapping, demonstrating the potential for these methods to support marine management while also highlighting the lack of consensus on the 'best' system and method (Kenny *et al.*, 2003; Brown *et al.*, 2011a; Diesing *et al.*, 2016).

The benefits of remote sensing, namely the ability to generate data for large areas in a non-destructive, rapid, repeatable way, providing information beyond human perception, access to inaccessible locations, and enabling automated, objective data interpretation (Pettorelli, 2014), are of particular relevance to the marine environment. Direct sampling of the seabed is possible in shallow seas for survey areas smaller than 1km^2, but disadvantages of direct sampling methods include high cost, the requirement for analyst expertise and the need for

high replication to yield statistical power (van Rein *et al.*, 2009). Benthic sampling methods such as grabs, cores, dredges, trawls and even video sensors on towed sleds can damage the seabed and are therefore inappropriate for surveying potential or existing MPAs (Sheehan *et al.*, 2010). Surveys by SCUBA divers are resource intensive and difficult to implement in deep or strongly current-swept areas, and such methods have been shown to be subjective and lead to variation in outputs within and between surveyors, even when the surveyors are experienced (Moore *et al.*, 2014).

Remote sensing therefore offers great potential for surveillance and monitoring in the marine environment, most of which is out of the range of direct survey methods, but there are many challenges to overcome in the implementation of this technology. Considerable technological expertise, processing power and specialist software are needed to pre-process and analyse remote sensing data, while ecological expertise is needed to define appropriate scales of analysis and ground truthing protocols. Because of this, the potential of remote sensing technology to inform conservation management and monitoring has been under-exploited and there is a growing call for interdisciplinary research and collaboration between the remote sensing and ecology communities (Nagendra *et al.*, 2013; Pettorelli, 2014; Pettorelli *et al.*, 2014; Buchanan *et al.*, 2015; Mairota *et al.*, 2015; Turner *et al.*, 2015). The wider range of sensors and platforms potentially available for marine and coastal applications create a particularly pressing need for such interdisciplinary research to evaluate the ability of different sensors to detect ecologically meaningful differences in benthic habitat type or quality.

1.3 Object-based image analysis

Remote sensing data from both active and passive sensors are typically processed to produce continuous georeferenced raster images made up of cells (pixels) which each contain a single value. Spatial resolution (pixel size) of remote sensing imagery is determined by ground sampling distance and ranges from hundreds of metres to less than one metre (Turner *et al.*, 2003). The interpretation of remote sensing imagery to produce land cover or habitat maps traditionally involved using statistical operators to classify each pixel based on its electromagnetic or acoustic frequency and the values of its neighbouring pixels (Lillesand *et al.*, 2015). Pixel-based classification methods prevailed when remote sensing imagery was predominantly available at low spatial resolution (e.g. from the

Landsat, Terra and Aqua satellite platforms), but as finer resolution imagery became available (e.g. from the WorldView, QuickBird and Ikonos platforms), analysts began to change their focus from single pixels to the spatial patterns they create, ushering in an object-based approach to image analysis (Blaschke *et al.*, 2000; Blaschke and Strobl, 2001).

Object-based image analysis (OBIA) involves segmenting the image into groups of pixels according to homogeneity criteria to create objects, and then classifying those objects based on their spectral and geometric properties, their relationship to other objects and to contextual data (Benz, 2004). OBIA has gained in popularity since around the year 2000 due to the increasing availability of high resolution remote sensing data, greater computer processing power and the availability of commercial software specifically developed for this purpose. Since then, hundreds of published studies have demonstrated the usefulness of OBIA for habitat, land cover and land use mapping and change detection (Blaschke, 2010). The majority of studies cited in Blaschke's review deal with OBIA of optical remote sensing data, predominantly satellite imagery, and all but two focus on terrestrial ecosystems (Lathrop *et al.*, 2006; Lucieer, 2008). Since then, a number of studies have started to evaluate OBIA methods with a wider range of sensors for marine habitat mapping both in tropical (Scopelitis *et al.*, 2010; Leon and Woodroffe, 2011; Estomata *et al.*, 2012; Phinn, 2012; Roelfsema *et al.*, 2013b; Zhang *et al.*, 2013; Wahidin *et al.*, 2015; Baumstark *et al.*, 2016; Xu *et al.*, 2016; McIntyre *et al.*, 2018) and temperate seas (de Oliveira *et al.*, 2006; Lucieer, 2008; Lucieer and Lamarche, 2011; Lucieer *et al.*, 2013; Diesing *et al.*, 2014; Hasan *et al.*, 2014; Hill *et al.*, 2014; Lacharite *et al.*, 2015; Lawrence *et al.*, 2015; Gavazzi *et al.*, 2016).

1.3.1 Benefits of OBIA

The large body of research in terrestrial remote sensing demonstrates the following advantages of OBIA, and the marine studies suggest how these advantages may be particularly relevant for benthic mapping (Table 1.1).

Table 1.1: Summary of benefits of OBIA and relevance to marine habitat mapping

Benefit of OBIA	**References**	**Relevance to marine mapping**	**Examples**	**References**
Segmentation and classification can be carried out at multiple, hierarchical levels of resolution to reflect ecologically meaningful objects in the ecosystem under investigation.	Hay *et al.* (2001) Hall *et al.* (2004) Hay *et al.* (2005)	Both tropical and temperate marine ecosystems can be classified hierarchically, from low to high levels of detail in biological communities and/or topographic features.	OBIA has been used to classify coral reefs at three levels of detail, from the whole reef system to individual biotopes/patches within the system, and to segment and classify environmental variables in both tropical and temperate regions to create a nested hierarchical model of seabed types.	Huang *et al.* (2011) Phinn (2012)
Image objects possess vastly more values than single pixels, any combination of which can be used in the classification process. Shape and texture can aid discrimination of classes which cannot be separated on spectral characteristics alone.	Blaschke and Strobl (2001) Hay and Castilla (2006) Visser *et al.* (2013)	The ability to use textural and geometric as well as spectral information is particularly useful for benthic mapping from acoustic imagery due to the low spectral resolution of this type of data.	Acoustic OBIA mapping studies have used a range of object values, notably mean backscatter intensity (seabed hardness), standard deviation of bathymetric position index or of sidescan sonar imagery (seabed roughness) and grey level co-occurrence values of backscatter (seabed texture).	Lucieer (2008) Lucieer *et al.* (2011) Diesing *et al.* (2014)
OBIA avoids the 'salt and pepper' effect which can be generated by pixel-based image analysis if the image is highly heterogeneous at a fine scale.	Blaschke *et al.* (2000)	Marine habitats often exhibit fine scale heterogeneity, particularly in coastal and intertidal environments.	'Salt and pepper' effect has been shown to reduced classification accuracy in pixel-based analysis of high resolution imagery for saltmarsh and rocky intertidal habitat mapping.	Hunter and Power (2002) Hennig *et al.* (2007)
Objects can be classified based on fuzzy logic using membership functions, which is useful for habitat mapping because it allows a more realistic reflection of the natural environment.	Benz (2004)	Marine biotopes rarely have distinct boundaries, but grade into one another along a continuum. It is seldom possible to separate marine habitats on spectral or spatial threshold values; large overlap in the values of classified objects is common, particularly when using acoustic data.	Several OBIA mapping studies illustrate the overlap in acoustic values of different benthic habitats.	See box plots in: Kloser *et al.* (2010) Lucieer *et al.* (2011) Diesing *et al.* (2014) Calvert *et al.* (2015)
			Membership functions used with OBIA to model seabed habitats from environmental data for a whole continent, and at a finer scale to map saltmarsh plants and predict distribution of intertidal algae.	Huang et al. (2011, fig.2) Ouyang *et al.* (2011) de Oliveira *et al.* (2006)

Benefit of OBIA	**References**	**Relevance to marine mapping**	**Examples**	**References**
OBIA enables users to apply their ecological knowledge and use contextual data to develop effective rules for segmenting and classifying remotely sensed data.	Lucas *et al.* (2007) Medcalf *et al.* (2014b) Medcalf *et al.* (2017)	Relevant contextual data for marine mapping includes light attenuation, tidal streams, wave energy, seabed geology, salinity, water temperature, nutrients, freshwater input, sediment sources or fishing intensity.	Environmental data is widely used in 'top down' marine habitat modelling studies but to date is rarely used in habitat mapping from remote sensing data, possibly because contextual data have not been available at a suitable spatial scale. OBIA modelling studies have used wave exposure and shore height to predict distribution of intertidal algae, and light attenuation, exposure and chemical data to predict distribution of seabed habitats.	Brown *et al.* (2011a) Diesing *et al.* (2016) de Oliveira *et al.* (2006) Huang *et al.* (2011)
OBIA enables interpretation of multiple layers of data simultaneously, enabling combination of data from different sensors and at different spatial resolutions.	Lucas *et al.* (2015) Mucher *et al.* (2015)	Acoustic and optical imagery can be combined for marine habitat mapping, using optical imagery collected via airborne sensors in clear tropical seas/intertidal zones, or via AUV or ROV in temperate seas. Acoustic data at different resolutions from different sensors can also be combined to increase coverage.	Marine OBIA studies have interpreted acoustic data in combination with derivative layers such as slope, curvature or aspect and in combination with optical imagery.	Lucieer *et al.* (2013) Diesing *et al.* (2014) McIntyre *et al.* (2018)

Few studies have directly compared pixel-based and object-based approaches using the same input data and classifiers, and such comparisons have seldom been carried out in marine or coastal ecosystems. Using satellite and acoustic imagery to map tropical benthic features, McIntyre *et al.* (2018) found OBIA outputs to be more accurate than pixel-based outputs except when pixel-based outputs had been contextually edited. Phinn (2012) found benthic community maps produced by OBIA more accurate than those produced by pixel-based analysis when using medium resolution satellite imagery to map coral reefs, but they caution that this may not be a fair comparison due to differences in the calibration and validation methods applied to both approaches. In contrast, Gavazzi *et al.* (2016) found OBIA outputs less accurate than pixel-based outputs when applied to acoustic imagery for mapping shallow lagoon habitats. Using very high resolution satellite imagery to map saltmarsh vegetation, Ouyang *et al.* (2011) found that OBIA produced more accurate results than pixel-based methods, primarily due to the ability to use fuzzy membership functions and a hierarchical, multi-scale approach. Further comparative studies are shown in Table 1.3.

The increasing prevalence of OBIA studies in peer-reviewed remote sensing literature is evidence of the benefits of this approach (Blaschke, 2010; Blaschke *et al.*, 2014) but is not proof that OBIA is always a better option than pixel-based analysis; the best approach will be determined by the spatial resolution of the data and the scale of the ecological question under investigation (Gao and Mas, 2008). The remit of this study is to evaluate the use of OBIA for interpreting high spatial resolution imagery (0.04m to 1m) to map and monitor intertidal and subtidal rock reefs which have fine-scale habitat complexity. Different OBIA approaches and compared but there is no comparison of OBIA with pixel-based approaches in this study.

1.3.2 Challenges of OBIA

Despite these benefits, OBIA presents challenges. Commercial software enables users to produce plausible, visually pleasing habitat maps from remotely sensed data relatively quickly and easily, but the development of robust, ecologically meaningful rules for segmentation and classification requires ecological expertise, a thorough understanding of the data, and an iterative, evaluative approach to developing the workflow. Throughout the segmentation and classification process, the analyst has to make a number of choices which will influence the accuracy and usefulness of the output map.

The first choices relate to image segmentation. Many methods of image segmentation have been developed, but the one most widely used for OBIA of remote sensing imagery is multi-resolution/hierarchical segmentation using fractal net evaluation (Dey *et al.*, 2010). When applying this approach, the analyst must decide which imagery layers to use and what weighting should be accorded to each layer, then define the scale parameter and homogeneity criteria for object shape and compactness (Baatz and Schape, 2000). The greater the number of objects, the slower the processing speed, so the aim is to create objects that are as small as necessary but as large as possible. Selection of inappropriate parameters will result in image objects that are not representative of real-world objects, which in turn leads to classification inaccuracy (Addink *et al.*, 2007; Laliberte and Rango, 2009; Gao *et al.*, 2011; Lucieer and Lamarche, 2011; Wahidin *et al.*, 2015). The critical dependence on appropriate segmentation parameters can be mitigated by taking a more flexible approach to segmentation, in which segmentations are revised and tailored for particular classes at later stages in the workflow (Lang *et al.*, 2010; Tiede *et al.*, 2010). A number of tools have been developed to statistically evaluate segmentation quality by calculating the local variance of object heterogeneity or the 'strength' of object borders (Moller *et al.*, 2007; Dragut *et al.*, 2010; Zhang *et al.*, 2010) which are useful where there is no *a priori* knowledge of the study site. However, expert interpretation 'by eye' remains the primary method of optimising the segmentation workflow, and this requires good knowledge of the ecosystem under investigation.

The classification step of OBIA also involves several choices, the first of which is the decision between a supervised or unsupervised approach. Unsupervised classification involves statistical clustering of data, e.g. spectral values, to identify natural groupings of pixels or objects, the total number of groups having been specified in advance by the analyst. A class description may then be assigned to each group using expert knowledge or ground truth data. In supervised classification, the user first defines the classes then develops a workflow to assign objects to these classes, either by setting threshold values or membership functions for class membership or by using samples to train a classification algorithm. Supervised classification is the most widely used approach in OBIA (Blaschke, 2010), while unsupervised classification has been the most common strategy for creating seabed habitat maps from acoustic data using pixel-based approaches (Brown *et al.*, 2011a). Unsupervised classification is objective and requires no prior knowledge of the study area, but it can be

difficult to determine the most suitable number of classes and there may be a mismatch between statistically derived clusters and real-world habitats as represented by ground truth data (Freitas *et al.*, 2003; Brown and Collier, 2008; Brown *et al.*, 2012). Recent OBIA studies have demonstrated the effectiveness of supervised classification for seabed mapping from acoustic or optical imagery (Lucieer, 2008; Phinn, 2012; Lucieer *et al.*, 2013; Diesing *et al.*, 2014; Gavazzi *et al.*, 2016), while others have demonstrated the value of combining both approaches, for example using the results of unsupervised classification to aid selection of training objects for supervised classification (Lucieer and Lamarche, 2011) or to inform choice of data layers for supervised classification (Duffy *et al.*, 2018). A potentially highly beneficial use of unsupervised classification of remotely sensed data is to ensure representative ground truth sampling to inform a supervised classification (Clements *et al.*, 2010).

The next decision to be made regards the choice of habitat classification system. Many remote sensing studies in both terrestrial (Bradter *et al.*, 2011; Lucas *et al.*, 2011; Lucas *et al.*, 2015) and marine environments (Brown and Collier, 2008; Lucieer, 2008; Shumchenia and King, 2010; Coggan and Diesing, 2011; van Rein *et al.*, 2011; Calvert *et al.*, 2015; Valentini *et al.*, 2015) have used national or international standard classification systems, which have the benefits of being widely understood, enabling comparison between sites and/or over time, and identifying habitats with statutory designations for conservation. Another advantage is that such systems are usually hierarchical, meaning that classes defined by biological community and the physical environment are nested within broader classes defined by the physical environment alone; this supports the OBIA approach of segmentation and classification on multiple hierarchical levels (Strasser and Lang, 2015).

However, standard classification systems may not correlate well to classes which can be detected from remote sensing data, particularly if the data are of low spectral and/or spatial resolution, and they may not adequately represent locally-specific habitats. This is particularly true of marine classifications which have been developed using coarse scale environmental and biological data due to the difficulty of sampling in this environment (Fraschetti *et al.*, 2008; Robinson *et al.*, 2011; Galparsoro *et al.*, 2012a; Galparsoro *et al.*, 2015). Thus the majority of remote sensing studies for marine habitat mapping have developed a classification system specific to their study area, either through statistical analysis of ground truth data (Freitas *et al.*, 2011; Serpetti *et al.*, 2011; Elvenes *et al.*, 2014;

Wahidin *et al.*, 2015; Biondo and Bartholoma, 2017) or visual assessment and categorisation of ground truth data (Bejarano *et al.*, 2010; Kloser *et al.*, 2010; Ierodiaconou *et al.*, 2011; Phinn, 2012; Lucieer *et al.*, 2013; Hasan *et al.*, 2014).

Whether using a standard or a site-specific classification system, the analyst needs to decide on an appropriate level of thematic resolution. The thematic resolution of seabed maps ranges from simple bathymetric features (Lucieer, 2007; Dekavalla and Argialas, 2017) to substratum types, for example based on sediment grades (Serpetti *et al.*, 2011; Diesing *et al.*, 2014; Calvert *et al.*, 2015; Biondo and Bartholoma, 2017) and finally biological communities (Ierodiaconou *et al.*, 2007; Holmes *et al.*, 2008; Rattray *et al.*, 2009; Kloser *et al.*, 2010; Ierodiaconou *et al.*, 2011; Elvenes *et al.*, 2014; Hasan *et al.*, 2014). Mapping at high thematic resolution is more challenging, particularly when data are of low spatial and/or spectral resolution and when the correlation between biological communities and environmental variables is imperfectly understood (Diaz, 2004; Reiss *et al.*, 2015). Maps at any level of thematic resolution can inform MSP; even simple geomorphological or 'seabed feature' maps have many uses (Harris *et al.*, 2014), including improving understanding of commercial fishery species (Lucieer and Pederson, 2008; Galparsoro *et al.*, 2009) and identifying optimal sites for MPAs (Banks and Skilleter, 2007; Harris and Whiteway, 2009). Species community maps are desirable, particularly for the management and monitoring of MPAs, but mapping at such high thematic resolution is costly in terms of requirements for high quality data, analyst expertise and knowledge of relationships between species and physical environmental factors (Buhl-Mortensen *et al.*, 2015). The choice of appropriate thematic resolution must therefore be informed by the desired purpose of the map and justified by the spatial and spectral resolution of the available remote sensing data and the taxonomic resolution of ground truth data.

The final decisions relate to the classification workflow itself, namely the choice of classification rules or algorithms and the selection of features to be used for classification. Commercial OBIA software enables analysts to develop sequential rule sets to classify objects based on threshold values or membership functions, or to apply one of a selection of standard classification algorithms which can be trained by sample objects (Trimble, 2014). An important benefit of developing customised rules is that it enables the analyst to apply their ecological knowledge to the rule development process, while the transparent, sequential workflow enables them to fine-tune the rules to maximise classification accuracy

(Visser *et al.*, 2016; Medcalf *et al.*, 2017). Another benefit is that this approach does not require training samples, although ground truth data may be used to inform the selection of threshold or membership function values. However, because it is based on expert knowledge, this approach can be subjective to the extent that classification workflows produced by different experts for the same data can produce significantly different results (Belgiu *et al.*, 2014). Furthermore, because of the 'trial and error' method of adjusting membership values to maximise accuracy, knowledge-based workflows can take a long time to develop and are seldom transferable from one dataset to another without adjustment (Arvor *et al.*, 2013).

In contrast, standard classification algorithms do not require expert knowledge and are therefore relatively quick and easy to implement. Brief descriptions of classification algorithms commonly used in habitat mapping from remote sensing data are provided in Table 1.2 and examples of marine and coastal applications are shown in Table 1.3.

Table 1.2: Summary of classification algorithms commonly used in habitat mapping

Algorithm	Description	Availability	References
k-Nearest Neighbour	Assigns objects to the class of the most similar training sample(s) in a defined feature space. 'k' represents the number of samples considered, i.e. if k = 1, the object is assigned to the class of the most similar sample, if k = 5, the object is assigned to the class held by the majority of the five most similar samples.	eCognition classifier class package in R	Lucieer *et al.* (2013) Lucieer (2008) Lawrence *et al.* (2015) Gavazzi *et al.* (2016)
Bayes	Calculates the probability of an object belonging to a class based on a number of features which are assumed to be independent from each other.	eCognition classifier e1071 package in R	Wahidin *et al.* (2015)
Fast Neural Network	Data is entered into an input layer which has a node for each feature. The output layer contains probability values for each class, which add up to 1. The input and output nodes are connected via a hidden layer of nodes.	nnet package in R	Marsh and Brown (2009)
Support Vector Machines	Predict which of two classes an object belongs to, based on identifying the best plane of separation between the two classes.	eCognition classifier e1071 package in R Segmentation and Classification Toolset in ArcGIS	Mountrakis *et al.* (2011) Hasan *et al.* (2012b)
Decision Tree	Classifies an object by applying a series of decisions based on if-then-else logical conditions which have been determined by training data. The model looks like a tree in which each decision is represented by a node which splits the data, assigning the object to one branch or another	eCognition classifier tree package in R	Lucieer *et al.* (2013) Holmes *et al.* (2008)
Random Forests	Aggregates the results of many randomly constructed decision trees, each of which has been trained using the same set of features but a different subset of the training data.	eCognition classifier randomForest package in R	Belgiu and Dragut (2016) Diesing *et al.* (2014)

In theory, classification algorithms offer a more objective and transferable classification method than a knowledge-based workflow, but the selection of training samples is a potential source of analyst bias which has a considerable influence on output and can lead to over-fitting the classification model to the data (Foody and Mathur, 2004; Belgiu and Dragut, 2016; Costa *et al.*, 2017). Furthermore, comparative studies show that the application of

different classifiers to the same data produces different results, and the classifier which produces the most accurate results varies from one study to another (Table 1.3). Variability in classifier performance may be mitigated through the use of classifier ensembles, although this approach has not yet been widely tested (Diesing and Stephens, 2015). Perhaps the most promising way to exploit the advantages of knowledge-based rules and of classification algorithms is to develop a workflow which combines both approaches. This could involve using knowledge-based rules to separate distinctive classes and/or to eliminate objects such as cloud or shadow from further classification, then applying a classification algorithm to separate more challenging classes in an objective, data-driven way (Heumann, 2011; Hsieh *et al.*, 2017; Jones *et al.*, 2017). Alternatively, a classification algorithm can be applied, followed by a sequence of knowledge-based rules to deliver post-classification enhancements as suggested by Diesing *et al.* (2016).

Table 1.3: Comparative studies of classification approaches for marine habitat mapping

Mapping study	Threshold rules (TR)	Membership functions MF)	Nearest Neighbour (NN)	Fast Neural Network (FNN)	Random Forests (RF)	Bayesian (B)	Decision Tree (DT)	Support Vector Machine (SVM)	Pixel-based (PB)	Manual (M)	Overall accuracy of classification
Coral reef morphology and substrata at three hierarchical levels using Landsat and Quickbird (Benfield *et al.*, 2007)		✓							✓		Landsat: Level 1: MF = 68% to 81%, PB = 57%, Level 2: MF = 63% to 76%, PB = 51%, Level 3: MF = 59% to 69%, PB = 45% Quickbird: Level 1: MF = 88% to 90%, PB = 77%, Level 2: MF = 85% to 87%, PB = 72%, Level 3: MF 81% to 84%, PB = 59%
Temperate benthic substrata from sidescan sonar (Lucieer, 2008)			✓							✓	Two classes: NN = 80%, M = 81% Three classes: NN = 60%, M = 72%
Coral reef morphology and substrata at three hierarchical levels from Quickbird and Ikonos imagery (Scopelitis *et al.*, 2010)	✓								✓	✓	TR = 55% to 60%, PB = 39% to 49% *The manual classification was used to evaluate the other methods.*
Coral reef geomorphology from Landsat imagery (Leon and Woodroffe, 2011)	✓		✓	✓							Coarse classes: TR = 56%, NN = 87%, FNN = 87% Fine classes: FNN = 75%
Saltmarsh vegetation from Quickbird imagery (Ouyang *et al.*, 2011)		✓	✓						✓		PB = 78% to 82%, NN = 80% to 81%, MF = 85% to 87%
Coral reef substrata from photographs and multibeam echosounder (MBES) data (Estomata *et al.*, 2012)	✓								✓		TR = 94%, PB = 85% to 93%
Coral reef mapping at three hierarchical levels from Quickbird imagery (Phinn, 2012)	✓								✓		Benthic communities: TR = 65%, PB = 57% *The validation methods differed between the two approaches.*
Temperate benthic substrata, rugosity and sponge structure classes from MBES data (Lucieer *et al.*, 2013)			✓		✓		✓				Substrata: NN = 49% to 57%, RF = 55% to 64%, DT = 48% to 57% Rugosity: NN = 60% to 63%, RF = 62% to 65%, DT = 61 to 62% Sponges: NN = 49% to 57%, RF = 50% to 54%, DT = 49% to 56%
Coral reef substrata and benthic communities from hyperspectral imagery (Zhang *et al.*, 2013)					✓				✓		Substrata: RF = 84%, PB = 70% Benthic communities: RF = 87%, PB = 60%
Temperate benthic substrata from MBES data (Diesing *et al.*, 2014)	✓				✓					✓	TR = 67%, RF = 76% Difference not statistically significant at 5% level
Temperate benthic substrata from MBES data (Lawrence *et al.*, 2015)			✓							✓	NN = 63%, M = 68% Angular response curve 75%
Coral reef substrata from Landsat imagery (Wahidin *et al.*, 2015)			✓		✓	✓	✓	✓			SVM = 73%, RF = 68%, NN = 67%, B = 66%, DT = 56%
Temperate lagoon sediments, submerged vegetation and sponges from MBES data (Gavazzi *et al.*, 2016)			✓						✓	✓	Five classes: NN = 51% to 52%, PB = 54% to 71% Four classes: NN = 55% to 61%, PB = 58% to 73% Three classes: NN = 64% to 66%, PB = 68% to 83%

The wealth of spectral, geometric and contextual information created by grouping pixels to form objects is considered a key benefit of OBIA (Blaschke, 2010), but it also presents a significant challenge. Using sub-optimal features reduces classification accuracy, but including too many features decreases processing speed and may also reduce accuracy (Diesing *et al.*, 2016). Determining the best selection of features from the hundreds available can be time-consuming and subjective (Laliberte *et al.*, 2012). Furthermore, features which are highly correlated may not actually be redundant, and features which are poor predictors when used alone may have very good predictive power when used in combination with other features (Guyon and Elisseeff, 2003). Automated feature selection methods which can be applied in an OBIA context are broadly categorised as filters, wrappers and embedded methods (Tang *et al.*, 2014). Filters are applied to training data before classification, ranking features without considering how they interact with each other or how they affect the performance of any specific classifier. Wrappers determine the best set of features by iteratively running a classifier with different subsets of features and evaluating the results, an approach which takes feature interaction into account but is computationally slow. Embedded methods are specific to a particular classifier and select features during the training stage, taking account of feature interaction and performance with the given classifier.

Some embedded feature selection methods commonly used with OBIA include feature space optimisation used with the Nearest Neighbour classifier (Lucieer, 2008; Na *et al.*, 2015; Son *et al.*, 2015), the generation of feature importance values by Decision Tree and Random Forests classifiers (Lucieer *et al.*, 2013), and recursive feature elimination for the Support Vector Machine classifier (Ma *et al.*, 2017). Comparative studies have shown that the extent to which feature selection improves classification accuracy varies from one classifier to another (Georganos *et al.*, 2017), and in some cases it actually reduces classification accuracy (Gilbertson and van Niekerk, 2017). Although feature selection may be aided by statistical methods, it is usually informed by the analyst's knowledge and experience, if only to produce an initial selection of features for further reduction (Duro *et al.*, 2012). The requirement for feature selection in OBIA therefore adds to the need for analyst expertise and is another potential source of subjectivity.

The above studies highlight the multitude of decisions confronting the OBIA analyst and demonstrate that there is no single 'best' choice in each case; the optimum parameters for segmentation and classification vary depending on the input data and purpose of the map.

1.4 Quality assessment

Quantitative evaluation of habitat maps derived from remote sensing data and clear presentation of the results of this evaluation are crucial, especially if the maps are intended to regulate activities through MSP. Evaluation methods may be used during the mapping process to refine the model as well as at the end of the process to communicate to users. The most commonly used method of evaluation is to compare the map to reference data to determine how closely it represents the ecosystem under observation, while other methods involve evaluating the quality of the input data and the robustness of the methods. A very simple quality assessment method is to score data and methods against set criteria, as exemplified by the Mapping European Seabed Habitats Confidence Assessment Scheme (MESH, 2010), which provides useful insight into the mapping process but does not quantify accuracy of the output.

Accuracy assessment methods evolved considerably during the first decades of remote sensing (Congalton, 1991; Congalton and Green, 2009). At the outset, maps were assessed only through basic visual appraisal, which is highly subjective and not quantitative. In the early 1980s, accuracy was quantified by comparing the predicted area of each habitat with its area in a reference dataset, thereby assessing the ability to predict extent but not the ability to predict distribution. To address this shortcoming, accuracy metrics were developed based on calculating the proportion of agreement between the map and reference data points; initially this consisted of a single figure for overall accuracy, which provided no information into the classification accuracy of particular habitats. By the early 1990s however, it had become standard practice to evaluate and communicate accuracy using a confusion matrix, or error matrix, a method which is still recommended and used today both for terrestrial and marine habitat mapping (Medcalf *et al.*, 2014b; Diesing *et al.*, 2016). The confusion matrix clearly illustrates where classification errors occur between habitats. This is valuable information, because classification errors between two habitats which have similar composition and ecological function may be more acceptable to users than errors between two very different habitats. Additional useful metrics can be derived

from the error matrix, such as producer's accuracy calculated as the proportion of reference data per class which agrees with the map, and user's accuracy calculated as the proportion of classified pixels/objects per class which agree with the reference data (Congalton, 1991). Low producer's accuracy therefore signifies high errors of omission, while low user's accuracy signifies high errors of commission. This insight into a model's tendency to over- or under-predict particular habitats can help to inform choice of classification method, particularly if maps are to be used to inform MSP, in which case the predicted extent of a given habitat will have a direct impact on regulation of activities. The error matrix data can be portrayed visually as a Bangdiwala agreement chart (Bangdiwala and Shankar, 2013). This visualisation can provide useful insight, for example if one dominant habitat class accounts for the majority of agreement between the map and reference data (Calvert *et al.*, 2015). Reference data rarely cover the entire area of the map, they usually represent a very small proportion of classified objects or pixels. Overall accuracy and user's and producer's accuracy are therefore estimates of probability of the map's accuracy, so it would be appropriate to add confidence limits when presenting these estimates although this is not common practice in remote sensing studies (Foody, 2008; Diesing *et al.*, 2016).

Another metric which can be derived from the error matrix is the Kappa coefficient (Cohen, 1960) which is uses the off-diagonal (i.e. incorrectly classified) elements of the matrix to calculate the amount of agreement that could be expected to occur by chance and is calculated as follows:

$$K = \frac{observed\ accuracy - chance\ agreement}{1 - chance\ agreement}$$

Endorsed by some as a useful additional measure of accuracy, a powerful technique for comparing error matrices and a discerning statistical tool for assessing the accuracy of different classifiers (Congalton, 1991; Fitzgerald and Lees, 1994), Kappa became increasingly widely used in remote sensing studies and integrated into mapping software, to the point that it has been described as a 'standard component' and a 'vital accuracy assessment measure' (Congalton and Green, 2009). Others have criticised Kappa and its variants, stating that these measures are unnecessarily complex, add no additional information to the primary accuracy metrics and can even be misleading (Foody, 1992; Liu *et al.*, 2007; Pontius and Millones, 2011). Despite these conflicting views, Kappa continues to be used in current OBIA studies (Gavazzi *et al.*, 2016; Onojeghuo and Onojeghuo, 2017; McIntyre *et al.*, 2018).

A shortcoming of the error matrix and its associated accuracy metrics is that they give no insight into the spatial distribution of accuracy. Spatially explicit accuracy measures have been developed based on geographically weighted regression (Foody, 2003; Foody, 2005), which have subsequently been extended by incorporating geographically weighted distance measures to produce measures of overall, user's and producer's accuracy within a moving window or kernel (Comber *et al.*, 2012; Comber, 2013). The majority of remote sensing studies do not, as yet, apply spatially explicit accuracy measures, perhaps due to insufficient density of reference data or because of the complexity of the method. However, application of these methods to evaluate the spatial accuracy of terrestrial habitat maps produced through OBIA has been successfully demonstrated by Medcalf *et al.* (2014b).

Classification accuracy is affected by the quantity and quality of the reference data. Interpretation of the error matrix is often based on the assumption that reference data are an accurate representation of real world habitats, but reference samples can contain positional errors and furthermore may not have been collected at the same time as the remote sensing data, which could be a cause of inaccuracy if the environment is dynamic (Diesing *et al.*, 2014). Classification of ground truth data by expert interpretation is another possible source of inaccuracy. Assigning habitat classes to seabed images has been shown to be subjective and inconsistent, particularly at more detailed levels of classification (Rattray *et al.*, 2014). Estimating percentage cover in a quadrat or photograph is also subject to operator bias, although this can be mitigated to some extent by software which aids the objective quantification of substrate coverage through the generation of random points in the image (Kohler and Gill, 2006). Use of an over-simplified classification, for example grouping different seabed sediment types into a single class due to the limitations of using seabed photographs to classify sediments, can lead to over-estimation of accuracy (Hasan *et al.*, 2014; Calvert *et al.*, 2015). In the absence of ground truth data, reference samples may be generated through expert interpretation of high quality remote sensing imagery (Olofsson *et al.*, 2014), which is also a source of subjectivity and potential error.

Common strategies for selecting sample locations and for splitting a reference dataset into subsets for training and validation are random, stratified random and systematic sampling. Choice of sampling protocol has been shown to affect validation results in an OBIA context, particularly when there is spatial autocorrelation between data points (Zhen *et al.*, 2013; Ma *et al.*, 2015). When reference data have been collected through field survey, it is often the

case that samples are unequally distributed amongst classes and that rare classes are under-sampled, which can render it impossible to produce meaningful accuracy statistics (Medcalf *et al.*, 2014b). Balanced error rate (BER) is an accuracy metric calculated as the mean proportion of incorrect classifications in each class. The lower the BER value, the higher the classification accuracy. BER compensates for unequal proportions of classes in the reference data and/or classified map by effectively giving higher weighting to rare classes. BER has not been widely used in remote sensing, but has been shown to be a useful measure of accuracy in seabed mapping studies with unbalanced class frequencies (Stephens and Diesing, 2014; Diesing and Stephens, 2015).

Where fuzzy classifications have been produced, for example through membership functions or a Nearest Neighbour classifier, classification stability can be calculated as the difference between an object's level of membership to its assigned class and to the second most similar class (Benz, 2004). This is not a measure of the map's accuracy, but does give insight into the robustness of the mapping method, i.e. the larger the difference, the more stable the classification. Thematic maps can be produced based on either class membership values or classification stability values, to determine whether there are spatial patterns in the robustness of the classification. Because different outputs can be produced from the same data by using different classifiers, or even by using the same classifier with different training samples, it is useful to compare maps produced by different methods on a pixel-by-pixel or object-by-object basis, calculating the percentage agreement overall and per habitat class (Visser and de Nijs, 2006). Agreement between models is not an indication of accuracy, but can be a useful way of quantifying the impact of methodological variability and visualising this in a spatially explicit way (Diesing *et al.*, 2014).

The above methods all measure agreement based on categorical classifications and are thus suitable for evaluating habitat maps. The standard method for measuring agreement between remote sensing outputs and ground truth data on a continuous scale is to calculate Root Mean Square Error (RMSE) by comparing predicted values with measured values and calculating the standard deviation of the residuals. This is widely used in remote sensing studies to quantify the horizontal accuracy of remotely sensed imagery and the vertical accuracy of digital elevation or bathymetry models generated by acoustic survey, LiDAR or photogrammetry (Dolan and Lucieer, 2014; Rapinel *et al.*, 2015; Ierodiaconou *et al.*, 2016).

The generation of accuracy statistics enables maps to be evaluated against a theoretical target value. A widely used target value in terrestrial remote sensing is 85% overall accuracy, but this has been criticised as arbitrary, inappropriate and inflexible to the requirements of different research questions and study areas (Foody, 2008; Pontius and Millones, 2011). There has been little discussion and no consensus amongst the marine research community regarding a minimum acceptable level of overall or per-class accuracy for marine habitat maps. This may be considered beneficial, in that it enables researchers and stakeholders to determine acceptable accuracy on a case-by-case basis. England's Marine Management Organisation have stated that maps derived from remote sensing must have a confidence score of ≥60% in order to inform marine spatial planning (MMO, 2014b).

A final point is that all habitat maps contain inaccuracies, including those created through ecological field surveys, but maps derived from remote sensing tend to be subject to more rigorous accuracy assessment than those derived from other methods (Foody, 2008). This rigorous approach helps to compare, evaluate and improve methods, but it should not lead to the perception that remote sensing maps are of lower quality than other maps which have simply not been subjected to the same level of assessment.

In conclusion, although research into remote sensing accuracy assessment is an evolving field and there is lack of consensus on certain details, such as the use of Kappa, the following five main best practice recommendations can be summarised from the body of research to date: (1) ground truth data for validation should be collected at the same time as remote sensing data where possible, (2) the sampling protocol should ensure sufficient sampling density and adequate representation of all habitat classes, (3) at least two accuracy metrics should be published, including overall and class-specific accuracy, (4) confidence limits for accuracy metrics should be defined and provided, and (5) the error matrix should be published.

1.5 Implications for management

The need for habitat maps to inform sustainable marine management as required by national and international legislation and policy was described in Section 1.1. This is particularly relevant in the UK, where recent legislation has led to an upsurge in the designation of MPAs (Figure 1.1). 23% of the UK's seabed is currently designated for conservation, but resources available for marine surveillance and monitoring are decreasing,

making it imperative to find cost-effective yet robust ways of meeting statutory obligations (Borja and Elliott, 2013; Rush and Solandt, 2017).

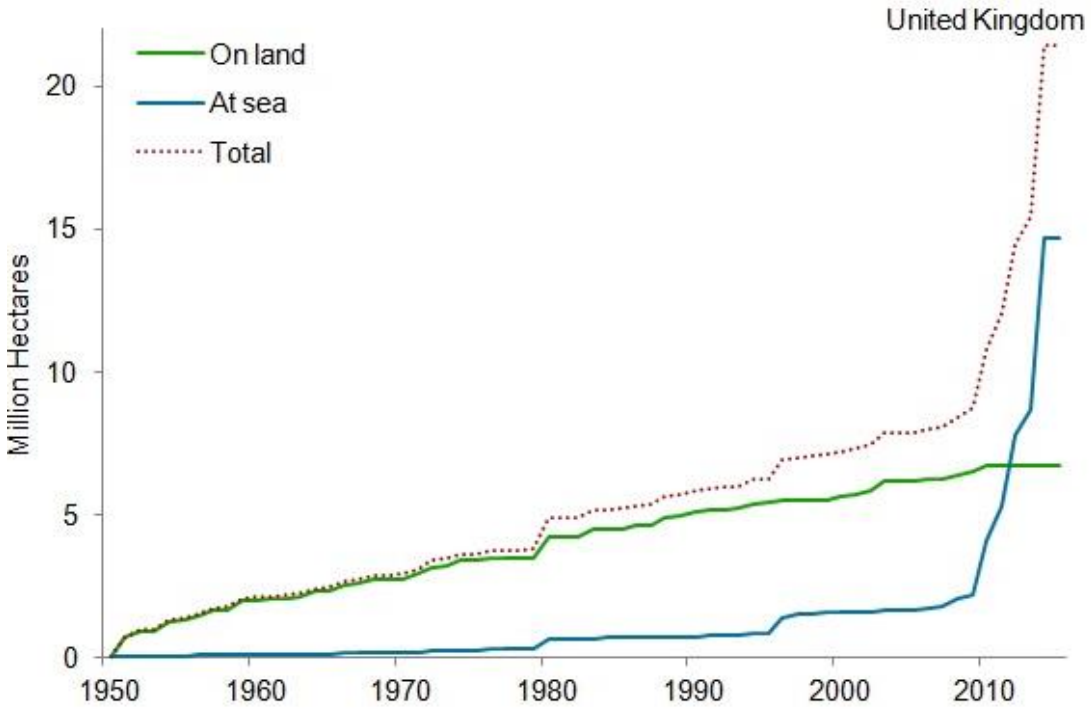

Figure 1.1: Extent of UK nationally and internationally important protected areas: on land (green); at sea (blue); in total (red), 1950 to 2015. Source: http://jncc.defra.gov.uk

Marine habitat maps are required by many areas of the UK's evolving marine governance framework, with potential to inform spatial planning and reporting under the Marine and Coastal Access Act 2009, the EU Marine Strategy Framework Directive 2008 and the Conservation of Habitats and Species Regulations 2010 (JNCC, 2013; Rodwell *et al.*, 2014). The establishment of an ecologically coherent network of MPAs is based on design principles which include criteria for representativity and replication of habitats (JNCC and Natural England, 2010). Habitat maps modelled from environmental variables informed initial network proposals (McBreen, 2011), but remote sensing surveys have since been conducted of recommended MPAs to produce more accurate, higher resolution habitat maps, in some cases using OBIA methods (Sotheran and Crawford-Avis, 2014; Curtis *et al.*, 2015; Mitchell and McIlwaine, 2015). England's emerging marine spatial plans have been based on a combination of modelled and remotely sensed habitat maps, with the provision that habitat maps derived from remote sensing, where available, should take priority over modelled data (MMO, 2014b; MMO, 2014a).

Remote sensing is thus already making a contribution to marine management, but the provision of baseline data is just the start of the process. The governance framework includes requirements for monitoring change in the extent and distribution of habitats, both within and outside MPAs. Variability in sampling and data interpretation methods prevent the use of marine habitat maps to monitor change in extent or distribution of habitats as it is impossible to distinguish real change from apparent change resulting from methodological inconsistency (Frost *et al.* 2013). Uncertainty arising from methodological variability could be addressed through the production of recommended operating guidelines and standard operating procedures for all aspects of marine mapping, from survey design to map production and quality assessment (Strong, 2015). Sample replication and distribution, the collection and processing of acoustic data, and the interpretation of data to produce habitat maps have been identified as the three highest priority areas for the development of agreed community standards (Lillis *et al.*, 2016).

Another issue which must be addressed in order to use remote sensing to monitor change in extent or distribution of habitats is the determination of ecologically meaningful thresholds of change. Mieszkowska *et al*. (2014) emphasise the importance of long-term sustained observations in the marine environment to remove the 'noise' of short-term environmental fluctuations and reveal genuine trends. In Europe, statutory obligations for monitoring require reporting on a six year cycle, but more frequent surveillance is required for highly dynamic habitats and for habitats which are particularly vulnerable to human impacts (Medcalf *et al.*, 2014b). The temperate marine environment is highly dynamic, for example experiencing considerable movement of sediment during winter storms, and higher biodiversity and biomass of seaweeds and sessile fauna on both intertidal and subtidal reefs during summer. Strong (2015) estimates the minimum percentage change in extent of a selection of temperate marine habitats that can be detected by recommended field or remote sensing survey methods, but cautions that these estimates do not take account of site-specific variables such as habitat heterogeneity, depth or wave exposure. Furthermore, there is a variety of methods for using remote sensing to detect change in extent and distribution of habitats, but few studies have directly compared methods through application to the same data and none has done so in the marine environment (Tewkesbury *et al.*, 2015; Gomez *et al.*, 2016). Further research leading to improved understanding of the magnitude of natural and seasonal fluctuations in this environment and of the change-

detection capabilities of different OBIA methods and sensors would aid adoption of these methods to fulfil statutory requirements for monitoring.

With greater standardisation of methods and improved understanding of ecologically meaningful rates of change in the marine environment, there is clear potential to use OBIA and remote sensing to monitor extent and distribution of marine habitats. However, environmental legislation also requires monitoring of habitat condition, which presents a far greater challenge. Remote sensing can be used to evaluate quality of terrestrial habitats by detecting key species, vegetative productivity, vegetation structure or landscape patterns as indicators of habitat condition (Nagendra *et al.*, 2013; Vaz *et al.*, 2015; Breyer *et al.*, 2016; Allard, 2017). This is made possible by the high spectral resolution of satellite imagery, notably the ability to generate indices for photosynthetic activity, soil moisture and plant water content, and by the insight into three-dimensional vegetation structure provided by LiDAR or SAR data. Change in habitat condition may not be detectable from remote sensing, for example if it takes place beneath a forest canopy or if habitat patches are smaller than image pixels, but coarse indicators of change derived from satellite imagery can be used to direct field survey effort to areas of interest (Nagendra *et al.*, 2013; Jones *et al.*, 2017).

The quality or condition of marine habitats can be defined in terms of species community, by comparison with an assumed 'natural' state, or through evaluation of functional integrity i.e. the ability to provide ecosystem good and services (Tillin, 2008). Remote sensing can be used to detect abundance or biomass of dominant, habitat forming species (Degraer *et al.*, 2008; Lindenbaum *et al.*, 2008; Limpenny *et al.*, 2010; McGonigle *et al.*, 2011), but in most cases a species-based approach to defining habitat quality from remote sensing is unlikely to be possible in the marine environment, especially in habitats where much of the fauna is hidden under a fucoid or kelp canopy or buried in sediment. A potentially useful indicator for habitat quality of intertidal and subtidal reefs is topographic complexity, because there are proven correlations between complexity and biodiversity in the marine environment (Johnson *et al.*, 2003; Frost *et al.*, 2005; Kostylev *et al.*, 2005; Meager *et al.*, 2011; Rees *et al.*, 2014). Topographic complexity of rock reefs can be altered through erosion and sedimentation, while that of biogenic reefs can be altered by any factors which affect the health of the habitat engineers. Topographic models can be derived from acoustic data, LiDAR and more recently from optical imagery through photogrammetry. Recent studies have demonstrated the use of topographic models derived from very high resolution

imagery to monitor coastal sediment habitats (Harwin & Lucieer 2012; Mancini *et al.* 2013; Goncalves & Henriques 2015; Ierodiaconou, Schimel & Kennedy 2016). Research into the consistency and feature detection capabilities of these methods would help to evaluate their potential as a proxy for habitat condition of temperate reefs, with potentially useful implications for marine monitoring.

1.6 Future research priorities

Interest in OBIA and remote sensing for habitat mapping has grown steadily for over a decade, to the extent that OBIA has been defined as a new paradigm (Blaschke *et al.*, 2014). This trend is likely to continue as remotely sensed data and processing software are becoming more widely available and there is strong Governmental support in Europe and the UK for the development of practical implementations (Medcalf *et al.*, 2014b; Medcalf *et al.*, 2014a; Lucas *et al.*, 2015; Medcalf *et al.*, 2015; Breyer *et al.*, 2016).

Nevertheless, this review reveals gaps in the knowledge required to inform the multitude of analyst decisions that affect the accuracy and usefulness of habitat maps. Although the current body of research gives valuable insight into the factors that must be considered, the majority of OBIA studies to date have focussed on satellite imagery and applications in terrestrial environments. Few studies have evaluated OBIA through application to other types of remotely sensed data in marine ecosystems, so there is a pressing need for comparative evaluation of methods through experimental applications in temperate subtidal and intertidal habitats. In particular, further research is needed to:

1. Evaluate the use of OBIA with remote sensing data from a range of sensors at different resolutions for temperate marine and coastal habitat mapping to better understand potential sources of error associated with each sensor and how these might be addressed.
2. Quantify the effect on map accuracy of different ground truth sampling protocols, classifiers, classification systems and thematic resolutions in this environment, leading to recommendations to inform appropriate choices in these areas.
3. Evaluate the accuracy and feature detection capability of topographic models derived from remotely sensed data, to ascertain their usefulness to aid predictive mapping in OBIA and to monitor change in physical habitat complexity.

4. Assess the change detection capability of OBIA and remotely sensed data through comparative evaluation of different workflows, leading to recommendations to inform adoption of these methods for intertidal monitoring.

Improved knowledge in these areas would help to overcome current barriers to adoption of such methods for mapping and monitoring temperate marine and coastal habitats by contributing to emerging standards and guidance (Strong, 2015; Lillis *et al.*, 2016). If applied in a robust and consistent way, OBIA and remote sensing have considerable potential to aid sustainable management of the marine environment and fulfil statutory conservation requirements, much as they are starting to do in terrestrial ecosystems (Lucas *et al.*, 2017). Coverage of remotely sensed data in the marine environment is patchy and incomplete, so the ability to integrate data from a wide range of sources is crucial; understanding the potential uses and limitations of different sensors will help to achieve this. Growing anthropogenic pressure on the marine environment poses a significant threat to biodiversity and to the ecosystem services on which the human population depends. Improved skills, knowledge and capacity in marine remote sensing will place us in a good position to take full advantage of future improvements in sensor technology, potentially moving beyond simple habitat mapping and change detection, to habitat condition monitoring and mapping of restoration opportunities.

1.7 Thesis aim and structure

The overall aim of this thesis is to evaluate the application of OBIA to multi-resolution remote sensing data for mapping and monitoring temperate marine and coastal habitats. The four knowledge gaps described in the previous section will be addressed through experimental studies in English North Sea MPAs using optical, acoustic and LiDAR data to produce habitat maps at different spatial and thematic scales. Knowledge gaps 1 and 2 are addressed by the thesis as a whole, while knowledge gap 3 is addressed specifically by chapter 3 and knowledge gap 4 by chapter 5. Findings will increase our understanding of the potential for using OBIA and remote sensing in this environment and inform adoption of suitable methods by the authorities responsible for marine spatial planning and monitoring in temperate seas.

Chapter 2 introduces and tests the concept of OBIA for marine habitat mapping through application to acoustic data to map circalittoral habitats over a large and relatively

homogeneous area at broad and fine thematic scales. This chapter investigates what can be achieved with simple two-band data at relatively low resolution, identifying both the potential benefits and the sources of error and uncertainty.

Chapters 3 and 4 build on these findings by developing workflows to interpret imagery at higher spectral and spatial resolution collected via an Unmanned Aerial Vehicle (UAV) in a small but highly heterogeneous area. Chapter 3 evaluates topographic models created by photogrammetry by validating their vertical accuracy and comparing rugosity indices derived from the models with those derived from manual measurements. Chapter 4 develops and tests three OBIA methods to interpret combined topographic and spectral information to produce and validate intertidal habitat maps at two thematic scales.

Chapter 5 evaluates the change detection capabilities of OBIA to determine its suitability for intertidal habitat monitoring. This chapter develops and applies three OBIA workflows to interpret freely available multi-temporal aerial imagery and LiDAR data to produce change detection maps at three levels of sensitivity.

Chapter 6 then provides a synthesis of key findings, addresses the limitations of the study, discusses wider implications of the findings and highlights areas for future research.

Chapter 2: Mapping temperate circalittoral habitats through object-based image analysis of acoustic data

2.1 Introduction

The growing human population depends on the marine environment for a wide range of goods and services (Millenium Ecosystem Assessment, 2005), but marine ecosystems are under increasing pressure from anthropogenic activities (Halpern *et al.*, 2008). An understanding of the distribution, extent and condition of seabed habitats and their associated biological communities is needed to inform sustainable use of the marine environment through Marine Spatial Planning (MSP) and to underpin biodiversity conservation through the designation and management of Marine Protected Areas (MPAs) (Cogan *et al.*, 2009).

Remote sensing offers a cost-effective, non-destructive method of producing habitat maps for large areas, and has made a considerable contribution to conservation management and monitoring environmental change in terrestrial ecosystems, predominantly through the use of satellite imagery (Pettorelli *et al.*, 2014; Corbane *et al.*, 2015). Satellite or aerial imaging of the seabed is feasible in clear tropical waters to a depth of around 20 metres (Phinn *et al.*, 2013), but due to the absorption and scattering of light, sonar technology offers the only solution for imaging large areas of seabed in deep water or in turbid shallow water (Kenny *et al.*, 2003; Brown *et al.*, 2011a).

Technology and techniques for acoustic remote sensing, georeferencing and data processing have improved and become more affordable in recent decades (Mayer, 2006; Brown and Blondel, 2009; Le Bas and Huvenne, 2009), and guidance has been developed to promote consistent standards in the application of these techniques for seabed mapping (Hopkins, 2007; Populus and Perrot, 2007; Henriques *et al.*, 2013). Various methods have been developed for the manual or automated interpretation of acoustic data, typically based on the statistical clustering of ground truth and acoustic data to identify and classify areas of seabed that share similar characteristics (Brown *et al.*, 2011a). Seabed mapping from acoustic data has traditionally focussed on pixel-based approaches (Dartnell and Gardner, 2004; Preston, 2009; Ierodiaconou *et al.*, 2011; Diesing and Stephens, 2015), signal-based methods such as analysis of the angular response curve (Fonseca and Mayer, 2007; Simons and Snellen, 2009; Hamilton and Parnum, 2011; Lamarche *et al.*, 2011) or interpretation of

integrated signal and image data (Fonseca *et al.*, 2009; Hasan *et al.*, 2012a; Hasan *et al.*, 2014). Research into the application of object-based image analysis (OBIA) for seabed mapping has not fully matured (Diesing *et al.*, 2016), but a few pioneering studies have demonstrated the potential of an object-based approach for mapping seabed substrata (Lucieer, 2008; Lucieer and Lamarche, 2011; Lucieer *et al.*, 2013; Diesing *et al.*, 2014; Lawrence *et al.*, 2015).

Producing even relatively simple substrate maps from acoustic data is difficult due to data variability, artefacts and gaps (McGonigle *et al.*, 2010; Collier and McGonigle, 2011), but mapping biological communities presents a far greater challenge (Diaz, 2004; Heap, 2011). Remote sensing can predict the distribution of biological communities either by detecting those communities directly or by detecting abiotic proxies. The ability of acoustic remote sensing to detect biological communities has so far been limited to communities defined by a single dominant species, notably habitat engineers such as *Modiolus modiolus* (Lindenbaum *et al.*, 2008), *Sabellaria spinulosa* (Limpenny *et al.*, 2010), *Lanice conchilega* (Degraer *et al.*, 2008) and *Laminaria* kelp species (McGonigle *et al.*, 2011). A more common approach to biological mapping is therefore to predict the distribution of biota from abiotic surrogates detectable from acoustic data. Several studies have modelled distribution of biota from acoustic data with some success using pixel-based approaches (Ierodiaconou *et al.*, 2007; Holmes *et al.*, 2008; Rattray *et al.*, 2009; Kloser *et al.*, 2010; Gonzalez-Mirelis *et al.*, 2011; Ierodiaconou *et al.*, 2011; Mielck *et al.*, 2014; Rinne, 2014) or OBIA methods (Lucieer *et al.*, 2013; Hill *et al.*, 2014). However, it should be noted that these studies used very broadly defined biological classes (for example 'macroalgae', 'rhodoliths', 'sessile invertebrates' (Holmes *et al.*, 2008)) and most were conducted in areas with considerable heterogeneity of environmental features likely to influence distribution of biota. There is thus a pressing need to test the application of OBIA methods to acoustic data for habitat mapping under relatively environmentally homogeneous conditions, which often prevail over large areas in temperate seas.

When creating maps of benthic substrata or communities, the option exists to use an existing habitat classification system or to develop one specifically for the survey area. An advantage of using an existing classification system is that the habitat map will be more easily understood by those responsible for marine management and spatial planning. For example, the OSPAR Biodiversity Committee agreed that the EUNIS classification system

should be used to characterise habitats throughout the OSPAR maritime area and to assess the representativity of the range of habitats covered by the MPA network (OSPAR Commission, 2006). Studies that develop and evaluate mapping methods to meet specific statutory marine conservation and monitoring requirements tend to use existing classification systems rather than developing a site-specific one (Brown and Collier, 2008; Shumchenia and King, 2010; Coggan and Diesing, 2011; van Rein *et al.*, 2011).

A disadvantage is that existing classification systems may not represent the full range of local variations of a particular habitat (Galparsoro *et al.*, 2012b) and may not correlate well with classes derived from acoustic data (Brown and Collier, 2008; Gonzalez-Mirelis *et al.*, 2011). The majority of studies on habitat mapping from acoustic data have used a classification system developed specifically for the study area through analysis of ground truth data (for example Kloser *et al.*, 2010; Serpetti *et al.*, 2011; Lucieer *et al.*, 2013; Hasan *et al.*, 2014; Biondo and Bartholoma, 2017). The benefit of this approach is that the habitat classes are ecologically meaningful and accurate for the study area and can be separated reliably using remote sensing data. Such an approach is well-suited for monitoring change within the study area, but wider application would likely require modification of the classification system, or even development of a new, regionally-specific system.

Commercially available software packages have been developed specifically for the interpretation of acoustic data, notably RoxAnn [Stenmar Ltd] for interpreting single-beam data, and QTC Multiview [Questor Tangent Corporation] for interpreting multi-beam data. These have proven effective for creating benthic habitat maps (Freitas *et al.*, 2003; McGonigle *et al.*, 2009; Brown *et al.*, 2011b; Serpetti *et al.*, 2011; Brown *et al.*, 2012) but one concern is that the user does not have access to the algorithms used as they are considered commercially sensitive (Davies *et al.*, 2001). In contrast, the commercial OBIA software eCognition enables users to develop classification rules using thresholds and membership functions to separate classes, and to apply a range of supervised classification algorithms trained by reference data drawn from ground truth samples (Trimble, 2014). A commonly used algorithm in OBIA habitat mapping studies is k-Nearest Neighbour, which assigns an object to the class which is most common amongst its closest training objects in a feature space, with k being the number of training objects considered (Lucieer, 2008; Lucieer and Lamarche, 2011; Lucieer *et al.*, 2013; Hill *et al.*, 2014; Lawrence *et al.*, 2015). Although a wide range of classification algorithms have been used in pixel-based and object-based

seabed mapping studies (Diesing *et al.*, 2016), Nearest Neighbour is a popular choice, particularly in OBIA studies, due to its simplicity, computational speed and its prevalence in eCognition's training and guidance documentation (Trimble, 2014).

Consisting of just two bands, bathymetry and backscatter, processed acoustic data contains far less information than the multi-spectral or hyperspectral optical data commonly used for terrestrial habitat mapping. However, information beyond depth and hardness can be provided by bathymetric derivatives such as slope, aspect and bathymetric position index and by textural analyses such as grey level co-occurrence matrix (Haralick, 1979) or standard deviation of bathymetry as a measure of structural complexity. This creates a potentially vast array of variables for use in seabed mapping, which presents a challenge because the inclusion of irrelevant features can increase processing time and decrease predictive performance (Stephens and Diesing, 2014). However, previous studies give insight into variables which have proven useful for separating seabed types from acoustic data, and methods have been developed to aid feature selection, such as eCognition's Feature Space Optimisation tool (Lucieer, 2008; Lucieer and Lamarche, 2011). This tool finds the combination of features that provides the largest average separation distance between classes; it does this by taking each training object of class A and finding the training object of class B with the smallest Euclidean distance to it for a given feature, then averaging these minimum Euclidean distances for all the class A and B objects and repeating this process for every class and every feature (Weise, 2014).

The aim of this study is to evaluate the application of OBIA to acoustic data for large scale habitat mapping in a relatively environmentally homogeneous area of the North Sea. Specific objectives are (1) to develop and evaluate an OBIA workflow for interpreting bathymetry and backscatter data and derivatives to produce broadscale habitat maps, (2) to evaluate the accuracy and consistency of a Nearest Neighbour classifier for predicting the distribution of biological communities on circalittoral rock and (3) to compare maps based on an existing standard habitat classification system with maps based on a site-specific classification system derived from cluster analysis of ground truth data.

2.2 Methodology

2.2.1 Study site

The Marine and Coastal Access Act 2009 enabled the designation of a network of Marine Conservation Zones (MCZs) in the territorial waters adjacent to England and Wales and UK offshore waters. Coquet to St Mary's rMCZ was one of 127 sites recommended for designation following a stakeholder-led site selection process (Net Gain, 2011; JNCC and Natural England, 2012) and prioritised for further evidence collection following a review and gap analysis (Defra, 2012). The data used in this chapter were collected between January and September 2014 as part of a dedicated survey programme initiated by Defra and coordinated by Cefas to collect and interpret new data at selected rMCZ sites. Coquet to St Mary's rMCZ was designated as an MCZ in January 2016. It is located in the northern North Sea on the Northumberland coast (Figure 2.1).

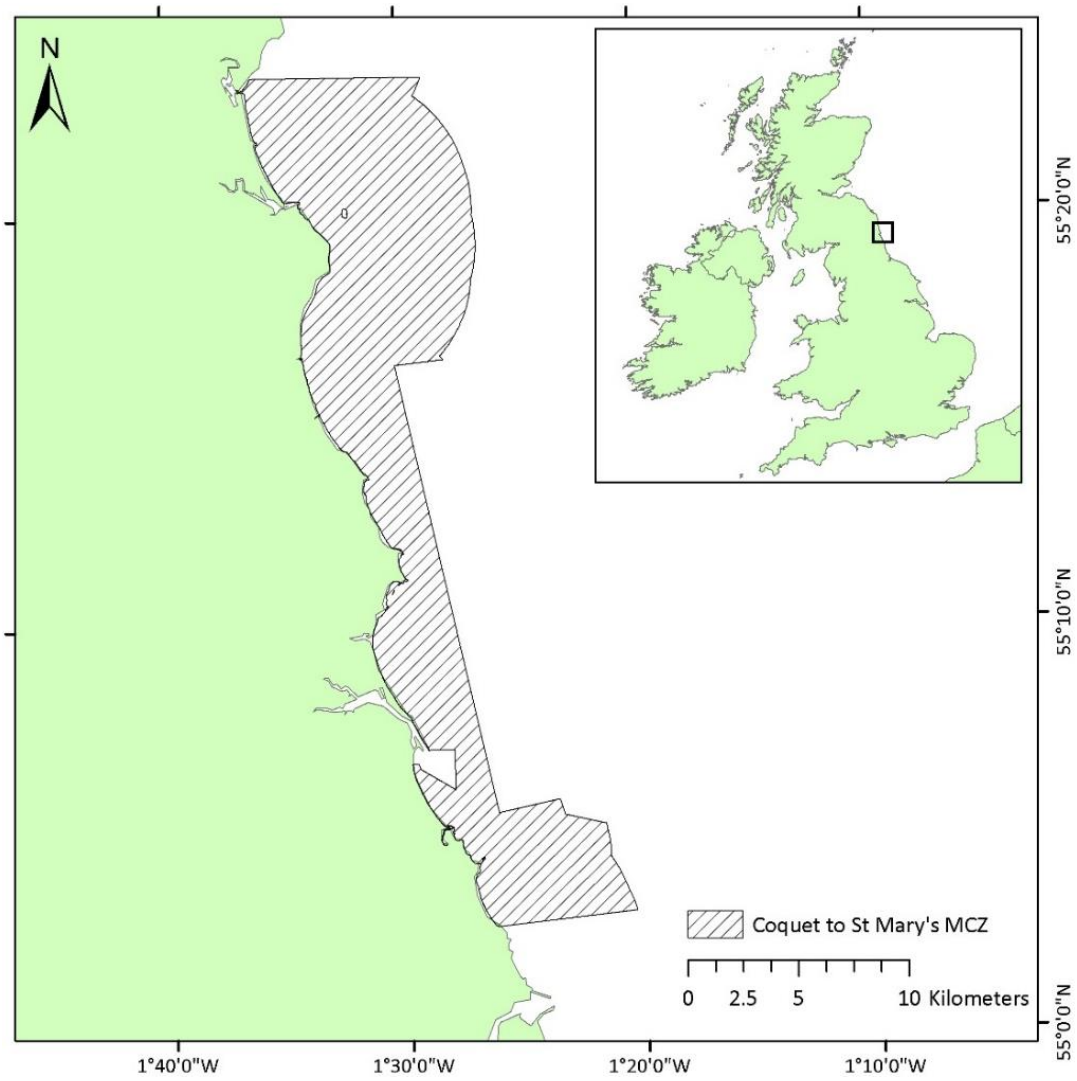

Figure 2.1: Location of Coquet to St. Mary's MCZ on the Northumberland coast

The inshore boundary extends from Whitley Bay in the south to Alnmouth in the north and includes both St Mary's Island and Coquet Island. The site covers an area of 198.75km^2, extending between 1.8km to 7.4km seawards from the mean high water springs mark, reaching a maximum depth of around 50 metres below Chart Datum. The original proposed MCZ boundary was amended prior to designation for practical reasons. The seaward boundary of the middle section was straightened and the areas around Blyth disposal site and the entrance to Blyth harbour were excluded. Figure 2.1 shows the final amended boundary, but all other maps in this chapter show the original proposed boundary, as this was the boundary used to inform data collection and analysis. Features designated for protection within Coquet to St Mary's MCZ include ten broadscale habitats, comprising four intertidal and six subtidal habitats.

2.2.2 Data

Acoustic data were acquired by the Environment Agency between January and March 2014 from the survey vessel CSV *Humber Guardian* using a side mounted Reson Seabat 7101 multibeam echosounder (MBES) system. This was used in conjunction with the Hypack Hysweep multibeam echosounder data collection and editing software module. An Ohmex Sonarmite v3 single beam echosounder and a Leica Viva GS10 GNSS receiver were used to collect ground truth single beam data at a number of indicative sites across the survey area to provide a quality control check of the MBES elevation data. CARIS HIPS/SIPS v.8.1.9 software was used to mosaic the backscatter and bathymetry data to produce 1 metre resolution geotiff files (Figure 2.2).

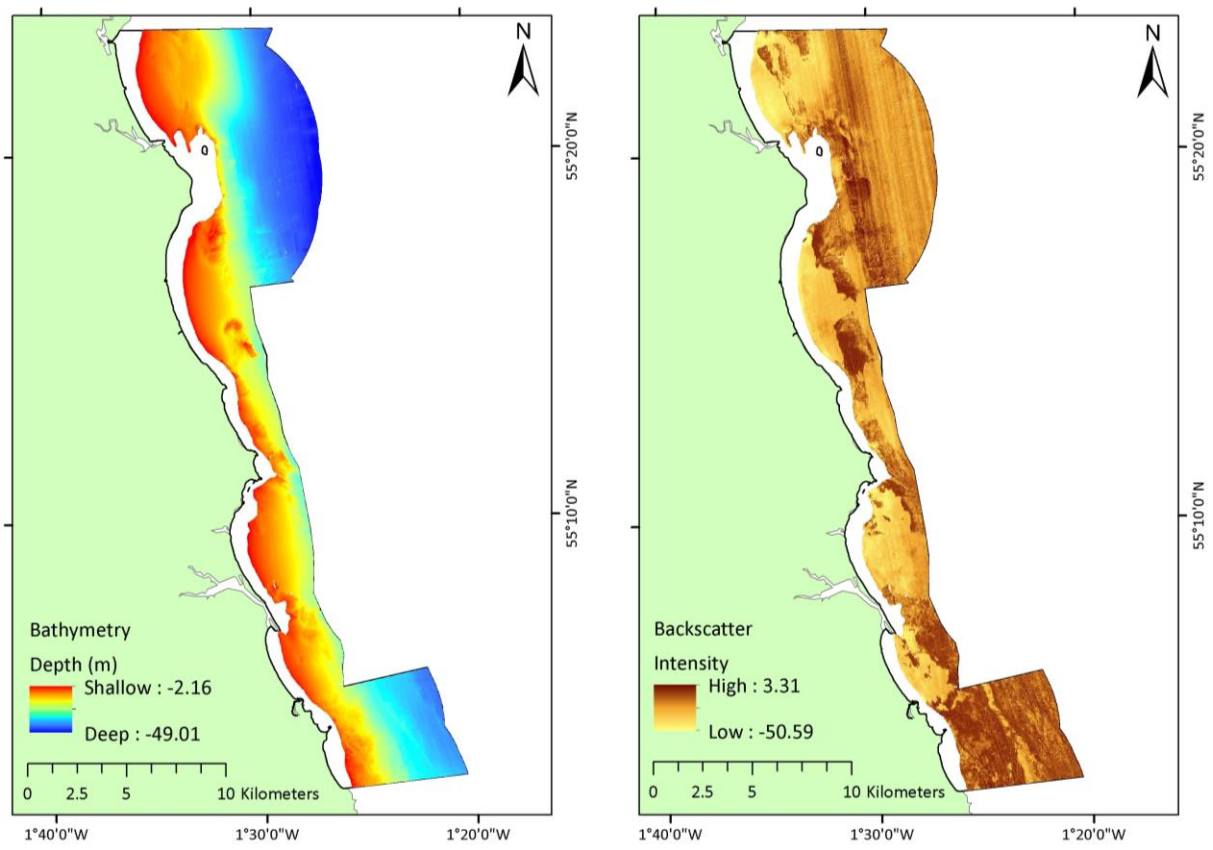

Figure 2.2: Mosaicked bathymetry and backscatter data collected between January and March 2014 in Coquet to St Mary's rMCZ

Bathymetric Position Index (BPI) derivatives were calculated from the bathymetric data using the Benthic Terrain Modeller add-in for ArcGIS. BPI indicates a pixel's elevation relative to its neighbouring pixels within a user-defined radius, aiding the identification of benthic features such as ridges and gullies (Verfaillie *et al.*, 2007). BPI layers were created using 10, 25, 50 and 100 pixel search radii. Visual interpretation in ArcGIS showed that the 50 and 100 search radii were the most appropriate for identifying features in the bathymetric data, so the BPI10 and BPI25 derivatives were not used in further analysis. A slope derivative was produced from the bathymetric data by calculating the maximum change in elevation between each pixel and its 8 neighbours to assign each pixel a value for slope in degrees.

Artefacts are present in the acoustic data due to the prevailing conditions and vessel motion. Gross artefacts were manually adjusted using the brightness and contrast adjustments in Caris HIPS/SIPS, but many could not be edited out. The Environment Agency, who collected and processed the acoustic data, state that areas of different bed type are visibly identifiable despite the artefacts, but that automated image analysis would be challenging due to the steps in the colour map/intensity (Environment Agency, 2014). Such artefacts have been shown to affect the accuracy of seabed maps produced by pixel-based approaches (Lecours

et al., 2017) but present specific challenges with an OBIA approach because artefacts cover areas larger than a single pixel and can thus affect segmentation, with affected pixels being grouped together into objects (Diesing, M. 2015, pers. comm. 7th January). Artefacts are particularly visible on homogeneous seabed, i.e. level areas of sediment, and in deeper water where the swath width is larger, such as the north east area of the study site (Figure 2.2). Artefacts present in the bathymetry data are intensified in the derived slope layer (Figure 2.3).

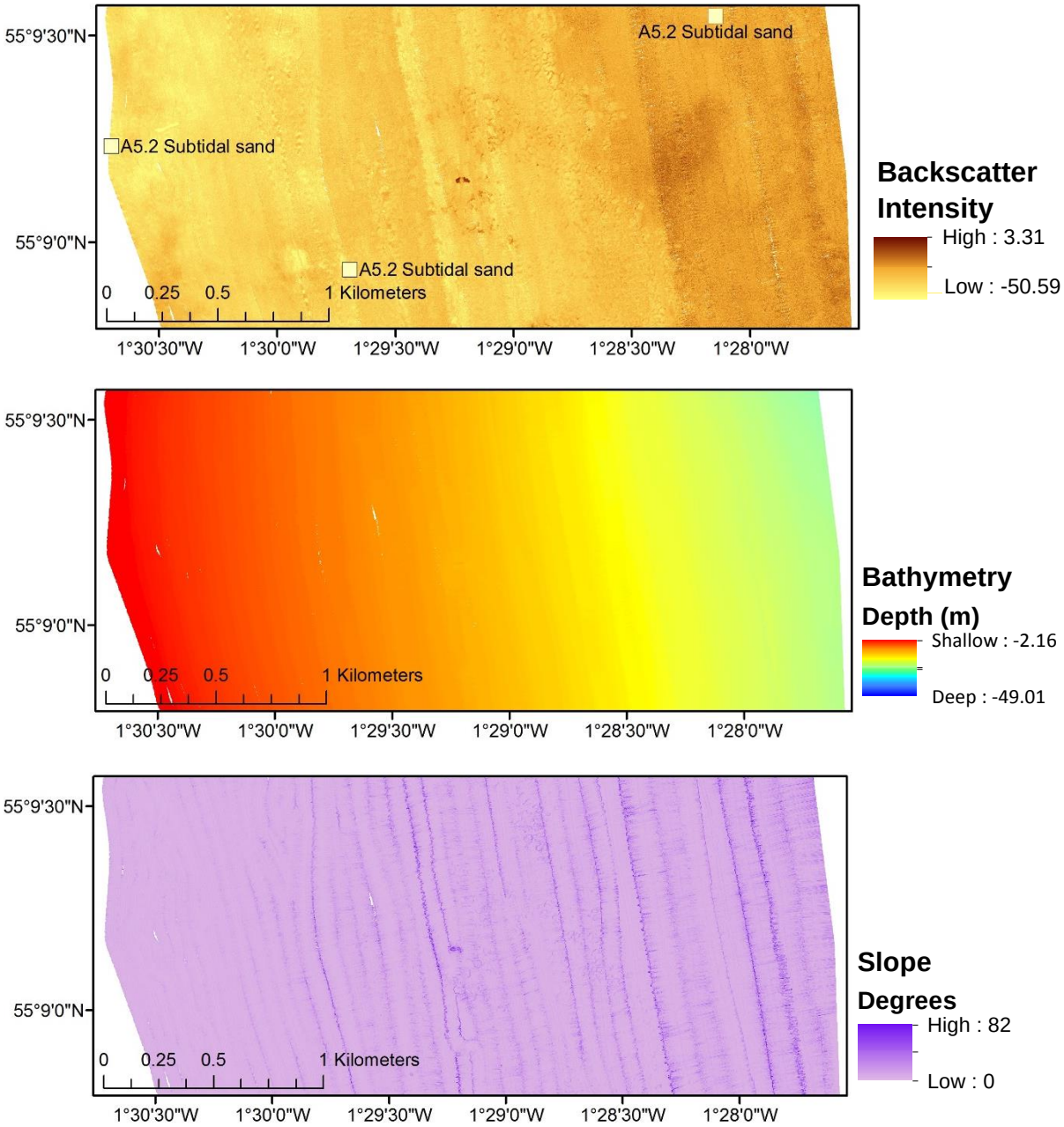

Figure 2.3: Backscatter, bathymetry and slope layers for an area of sediment seabed north of Blyth. The location of ground truth grab sampling points are overlain on the backscatter data.

Ground truth data were acquired by the Environment Agency between July and September 2014 from the survey vessel CSV *Humber Guardian*. Ninety-five ground truth sampling

stations were selected (Figure 2.4), stratified by substratum and depth based on interpreted MBES bathymetry and backscatter data and UKHO Admiralty charts to give the best possible representation of broadscale habitats within the study site.

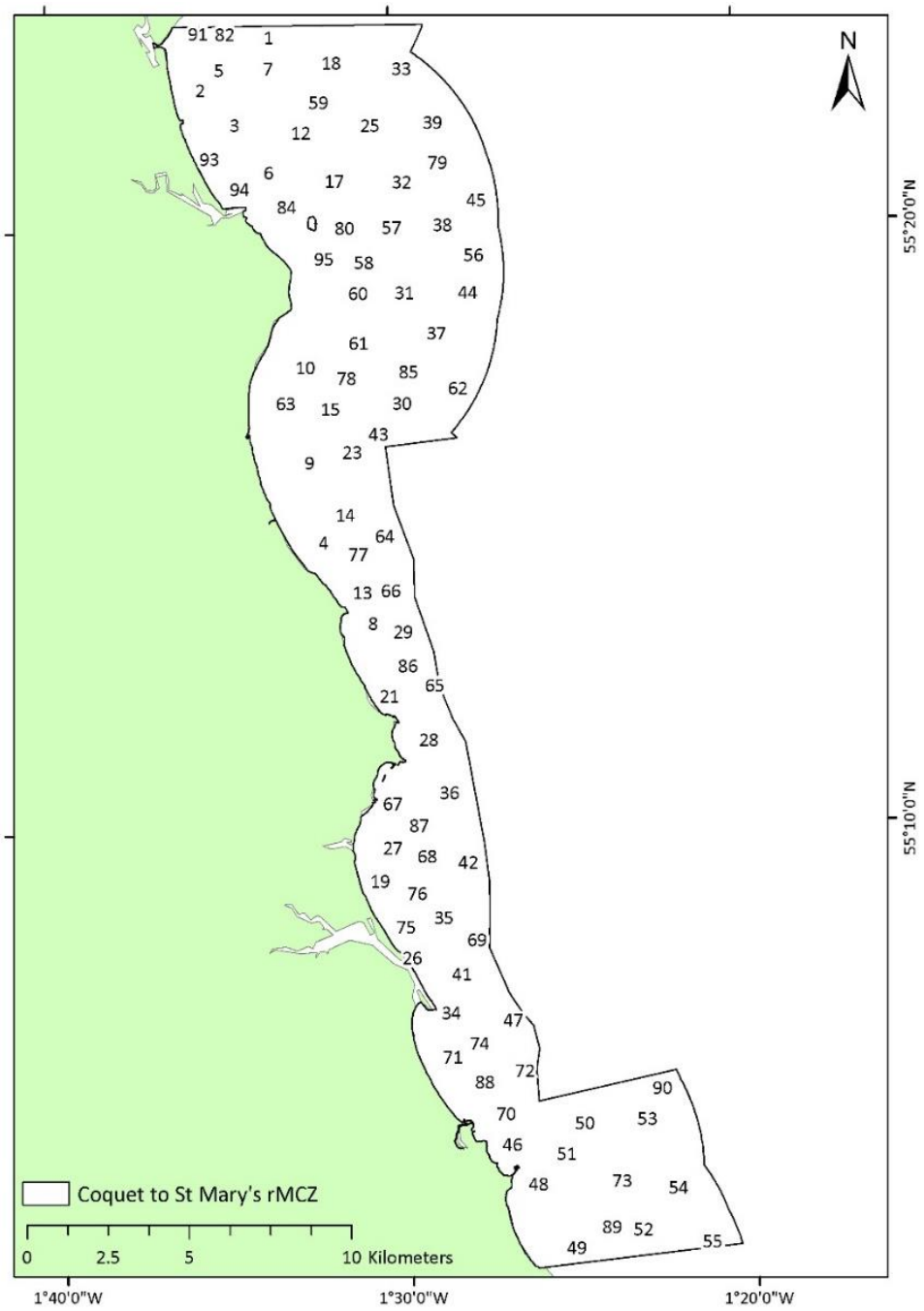

Figure 2.4: Location of 95 sampling stations used for the collection of ground truth data through video and grab sampling between July and September 2014 in Coquet to St Mary's rMCZ

Video and still images of the seabed were captured using an SES SeaSpyder drop camera system in accordance with the MESH recommended operating guidelines for underwater video and photographic imaging techniques (Coggan *et al.*, 2007). Images of the seabed were captured approximately every 10 to 15 metres, with extra photographs being taken in

heterogeneous areas. Of the 95 sampling stations, 50 were selected for grab sampling based on observation of suitable sediment in the images, and a mini-Hamon grab was deployed to collect sediment and infauna. Samples were analysed using Particle Size Analysis (PSA).

2.2.3 Derivation of habitat classes from ground truth data

Broadscale habitat classes were assigned to each of the 50 grab samples and the 2,238 still images using the European Nature Information System (EUNIS, 2012). 'A4.2 Moderate energy circalittoral rock', 'A5.2 Subtidal sand' and 'A5.3 Subtidal mud' are the predominant broadscale habitats identified from the combined data, while 'A5.1 Subtidal coarse sediment' and 'A5.4 Subtidal mixed sediments' constitute a far smaller proportion of samples (Table 2.1).

Table 2.1: Broadscale habitats identified from ground truth data collected in Coquet to St Mary's rMCZ in 2014 (n=2,288)

Broadscale Habitat	Number of grab samples	Number of still images	Total number of ground truth samples
A4.2: Moderate energy circalittoral rock	0	905	905
A5.1: Subtidal coarse sediment	0	15	15
A5.2: Subtidal sand	26	770	796
A5.3: Subtidal mud	19	506	525
A5.4: Subtidal mixed sediments	5	42	47

The 95 sampling station transects range in length from 66m to 498m with a mean length of 187 m. The ground truth data indicates the presence of just 1 broadscale habitat at 53 stations, 2 broadscale habitats at 21 stations, 3 broadscale habitats at 20 stations and 4 broadscale habitats at 1 station (Table 2.2).

Table 2.2: Summary of broadscale habitats assigned to ground truth data collected at the sampling stations in Coquet to St Mary's rMCZ (DC = drop camera, HG = Hamon Grab) (n=95)

Station numbers	A4.2 Moderate energy circalittoral rock	A5.1 Subtidal coarse sediment	A5.2 Subtidal sand	A5.3 Subtidal mud	A5.4 Subtidal mixed sediments
01, 10, 11, 14, 15, 21, 23, 28, 48, 51, 55, 77, 95	DC				
04, 07, 09, 20, 63, 65, 86, 91			DC		
02, 03, 12, 19, 34, 35, 42, 45, 59, 61, 68, 69, 70, 75, 76, 83, 92, 93			DC & HG		
29, 66				DC	
25, 31, 32, 33, 37, 38, 39, 43, 44, 52, 56, 57				DC & HG	
22, 47	DC	DC			
05, 26, 36, 46, 67, 78, 82	DC		DC		
27, 71, 87, 88	DC		DC & HG		
06, 16, 40, 79			DC	HG	
18, 94			HG	DC	
13	DC				DC
24			DC		HG
08	DC	DC	DC		
41, 74	DC	DC	DC & HG		
81	DC		DC	DC & HG	
17, 30, 49, 53, 60, 64, 72, 80, 84, 89, 90	DC		DC		DC
50, 54, 73, 85	DC		DC		DC & HG
58	DC			DC & HG	DC
62	DC		DC	DC & HG	DC

Table 2.2 shows that rock and sediment habitats co-occur along the same transect at 35 out of 95 sampling stations. Images collected by drop camera at several sampling stations show a fine-scale mosaic of sediment and rock supporting sessile fauna including *Alcyonium digitatum*, *Flustra foliacea* and *Urticina* spp. (Figure 2.5).

Figure 2.5: Seabed photographs collected by drop camera showing sediment overlying functional reef supporting sessile fauna. Clockwise from top left: station 53 (image width 0.6m), station 50 (image width 0.8m), station 54 (image width 1m) and station 85 (image width 0.7m).

A total of 886 still images from 45 stations were classified as moderate energy circalittoral rock. These images were classified on the basis of their biological community using the Marine Habitat Classification for Britain and Ireland v04.05 (Connor *et al.*, 2004). Of all the images collected, 14% contained insufficient information to be classified according to biological community and were assigned to the biotope complex 'moderate energy circalittoral rock'. A further 49% of images were classified as the biotope 'faunal and algal crusts', and 36% as sub-biotopes of 'faunal and algal crusts' (Table 2.3).

Table 2.3: Circalittoral rock biotopes and biotope complexes identified from ground truth data collected in Coquet to St Mary's rMCZ (n = 886)

Biotope or biotope complex	**Number of images**	**Number of stations**
CR.MCR Moderate energy circalittoral rock	120	36
CR.MCR.EcCr.FaAlCr Faunal and algal crusts on exposed to moderately wave-exposed circalittoral rock	438	37
CR.MCR.EcCr.FaAlCr.Adig *Alcyonium digitatum*, *Spirobranchus triqueter*, algal and bryozoan crusts on wave-exposed circalittoral rock	182	33
CR.MCR.EcCr.FaAlCr.Flu *Flustra foliacea* on slightly scoured silty circalittoral rock	69	17
CR.MCR.EcCr.FaAlCr.Pom Faunal and algal crusts with Pomatoceros triqueter and sparse *Alcyonium digitatum* on exposed to moderately wave-exposed circalittoral rock	66	11
CR.MCR.EcCr.FaAlCr.Bri Brittlestars on faunal and algal encrusted exposed to moderately wave-exposed circalittoral rock	3	2
CR.MCR.CSab.Sspi *Sabellaria spinulosa* encrusted circalittoral rock	8	2

The ground truth data indicates the presence of just 1 biotope/biotope complex at 4 stations, 2 biotopes/biotope complexes at 12 stations, 3 biotopes/biotope complexes at 15 stations, 4 biotopes/biotope complexes at 13 stations and 5 biotopes/biotope complexes at 1 station (Table 2.4).

Table 2.4: Summary of biotopes and biotope complexes assigned to ground truth data collected at sampling stations on circalittoral rock in Coquet to St Mary's rMCZ (DC = drop camera) (n = 45)

Station numbers	FaAlCr.Adig	FaAlCr.Bri	CR.MCR	FaAlCr	FaAlCr.Flu	FaAlCr.Pom	CSab.Sspi
26, 55			DC				
21, 84				DC			
73, 90	DC		DC				
15, 23, 85, 87	DC			DC			
54	DC				DC		
49, 82				DC		DC	
05, 08, 74			DC	DC			
14, 22, 50, 53, 58, 77, 89	DC		DC	DC			
13, 51	DC			DC	DC		
41	DC		DC		DC		
47	DC		DC			DC	
67, 81			DC	DC	DC		
71			DC	DC		DC	
10				DC	DC	DC	
30	DC	DC	DC	DC			
01, 28, 36, 73, 80, 88	DC		DC	DC	DC		
17, 60	DC		DC	DC			DC
48, 78	DC		DC	DC		DC	
64	DC			DC	DC	DC	
46	DC		DC		DC	DC	
11	DC		DC	DC	DC	DC	

The abundance of taxa identified in the 886 images classified as circalittoral rock was recorded using the semi-quantitative SACFOR scale (Connor *et al.*, 2004). The SACFOR scale provides a unified system for deriving standard abundance values from species density or percentage cover, taking account of organism/colony size and growth form. Sixty-five taxa or morphological groups were identified, of which 12 occur in over 10% of the images (Table 2.5).

Table 2.5: Taxa and morphological groups which occur in >10% of seabed images classified as circalittoral rock in Coquet to St Mary's rMCZ (n = 886)

Taxon	Total	Superabundant	Abundant	Common	Frequent	Occasional	Rare
Spirobranchus sp.	562	0	1	8	39	57	457
Hydroid turf	554	1	23	58	133	251	88
Alcyonium digitatum	536	32	134	155	101	72	42
Asterias rubens	442	1	2	43	312	83	1
Algal crusts	329	0	1	0	14	85	229
Faunal crusts	307	0	0	0	4	27	276
Thuiaria thuja	211	0	1	1	27	113	69
Echinus esculentus	183	0	6	172	5	0	0
Ophiuroidea	161	0	16	30	85	30	0
Ophiura albida	104	0	2	15	40	45	2
Urticina sp.	100	0	0	3	93	3	1
Flustra foliacea	96	19	28	25	9	10	5
Galatheoidea	86	0	0	2	45	37	2

SACFOR values were converted to numeric values S=6, A=5, C=4, F=3, O=2 and R=1. This process balances the weighting of common and rare species in the dataset, eliminating the need for further transformation of the data prior to multivariate analysis. One sample from station 49 was removed from the dataset because it contained no taxonomic data. Hierarchical cluster analysis of the remaining 885 samples based on a Bray-Curtis similarity matrix was performed using PRIMER v.7 (Clarke *et al.*, 2014). The resulting cluster dendrogram and non-metric MDS plot comprised 31 groups. ANOSIM and SIMPER analyses were performed in PRIMER v.7 to quantify the statistical similarity within and between these groups. Pairs of statistically similar groups were combined, with ANOSIM and SIMPER analyses performed after each combination to identify the next pair for combination, until the dataset had been divided into 7 groups (Table 2.6).

Table 2.6: Groups produced by hierarchical cluster analysis of species abundance data from seabed images in Coquet to St Mary's rMCZ (n = 885)

Group name	No. of samples	Average similarity	Characterising taxa					
Algal crusts and keelworms (ACKW)	38	28.93	Species	Av.Abund	Av.Sim	Sim/SD	Contrib%	Cum.%
			Spirobranchus	1.26	17.45	1.10	60.32	60.32
			Corallinaceae (crusts)	0.76	5.33	0.54	18.40	78.73
Hydroid turf and keelworms (HTKW)	87	40.80	Species	Av.Abund	Av.Sim	Sim/SD	Contrib%	Cum.%
			Hydrozoa	2.09	24.91	1.78	61.04	61.04
			Spirobranchus	0.80	7.88	0.83	19.32	80.36
Hydroid turf, squat lobsters and urchins (HTLU)	17	34.03	Species	Av.Abund	Av.Sim	Sim/SD	Contrib%	Cum.%
			Galatheoidea	2.24	12.27	1.04	36.07	36.07
			Hydrozoa	2.00	9.30	1.03	27.34	63.41
			Echinus esculentus	1.41	3.20	0.35	9.39	72.80
Flustra foliacea and *Alcyonium digitatum* (FFAD)	78	51.01	Species	Av.Abund	Av.Sim	Sim/SD	Contrib%	Cum.%
			Flustra foliacea	4.54	32.97	2.09	64.64	64.64
			Alcyonium digitatum	2.18	6.87	0.63	13.48	78.11
Hydroid turf and *Alcyonium digitatum* (HTAD)	26	41.75	Species	Av.Abund	Av.Sim	Sim/SD	Contrib%	Cum.%
			Hydrozoa	2.00	12.57	1.71	30.10	30.10
			Alcyonium digitatum	2.62	11.89	1.24	28.48	58.58
			Caridea	2.15	10.89	1.25	26.07	84.66
Alcyonium digitatum and hydroid turf (ADHT)	340	46.68	Species	Av.Abund	Av.Sim	Sim/SD	Contrib%	Cum.%
			Alcyonium digitatum	3.91	28.51	2.18	61.06	61.06
			Hydrozoa	1.56	6.33	0.76	13.57	74.63
Starfish, urchins and keelworms (SUKW)	299	44.18	Species	Av.Abund	Av.Sim	Sim/SD	Contrib%	Cum.%
			Asterias rubens	2.45	16.47	1.29	37.28	37.28
			Echinus esculentus	2.14	8.24	0.61	18.65	55.93
			Spirobranchus	1.22	6.84	1.13	15.49	71.42

2.2.4 OBIA workflow

Broadscale habitat mapping

Segmentation of the image composed of the bathymetry and backscatter layers was carried out using the multi-resolution segmentation algorithm in eCognition Developer v9.0.3 (Trimble, 2014). This algorithm enables users to influence the size of objects by defining a scale parameter which determines the maximum allowable heterogeneity within an object; the larger the scale parameter, the larger the objects. The scale parameter operates in combination with weighting criteria defined by the user to determine the degree to which segmentation is influenced by homogeneity of shape versus colour, and by object compactness versus smoothness. In this study, a scale parameter of 23 was used in combination with homogeneity criteria which weighted shape (0.1) versus colour (0.9), and object compactness (0.9) versus smoothness (0.1). These segmentation settings were selected by starting from scale parameter 80 and trialling progressively smaller scales with different combinations of shape and compactness criteria, evaluating each output by visual

comparison with the bathymetry and backscatter data. The Estimation of Scale Parameters (ESP) tool (Dragut *et al.*, 2010) had been applied to the data in an attempt to find the optimum segmentation scale through an automated iterative process, but visual evaluation of the outputs showed poor delineation of features that were clearly detectable in the imagery, for example many objects contained a mixture of hard and soft seabed types, so the manual iterative process was used as this produced better results. Scale parameter 23 performed best at identifying seabed features such as small (100-200m^2) rock outcrops surrounded by sediment, whilst minimising the erroneous creation of objects from artefacts in the acoustic data. Application of multi-resolution segmentation to the data created 78,875 objects with an average area of 2,061m^2.

The ground truth dataset was divided into two approximately equal sized subsets to create a training dataset and a validation dataset. The division was carried out on the basis of stations rather than individual samples, to avoid sample pseudoreplication caused by spatial autocorrelation of samples taken from the same video tow (Clements *et al.*, 2010). Because PSA data is more reliable than video data as evidence of sediment type, stations at which grab samples were taken were allocated to the training dataset. Three of the 95 sampling stations did not overlap the area covered by the acoustic survey, so the training and validation datasets each consisted of 46 stations, comprising 1,015 samples in the training dataset and 1,208 samples in the validation dataset.

Feature values of objects overlying training samples were compared to find suitable values for separating the habitat classes represented by the ground truth data. Mean backscatter intensity and mean slope were identified as the best features for distinguishing rock from sediment habitats (Figure 2.6).

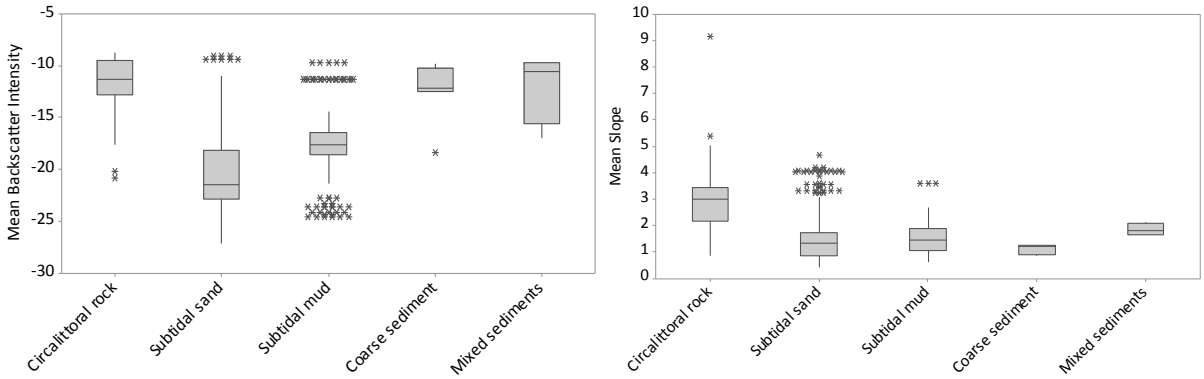

Figure 2.6: Mean backscatter intensity and mean slope values of objects overlying sample points in the training dataset (n = 1,015)

Objects were classified as 'A4.2 Moderate energy circalittoral rock' via a two-stage process using the following threshold parameters of mean slope and mean backscatter intensity:

Stage 1: Mean backscatter ≥ -14.5

or

Mean backscatter ≥ -17 and mean slope ≥ 4.8

Stage 2: Border with object already classified as rock and mean backscatter ≥ -19.58 and mean slope ≥ 3

or

Border with object already classified as rock and mean backscatter ≥ -16.5 and mean slope ≥ 2.02

or

Border with object already classified as rock and mean backscatter ≥ -14.3 and mean slope ≥ 1.85

Stage 2 was repeated for five cycles. The threshold values above were informed by analysis of the values of objects overlying rock sample points (Figure 2.6) and refined through experimental application to the data and visual interpretation of the results.

To classify the remaining objects, unclassified objects overlying ground truth samples identified by PSA as 'A5.2 Subtidal sand' or 'A5.3 Subtidal mud' were defined as training objects. This created 24 training objects for 'A5.2 Subtidal sand' and 15 training objects for 'A5.3 Subtidal mud'. The ground truth survey provided evidence that 'A5.1 Subtidal coarse sediment' and 'A5.4 Subtidal mixed sediments' were present within the study site, but provided insufficient data to predict their distribution reliably (Table 2.1) so these were not included in the training dataset. Figure 2.7 shows the location of the PSA samples that were used to create training objects for mud and sand, the mud samples being predominantly in the deep area in the north east of the study site.

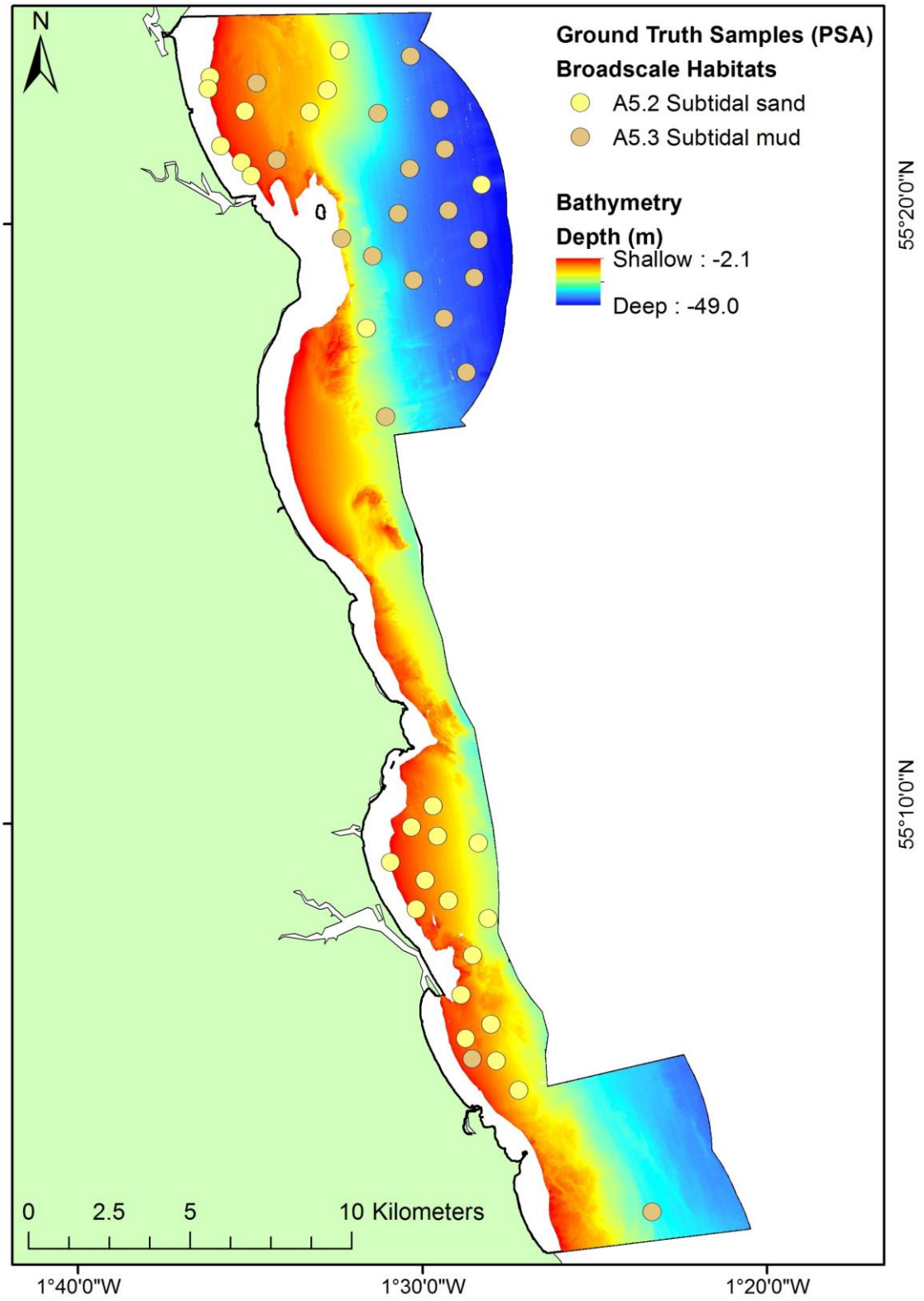

Figure 2.7: Location of PSA samples of mud and sand used to create training objects for object-based image analysis of bathymetry and backscatter data

In order to reduce dimensionality, eCognition's Feature Space Optimisation tool was used to identify the best combination of feature values for distinguishing 'A5.2 Subtidal sand' from 'A5.3 Subtidal mud' in conjunction with a nearest neighbour classifier. By calculating the Euclidean distance between all training objects of both classes for 42 feature values, ten

features were selected that, in combination, produce the largest average minimum separation distance (1.49) between the two substratum classes (Table 2.7). Correlation was expected between some features, notably mean, mode and maximum bathymetry, but the results of Feature Space Optimisation show that reducing dimensionality further would weaken the separation distance between classes, so all ten features were retained and used for classification.

Table 2.7: Features selected for the Nearest Neighbour classification of sediments in Coquet to St. Mary's MCZ through Feature Space Optimisation analysis of training objects (n = 39)

Feature	**Layer**	**Description**
Skewness	Backscatter Bathymetry Slope	The distribution of the layer intensity values of all the pixels in the object. A value of 0 indicates normal distribution. A positive value indicates that the object contains more pixels with a layer intensity value greater than the mean, a negative value indicates that the object contains more pixels with a layer intensity value less than the mean.
Mode	Bathymetry	The most frequently occurring layer intensity value of all the pixels in the object. If more than one value has equal frequency, the minimum value is chosen.
GLCM correlation	Backscatter	The grey level co-occurrence matrix (GLCM) is a measure of object texture, calculated by tabulating the occurrence of neighbouring pixel values as a proportion of all occurrences. A matrix with most co-occurrence values on the diagonal element would indicate a 'smooth' object, in which many neighbouring pixels have equal values. Co-occurrence values a large distance from the diagonal element of the matrix indicate a 'rough' object in which neighbouring pixels have very different layer values. GLCM correlation measures the linear dependency of neighbouring pixel values, a value of 0 indicating no correlation and 1 indicating perfect correlation. (Haralick *et al.*, 1973; Haralick, 1979)
Mean	Bathymetry	The mean layer intensity value of all the pixels in the object
Border contrast	Backscatter	The mean of the difference in pixel values between all the edge pixels in the object and their neighbouring pixels in adjacent objects.
Max	Backscatter Bathymetry	The maximum layer intensity value of all the pixels in the object
GLCM homogeneity	Bathymetry	See above definition of GLCM. GLCM homogeneity measures the homogeneity of the object's texture by measuring the distance of the co-occurrence values from the diagonal element of the matrix. A homogeneity value of 1 indicates a perfectly symmetrical GLCM with all co-occurrence values on the diagonal element.

A supervised classification was carried out to classify unclassified objects as 'A5.2 Subtidal sand' or 'A5.3 Subtidal mud' using eCognition's Standard Nearest Neighbour algorithm and the feature values and training objects described above. A class membership value was produced for each object by comparing its feature values with those of the training objects. A class membership value of 1 indicates that the object's feature values are identical to the training object feature values. The difference between the object's membership value to the assigned class and to the second most similar class is an indication of classification stability; the larger the difference, the more stable the classification (Benz, 2004).

Following the supervised classification, objects with a class membership value of less than 0.1 on all features were left unclassified, resulting in 2,201 unclassified objects. These were predominantly very small objects, of which over 60% consisted of a single pixel, and together they comprised less than 0.7% of the study area. The creation of very small objects with extreme bathymetry and/or backscatter values was caused by artefacts in the acoustic data (Environment Agency, 2014), so to produce a cleaner map these objects were classified as the same habitat class as their surrounding or neighbouring objects. Objects of the same habitat class were then merged, and the results exported as an ESRI shapefile. Finally, objects which had been erroneously classified as circalittoral rock due to artefacts in the acoustic data (Environment Agency, 2014) were reclassified as either sand or mud in accordance with ground truth data using a semi-automated process in ArcGIS v10.2 based on intersection with user-defined polygons. A classification stability assessment based on class membership values was performed after the initial supervised classification.

An error matrix was produced for the final map by comparing the modelled habitat objects with the ground truth samples from the 46 sampling stations that were not used in the training dataset. Cross-validation was not performed because samples had not been allocated randomly to the training and validation datasets due to the decision to use all available PSA samples to train the model.

Biological community mapping

Objects classified as 'A4.2: Moderate energy circalittoral rock' were segmented using the multi-resolution segmentation algorithm in eCognition using a scale parameter of 3 in combination with homogeneity criteria which weighted shape (0.1) versus colour (0.9) and object compactness (0.9) versus smoothness (0.1). Only the backscatter and bathymetry

layers were used in segmentation. Scale parameter 3 was selected by trialling progressively smaller scales from 23 to 1 and comparing the mean size of objects and the presence of conflicting ground truth samples within objects. The minimum size for defining a homogeneous biological community is considered to be 25m^2 (Connor *et al.*, 2004). Scale parameter 3 produces 1,716,821 objects with a mean area of 37m^2, 40% of objects have an area < 25m^2 and 9% of objects overlying ground truth samples contain two or more conflicting samples. Larger scales increase the number of objects containing conflicting ground truth points, smaller scales increase the number of objects with an area less than 25m^2.

The 886 circalittoral rock ground truth samples, classified according to their biological community (Table 2.3 and Table 2.6), were divided to create training and validation datasets using a stratified 4-fold process. The samples assigned to each habitat class were divided randomly into four equal subsets, which were then combined to create a training dataset comprising 75% of the data and a validation dataset comprising 25% of the data. The subsets were rotated to create eight different training and validation datasets, four using the Marine Habitat Classification for Britain and Ireland v04.05 and four using the habitat classes derived from cluster analysis of species abundance data in the ground truth samples. Objects overlying these ground truth sample points were defined as training objects.

eCognition's Feature Space Optimisation tool was used to identify the best combination of ten feature values for distinguishing habitat classes in conjunction with a nearest neighbour classifier. The best combination of features and the best and worst separation values varied according to the training dataset used (Table 2.8).

Table 2.8: Feature values selected to predict the distribution of biological communities on circalittoral rock through Feature Space Optimisation analysis of training objects

	Marine Habitat Classification for Britain and Ireland v04.05				**Classes derived from cluster analysis of ground truth samples**			
	Training dataset:				Training dataset:			
Feature and layer	A (n=508)	B (n=510)	C (n=517)	D (n=520)	A (n=515)	B (n=517)	C (n=515)	D (n=512)
Skewness BPI100	✓	✓	✓	✓	✓	✓	✓	✓
Skewness bathymetry	✓	✓	✓	✓	✓	✓	✓	✓
Skewness BPI50	✓		✓	✓	✓	✓	✓	✓
Skewness backscatter	✓	✓	✓	✓	✓	✓	✓	✓
Skewness slope	✓	✓	✓	✓	✓	✓	✓	✓
StDev BPI100	✓							
StDev slope	✓	✓						
StDev backscatter		✓		✓				
StDev bathymetry				✓	✓	✓		✓
Mean bathymetry			✓					
Mean BPI50			✓					✓
Mean BPI100				✓	✓	✓	✓	
Mode backscatter		✓		✓	✓	✓	✓	✓
Mode bathymetry	✓	✓				✓	✓	✓
Max backscatter	✓		✓					
GLCM correlation backscatter	✓	✓	✓	✓	✓	✓	✓	✓
GLCM entropy bathymetry		✓	✓		✓		✓	
Best separation	5.1	4.8	6.5	7.0	4.5	4.8	5.2	5.5
Worst separation	1.3	1.2	1.3	1.2	1.2	1.2	1.2	1.1

A supervised classification was carried out using eCognition's Standard Nearest Neighbour algorithm and the feature values and training datasets outlined above. Objects with a class membership function < 0.1 were left unclassified. An error matrix was produced for each of the eight output maps by comparing the modelled habitat objects with the ground truth sample points. Classification stability and best classification assessments were performed for all eight maps based on the membership values of each classified object. The consistency of the outputs was evaluated by calculating the proportion of objects which received the same classification in each of the four maps produced by the different training datasets.

2.3 Results

2.3.1 Broadscale habitat map

The spatial extent of each broadscale habitat predicted by the OBIA methods described above is shown in Table 2.9 and the predicted distribution is shown in Figure 2.8. For comparison, the extent of each broadscale habitat predicted for the same area by UKSeaMap 2010 (McBreen, 2011) is also shown in Table 2.9 and the predicted distribution is shown in Figure 2.9.

Table 2.9: Spatial extent and proportion of total MCZ area of broadscale habitats in Coquet to St Mary's MCZ predicted by object-based image analysis of MBES data and by UKSeaMap 2010. Full descriptions for EUNIS codes: A3.1 High energy infralittoral rock, A3.2 Moderate energy infralittoral rock, A4.2 Moderate energy circalittoral rock, A5.1 Subtidal coarse sediment, A5.2 Subtidal sand, A5.3 Subtidal mud and A5.4 Subtidal mixed sediments.

		A3.1	**A3.2**	**A4.2**	**A5.1**	**A5.2**	**A5.3**	**A5.4**
Ground Truth Samples	Number	0	0	905	15	796	525	47
	Proportion	0.00	0.00	0.40	0.01	0.35	0.23	0.02
Spatial extent predicted by OBIA of MBES data	Area (km^2)	0	0	64.2	0.0	54.3	44.4	0.0
	Proportion	0.00	0.00	0.33	0.00	0.28	0.23	0.00
Spatial extent predicted by UKSeaMap 2010	Area (km^2)	73.4	48.3	69.4	1.0	0.1	0.2	2.6
	Proportion	0.37	0.24	0.35	0.01	<0.01	<0.01	0.01

The area of A4.2 Moderate energy circalittoral rock predicted by OBIA is similar to that predicted by UKSeaMap 2010, but the predicted distribution differs greatly. UKSeaMap 2010 predicted circalittoral rock only in the north and south of the MCZ in the deeper waters at the seaward boundary, while OBIA predicted patchy distribution throughout the MCZ, extending to shallower waters at the shoreward extent of the survey area. OBIA did not predict infralittoral rock because neither the acoustic nor the ground truth survey covered the infralittoral. OBIA did not predict coarse or mixed sediments because these were omitted from the model due to insufficient reference data, but the extent of these habitats predicted by UKSeaMap 2010 was extremely small, representing about 1% of the MCZ area each. The greatest difference is in the predicted extent of mud and sand; these two sediment classes combined represent less than 1% of the total MCZ area on UKSeaMap 2010, but over 50% of the total MCZ area on the map created from new survey data using OBIA methods.

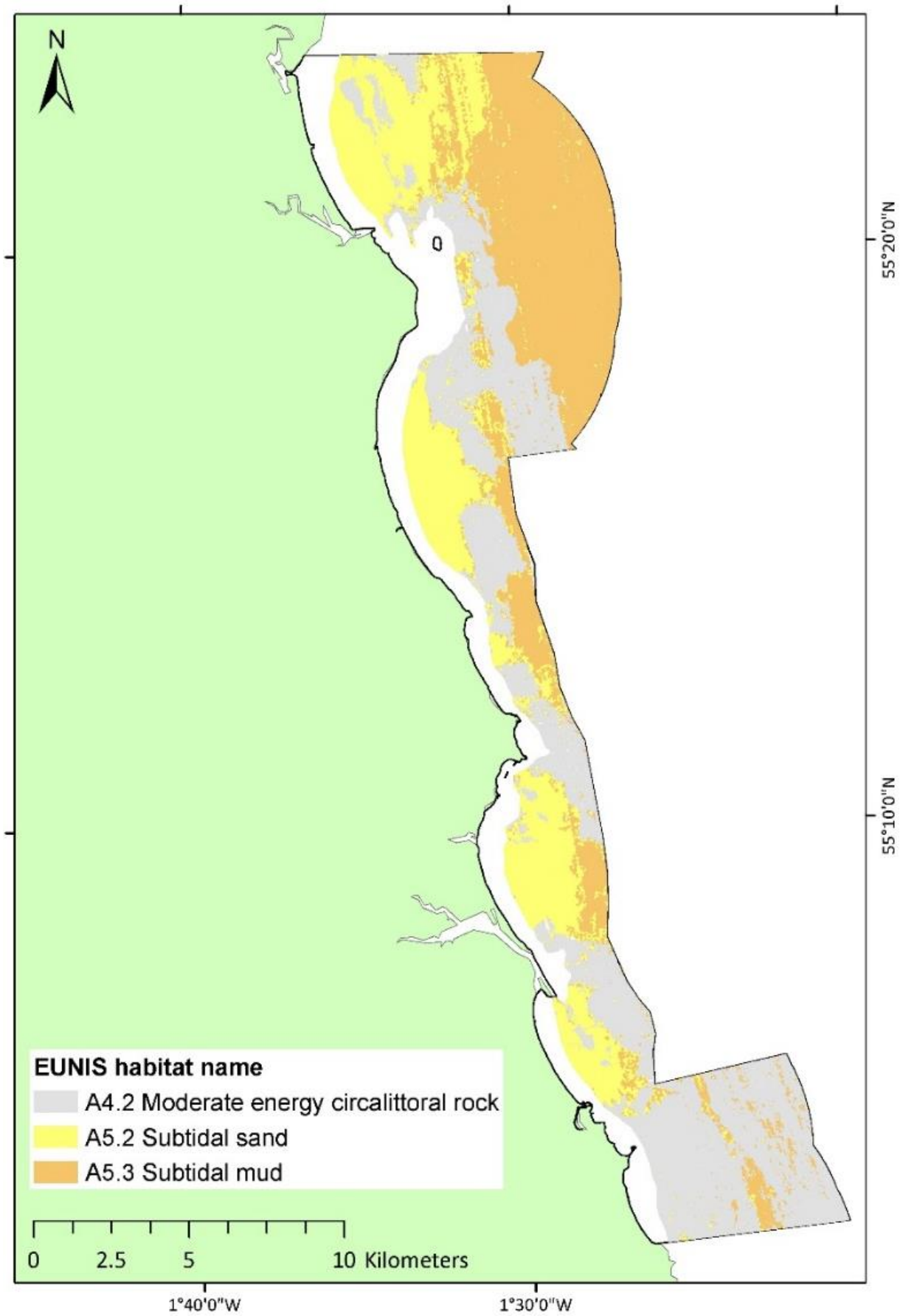

Figure 2.8: Distribution of broadscale habitat maps in Coquet to St. Mary's MCZ predicted by object-based image analysis of MBES data

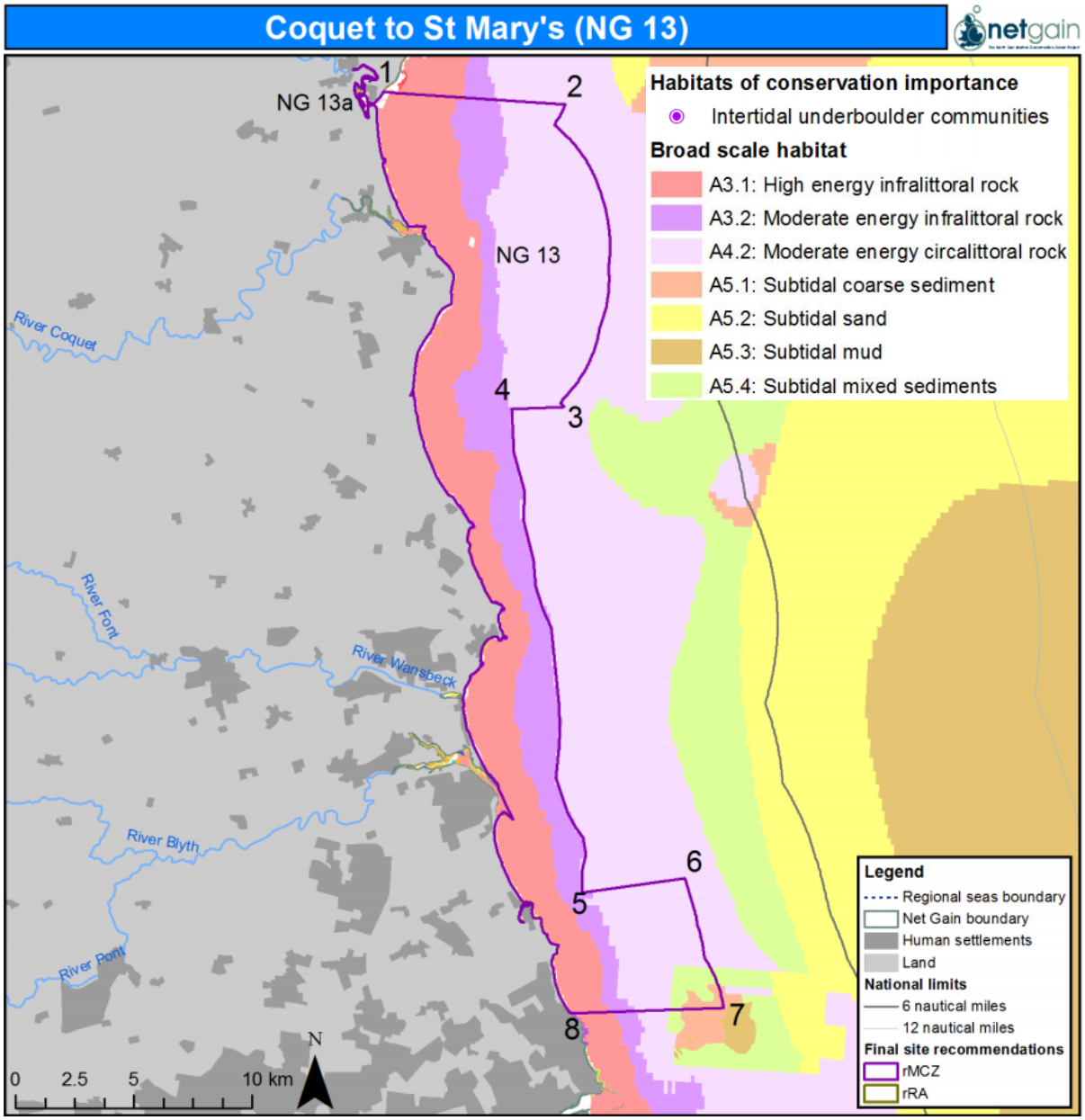

Figure 2.9: Broadscale habitat map of Coquet to St Mary's rMCZ and the surrounding area produced in 2010 by top-down predictive modelling (McBreen, 2011)

Comparison of the predicted habitat objects with the ground truth validation dataset (*n* = 1,208) showed that the broadscale habitat map had an overall accuracy of 80%, kappa coefficient of 0.66 and balanced error rate of 54% (Table 2.10). Both user's and producer's accuracy were higher for rock than for the two sediment classes that were mapped. Producer's accuracy was higher than user's accuracy for rock and mud, showing that this workflow over-predicts those classes and under-predicts sand. Misclassification occurred between the two dominant sediment classes, with 50 sand ground truth samples occurring in areas classified as mud, and 60 mud ground truth samples occurring on areas classified as

sand. The majority of coarse and mixed sediment ground truth samples occurred in areas classified as rock, as did 73 ground truth samples of sand.

Table 2.10: Error matrix for the broadscale habitat map of Coquet to St Mary's MCZ

		OBIA Modelled Habitat Objects					
		Circalittoral Rock	Coarse sediment	Mixed sediments	Mud	Sand	Total
Ground Truth Points	Circalittoral Rock	**655**	0	0	0	6	661
	Coarse sediment	6	**0**	0	0	0	6
	Mixed sediments	40	0	**0**	3	0	43
	Subtidal mud	0	0	0	**128**	50	178
	Subtidal sand	73	0	0	60	**187**	320
	Total	774	0	0	191	243	1208

Overall accuracy	80%				
User accuracy	85%			67%	77%
Producer accuracy	99%	0%	0%	72%	58%
Kappa	0.66				
Balanced Error Rate	54%				

Figure 2.10 compares the range of values of training objects and classified objects for the ten features used in the classification, demonstrating correlation between mean, mode and max bathymetry. The range of values for mud and sand training objects overlapped for every feature value. The only features with minimal or no overlap between the interquartile ranges of the mud and sand training objects were mode, mean and maximum bathymetry and maximum backscatter. Mud training objects had lower bathymetry and higher backscatter values than sand training objects, but as Figure 2.3 shows, backscatter intensity values of homogeneous sediment areas increased with depth as a result of artefacts in the data. The large number of outlier values of both classified and unclassified objects for all 10 features is due to the presence of small objects with extreme values caused by artefacts in the acoustic data as discussed above.

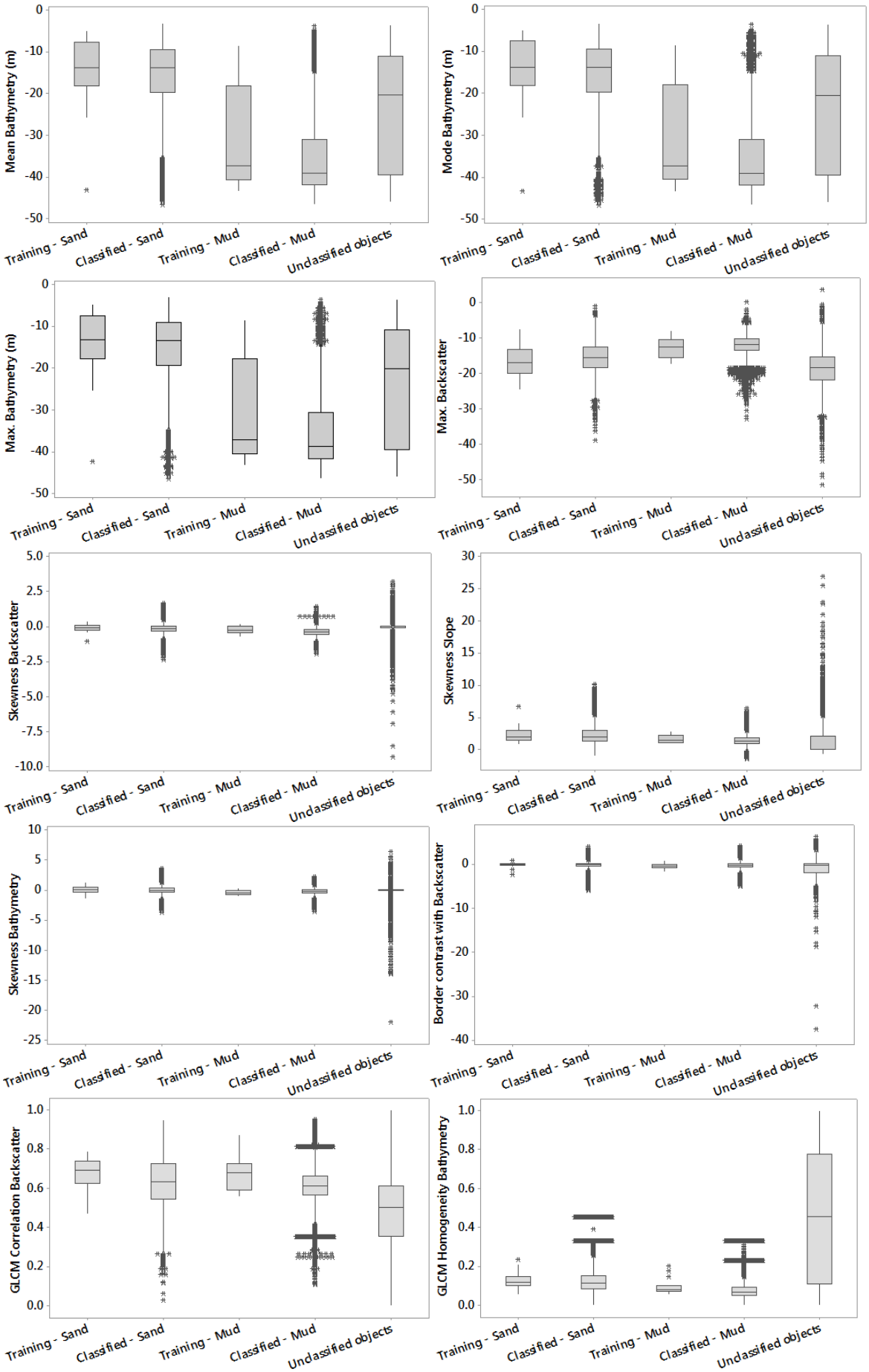

Figure 2.10: Range of values of training objects for sand (n = 24) and mud (n = 15), objects classified as sand (n = 17,975) and mud (n = 18,267) and unclassified objects (n = 2,201) for the 10 features used in SNN classification.

Objects classified as mud had a mean membership value of 0.72 and mean stability value of 0.29, while objects classified as sand had a mean membership value of 0.65 and mean stability value of 0.22 (Table 2.11). This suggests a reasonably stable classification overall, with greater stability in the classification of mud than of sand, but the standard deviation of both classification stability and membership values shows a degree of variability in the data.

Table 2.11: Results of classification stability assessment and best classification result assessment for A5.2 Subtidal sand and A5.3 Subtidal mud

		Classification stability		**Membership value**	
	No. of objects	Mean	Standard deviation	Mean	Standard deviation
A5.2 Subtidal sand	17,975	0.22	0.16	0.65	0.19
A5.3 Subtidal mud	18,267	0.29	0.18	0.72	0.18

2.3.2 Biological community maps

Eight biological community maps were produced by the OBIA methods described above, four using classes defined in the Marine Habitat Classification and four using classes derived from hierarchical cluster analysis of the ground truth data. There was correlation between the predicted area of each habitat and its proportion of the ground truth dataset with both classification systems (Figure 2.11 and Figure 2.12).

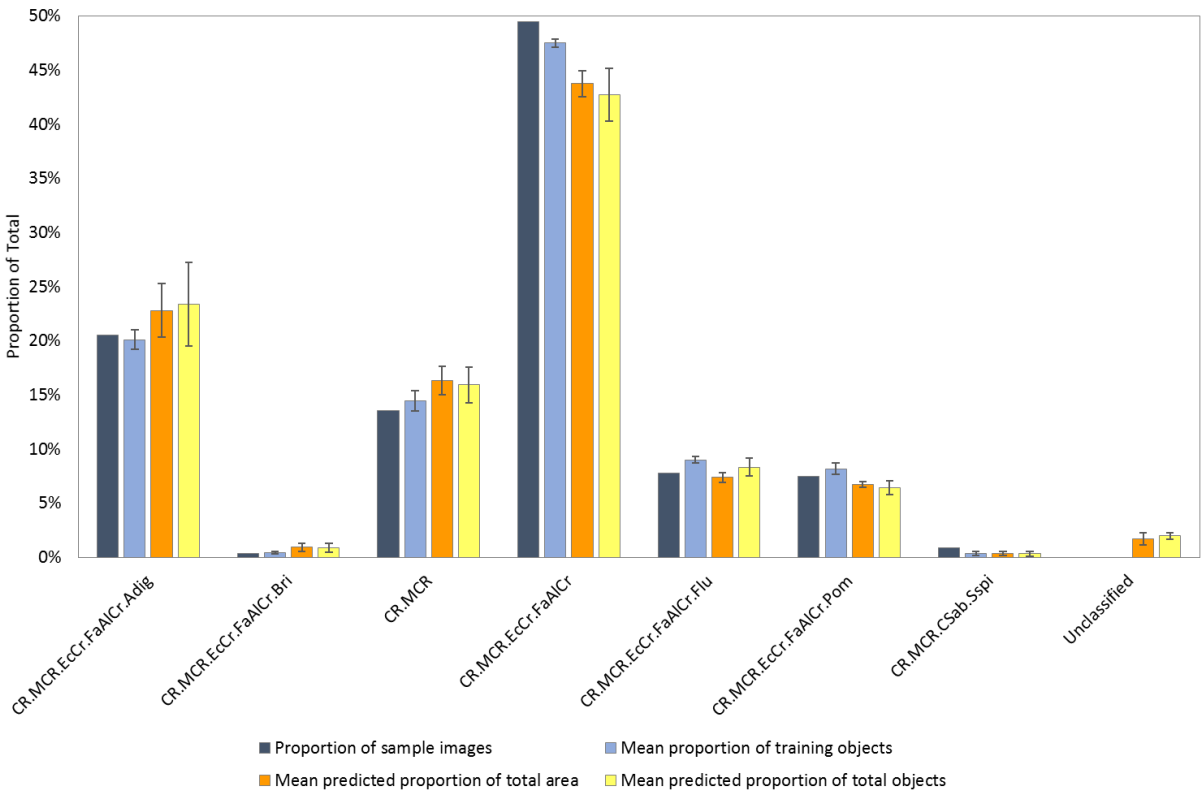

Figure 2.11: Mean proportion of training objects, predicted objects and predicted area represented by each biological community class assigned from the Marine Habitat Classification System v 04.05. Error bars represent standard deviation.

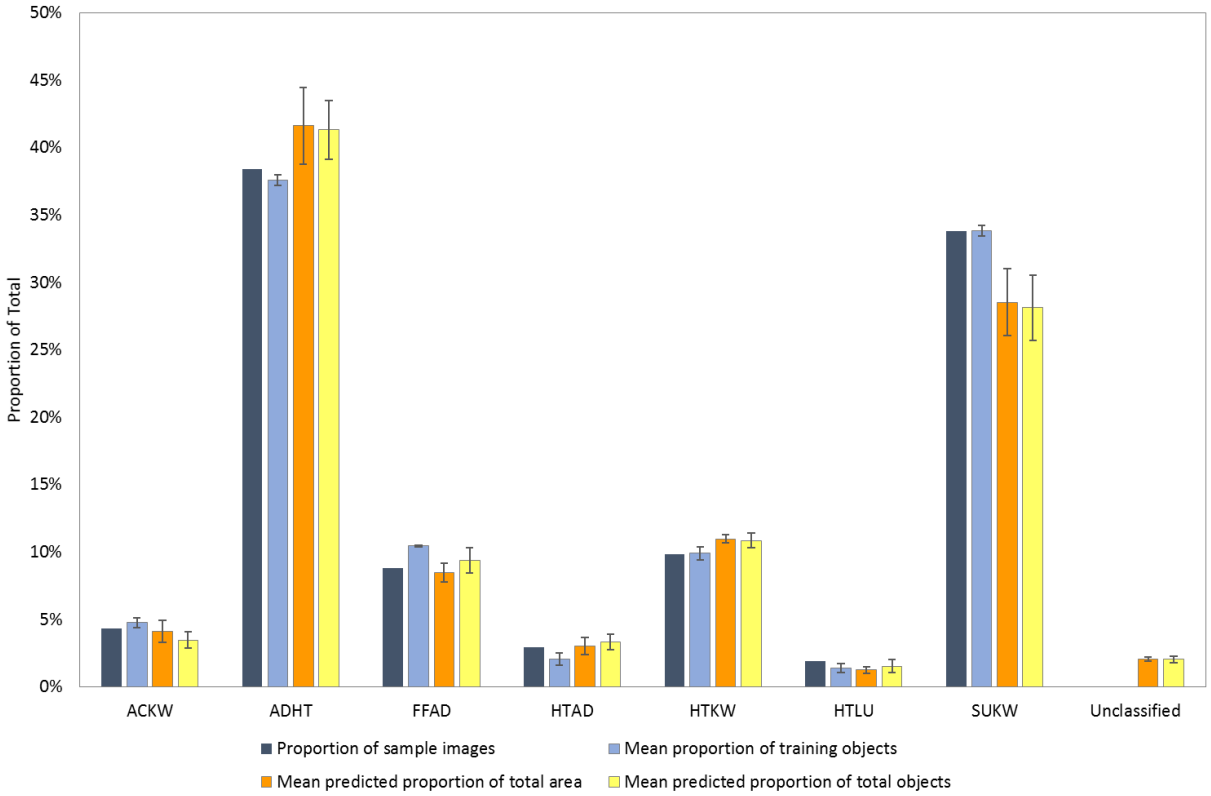

Figure 2.12: Mean proportion of training objects, predicted objects and predicted area represented by each biological community class derived from hierarchical cluster analysis of ground truth data. Error bars represent standard deviation. For explanation of abbreviations of community class names see Table 2.6.

Overall accuracy of the eight predictive biological community maps was very low, ranging from 35% to 46% (Table 2.12 and Table 2.13). Classification system had little effect on overall accuracy; mean overall accuracy of the four maps produced using the Marine Habitat Classification was 43% compared to 40% for the maps using habitat classes derived from ground truth data. User's and producer's accuracy were higher than overall accuracy for the classes which dominated the ground truth dataset and accounted for the majority of predicted map area, namely the Faunal and Algal Crusts biotope (CR.MCR.EcCr.FaAlCr) in the Marine Habitat Classification, and the *Alcyonium digitatum* and hydroid turf (ADHT) and Starfish, urchins and keelworms (SUKW) classes in the site-specific classification.

Table 2.12: Results of 4-fold cross validation of predictive maps produced using the Marine Habitat Classification for Britain and Ireland v 04.03

		Training dataset:			
		A	**B**	**C**	**D**
	Overall accuracy	0.46	0.43	0.42	0.41
	Kappa	0.19	0.16	0.15	0.15
	Balanced Error Rate	0.62	0.70	0.78	0.77
User Accuracy	CR.MCR.EcCr.FaAlCr.Adig	0.35	0.32	0.30	0.30
	CR.MCR.EcCr.FaAlCr.Bri	0.00	0.00	0.00	n/a
	CR.MCR	0.35	0.31	0.19	0.26
	CR.MCR.EcCr.FaAlCr	0.57	0.56	0.60	0.58
	CR.MCR.EcCr.FaAlCr.Flu	0.26	0.25	0.23	0.23
	CR.MCR.EcCr.FaAlCr.Pom	0.30	0.25	0.24	0.22
	CR.MCR.CSab.Sspi	0.33	0.33	0.00	n/a
Producer Accuracy	CR.MCR.EcCr.FaAlCr.Adig	0.23	0.28	0.33	0.33
	CR.MCR.EcCr.FaAlCr.Bri	n/a	0.00	0.00	0.00
	CR.MCR	0.27	0.32	0.17	0.17
	CR.MCR.EcCr.FaAlCr	0.64	0.60	0.59	0.58
	CR.MCR.EcCr.FaAlCr.Flu	0.31	0.24	0.18	0.23
	CR.MCR.EcCr.FaAlCr.Pom	0.35	0.18	0.25	0.22
	CR.MCR.CSab.Sspi	0.50	0.50	0.00	0.00

Table 2.13: Results of 4-fold cross validation of predictive maps produced using habitat classes derived from hierarchical cluster analysis of ground truth data

		Training dataset:			
		A	**B**	**C**	**D**
	Overall accuracy	0.35	0.41	0.39	0.44
	Kappa	0.09	0.18	0.14	0.22
	Balanced Error Rate	0.79	0.74	0.78	0.73
User Accuracy	Algal crusts and keelworms (ACKW)	0.15	0.33	0.00	0.11
	Alcyonium digitatum and hydroid turf (ADHT)	0.46	0.52	0.46	0.57
	Flustra foliacea and *Alcyonium digitatum* (FFAD)	0.06	0.21	0.17	0.33
	Hydroid turf and *Alcyonium digitatum* (HTAD)	0.17	0.20	0.29	0.09
	Hydroid turf and keelworms (HTKW)	0.22	0.14	0.15	0.24
	Hydroid turf, squat lobsters and urchins (HTLU)	0.00	0.00	0.00	0.00
	Starfish, urchins and keelworms (SUKW)	0.39	0.50	0.48	0.48
Producer Accuracy	Algal crusts and keelworms (ACKW)	0.22	0.30	0.00	0.10
	Alcyonium digitatum and hydroid turf (ADHT)	0.42	0.55	0.44	0.59
	Flustra foliacea and *Alcyonium digitatum* (FFAD)	0.05	0.16	0.16	0.35
	Hydroid turf and *Alcyonium digitatum* (HTAD)	0.14	0.17	0.29	0.17
	Hydroid turf and keelworms (HTKW)	0.23	0.18	0.14	0.23
	Hydroid turf, squat lobsters and urchins (HTLU)	0.00	0.00	0.00	0.00
	Starfish, urchins and keelworms (SUKW)	0.42	0.45	0.54	0.44

Four-fold cross validation showed that changing the training dataset with the Standard Nearest Neighbour classifier affected the accuracy (Table 2.12 and Table 2.13) and consistency (Table 2.14) of outputs. Of the maps created using the Marine Habitat Classification, 14% of objects received the same classification in all four maps and a further 37% received the same classification in three maps, compared to 21% and 43% respectively for the maps created using the site-specific classification.

Table 2.14: Consistency of object classification using the Standard Nearest Neighbour method with the Marine Habitat Classification and the site-specific classification system. Total number of objects = 1,716,821.

		Marine Habitat Classification	**Site-Specific Classification**
Proportion of total objects with the same classification in:	4 maps	0.14	0.21
	3 maps	0.37	0.43
	2 maps	0.45	0.34
Proportion with different classification in all 4 maps		0.04	0.02

Mean class membership values were reasonably high, ranging from 0.63 to 0.83 for maps created using the Marine Habitat Classification and from 0.59 to 0.77 for the site-specific classification, but classification stability was extremely low, ranging from 0.05 to 0.09 for the Marine Habitat Classification and from 0.05 to 0.1 for the site specific classification (Table 2.15 and Table 2.16). In both cases, the classes defined by the bryozoan *Flustra foliacea* (CR.MCR.EcCr.FaAlCr.Flu and FFAD) had lower membership values than the other classes.

Table 2.15: Results of classification stability assessment and best classification assessment for biological community maps produced using the Marine Habitat Classification for Britain and Ireland v. 04.05

			Classification Stability		**Membership value**	
Training dataset	Habitat Class	No. of objects	Mean	Standard deviation	Mean	Standard deviation
A	CR.MCR.EcCr.FaAlCr.Adig	381,996	0.08	0.08	0.75	0.19
	CR.MCR.EcCr.FaAlCr.Bri	17,414	0.05	0.05	0.78	0.15
	CR.MCR	287,132	0.06	0.06	0.78	0.16
	CR.MCR.EcCr.FaAlCr	733,754	0.08	0.08	0.74	0.20
	CR.MCR.EcCr.FaAlCr.Flu	159,420	0.08	0.10	0.66	0.22
	CR.MCR.EcCr.FaAlCr.Pom	97,297	0.05	0.05	0.76	0.20
	CR.MCR.CSab.Sspi	5,628	0.06	0.07	0.71	0.20
B	CR.MCR.EcCr.FaAlCr.Adig	417,102	0.08	0.07	0.65	0.18
	CR.MCR.EcCr.FaAlCr.Bri	20,950	0.07	0.06	0.68	0.14
	CR.MCR	267,443	0.07	0.06	0.68	0.17
	CR.MCR.EcCr.FaAlCr	725,424	0.09	0.07	0.66	0.18
	CR.MCR.EcCr.FaAlCr.Flu	124,754	0.07	0.10	0.64	0.19
	CR.MCR.EcCr.FaAlCr.Pom	122,607	0.06	0.05	0.69	0.17
	CR.MCR.CSab.Sspi	10,521	0.06	0.06	0.68	0.15
C	CR.MCR.EcCr.FaAlCr.Adig	482,003	0.08	0.08	0.72	0.18
	CR.MCR.EcCr.FaAlCr.Bri	18,438	0.07	0.06	0.72	0.16
	CR.MCR	237,413	0.06	0.06	0.74	0.17
	CR.MCR.EcCr.FaAlCr	686,461	0.09	0.08	0.70	0.20
	CR.MCR.EcCr.FaAlCr.Flu	144,809	0.08	0.07	0.63	0.21
	CR.MCR.EcCr.FaAlCr.Pom	109,677	0.06	0.07	0.71	0.22
	CR.MCR.CSab.Sspi	4,599	0.04	0.03	0.83	0.09
D	CR.MCR.EcCr.FaAlCr.Adig	323,126	0.06	0.06	0.75	0.20
	CR.MCR.EcCr.FaAlCr.Bri	3,922	0.07	0.08	0.68	0.24
	CR.MCR	302,964	0.06	0.06	0.75	0.17
	CR.MCR.EcCr.FaAlCr	788,637	0.08	0.08	0.72	0.21
	CR.MCR.EcCr.FaAlCr.Flu	144,164	0.08	0.11	0.65	0.23
	CR.MCR.EcCr.FaAlCr.Pom	112,081	0.05	0.05	0.75	0.20
	CR.MCR.CSab.Sspi	1,791	0.05	0.04	0.75	0.14

Table 2.16: Results of classification stability assessment and best classification assessment for biological community maps produced using the site-specific classification

			Classification Stability		**Membership value**	
Training dataset	Habitat Class	No. of objects	Mean	Standard deviation	Mean	Standard deviation
A	ACKW	68,694	0.06	0.07	0.72	0.21
	ADHT	654,079	0.08	0.07	0.74	0.20
	FFAD	171,589	0.09	0.11	0.62	0.22
	HTAD	42,936	0.06	0.06	0.75	0.17
	HTKW	179,703	0.06	0.06	0.76	0.18
	HTLU	20,851	0.05	0.05	0.74	0.19
	SUKW	540,684	0.07	0.07	0.72	0.21
B	ACKW	46,195	0.06	0.06	0.74	0.20
	ADHT	738,084	0.09	0.08	0.76	0.18
	FFAD	159,458	0.08	0.08	0.61	0.23
	HTAD	61,338	0.06	0.06	0.76	0.15
	HTKW	199,973	0.06	0.07	0.74	0.19
	HTLU	33,669	0.06	0.05	0.76	0.14
	SUKW	442,722	0.08	0.07	0.71	0.21
C	ACKW	57,404	0.05	0.05	0.77	0.16
	ADHT	719,242	0.10	0.08	0.71	0.19
	FFAD	174,109	0.08	0.09	0.61	0.23
	HTAD	65,925	0.07	0.06	0.76	0.12
	HTKW	185,965	0.07	0.07	0.71	0.18
	HTLU	16,890	0.05	0.04	0.77	0.13
	SUKW	468,330	0.08	0.08	0.69	0.21
D	ACKW	66,238	0.05	0.06	0.75	0.20
	ADHT	725,920	0.08	0.07	0.76	0.18
	FFAD	138,493	0.08	0.08	0.59	0.24
	HTAD	57,007	0.07	0.07	0.74	0.17
	HTKW	180,172	0.06	0.06	0.77	0.17
	HTLU	32,939	0.06	0.06	0.74	0.16
	SUKW	479,043	0.08	0.07	0.72	0.20

2.4 Discussion

2.4.1 Broadscale habitat mapping

The spatial extent and distribution of broadscale habitats predicted by OBIA methods were considerably different to those predicted by UKSeaMap 2010, which prior to this study represented the most recent full coverage habitat map available for the study area. Expert evaluation and the accuracy metrics derived from comparison with ground truth data both suggest that the map produced by this study provides the more reliable representation of

seabed habitats at the site. This is to be expected, because although UKSeaMap 2010 is considered an improvement on its predecessor UKSeaMap 2006 (Connor *et al.*, 2006) due to refined modelling techniques and higher resolution data from a greater number of sources, top-down predictive modelling from environmental variables cannot produce such reliable, fine scale habitat maps as can be achieved through interpretation of acoustic survey data (McBreen, 2011).

The overall accuracy of the broadscale habitat map compares well with other studies. Previous attempts to map geological substrata from acoustic data using a similar number of classes have produced maps with accuracies ranging from 46%-56% (Calvert *et al.*, 2015), 60-66% (Lucieer *et al.*, 2011), 60-80% (Lucieer, 2008), 63-75% (Lawrence *et al.*, 2015), 67-76% (Diesing *et al.*, 2014), 63.5% (Biondo and Bartholoma, 2017), 72% (Dartnell and Gardner, 2004; Ierodiaconou *et al.*, 2007), 75%-83% (Hasan *et al.*, 2012b) to 83% (Serpetti *et al.*, 2011). Comparison of overall accuracy with UKSeaMap 2010 is not possible as this modelled output was not validated through comparison with ground truth data. UKSeaMap 2010 was evaluated using a modified version of the MESH confidence assessment method (MESH, 2010) in which confidence scores were assigned to each cell of the main input data layers (biological zones, seabed substrata, wave energy and tidal current) and then multiplied to produce an overall confidence map for the whole area.

User's and producer's accuracy for rock were higher than the map's overall accuracy, while user's and producer's accuracy for sand and mud were lower than the map's overall accuracy. Analysis of training object values showed that rock could be separated from sediment fairly reliably using mean backscatter intensity and mean slope. Rock training objects generally had higher values than sediment training objects for both features, although the slight overlap in value ranges necessitated the development of iterative rules with different combinations of the two features. In contrast, there was considerable overlap in training object value ranges for all ten features used to separate mud and sand, with only mean, mode and maximum bathymetry providing any visible separation of classes). Some misclassification of mud as sand, and vice versa, was expected due to this overlap in training object values and the consequently low separation distance of 1.49 between the two classes. Few seabed mapping studies have published training object value ranges, but those that have show similar findings; Stephens and Diesing (2014) and Diesing *et al.* (2014) publish box plots showing considerable overlap between bathymetry and backscatter values

for four sediment classes at two sites in the English North Sea, Lucieer *et al.* (2011) demonstrate overlap in mean backscatter training object values for six reef and sediment classes at a site in Eastern Tasmania, and Calvert *et al.* (2015) show overlap in backscatter values for rock and coarse sediment, and for three classes of muddy sediment based on samples collected in the Irish Sea.

In the present study, mud training objects tended to have higher backscatter intensity and lower bathymetry values than sand training objects, but the higher backscatter intensity is a product of artefacts, whose impact increases with depth. The majority of mud samples were collected in the north east part of the site, which is the area worst affected by artefacts. Using training objects derived from these samples and a feature space which included three correlated bathymetry features, the SNN classifier tended to predict mud in deeper areas and sand in shallower areas. Lucieer and Lamarche (2011) found similar correlation between depth and spatial distribution of classes predicted by OBIA with a SNN classifier, despite their feature space including only one bathymetric feature (mean bathymetry) alongside several features representing seabed hardness and texture. Other acoustic mapping studies have shown correlation between sediment grain size and depth (Freitas *et al.*, 2003; Bellec *et al.*, 2009; Freitas *et al.*, 2011) which can be explained by the influence of depth on wave energy, which in turn affects sediment sorting (George and Hill, 2008). In our study, OBIA of acoustic data produced a reasonably accurate and stable classification, evidenced by the mean membership and classification stability values for mud and sand, but this classification relied heavily on the observed correlation between depth and sediment grade at the study site.

Post-classification enhancements had to be carried out to classify unclassified objects and to correct misclassifications which had occurred due to backscatter artefacts. These consisted of rule-based alterations in eCognition as well as semi-automated manual editing in ArcGIS. Few other studies report applying post-classification enhancements to habitat maps derived from acoustic data (Costa and Battista, 2013; Diesing *et al.*, 2014), but Diesing *et al.* (2016) suggest that such enhancements will be applied more frequently as the science of image-based seabed mapping matures.

2.4.2 Biological community mapping

It was expected that the overall accuracy of the biotope map would be lower than that of the broadscale habitat map, because increasing the number of habitats in a predictive model has been shown to decrease overall prediction accuracy (White *et al.*, 2003; Lucieer, 2008). Other studies have produced biological community maps from acoustic data with accuracy ranging from 62% (Mielck *et al.*, 2014), 68%-72% (Elvenes *et al.*, 2014), 78% (Brown and Collier, 2008), 38%-80% (Ierodiaconou *et al.*, 2011), 83% (Ierodiaconou *et al.*, 2007) 57%-84% (Holmes *et al.*, 2008) 70%-85% (Hasan *et al.*, 2012b) to 70%-87% (Rattray *et al.*, 2009). These studies use a small number of simplified biota classes (e.g. 'seagrass', 'mixed green algae', 'mixed brown algae', 'mixed red algae', 'invertebrates' (Ierodiaconou *et al.*, 2007)), each strongly associated with physical factors such as depth, rugosity and substratum, factors which are detectable from acoustic data and, crucially, exhibit a wide range of values throughout the study area. Only one study has attempted to map complex biological communities defined by a national standard classification; this was successful but used only four classes which were clearly separated by substratum type and depth (Brown and Collier, 2008).

In contrast, the circalittoral rock biotopes and sub-biotopes recorded in the study area are very similar to each other in terms of species composition and environmental preferences. The dominant species, such as *Alcyonium digitatum*, *Flustra foliacea*, *Spirobranchus* sp, *Urticina* spp and *Echinus esculentus* are ubiquitous generalists [www.marlin.ac.uk/biotic], tolerant of the levels of turbidity, siltation and scour that prevail throughout the study area (Brazier *et al.*, 1998). All require hard substratum and some require moderate-strong current, but these factors do not vary within the study area at sufficient levels to limit species distribution. In a North Sea species distribution modelling study, Reiss *et al.* (2011) evaluate several models and find that performance is consistently less accurate for species with a broad ecological niche, which may not be limited by any of the environmental variables at that spatial scale. Other distribution modelling studies have demonstrated correlations between individual species or broad community types and environmental parameters which can be derived from acoustic data, such as seabed depth, hardness and roughness (Kloser *et al.*, 2010; Hill *et al.*, 2014; Rees *et al.*, 2014; Rinne, 2014), but these correlations are fairly simplistic, e.g. depth as a predictor of algal- versus faunal-dominated communities, or rugosity and hardness as predictors of sessile fauna versus infauna.

Correlation with abiotic factors at the biotope level of detail remains elusive; Richmond (2014) found abiotic variables to be poor predictors of biological community distribution, recommending that surveys be carried out to establish relationships between abiotic surrogates and patterns of biodiversity on a site-by-site basis if producing habitat maps to inform marine conservation management. In the present study, the similarity of species communities and homogeneity of environmental parameters in the study area result in low separation distances between classes and consequently low mean classification stability, overall accuracy, user's and producer's accuracy of the predictive maps.

These measures of accuracy and stability did not differ between the maps created using the national standard habitat classification system and those produced using the site-specific classification. Classes derived from cluster analysis did not align exactly with the standard classification, but this is likely due to the different methods of collecting the data that underpin each classification. The empirical data used to develop the standard classification were collected by *in situ* recording of epibiota (Connor *et al.*, 2004) while the data used for cluster analysis in this study consisted only of still images; recording biota from seabed images results in data with low taxonomic resolution and potentially skewed estimates of abundance (Foster-Smith and Sotheran, 2003; Calvert *et al.*, 2015). The classes derived from cluster analysis had fairly low average similarity due to variability in quantitative data derived from individual photographs. Although 65 taxa were identified in the photographs, only 12 occurred in >10% of the samples and consequently dominated the cluster analysis. These are the same taxa that characterise the biotopes in the standard classification, e.g. *Alcyonium digitatum* and *Flustra foliacea*. These taxa have broad environmental niches, as mentioned above, so the dominance of these same taxa in both classification systems explains why neither system provided an advantage in classification accuracy.

The low consistency between maps produced with different subsets of the training data suggests that the SNN model over-fits the model to the training data. Reducing the feature space further and removing correlated variables could help to overcome this, but this was not explored here because Feature Space Optimisation showed that reducing the number of features reduced the separation distance between classes.

In both classifications, user's and producer's accuracy is higher than overall accuracy only for the habitats which account for the largest proportion of ground truth data and predicted area, namely CR.MCR.FaAlCr (Faunal and algal crusts on moderate energy circalittoral rock)

in the biotope maps, and ADHT (*Alcyonium digitatum* and hydroid turf) and SUKW (starfish, urchins and keelworms) in the maps produced using the site-specific classification. Locally rare classes have the lowest classification accuracy due to the small number of objects available both for training and validation. In view of the low separation distances between classes and consequent low classification accuracy and stability, the observed correlation between predicted area and number of ground truth samples in both classifications is likely to be an artefact of the classification method rather than a reliable indication of the extent and distribution of species communities in the study area. These issues highlight the need to establish the required ground truth sampling effort for each class through analysis of acoustic data in order to achieve a statistically robust validation (Clements *et al.*, 2010), although in practice ground truth data collection is often limited by time and budget constraints as discussed in sections 2.4.3 and 2.4.4.

2.4.3 Sources of error and uncertainty

Seabed photographs were used for validation, but assigning a habitat class to a photograph is error prone (Rattray *et al.*, 2014), so the error matrix may not give a true representation of classification accuracy, particularly in the case of sediments. There is disagreement between the sediment class assigned to the grab sample and that assigned to seabed photographs at 14 out of 95 sampling stations. This could reflect genuine fine-scale heterogeneity of sediment classes or misclassification of the photographs. The ground truth photographs show a veneer of sediment overlying functional reef at several stations, a fact which has been identified as a cause of classification error in acoustic mapping studies (Calvert *et al.*, 2015; Lawrence *et al.*, 2015). In the present study, the error matrix shows coarse sediment, mixed sediment and sand misclassified as rock due to high values of backscatter and/or slope; these could be due to underlying rock giving a strong backscatter return, or simply due to artefacts in the data.

Artefacts in acoustic data, in the form of backscatter specular reflection along the nadir stripe, have been shown to be a source of error in both segmentation and classification, particularly in deeper water (Lucieer and Lamarche, 2011; Lecours *et al.*, 2017). In the present study, these artefacts caused classification errors, notably in the deeper waters in the south east and north east of the study site, but these errors were corrected by post-classification enhancements.

Inadequate ground truth sampling can be a major source of error in benthic mapping from acoustic data (Clements *et al.*, 2010). In this study, ground truth data collection was stratified by depth and substratum through expert interpretation of the acoustic data. The data generated were suitable for predicting and validating distribution of the three dominant broadscale classes, but did not include sufficient samples of the two rare sediment classes to enable them to be mapped reliably. Ground truth data were collected at least four months after the acoustic data. It is possible that some sediment movement could have occurred in that time, especially at reef edges, which could result in a change of broadscale habitat class at the location.

At the biotope level, under-sampling of locally rare habitat classes was more pronounced. The ground truth data included only 8 and 3 samples respectively of the biotopes CR.MCR.EcCr.FaAlCr.Bri (brittlestars on faunal and algal encrusted rock) and CR.MCR.CSab.Sspi (*Sabellaria spinulosa* encrusted rock), which is insufficient data to train or validate a predictive map, as evidenced by the extremely low user's and producer's accuracy for these classes. The inherent transience of these two biotopes is another source of uncertainty.

Assigning biological community classes to photographs relies on the assumption that the photograph is representative of the surrounding area. The area covered by a photograph was typically around $1m^2$, equivalent to one pixel in the acoustic data, while the average size of objects produced by segmentation at scale 3 was $58m^2$. While some sampling stations showed consistency of biotopes at this scale, there is evidence of fine-scale heterogeneity of biotopes at others, so this assumption will not be valid in every case and is an inevitable source of uncertainty.

2.4.4 Methodological improvements

Artefacts in acoustic data could be reduced by conducting surveys during calm sea conditions. Ground truth data cannot be collected simultaneously with acoustic data because acoustic data are needed to inform stratified sampling, but should be collected with the least delay possible in order to reduce uncertainty due to sediment mobility and transient habitats. Collection of ground truth data is limited by cost considerations, but grab sampling should be used wherever possible to determine sediment type, due to the uncertainty of assigning sediment classes to video or photographs. Because the mean

bathymetry values of mud and sand training objects overlap and the sample size is relatively small (*n* = 45), further grab sampling stratified by bathymetry would be advisable to ascertain whether depth is a reliable predictor of the distribution of mud and sand in the study area. The ground truth sampling protocol used in this study was intended to support broadscale habitat mapping, not biological community mapping. In order to identify and predict circalittoral rock biotopes, a sampling protocol stratified by features with potential to affect distribution of biota, such as rugosity and slope, would be advisable, while noting that 1m resolution data will be too coarse to identify fine-scale topographic features that may affect distribution of certain species (Lucieer *et al.*, 2013).

The ability to use contextual data layers to inform predictions, which is one of the advantages offered by OBIA, was not exploited here. Current and wave energy can aid prediction of biological communities (Robinson *et al.*, 2011), but even where relationships between species and environmental variables are understood, data may not be available at appropriate resolution to model distribution (Reiss *et al.*, 2015). Existing hydrodynamic models for the study area are too low resolution to be useful predictors of biota distribution in this relatively homogeneous environment (ABP Marine Environmental Research Ltd, 2008; Burrows, 2012). Where correlation can be established between hydrodynamic variables and the distribution of dominant species or communities, allowing for temporal variability in such data, research into fine scale hydrodynamic modelling to produce contextual layers for use in OBIA would be beneficial.

A limitation of this study was that the infralittoral zone was not covered by the acoustic survey due to the operational depth restrictions of the survey vessel and the turbidity of the study site. This is a serious shortcoming because kelp-dominated habitats support considerable biodiversity and provide many ecosystem services (Smale *et al.*, 2013) and previous surveys have shown such habitats to be widespread in the study area at depths shallower than 10m (Brazier *et al.*, 1998). Most studies which have mapped macroalgal communities from acoustic data were conducted at sites where water clarity extends the infralittoral zone to depths accessible to acoustic survey (Ierodiaconou *et al.*, 2007; Brown and Collier, 2008; Holmes *et al.*, 2008; Rattray *et al.*, 2009; Lucieer *et al.*, 2011), but one study conducted surveys in shallow turbid waters from a vessel with a low draught using equipment with a shallow technical limit and predicted macroalgal distribution through pixel-based analysis and manual interpretation of imagery (Mielck *et al.*, 2014). Other

studies have demonstrated the potential for using bathymetric LiDAR to predict habitat distribution in shallow turbid waters using pixel-based approaches (Collin *et al.*, 2011; Zavalas *et al.*, 2014). Future studies should evaluate OBIA methods for mapping infralittoral broadscale habitats and biotopes from shallow acoustic data and bathymetric LiDAR, but were not explored here because no such data are available for the study area.

The low spectral resolution of acoustic data is a limitation of all seabed mapping studies to date. The emerging ability to collect backscatter data at multiple frequencies simultaneously (Hughes Clarke, 2015) holds great promise for improving benthic habitat mapping. OBIA's ability to interpret multiple data layers concurrently, developed through over a decade of applications to multispectral and hyperspectral optical imagery (Blaschke *et al.*, 2014), make this an ideal approach to mapping seabed habitats from multispectral acoustic backscatter when such data become commercially available.

Only two OBIA classification methods were applied, namely threshold-based rules and the SNN algorithm. The SNN classifier was chosen because its simplicity, speed of implementation and prevalence in the software documentation (Trimble, 2014) make it very likely to be selected by users; an evaluation of this method's application to a policy-relevant case study was therefore deemed useful. Diesing *et al.* (2016) recommend conducting comparative studies of classification algorithms to address knowledge gaps in benthic acoustic mapping. To date, little comparative evaluation has been carried out, and variability in findings suggests that the 'best' classification method is influenced by the site and the data. In pixel-based studies, Ierodiaconou *et al.* (2011) found that decision tree classifiers outperformed maximum likelihood classifiers, while Hasan *et al.* (2012b) found that support vector machines and random forests classifiers outperformed decision trees, and in a North Sea application Diesing and Stephens (2015) found negligible difference in overall accuracy of maps produced by random forests, naïve Bayes, neural networks and decision tree classifiers, but found that these four methods outperformed support vector machines and nearest neighbour. Two studies have compared OBIA with pixel-based methods; Lawrence *et al.* (2015) found that automated interpretation of backscatter angular response curves and manual segmentation and classification through visual analysis of acoustic imagery both produced more accurate results than OBIA with a SNN classifier; Diesing *et al.* (2014) found that an OBIA threshold-based rule set produced less accurate results than both a geostatistics approach and a random forests classifier, although the

differences in accuracy were not statistically significant. Only one study has compared the performance of different OBIA classifiers through application to the same acoustic data, finding that a random forests classifier performed best at distinguishing substrates while a nearest neighbour classifier performed best at predicting distribution of biota (Lucieer *et al.*, 2013). Further comparison of different object-based algorithms is therefore strongly recommended for future studies, but was not pursued here because the data and study site provide a poor testing ground for different classification methods due to the broad environmental niche of the modelled communities, the homogeneity of environmental variables, the confounding influence of artefacts, insufficiency of ground truth samples and uncertainty in their analysis.

2.4.5 Wider implications

Broadscale habitat maps produced using the OBIA methods described in this chapter contributed to the evidence base for the designation of Coquet to St Mary's MCZ and Runswick Bay MCZ in 2016 (Fitzsimmons *et al.*, 2015a; Fitzsimmons *et al.*, 2015b). The maps informed the establishment of conservation objectives and continue to inform the design and implementation of spatial management measures by regulatory bodies. The remit of the UK's MPA network is "to protect flora and fauna that are rare, threatened or representative of UK biodiversity"(Defra, 2010), and MCZ design principles aim to achieve protection of both broadscale habitats and features of conservation importance, namely habitats or species that are rare or threatened (JNCC and Natural England, 2010). The remote sensing methods used in this study are unlikely to be suitable for monitoring rare habitats or species. The prevalent species detectable in the seabed imagery were large, common, locally abundant species such as *Flustra foliacea* and *Alcyonium digitatum*. Rare, mobile, small or cryptic species are unlikely to be captured in seabed imagery at this scale.

Furthermore, although these methods were able to distinguish mud and sand broadscale habitats through interpretation of acoustic data informed by PSA of grab samples, this provides no insight into the infaunal communities present in these sediments. Within the 'A5.2 Subtidal sand' habitat complex there are 17 biotopes, of which 4 are found in circalittoral waters, while in the 'A5.3 Subtidal mud' habitat complex here are 33 biotopes of which 8 are found in circalittoral waters, but classification to this level would require taxonomic analysis of sediment infauna (EUNIS, 2012). Acoustic remote sensing can be used to predict the distribution of sediment biotopes in areas where there is a strong relationship

between backscatter signal and grain size, and between grain size and infaunal community (Brown and Collier, 2008), but this was not pursued in this due to insufficient ground truth data.

These methods show promise for meeting statutory requirements for broadscale marine habitat monitoring, such as the EU Habitats Directive, Marine Strategy Framework Directive and Water Framework Directive (EC, 1992; EC, 2000; EC, 2008). This legislation requires the extent and condition of features to be monitored. Feature extent can be derived from broadscale habitat maps and if future surveys are carried out, maps produced using the same methods could be compared to monitor change in extent, allowing for the margin of error defined by the maps' accuracy. The seabed imagery examined in this study shows a fine-scale mosaic of different substrata at the interface between more extensive areas of reef or sediment, suggesting that sediments are mobile, which is to be expected at the depths and energy levels present in the study site (Brazier *et al.*, 1998). The remote sensing methods presented here could detect changes in the boundaries between broadscale habitats, although there is likely to be natural fluctuation in these boundaries due to wave action in winter storms so repeat surveys would be needed initially to determine the background level of natural change to inform future monitoring. The seabed imagery also provides evidence of a veneer of sediment overlying functional reef in many parts of the study site. Even a thin layer of sediment can soften the acoustic return and result in the area of seabed being classified as sediment rather than reef (Calvert *et al.*, 2015; Lawrence *et al.*, 2015). MPA management is often feature-based, with activities such as benthic trawling permitted on sediment habitats and prohibited on reef habitats, so the classification of functional reef as sediment due to an overlying veneer can result in lack of protection for the associated fauna (Sheehan *et al.*, 2013). The methods described here could be used to produce broadscale habitats maps from acoustic data to inform feature-based MPA management (Defra, 2013b), but ground truth data should be collected, at least initially, to determine whether sediment veneers are present and a buffer zone should be placed around features to allow for shifting boundaries (Halpern *et al.*, 2010).

Measures of the condition of subtidal reefs include the extent and distribution of biotopes within the reef and the total number of biotopes present (Davies *et al.*, 2001). The low accuracy of output maps and low separation distance between classes suggest that these methods are not recommended for monitoring change in the extent, distribution or number

of biotopes in areas with homogeneous environmental conditions, although their application in areas with greater spatial heterogeneity of depth, substratum and topography should be explored. On reefs where the biological community appears to be homogeneous there may be subtle differences in biota that are not detectable from video surveys. An alternative measure of condition could therefore be topographic complexity, which is correlated with biodiversity in this environment (Johnson *et al.*, 2003; Frost *et al.*, 2005; Kostylev *et al.*, 2005). OBIA methods could be developed to segment and classify multiple layers of acoustic imagery and derivatives to map and monitor change in topography at different scales, building on previously developed pixel-based approaches to topographic feature mapping (Lucieer, 2007; Diesing *et al.*, 2009).

Although site-specific habitat classes can be locally relevant and easier to separate using remote sensing data, in this case the site-specific classification did not improve accuracy and therefore is not recommended, as maps based on existing standard classifications are better suited to meet statutory conservation and monitoring requirements. The hierarchical structure of the biotope classification system has the benefit of enabling classification at a higher level if there is insufficient data to separate classes at finer levels of detail. This was not applied in this study because four classes were sub-biotopes of another class so mapping at a higher level would have reduced the classification to three classes, one of which was defined by absence of visible biota.

Although the cost of conducting full coverage MBES surveys and collecting video and grab sample data is high, OBIA provided a very cost-effective way of interpreting the data to produce maps. Despite the need for post-classification enhancements, segmentation and classification of the acoustic data were performed far more quickly and reproducibly than could be achieved by manual interpretation of the data. Once developed, the OBIA rule set can be applied to other datasets, with adjustments in threshold values and SNN feature space as required.

2.5 Conclusions

This study applied OBIA to acoustic data to produce a broadscale habitat map with high overall accuracy that considerably improved our understanding of the extent and distribution of benthic substrata. This improved knowledge had immediate practical implications in terms of conservation designation and management of the study area. This

demonstrates that despite challenges presented by artefacts and limited spectral resolution of acoustic data and by uncertainties in interpreting ground truth data, these methods can contribute to MPA planning and management in temperate seas. The methods separated rock from sediment reliably; classification errors were rare and are likely explained by the observed veneer of mobile sediment overlying rock. Sediment classification was reasonably accurate, but this accuracy was largely due to the observed correlation between sediment grade and depth at the study site rather than to detectable differences in backscatter signal. The reliability of sediment classifications could be improved by modifying the sampling strategy to ensure adequate representation of locally rare classes and collecting more grab samples to remove the uncertainty inherent in classifying sediments from video data.

The low accuracy and classification stability of biological community maps produced by this study were due to the broad environmental niche of the dominant biota and the homogeneity of environmental parameters in the study area. However, the proven ability to map biotic classes from acoustic data in more heterogeneous areas using pixel-based approaches (Brown and Collier, 2008; Holmes *et al.*, 2008; Rattray *et al.*, 2009) and the demonstrated advantages of object-based over pixel-based methods in terrestrial environments (Blaschke, 2010) suggest that it would be beneficial to continue to explore OBIA methods for mapping benthic biota. Future studies conducted in areas with greater heterogeneity of abiotic variables and demonstrable correlation between those variables and the distribution of species communities can compare the performance of different OBIA classification algorithms, assess the benefits of using imagery with higher spatial and/or spectral resolution and evaluate the potential of contextual data to improve classification accuracy, where suitable data exist.

While demonstrating that object-based analysis of acoustic imagery can inform marine spatial planning at a coarse thematic scale, this study has provided essential insight into multiple factors affecting the reliability of methods for producing and validating habitat maps, which should inform both future research and practical applications of these methods.

Chapter 3: Measuring intertidal reef rugosity using structure-from-motion photogrammetry and UAV imagery

3.1 Introduction

Relationships between benthic habitat physical structural complexity and biodiversity in the marine environment have been established by a number of studies on habitats including coral reefs (Graham and Nash, 2013), algal and seagrass beds (Gratwicke and Speight, 2005), mangrove forests (MacKenzie and Cormier, 2012), intertidal and subtidal rock reefs (Johnson *et al.*, 2003; Frost *et al.*, 2005; Kostylev *et al.*, 2005; Meager *et al.*, 2011; Medeiros *et al.*, 2011) and artificially engineered habitats (Hunter and Sayer, 2009; Borsje *et al.*, 2011; Firth *et al.*, 2014). Relationships vary depending on the habitat and species under investigation, but the majority of studies report a positive correlation between habitat structural complexity and species richness and/or abundance (Beck, 2000; Schlacher *et al.*, 2007; Wilson *et al.*, 2007b; Matias *et al.*, 2010; St Pierre and Kovalenko, 2014; Newman *et al.*, 2015; Trebilco *et al.*, 2015). Mechanisms driving this correlation are incompletely understood but include the influence of structural complexity on water and sediment movement, light availability, protection from predation and surface area for attachment, factors which are likely to operate in combination and at multiple spatial scales (Kovalenko *et al.*, 2012). Structural complexity is used as an abiotic surrogate in species distribution modelling (Pittman *et al.*, 2009; Pittman and Brown, 2011), predictive habitat mapping (Wilson *et al.*, 2007a), ecological monitoring (Murray *et al.*, 2001; Hill and Wilkinson, 2004) and marine spatial planning (Banks and Skilleter, 2007; McArthur *et al.*, 2010).

Various methods have been developed with the aim of measuring structural complexity in a standard, repeatable way at ecologically relevant scales. These include visual assessment (Wilson *et al.*, 2007b), counting and measuring refugia (Menard *et al.*, 2012), using a falling-rod gauge to record the profile of the contoured surface (Underwood and Chapman, 1989) and using a chain (Risk, 1972), distance-wheel (Wilding *et al.*, 2010) or laser (Lambert, 2012) to record the length of the contoured surface. Indices generated to characterise terrain complexity from surface measurements include root mean square difference in height between sequential measurements or the angular standard deviation of vectors along a line (McCormick, 1994), scale-invariant fractal dimensions (Kostylev *et al.*, 2005) and linear rugosity derived from the ratio of the contoured surface to a horizontal straight line distance (Risk, 1972; Luckhurst and Luckhurst, 1978). Comparative studies have found varying levels

of correlation between different methods of measuring structural complexity (McCormick, 1994; Beck, 1998; Frost *et al.*, 2005; Leon *et al.*, 2015). Manual methods of taking surface measurements are labour-intensive and restricted to accessible areas such as intertidal or shallow subtidal reefs. Measurements are limited to a single scale defined by the length and link size of a chain or the length and rod size of a profile gauge. Furthermore, manual methods require contact with the seabed and could cause environmental damage.

Remote sensing techniques enable the creation of three-dimensional topographic models of the seabed or shore without risk of harm to benthic communities. Indices of structural complexity can be derived from these models at far greater sampling density than could be achieved from manual measurements. Remotely sensed models also enable the generation of more sophisticated indices than could be easily derived from manual measurements, such as root mean square of heights within a planar area (Leon *et al.*, 2015), ratio of contoured surface area to horizontal planar area (Jenness, 2004) and two- and three-dimensional arc-chord ratios (Du Preez, 2015). Techniques such as sonar, LiDAR and terrestrial laser scanning (TLS) are widely used to generate three-dimensional models of marine and coastal environments, but data capture is expensive and data processing requires specialist software and expertise. Although topographic complexity can be characterised from sonar or LiDAR data at coarse scales over large areas, the resolution of processed imagery is too low to resolve finer scale rugosity (Zawada and Brock, 2009; Zawada *et al.*, 2010). Digital photogrammetry enables the reconstruction of scene geometry from overlapping photographs, providing a relatively low-cost and accessible method of producing high resolution topographic models. While acoustic or laser surveys capture only the physical characteristics of the landscape, photogrammetry combines spectral and geometric information to create a photorealistic model which could be used in ecological analyses, for example to assess the extent, distribution and condition of algal and sessile faunal communities and their relationship with topographic features.

Traditional photogrammetric techniques used trigonometric equations to calculate the location of points in an image from the known locations of the camera(s) (Baily *et al.*, 2003). Early applications of stereo photogrammetry in the intertidal environment produced topographic complexity indices that correlated with species density at scales of habitat patches (Beck, 1998) and whole sites (Guichard *et al.*, 2000), but Frost *et al.* (2005) found stereo photogrammetry more error-prone than manual methods of taking surface

measurements, leading to overestimation of rugosity on smooth surfaces. The more recent development of Structure-from-Motion (SfM) photogrammetry enables the geometry of a scene to be resolved from overlapping photographs without the prior specification of camera positions and ground target coordinates (Snavely *et al.*, 2008). To enable their use in geoscience applications, models created by SfM photogrammetry can be georeferenced by aligning points in the imagery with features of known coordinates, which can be facilitated by deploying high contrast physical targets (Ground Control Points) within the survey area prior to image collection (Westoby *et al.*, 2012; Micheletti *et al.*, 2015). A range of open source and low-cost commercial software packages are available, enabling users to create 3D models from photographs captured by consumer grade cameras without the need for specialist skills (Remondino *et al.*, 2012).

As with all remote sensing techniques, there is a trade-off between spatial resolution and extent of coverage. Close-range (< 5m) photogrammetry has been applied in marine environments to produce topographic models of small areas (< 500m^2) from which rugosity indices can be derived (Friedman *et al.*, 2012; He *et al.*, 2012; Burns *et al.*, 2015; Figueira *et al.*, 2015; Leon *et al.*, 2015) and measurements of benthic organisms recorded (Courtney *et al.*, 2007; Lavy *et al.*, 2015). Only three of the above studies compared rugosity indices derived from models with those derived from manual measurements; Friedman *et al.* (2012) and Figueira *et al.* (2015) both observed that photogrammetric measurements underestimated rugosity compared to manual measurements, while He *et al.* (2012) found no significant difference between measurements.

To cover a larger area, SfM photogrammetry has been applied to imagery captured by unmanned aerial vehicle (UAV) to create georeferenced topographic models for purposes including forest biomass monitoring (Mlambo *et al.*, 2017), assessing earthquake damage to urban areas (Menderes *et al.*, 2015) and informing hydrographic modelling in fluvial (Javernick *et al.*, 2014; Woodget *et al.*, 2016), agricultural (Ouedraogo *et al.*, 2014) and polar environments (Lucieer *et al.*, 2014; Rippin *et al.*, 2015). SfM photogrammetry of UAV imagery has been tested in coastal and estuarine environments, demonstrating the potential of these methods for monitoring erosion of sediment habitats (Harwin and Lucieer, 2012; Mancini *et al.*, 2013; Goncalves and Henriques, 2015; Ierodiaconou *et al.*, 2016) but to date the technique has not been evaluated as a means of recording the rugosity of intertidal reefs.

This study aims to evaluate SfM photogrammetry of ultra-high resolution multispectral UAV imagery as a method for quantifying rugosity by conducting an experimental study on a temperate intertidal reef. Specific objectives are (1) to produce topographic models of the shore under different processing parameters and in different formats (point cloud and digital elevation model) to assess the influence of these factors on processing time and quality of output, (2) to assess the vertical accuracy of all models by comparison with ground truth data, (3) to compare linear rugosity indices derived from the models with indices derived from manual measurements using the chain-and-tape method (Risk, 1972), applying statistical tests to evaluate the consistency of indices generated by photogrammetric and by manual methods. The cost, time and ease of use of both methods will also be compared.

3.2 Methods

3.2.1 Study site

The study was conducted at Kettleness headland, North Yorkshire, UK (54° 32.050' N, 0° 42.800' W) (Figure 3.1) because of this site's high topographic diversity and conservation interest.

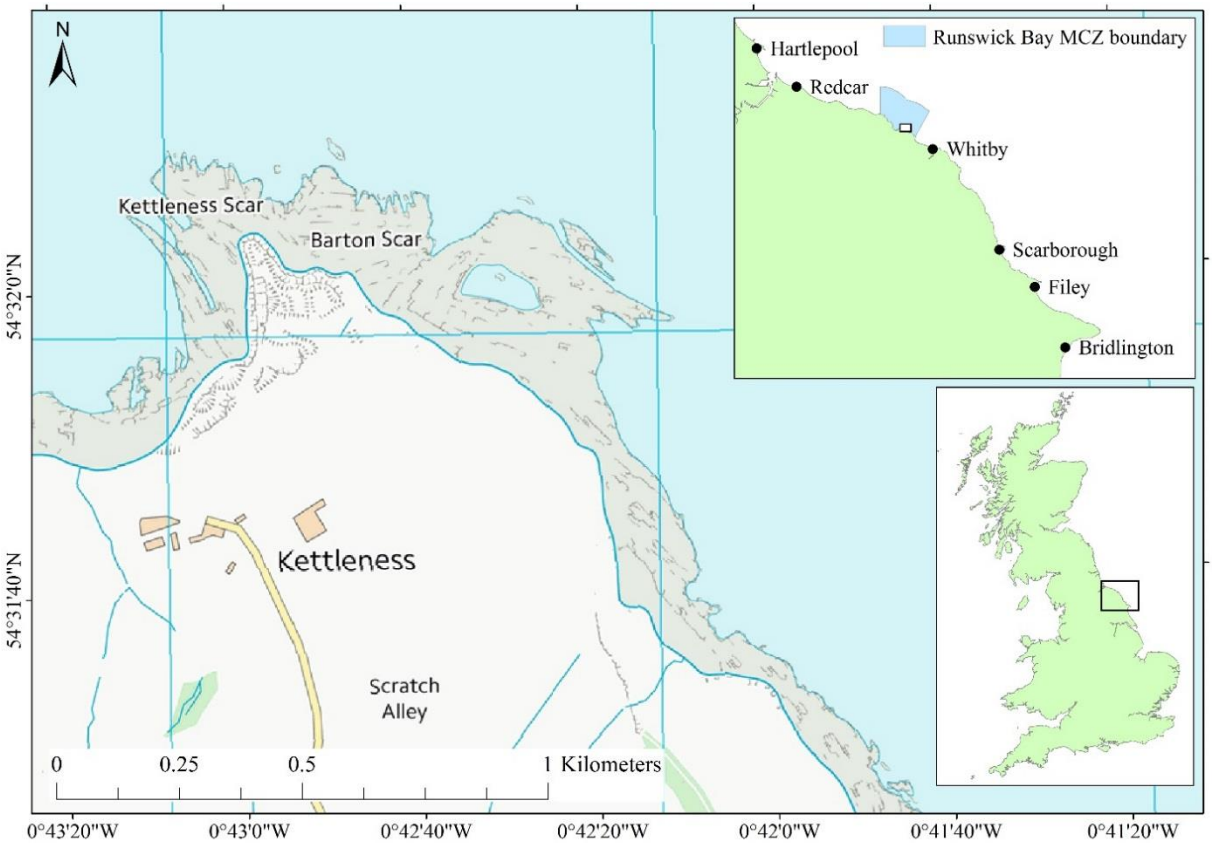

Figure 3.1: Map showing the location of Kettleness headland and (inset) the boundary of Runswick Bay Marine Conservation Zone. Contains Ordnance Survey data © Crown copyright and database right (2018).

Kettleness lies within Runswick Bay Marine Conservation Zone which was designated in January 2016 under the UK's Marine and Coastal Access Act 2009 to maintain a number of features including intertidal rock in favourable condition. The intertidal area consists of a ~300m wide wave-cut platform of Cleveland ironstone at the base of 80m to 100m high cliffs comprising deposits of grey shale and alum shale capped by carboniferous sandstone. The site's topography was heavily modified by alum production and jet mining in the 18th and 19th centuries and continues to be affected by landslips (Miller, 2002; Jecock *et al.*, 2003). As a result, the stepped bedrock of the upper shore is strewn with large boulders deposited by quarrying and cliff falls, while the lower shore is cut by gullies and channels, some naturally occurring and some man-made to aid the transport of quarried materials or the run-off of waste products from alum processing.

Kettleness is a north-facing headland, exposed to prevailing wind and wave action. Due to the high exposure, the fucoid canopy is reduced and the mid-shore dominated by turf-forming red seaweeds, predominantly *Osmundea pinnatifida* and *Corallina officinalis*, while the upper shore is dominated by dense communities of the barnacle *Semibalanus balanoides*. Tides are diurnal with a mean tidal range of 4.8m on spring tides and 2.4m on neap tides.

3.2.2 Aerial imagery acquisition

Ultra-high resolution aerial imagery was collected during a low spring tide on the 3rd July 2015 using a senseFly eBee UAV (www.sensefly.com/drones/ebee). The eBee is a fixed wing UAV weighing 0.7kg with a 0.96m wingspan. Flights were pre-programmed using senseFly's ground station software eMotion 2 to collect imagery of the study site at 0.04m ground sampling distance with 60% lateral overlap and 75% forward overlap between images. The flight plan consisted of perpendicular intersecting flight lines to maximise image overlap and reduce the impact of crosswinds on image acquisition. Two flights were conducted using the eBee's onboard GPS to follow the flight plan, each flight lasting eleven minutes. On the first flight, a Canon IXUS 127 HS 16.1 megapixels camera was used to capture red-green-blue (RGB) imagery (390nm to 700nm). On the second flight a Canon Powershot ELPH 110 HS 16.1 megapixels camera was used to capture red edge imagery (680nm to 750nm). The eBee's flight recorder logged the time of image capture, horizontal and vertical location (x, y, z) and rotation angle (pitch: ω, roll: ϕ and yaw: κ) of the sensor for every image. A summary of image acquisition is provided in Table 3.1.

Table 3.1: Flight and imagery details of UAV surveys conducted in Runswick Bay on 3rd July 2015

Camera	Flight times (GMT+1)	Tide height above Chart Datum (m)	Number of images	Survey Area (km^2)	Mean Ground Sampling Distance (m)
Canon IXUS 127 HS RGB	11:49 – 12:00	0.78 – 0.79	113	0.2246	0.0392
Canon Powershot ELPH 110 Red Edge	12:23 – 12:34	0.88 – 0.97	133	0.1988	0.0346

There was no cloud cover during either flight, so lighting conditions were as consistent as possible. The flights were carried out close to midday (Table 3.1) to minimise the impact of shadows in the imagery.

Seven ground control points (GCPs) consisting of 0.5m x 0.5m squares marked with a white cross on a black background were distributed throughout the survey area and remained in place during both flights. The horizontal and vertical coordinates at the centre of each GCP were logged using a Leica Viva GS10 high-precision receiver (Leica Geosystems), which recorded one observation per second for three minutes. The logged coordinates were differentially corrected in Leica Geo Office software (Leica Geosystems) using reference data from the Global Navigation Satellite System (GNSS) base station network downloaded from Leica's SmartNet website (http://uk.smartnet-eu.com/) in RINEX format. The processed coordinates had a horizontal and vertical accuracy of between 0.001m and 0.003m. The same method was used to collect and process coordinates at an additional 162 points distributed throughout the survey area to provide a dataset for validating the vertical accuracy of 3D models.

The images were processed using PostFlight Terra 3D software (senseFly) to create orthomosaics and digital elevation models (DEM) for both flights at 0.04m resolution. The georeferencing RMS error was 0.011m for the RGB orthomosaic and 0.006m for the red edge orthomosaic. ArcGIS v.10.3 (ESRI) was used to clip all the raster layers to the same boundary to remove cliffs and sea, leaving only the intertidal area (Figure 3.2).

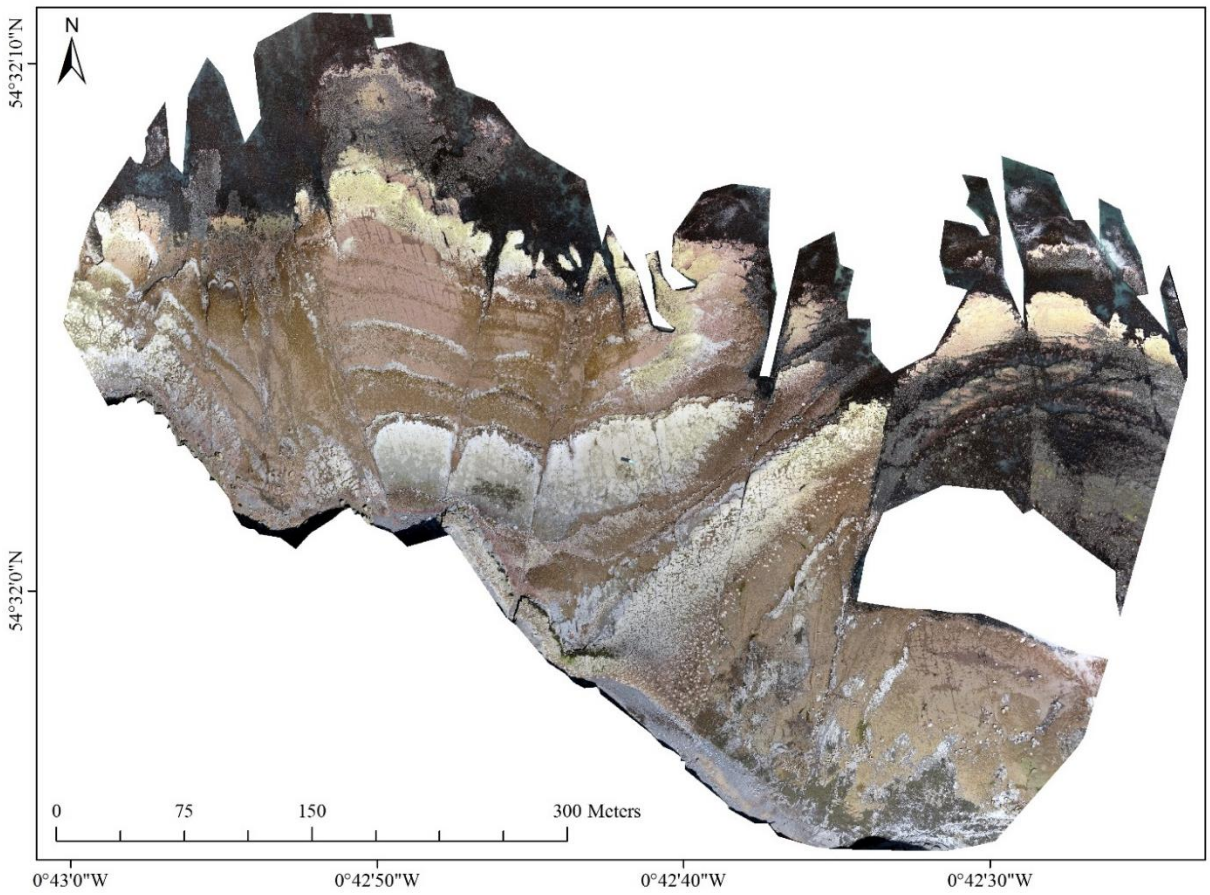

Figure 3.2: Orthomosaic of the intertidal area of Kettleness produced by SfM photogrammetry of RGB imagery and clipped to remove sea and cliffs.

3.2.3 Manual surface measurements

Object-based image analysis was used to define a stratified random sampling protocol for the collection of rugosity measurements. eCognition Developer v.9.0.3 produced a chessboard segmentation of the DEM at 255 pixel scale, creating 1,923 10m x 10m square objects. These objects were exported to ArcGIS with the attribute value of standard deviation of elevation values within each object. This value was used to divide the dataset into five quantiles to produce five classes of rugosity from least rugose (standard deviation of elevation: 0 to 0.064) to most rugose (standard deviation of elevation: 0.262 to 3.313) (Figure 3.3).

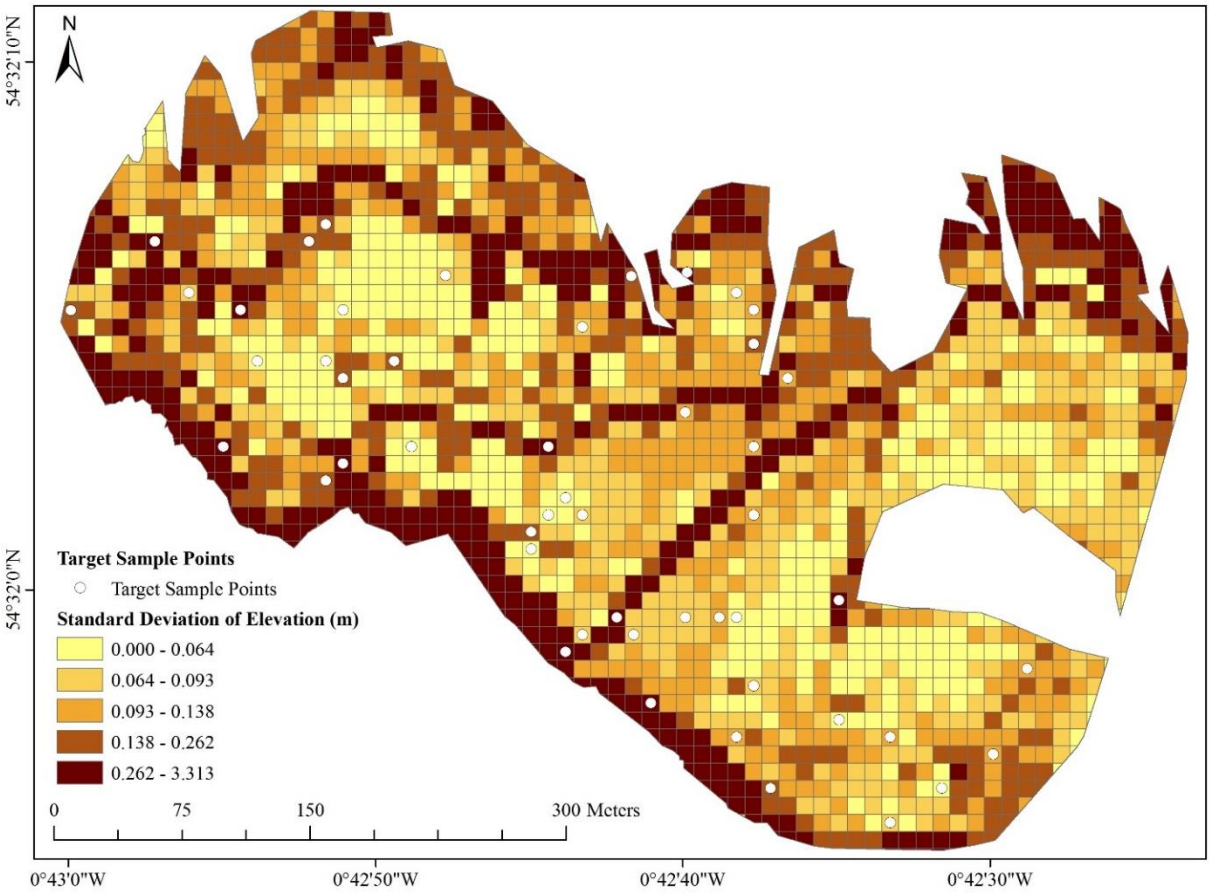

Figure 3.3: Overview of stratified random sampling method showing the location of the 50 target sample points against the grid produced by chessboard segmentation of the digital elevation model and categorised based on standard deviation of elevation values within each object.

A random number generator was used to select ten squares from each of the five rugosity classes, creating fifty target sampling points located at the centroid of each randomly selected 10m x 10m square (Figure 3.3). Linear surface measurements were collected during low spring tides on the 24th, 25th and 26th March 2016 using the 'chain-and-tape' method. A 5m long chain with 0.04m links was used to match the spatial resolution of the imagery. At each sampling point, the chain was laid either north-south or east-west, whichever direction was deemed to give the best representation of the rugosity class being sampled. If rockpools or overhangs occurred along the transect, their contours were followed as closely as possible with the chain and their presence was noted on a recording form. The coordinates of the start and end point of each transect were logged using a Leica Viva GS10 high-precision receiver and post-processed as described above. The distance between the start and end point of the transect was measured on a horizontal plane using a tape measure. Every transect was photographed.

3.2.4 Creation and validation of 3-dimensional models

To create georeferenced 3D models from the UAV imagery, structure-from-motion photogrammetric processing was carried out in PhotoScan Professional v. 1.3.0 (Agisoft), because it is widely used commercial stand-alone software with a practical user interface. The following photogrammetric processes were applied to the imagery from the first flight (RGB), the imagery from the second flight (red edge) and to the combined imagery from both flights. The coordinate system was defined as WGS84 / UTM zone 30N and the sensor position data (x, y, z, ω, ϕ, κ) from the eBee's flight log were used to aid the initial photo alignment process. The horizontal and vertical coordinates of the GCPs were then used to optimise triangulation and improve the accuracy of the georeferenced outputs. Place markers were automatically added to all photographs containing the GCP coordinates (60 photographs from flight 1 and 61 photographs from flight 2). Manual adjustments were made to align the place marker in each photograph with the centre of the cross marked on the GCP. The PhotoScan workflow for building a dense point cloud from the imagery enables users to select pre-set quality parameters defined by the level of compression of the original photographs (lowest, low, medium, high, ultra-high) and different strengths of depth filtering, i.e. the removal of points which appear to be outliers (disabled, mild, moderate, aggressive). The quality parameters used in this study were medium (images compressed to 25% of their original size), high (images compressed to 50% of their original size) and ultra-high (no compression applied). The depth filtering parameters used were aggressive, which is least tolerant of outliers and therefore removes the largest number of points, moderate, which is more tolerant of outliers, and mild, which is the most tolerant of outliers and therefore removes the smallest number of points. Nine dense point clouds were created for each of the three sets of imagery using every combination of medium, high and ultra-high quality and mild, moderate and aggressive depth filtering. The results were exported as georeferenced LAS files. Vertical accuracy of each model was validated by comparing the elevation measured by GNSS equipment at the 162 sampling points with the elevation (z) value of the point cloud at the same coordinates and calculating root-mean-square error (RMSE) from the differences. RMSE was chosen as a standard measure of accuracy because it is an easily understood metric which is widely used when the ground truth data consist of points rather than a continuous surface (Harwin and Lucieer, 2012).

3.2.5 Generation and comparison of rugosity indices

Linear rugosity indices were calculated using the formula

$$R_{chain} = \frac{L_{chain}}{D_{chain}}$$

in which L_{chain} is the length of the contoured surface and D_{chain} is the horizontal straight line distance between the start and end points of the contoured surface. R_{chain} was therefore calculated from the manual measurements by dividing the chain length (5 m) by the horizontal distance measured by tape measure.

In order to derive rugosity indices from the 3D models, a polyline shapefile was created in ArcGIS using the post-processed coordinates for the start and end points of the 50 transects. The straight line distance between each set of points was measured using the Calculate Geometry command to provide a virtual value for D_{chain}. The Add Surface Information tool in the 3D Analyst toolbox was used to calculate L_{chain} values for the 50 transects from each of the 3D models. R_{chain} values were calculated from these virtual measurements as described above. R_{chain} values derived from photogrammetry were compared to those derived from manual measurements and RMSE was calculated from the differences. A Wilcoxon signed-rank test (Wilcoxon, 1945) was conducted to determine whether the indices derived from photogrammetry were significantly different to those derived from manual measurements. This test was used because the data are paired but not normally distributed and met the assumptions of the test. Digital Elevation Models (DEMs) were then produced in PhotoScan from the dense point clouds with the lowest RMSE rugosity values for each of the three sets of imagery. Rugosity indices were derived from the DEMs using the same methods described above.

3.3 Results

3.3.1 Vertical accuracy

Comparison of elevation values between the models and the 162 ground points measured with GNSS produced RMSE values ranging from 0.061m to 0.128m. Accuracy increased with increasing point density, with the ultra-high quality parameter producing point clouds with the highest vertical accuracy in all but one case, namely the model produced from RGB imagery with mild depth filtering (Figure 3.4). Differences between vertical RMSE produced

by different depth filtering parameters were in the order of millimetres; mild depth filtering produced highest RMSE values in the ultra-high point density models, but aggressive depth filtering produced highest RMSE values at medium and high point densities. Vertical RMSE values of DEMs were within millimetres of the vertical RMSE values of the ultra-high quality point clouds from which they were created (Figure 3.4).

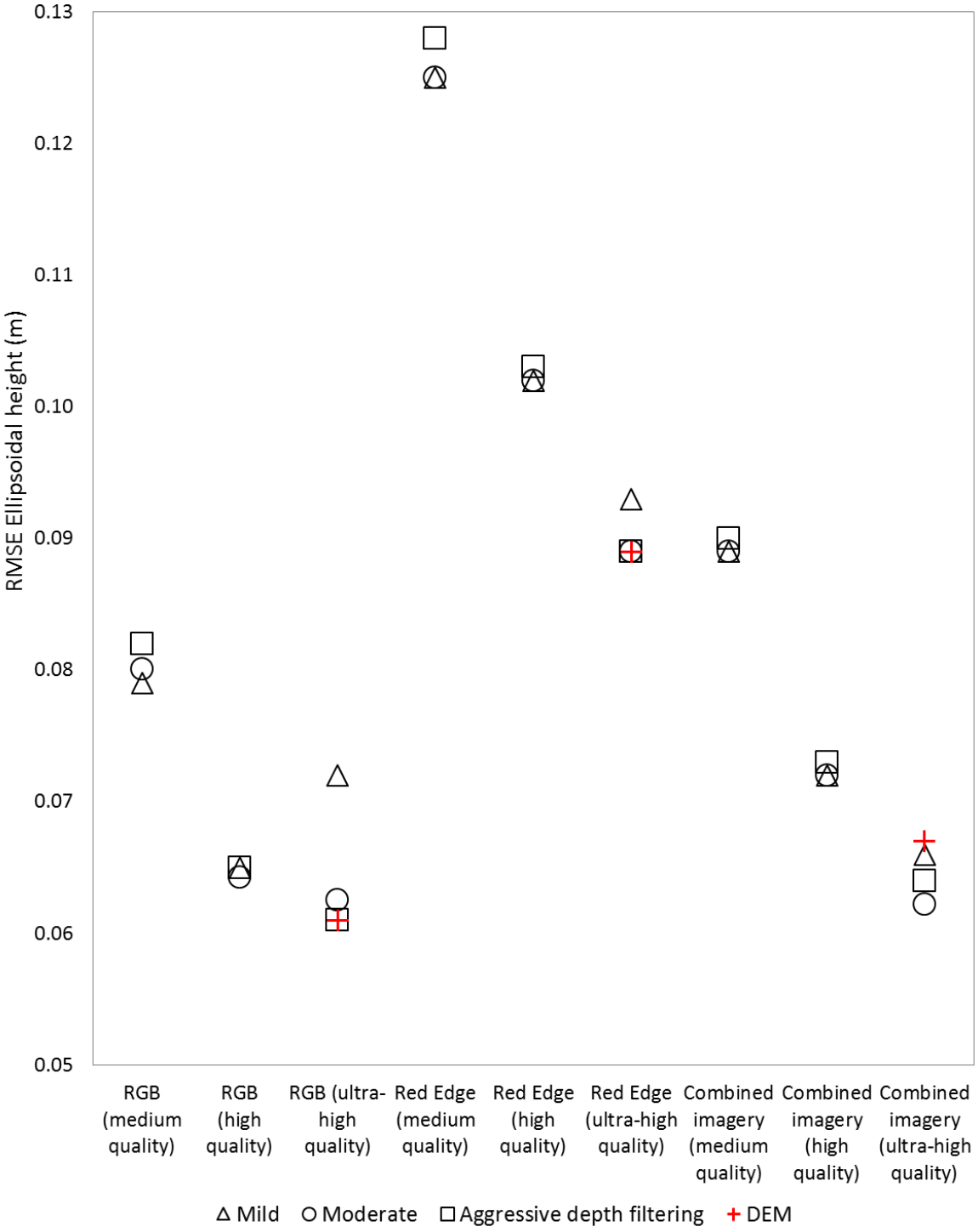

Figure 3.4: Vertical RMSE values of point clouds produced using different combinations of point density and depth and DEMs produced from the point cloud with the lowest RMSE rugosity value in each of the three sets of imagery. RMSE values were produced by comparing elevation values derived from the 3D models with elevation values measured by GNSS (n = 162).

The vertical difference between elevation values derived from photogrammetry and those measured using GNSS are shown for the model with the lowest vertical RMSE produced from each set of imagery (Figure 3.5). Values are distributed evenly around zero for the model derived from the RGB imagery, while the values derived from the red edge imagery are positively skewed, i.e. elevation values derived from the model tend to be higher than those measured using GNSS. The vertical accuracy of models produced by combining the imagery from both flights was on a par with that of models produced from the RGB imagery alone.

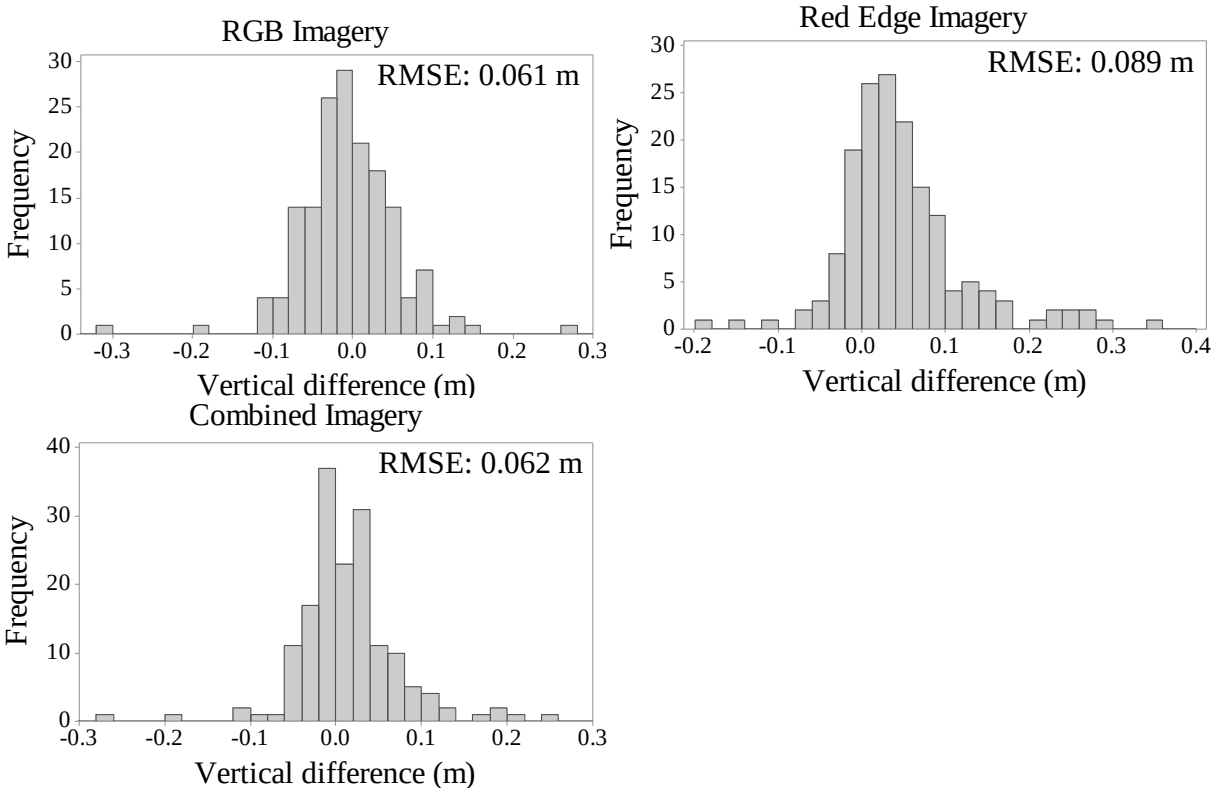

Figure 3.5: Vertical difference between elevation values derived from point clouds and those measured using GNSS for the models with the lowest vertical RMSE values produced from each set of imagery (n = 162)

3.3.2 Comparison of photogrammetric and manual rugosity measurements

Comparison of rugosity indices values derived from the models with those measured manually produced rugosity (R_{chain}) RMSE values ranging from 0.044 to 0.077 and surface length (L_{chain}) RMSE values ranging from 0.189m to 0.325m (Table 3.2), which represents 3.8% to 6.5% of the 5m sampling distance. Consistency between photogrammetric and manual rugosity measurements increased with increasing point density, but the choice of depth filtering parameter did not appear to have a consistent influence; the models with lowest R_{chain} RMSE values for RGB, red edge and combined imagery were produced by moderate, aggressive and mild depth filtering respectively (Figure 3.6). Increasing the

number of photographs by combining the imagery from both flights did not appear to increase correlation between photogrammetric and manual rugosity measurements.

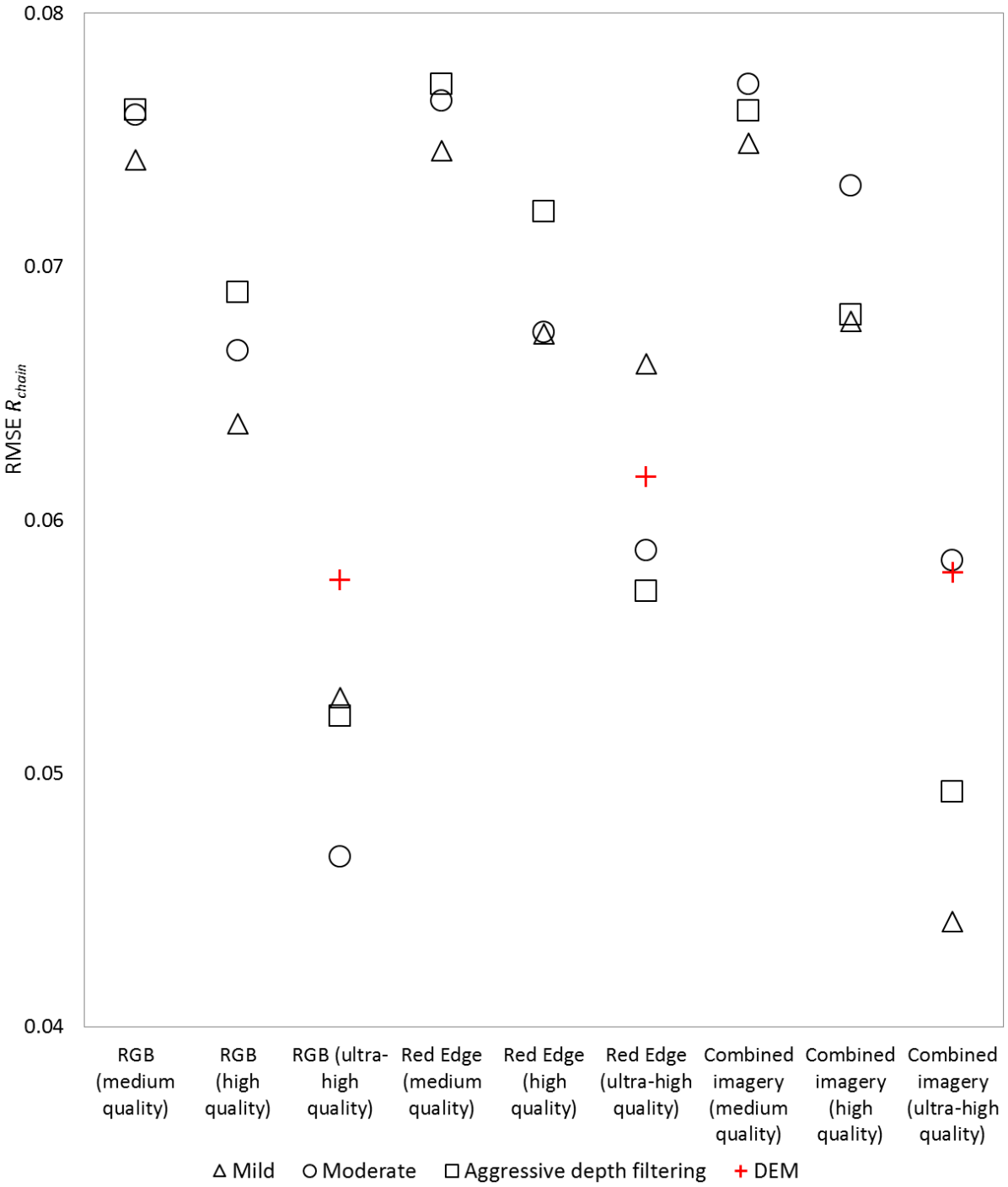

Figure 3.6: Rugosity RMSE values of point clouds produced using different combinations of point density and depth and DEMs produced from the point cloud with the lowest RMSE rugosity value in each of the three sets of imagery. RMSE values were produced by comparing R_{chain} values derived from the 3D models with R_{chain} values measured manually using the chain-and-tape method (n = 50).

There was a significant difference between rugosity indices derived from manual measurements and those derived from medium and high quality point clouds (Wilcoxon signed rank $p < 0.001$) or from ultra-high quality point clouds with mild depth filtering of RGB

imagery (Wilcoxon signed rank $p < 0.01$) and red edge imagery (Wilcoxon signed rank $p < 0.05$) (Table 3.2). The vertical RMSE and R_{chain} RMSE values of DEMs are comparable with the RMSE values of the ultra-high quality point clouds from which the DEMs were produced, but there was a significant difference between rugosity indices derived from DEMs and those derived from manual measurements (Wilcoxon signed rank $p < 0.001$).

Table 3.2: Table of point density, vertical RMSE, rugosity RMSE and Wilcoxon signed-rank test results for 27 point clouds and 3 DEMs produced using different combinations of quality and depth filtering parameters in PhotoScan

Camera	Point cloud quality	Point cloud depth filtering	Mean point density (m^{-3})	Vertical RMSE (m)	D_{chain} RMSE (m)	L_{chain} RMSE (m)	R_{chain} RMSE	Significant difference between photogrammetric and manual R_{chain} values
Canon IXUS 127 HS (RGB)	Medium	Mild	43	0.079	0.050	0.312	0.074	Yes ($p < 0.001$)
		Moderate	43	0.080	0.050	0.319	0.076	Yes ($p < 0.001$)
		Aggressive	43	0.082	0.050	0.320	0.076	Yes ($p < 0.001$)
	High	Mild	173	0.065	0.050	0.268	0.064	Yes ($p < 0.001$)
		Moderate	175	0.064	0.050	0.282	0.067	Yes ($p < 0.001$)
		Aggressive	176	0.065	0.050	0.293	0.069	Yes ($p < 0.001$)
	Ultra-high	Mild	698	0.072	0.050	0.223	0.053	Yes ($p < 0.01$)
		Moderate	706	0.063	0.050	0.207	0.047	No
		Aggressive	719	0.061	0.050	0.226	0.052	No
	Ultra-high	Moderate	DEM	0.061	0.050	0.25	0.058	Yes ($p < 0.001$)
Canon Powershot ELPH 110 (Red Edge)	Medium	Mild	56	0.125	0.050	0.300	0.075	Yes ($p < 0.001$)
		Moderate	56	0.125	0.050	0.321	0.077	Yes ($p < 0.001$)
		Aggressive	56	0.128	0.050	0.324	0.077	Yes ($p < 0.001$)
	High	Mild	223	0.102	0.050	0.283	0.067	Yes ($p < 0.001$)
		Moderate	224	0.102	0.050	0.283	0.067	Yes ($p < 0.001$)
		Aggressive	228	0.103	0.050	0.306	0.072	Yes ($p < 0.001$)
	Ultra-high	Mild	909	0.093	0.050	0.298	0.066	Yes ($p < 0.05$)
		Moderate	923	0.089	0.050	0.254	0.059	No
		Aggressive	936	0.089	0.050	0.244	0.057	No
	Ultra-high	Aggressive	DEM	0.089	0.050	0.264	0.062	Yes (P < 0.001)
Combined imagery	Medium	Mild	54	0.089	0.050	0.315	0.075	Yes ($p < 0.001$)
		Moderate	55	0.089	0.050	0.325	0.077	Yes ($p < 0.001$)
		Aggressive	55	0.090	0.050	0.320	0.076	Yes ($p < 0.001$)
	High	Mild	219	0.072	0.050	0.283	0.068	Yes ($p < 0.001$)
		Moderate	222	0.072	0.050	0.307	0.073	Yes ($p < 0.001$)
		Aggressive	224	0.073	0.050	0.285	0.068	Yes ($p < 0.001$)
	Ultra-high	Mild	883	0.066	0.050	0.189	0.044	No
		Moderate	897	0.062	0.050	0.251	0.058	No
		Aggressive	915	0.064	0.050	0.208	0.049	No
	Ultra-high	Mild	DEM	0.067	0.050	0.252	0.058	Yes ($p < 0.001$)

The rugosity indices derived from point clouds were higher than those derived from manual measurements for 64% (RGB), 65% (red edge) and 68% (combined imagery) of the samples (Figure 3.7). In contrast, the indices derived from DEMs were lower than those derived from manual measurements for 73% (RGB), 76% (red edge) and 80% (combined imagery) of the samples. In both cases, photogrammetric measurements were increasingly lower than

manual measurements at higher rugosity index values.

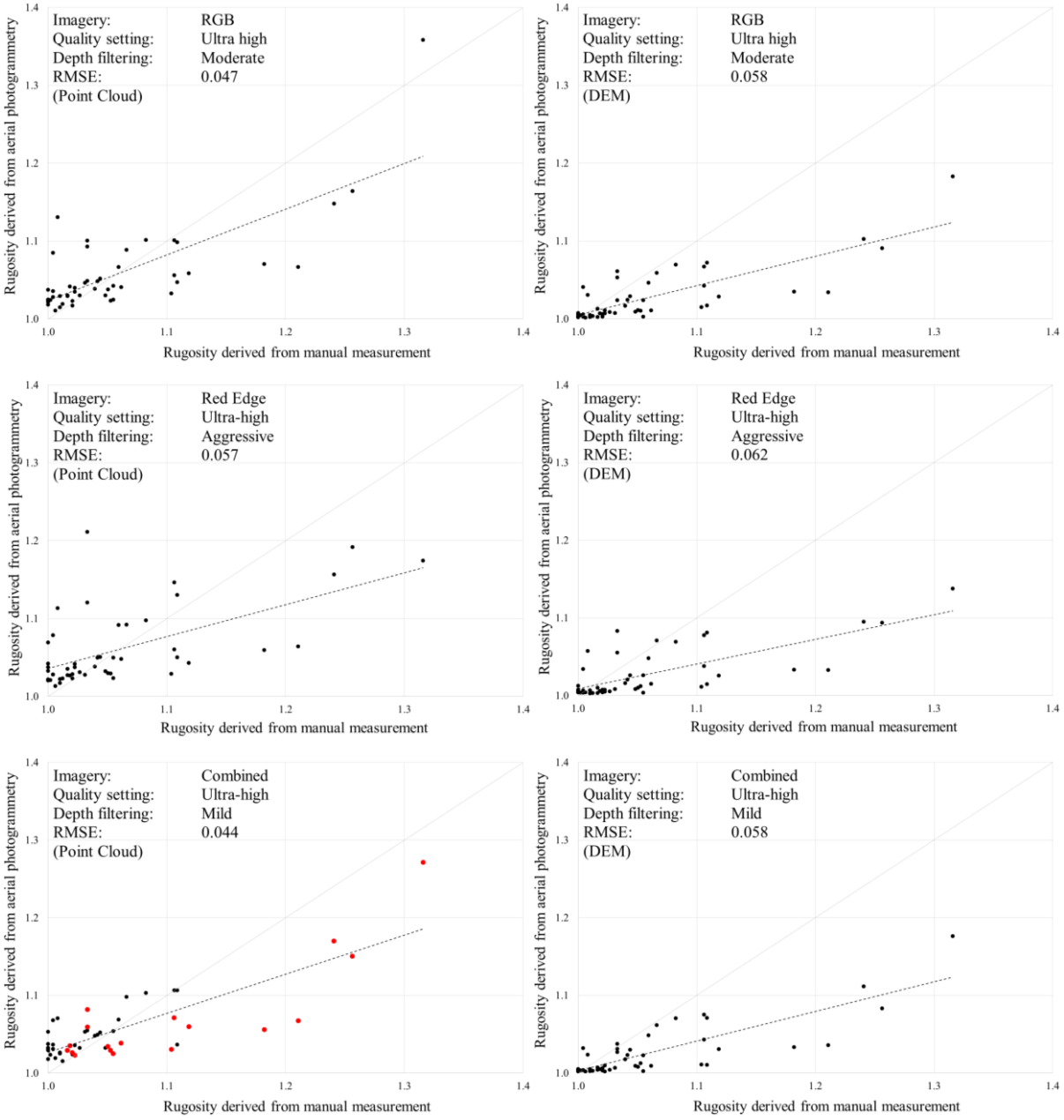

Figure 3.7: Rugosity indices derived from photogrammetry against those derived from manual measurements for the three point clouds with the lowest rugosity RMSE values and the three DEMs produced from those point clouds (n = 50). The dashed line is the line of best fit and the grey unbroken line represents 1:1 correspondence. Transects at which overhangs were present are highlighted in red on the bottom left plot only.

Three transect profiles derived from point clouds and DEMs illustrate inconsistencies in surface contours derived from different sets of imagery (which can lead to over- or underestimation of rugosity), and the 'smoothing' effect of DEMs which leads to underestimation of rugosity.

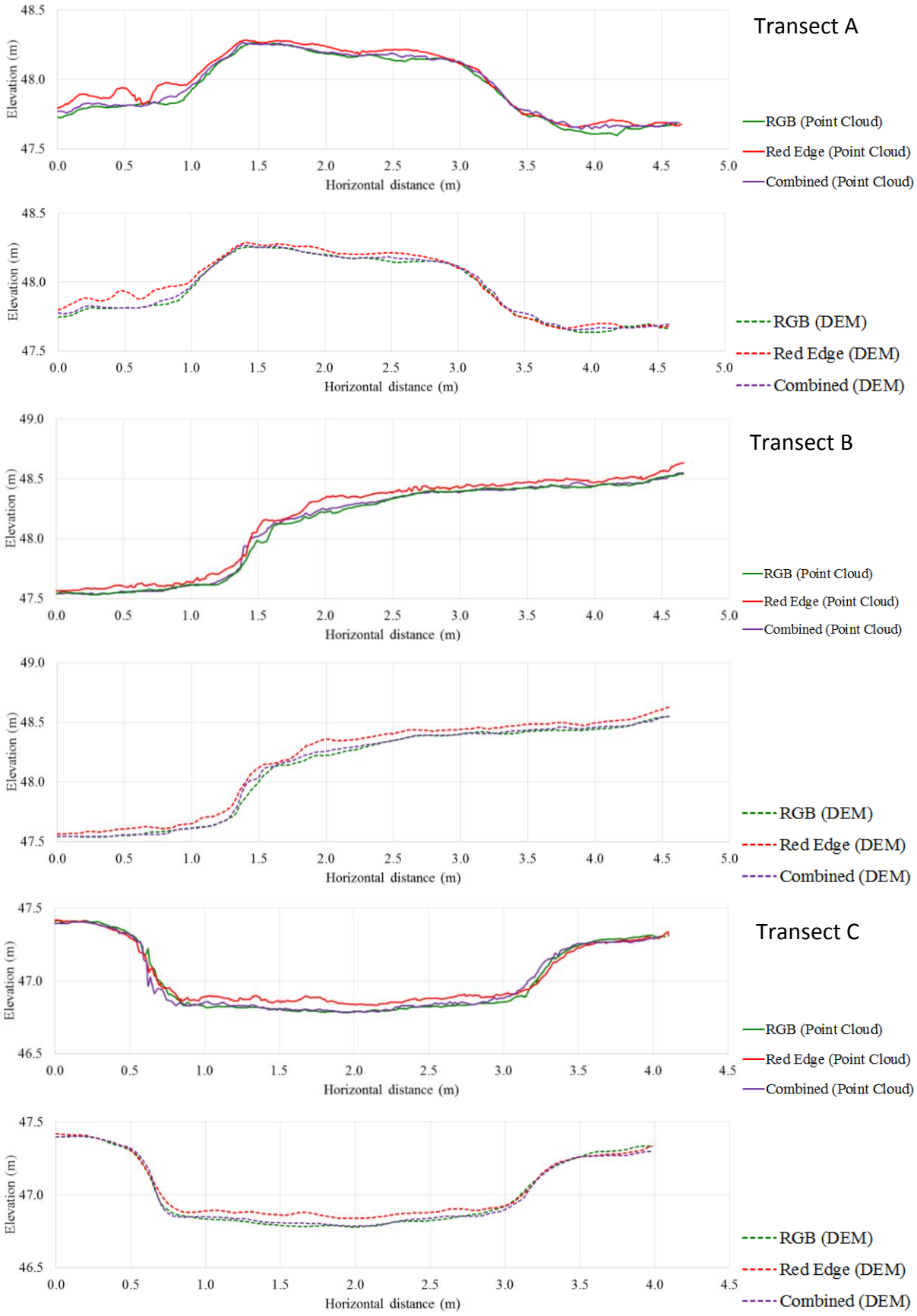

Figure 3.8: Profiles of three 5m transects showing the contoured surface derived from ultra-high density point clouds and DEMs created from RGB, Red Edge and combined imagery.

L_{chain}, D_{chain} and R_{chain} values derived from manual and photogrammetric measurements for three transects (Figure 3.8) illustrate the variation in surface contours derived from different imagery and file formats, which caused the inconsistency between photogrammetric and manual rugosity measurements (Figure 3.7 and Table 3.3). However, despite this centimetre-scale variability in surface contours, decimetre-scale terrain features such as ridges, steps and channels were consistently identified (Figure 3.8).

Table 3.3: L_{chain}, D_{chain} and R_{chain} values for the three 5m transects shown in Figure 3.8

Transect	Rugosity index derived from:		L_{chain} (m)	D_{chain} (m)	R_{chain}	Difference between photogrammetric and manual R_{chain} measurements
A	Chain-and-tape		5.000	4.520	1.106	
	Point Cloud	RGB	5.007	4.548	1.101	-0.5%
		Red Edge	5.212	4.548	1.146	3.6%
		Both	5.032	4.548	1.106	0.0%
	DEM	RGB	4.852	4.548	1.067	-3.5%
		Red Edge	4.902	4.548	1.078	-2.6%
		Both	4.890	4.548	1.075	-2.8%
B	Chain-and-tape		5.000	4.510	1.109	
	Point Cloud	RGB	5.038	4.586	1.099	-0.9%
		Red Edge	5.183	4.586	1.130	1.9%
		Both	5.075	4.586	1.107	-0.2%
	DEM	RGB	4.918	4.586	1.072	-3.3%
		Red Edge	4.957	4.586	1.081	-2.5%
		Both	4.911	4.586	1.071	-3.4%
C	Chain-and-tape		5.000	4.030	1.241	
	Point Cloud	RGB	4.571	3.982	1.148	-7.5%
		Red Edge	4.606	3.982	1.157	-6.8%
		Both	4.658	3.982	1.170	-5.7%
	DEM	RGB	4.390	3.982	1.103	-11.1%
		Red Edge	4.360	3.982	1.095	-11.7%
		Both	4.426	3.982	1.112	-10.4%

Transect lengths (D_{chain}) measured by tape measure were systematically higher than those measured by GNSS (Figure 3.9).

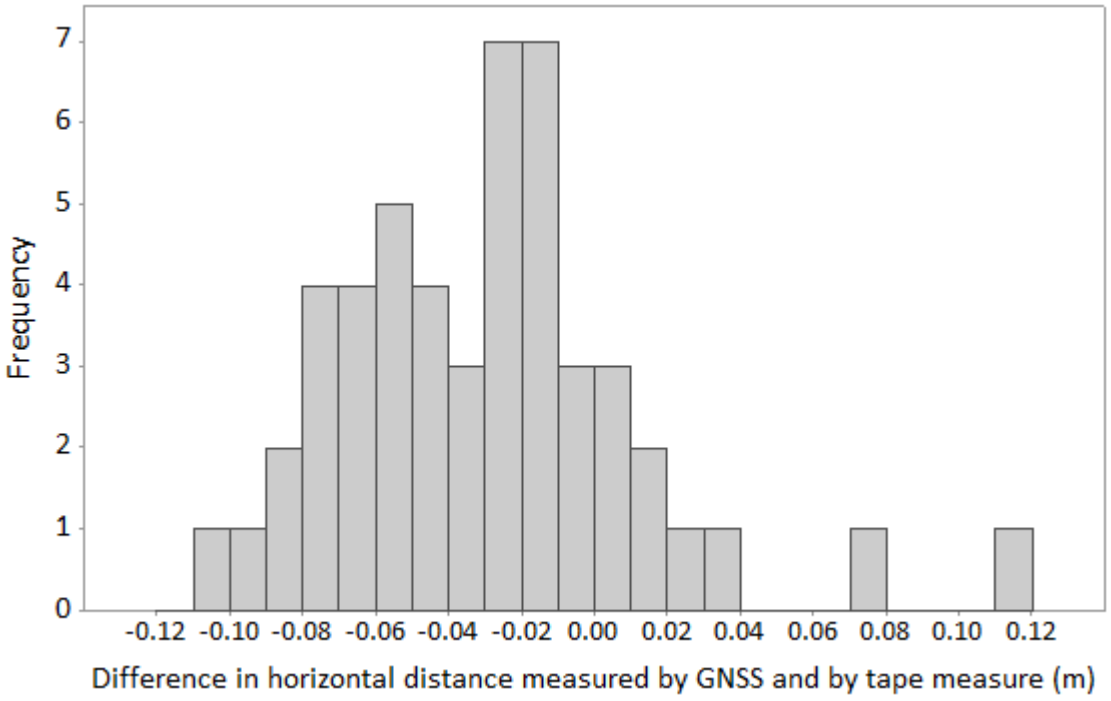

Figure 3.9: Differences between horizontal distance between the start and end point of transects measured by GNSS and by tape measure (n = 50)

3.4 Discussion

3.4.1 Evaluation of topographic models

This study was the first to evaluate SfM photogrammetry of UAV imagery as a method for quantifying rocky shore rugosity. Production of topographic models under different processing parameters showed that compression of source imagery had a considerable negative impact on accuracy. Image compression is desirable to increase processing speed and reduce the size of the output models, but the results of this study suggest that image compression should not be applied if the models need to faithfully represent fine-scale topographic detail. In contrast, depth filtering did not appear to affect accuracy significantly or in a consistent way. The aim of depth filtering is to reduce 'noise' in topographic models by eliminating outlier points above or below the connected surface, mild depth filtering is recommended for scenes with a lot of vertical variation and aggressive depth filtering for scenes with relatively smooth topography (Agisoft LLC, 2017). Aggressive depth filtering produced more accurate results with the red edge imagery, but the models derived from this imagery had lower accuracy overall than the models derived from RGB or combined imagery and the transect profiles showed that there is a lot of 'noise' in the red edge imagery. It is therefore likely that aggressive filtering was necessary with this dataset, but that mild or moderate depth filtering would be a more appropriate choice for modelling rocky shores

which often have high vertical variation due to the presence of boulders and channels, as was the case here.

The analysis also showed that file format affects model accuracy. Although DEMs had comparable vertical accuracy to the ultra-high point cloud from which they were created, the rugosity RMSE values of DEMs were higher than those of their source point clouds and DEMs were shown to under-estimate rugosity by 'smoothing' the fine topographic detail captured in the point clouds. DEMs are more widely used than point clouds or triangular irregular networks (TINs) in spatial ecology and geoscience applications due to advantages including faster processing speed, data availability and more consistent, comparable outputs, but surface area measurements derived from DEMs tend to be lower and less accurate than those derived from vector data (Jenness, 2004). Until recently, DEMs were the only format in which topographic data could be interpreted using object-based image analysis (OBIA), but recent developments in commercial software will in future enable the analysis of point clouds using OBIA (Blaschke and Tomljenovic, 2017). Although this novel technology was not available at the time of this investigation, these results suggest that it would be beneficial for future studies to evaluate the use of OBIA with point clouds derived from photogrammetry for marine habitat mapping.

Comparison with ground truth data showed that all the topographic models had a high level of vertical accuracy. RMSE vertical accuracy values ranged from 0.061m to 0.128m, and the mean vertical accuracy for the models created without compressing the source imagery was 0.07m ± 0.01m. These results compare favourably with those of other studies which applied SfM photogrammetry to UAV imagery in different environments, achieving vertical RMSE of 0.021m – 0.171m (Harwin and Lucieer, 2012), 0.038m – 0.046m (Goncalves and Henriques, 2015), 0.11m (Mancini *et al.*, 2013), 0.139m (Ouedraogo *et al.*, 2014) and 0.29m (Hugenholtz *et al.*, 2013). Harwin and Lucieer (2012) demonstrate that the density of GCPs has a major influence on vertical accuracy, but there are several other methodological differences between these studies which could affect vertical accuracy, such as ground sampling distance, type of camera (compact/DSLR), capture of oblique imagery, image overlap and resolution and format of processed data. The results also compare favourably with the vertical accuracy achieved by LiDAR surveys, for example 0.17m to 0.26m (Hodgson and Bresnahan, 2004) or 0.03m to 0.25m (Hladik and Alber, 2012).

Despite the high vertical accuracy achieved in this investigation, no correlation was found between rugosity indices derived from manual measurements and those derived from any of the topographic models except for the point clouds created with no compression of source imagery. No previous study has compared long-range photogrammetry with manual methods for calculating rugosity indices, but these findings corroborate studies of close-range photogrammetry which report a tendency for photogrammetric measurements to under-estimate rugosity compared to manual or laser-scanning methods (Friedman *et al.*, 2012; Figueira *et al.*, 2015) and to overestimate rugosity at low rugosity values (Frost *et al.*, 2005). However, inconsistencies between manual and photogrammetric measurements of rugosity may also be due to sources of error in the manual measurements, which are discussed below.

3.4.2 Sources of error and uncertainty

Although manual 'chain-and-tape' measurements were used as reference values for comparison with photogrammetric measurements, sources of error and uncertainty in this method are likely to have contributed to the observed inconsistencies between measurements. The observed differences between manual and photogrammetric transect lengths (D_{chain}) could be caused by not holding the tape measure completely taut or level. This is likely to be a major contributing factor to the 0.05m RMSE D_{chain} values (Table 3.2). Other potential sources of discrepancy between manual and photogrammetric measurements include failing to lay the chain in a perfectly straight line and allowing an open-linked chain to bunch up under its own weight, both of which lead to overestimation of rugosity (Friedman *et al.*, 2012).

A benefit of the chain-and-tape method is the ability to capture overhanging areas provided that they are small enough to be accessible and that care is taken to follow their contours when laying the chain. Overhangs were present on 18 of the 50 transects (Figure 3.7, bottom left plot), the majority of which consistently had lower rugosity indices derived from photogrammetry than from manual measurements. This is likely to be a source of inconsistency between manual and photogrammetric measurements in this study.

3.4.3 Methodological improvements

Accuracy and precision of terrain models derived from UAV photogrammetry can be improved by reducing ground sampling distance, obtaining oblique as well as nadir imagery

and increasing GCP density (Harwin and Lucieer, 2012; Micheletti *et al.*, 2015). Future studies could evaluate whether these methodological adjustments improve the consistency between manual and photogrammetric rugosity measurements, and at what cost in terms of data collection and processing time. A critical limitation of UAV photogrammetry for evaluating rugosity which is unlikely to be overcome by improvements in sensor technology is the difficulty of capturing overhangs. Flying at lower altitude and capturing oblique imagery may help to some extent, but for complex sites a combination of long-range and short-range photogrammetry may be the best way to capture topographic detail.

Linear indices were used in this study for pragmatic reasons, but rugosity is not isotropic and 2-dimensional indices are not the best way of measuring 3-dimensional topographic heterogeneity. Frost et al. (2005) recommend making as many chain-and-tape measurements as logistically feasible to compensate for this. Furthermore, the appropriate scale for measuring topographic complexity varies with the species or system being studied (McCormick, 1994; Beck, 1998) so multiple metrics of topographic complexity often have to be combined (Gratwicke and Speight, 2005; Wilson *et al.*, 2007b). This comparison of linear rugosity indices provides useful insight into levels of consistency between photogrammetric and manual measurements and into the optimum parameters for producing 3D models from UAV imagery for assessing rugosity. With this understanding, more sophisticated and robust techniques can be applied to 3D models to derive rugosity indices relevant to the ecological question being studied. At the simplest level, multiple linear measurements at different scales and in different directions could be taken in order to represent 3D rugosity, achieving a sampling density that would not be possible using manual techniques. Other measures could include calculating scale-invariant fractal dimensions, root mean square height or the index between surface area and projected planar area (Leon *et al.*, 2015) or calculating 2- or 3-dimensional rugosity indices in which rugosity is decoupled from slope by projecting the surface onto a plane of best fit (Friedman *et al.*, 2012; Du Preez, 2015)

3.4.4 Cost, time and ease of use

The cost of a senseFly eBee equipped with cameras and flight planning and image processing software ranged from GBP 19,800 – 22,200 in 2017. However, a range of portable aerial platforms are available to suit different budgets, and include balloons and kites as well as remotely-controlled or pre-programmed fixed wing or rotary UAVs (Colomina and Molina, 2014; Klemas, 2015) so the methods described here could be adapted to lower cost

platforms. Fonstad *et al.* (2013) found that SfM photogrammetry of imagery captured by a hand-held helikite flown at 10m – 70m generated digital elevation models with vertical accuracy of 0.07m ± 0.15m which is comparable with the results of this study, although they do not attempt to derive surface complexity from the models.

This investigation used professional-grade GNSS survey equipment, specialist software for differential correction and a SmartNet user license, which together may be beyond the budget of some potential users. The majority of studies into applications of UAVs for topographic modelling use similar professional-grade equipment with either real time kinematic processing or post-processing, but Bryson *et al.* (2013) used a consumer-grade hand-held GPS to record ground control locations, reporting low 'global accuracy' with residual errors of over 1m relative to absolute coordinates, but high 'local accuracy' with errors of just a few cm relative to other points in the model. Accurate georeferencing relative to an absolute coordinate system was necessary in this study to ensure like-for-like comparison of rugosity measurements, but for some applications good 'local' accuracy would suffice, removing the need for high-cost GNSS equipment.

Although the two flights lasted only eleven minutes each, the complete process of collecting aerial imagery, including flight programming, distributing GCPs, downloading data between flights, took a team of four people around three hours. The process of manually aligning images with GCP coordinates took around one hour per set of imagery, based on seven GCPs present in at least seventy images per flight, i.e. less than 1 minute per image. Image processing time depended on the quality setting used, requiring less than one hour to create a point cloud at medium density, around four hours at high density and around twelve hours at ultra-high density. However, this is an automated process and the operator can carry out other tasks while the software is processing the data so this has no implications in terms of staff costs. Once the point clouds had been generated, the additional time taken to create TINs and DEMs was negligible. Processing time was not affected by choice of depth filtering parameter or by the number of photographs. The computer used for image processing had 64 GB RAM, an Intel® Xeon® 2.4 GHz processor and an NVIDIA GeForce GTX 780 graphics processing unit. Collection of rugosity measurements using manual methods took two people around twelve hours, spread over three days. Given the time restrictions imposed by the tidal cycle, reducing data collection time is a greater priority than reducing automated processing time when working in this environment.

3.4.5 Wider implications

SfM photogrammetry of UAV imagery has potential to meet the growing need for non-invasive, rapid, cost-effective topographic survey methods, particularly in environments with limited accessibility such as the intertidal zone. Growing affordability of data capture platforms and data processing software mean that these methods are likely to be increasingly widely used in future, but Micheletti *et al.* (2015) caution that "the high level of automation of SfM data processing creates both opportunities and threats, particularly because user control tends to focus upon visualisation of the final product rather than upon inherent data quality". The aims of this research were to evaluate consistency between rugosity indices derived from photogrammetry and those derived from manual measurements and to assess the influence of data processing parameters on this consistency. This study found that only point clouds created without prior compression of source imagery generated rugosity indices that were significantly correlated with manual measurements, and that even where correlation was observed, there was considerable scatter of data points. This suggests a need for caution if attempting to quantify fine-scale rugosity from terrain models created using long-range photogrammetry.

One of the aims of this thesis is to evaluate OBIA methods of interpreting UAV imagery to map temperate intertidal habitats through an experimental field study which is described in the next chapter. Inclusion of topographic information from LiDAR has been shown to improve the accuracy of predictive habitat maps in both marine and terrestrial environments (Chust *et al.*, 2008; Medcalf *et al.*, 2014b). This accuracy assessment of terrain models derived from UAV photogrammetry has helped to quantify the confidence with which these models and potential derivatives, such as slope, can be used for intertidal habitat mapping. Despite variability between manual and photogrammetric rugosity measurements, decimetre-scale topographic features were consistently detectable in all the terrain models created by SfM photogrammetry of UAV imagery, including the DEMs which are the current preferred format for OBIA. These high resolution terrain models can therefore inform ecological analysis and predictive mapping on intertidal temperate reefs, where sub-metre scale topographic complexity has been shown to influence the distribution and behaviour of species communities (Johnson *et al.*, 1997; Guichard *et al.*, 2000).

3.5 Conclusions

This study demonstrates the potential benefits of SfM photogrammetry and UAV technology methods for topographic survey in intertidal environments and their current limitations for measuring centimetre-scale terrain rugosity. Ongoing improvements in sensor technology can only increase the benefits and may help to overcome some of the limitations, particularly in combination with methodological adjustments such as increasing the number of GCPs and reducing ground sampling distance.

The methods described here have particular benefits in the intertidal environment due to its dynamic nature, high spatial heterogeneity and limited accessibility. Fine-scale topographic models are a valuable tool for ecological analysis and spatial planning in this environment, in which species communities exhibit strong fidelity to vertical zones with specific periods of emersion and immersion. However, these methods are far more widely applicable and have considerable potential to inform conservation monitoring and environmental decision-making in a range of habitats. As SfM methods become more accessible and increasingly automated, it is crucial that data, workflows and outputs continue to be critically evaluated in order to ensure robust and ecologically meaningful final products.

Chapter 4: Mapping temperate intertidal habitats from UAV imagery: a comparison of OBIA methods

4.1 Introduction

Temperate intertidal rock reefs support high levels of biodiversity and provide important ecosystem services (Wilson *et al.*, 2005). They are susceptible to anthropogenic degradation due to pollution, resource extraction, introduction of non-native species and modification of coastal processes through development, but are more amenable to management than subtidal benthic habitats (Thompson *et al.*, 2002). International legislation calls for the conservation of temperate reefs and evaluation of their condition in response to human-induced pressures (EC, 1992; EC, 2008). Intertidal habitat mapping is a widely used tool for informing the designation and monitoring of intertidal protected areas, and such maps have predominantly been produced through a combination of field survey and manual interpretation of aerial imagery (Bunker *et al.*, 2001; JNCC, 2004; Wyn *et al.*, 2006). These methods can produce accurate maps, but are time-consuming and prone to subjectivity (Ekebom and Erkkila, 2003; Thorner *et al.*, 2013).

Automated interpretation of remote sensing data provides a cost-effective, consistent way of generating contiguous habitat or land cover maps for large areas (Kerr and Ostrovsky, 2003; Turner *et al.*, 2003; Aplin, 2005; Wang *et al.*, 2010). The adoption of remote sensing techniques for the coastal zone has lagged behind applications in the terrestrial and marine environments, largely due to the low temporal and spatial resolution of hitherto available data (Cracknell, 1999; Malthus and Mumby, 2003; Peterson *et al.*, 2003). Temperate intertidal reefs have very high spatial and temporal heterogeneity; complex interactions of abiotic and biotic factors influence the distribution of species communities, which may also undergo seasonal change, cyclical succession and rapid response to stochastic weather events (Hartnoll and Hawkins, 1980). Unless remote sensing data are collected to order, the probability of obtaining imagery of the intertidal area under optimal tidal, seasonal and weather conditions is extremely low (Thomson *et al.*, 2003).

However, some advantages of remote sensing are particularly relevant to the intertidal environment. Extensive areas of coastline are inaccessible for ground survey, making remote sensing the only practical option for surveillance and monitoring. Remote sensing can produce elevation data with high vertical resolution which can be used to improve the

accuracy of terrestrial habitat maps (Mucher *et al.*, 2013; Mucher *et al.*, 2015; Rapinel *et al.*, 2015); such data are especially useful in the intertidal environment in which species communities exhibit strong fidelity to vertical zones with specific periods of emersion and immersion (Chust *et al.*, 2008). Intertidal habitats have high spectral diversity due to the distinct combinations of photosynthetic and accessory pigments found in red, green and brown algal species, and the results of *in situ* spectral analysis highlight the potential for separating seaweed communities or even individual species from optical remotely sensed data (Zacharias *et al.*, 1992; Smith and Alberte, 1994; Kotta *et al.*, 2014).

Relatively few studies have been published on the automated interpretation of remote sensing data for intertidal habitat mapping. While a few have used satellite imagery (Larsen *et al.*, 2004; Lucas *et al.*, 2011; Lyons *et al.*, 2012), the majority used airborne remote sensing for its finer spatial resolution and the flexibility to collect data at optimal times, with a notable preference for hyperspectral imagery (Bajjouk *et al.*, 1996; Hunter and Power, 2002; Thomson *et al.*, 2003; Garono *et al.*, 2004; Hennig *et al.*, 2007; Garono *et al.*, 2008; Oppelt *et al.*, 2012; Valle *et al.*, 2015). Hyperspectral sensors have a high number of narrow bands able to discriminate vegetation on subtle differences in spectral response, but data collection is expensive and the computational cost of data storage and processing is high. Unmanned aerial vehicles (UAVs) offer an increasingly cost-effective and flexible means of data collection (Eisenbeiss and Sauerbier, 2011; Mancini *et al.*, 2013; Colomina and Molina, 2014), but to date only one study has interpreted UAV imagery for intertidal habitat mapping (Burrows *et al.*, 2014), although several have evaluated UAV technology for monitoring intertidal topography (Perez-Alberti and Trenhaile, 2014; Goncalves and Henriques, 2015; Ierodiaconou *et al.*, 2016) or intertidal species (Konar and Iken, 2017; Murfitt *et al.*, 2017).

The majority of intertidal habitat mapping studies used pixel-based classification methods, notably the Maximum Likelihood Classifier and/or Spectral Angle Mapper techniques for supervised classification (Hunter and Power, 2002; Hennig *et al.*, 2007; Chust *et al.*, 2008; Lyons *et al.*, 2012; Oppelt *et al.*, 2012; Burrows *et al.*, 2014), ISODATA cluster analysis for unsupervised classification (Larsen *et al.*, 2004), or a combination of these supervised and unsupervised methods (Thomson *et al.*, 2003; Garono *et al.*, 2004; Garono *et al.*, 2008).

Only one of the above studies discusses any limitations of a pixel-based approach, namely the patchy ‘salt-and-pepper’ effect of classifying individual pixels and the ‘edge effect’ of

misclassified pixels at habitat boundaries (Hennig *et al.*, 2007). Object-based image analysis (OBIA) overcomes these problems, enabling users to create ecologically meaningful objects at multiple, hierarchical levels and to classify them using combinations of spectral, geometric and contextual properties (Hay and Castilla, 2006; Blaschke, 2010). These benefits over traditional pixel-based approaches hold promise for the development of OBIA methods for mapping the complex and dynamic intertidal environment, but to date few studies have been published on the application of OBIA methods for mapping the distribution of intertidal habitats (de Oliveira *et al.*, 2006; Lucas *et al.*, 2011). Commercially available OBIA software enables users to apply ecological knowledge to develop sequential rule-sets using Boolean operations and membership functions to separate classes (Lucas *et al.*, 2011), as well as offering a range of standard algorithms for supervised classification that can be trained with samples (Trimble, 2014). The standard nearest neighbour (SNN) classifier is a widely used method which assigns objects to the class of the sample they most closely resemble within a given feature space; this supervised classifier has been used for habitat mapping in terrestrial and, more recently, marine environments (Conchedda *et al.* (2008), Lucieer *et al.* (2013), Na *et al.* (2015), Stephens and Diesing (2014), Varela *et al.* (2008), Zhang (2015)). Random forests (RF) is an ensemble classifier that creates a number of classification and regression trees (CARTs), each trained by a subset of training data with randomly sampled variables, and classifies objects as the class assigned by the majority of trees in the forest (Breiman, 2001). RF has grown in popularity for classifying remote sensing data due to its processing speed, classification accuracy and ability to handle a large number of variables (Belgiu and Dragut, 2016). Although it is a more recent and less well documented addition to the commercial OBIA toolkit than the SNN classifier (Trimble, 2014), several studies have evaluated the RF classifier through applications to various types of remote sensing data and environments, finding it compares favourably with other supervised classification algorithms (Wahidin *et al.*, 2015; Li *et al.*, 2016; Onojeghuo and Onojeghuo, 2017), with pixel-based approaches (Jhonnerie *et al.*, 2015) and with manual methods (Husson *et al.*, 2016).

The thematic resolution of intertidal habitat maps produced from remote sensing data varies; some studies map only physical characteristics (Lucas *et al.*, 2011; Thorner *et al.*, 2013), the majority map broadscale habitats e.g. seagrass, red, brown or green algae, (Hunter and Power, 2002; Thomson *et al.*, 2003; Garono *et al.*, 2004; Larsen *et al.*, 2004; Hennig *et al.*, 2007; Garono *et al.*, 2008) and only a few have attempted to map individual

species or communities (Bajjouk *et al.*, 1996; de Oliveira *et al.*, 2006; Chust *et al.*, 2008; Valle *et al.*, 2015). To our knowledge, none has yet attempted to apply an existing national or international standard habitat classification system.

The aim of this research is to evaluate object-based methods of interpreting very high resolution UAV imagery to map the extent and distribution of temperate intertidal rock reef habitats. Specific objectives are (1) to develop OBIA workflows to produce intertidal habitat maps at broad and fine thematic scales using a SNN classifier, a RF classifier and a knowledge-based rule set, (2) to evaluate the accuracy of all three methods by validating the output maps against ground truth data; (3) to evaluate the consistency of the SNN and RF methods by 2-fold cross validation and (4) to evaluate the reproducibility of all three methods by applying them to a separate dataset of UAV imagery.

4.2 Methodology

4.2.1 Study site

The study site is Kettleness headland in Runswick Bay Marine Conservation Zone (54° 32.050' N, 0° 42.800' W), the same location as the study site for chapter 3 (Figure 3.1). Kettleness is a north-facing headland, exposed to prevailing wind and wave action. Due to the high exposure, the fucoid canopy is reduced and the mid-shore dominated by turf-forming red seaweeds, predominantly *Osmundea pinnatifida* and *Corallina officinalis*, while the upper shore is dominated by dense communities of the barnacle *Semibalanus balanoides*. Tides are diurnal with a mean tidal range of 4.8m on spring tides and 2.4m on neap tides.

4.2.2 Data acquisition and processing

Reference data

Reference data for training and validation were collected between April and July 2015 from 164 locations selected by stratified random sampling based on four shore height strata derived from LiDAR data, and in March 2016 from a further 100 locations selected by stratified random sampling based on five shore rugosity strata derived from a digital elevation model (see chapter 3). Biotopes were assigned to each sample using the Marine Habitat Classification for Britain and Ireland v04.05 (Connor *et al.*, 2004). Broadscale habitat classes of red algae, green algae, brown algae and barnacles were assigned to a subset of

samples; they could not be assigned to every sample because some samples contained a mixture of classes, for example red and brown algae. The biotopes recorded in the reference data are shown in Table 4.1 with the number of samples assigned to each biotope and the abbreviations that will be used to refer to these biotopes throughout this chapter.

Table 4.1: List of biotopes recorded through ground survey at Kettleness headland

Biotope code	Biotope name	Abbreviation	Samples
LR.HLR.FR.Osm	*Osmundea pinnatifida* on moderately exposed mid eulittoral rock	Osm	59
LR.HLR.FR.Coff	*Corallina officinalis* on exposed to moderately exposed lower eulittoral rock	Coff	47
LR.HLR.MusB.Sem	*Semibalanus balanoides* on exposed to moderately exposed or vertical sheltered eulittoral rock	Sem	43
LR.HLR.MusB.Sem.FvesR	*Semibalanus balanoides*, *Fucus vesiculosus* and red seaweeds on exposed to moderately exposed eulittoral rock	FvesR	42
IR.MIR.KF.Ldig.Ldig	*Laminaria digitata* on moderately exposed sublittoral fringe bedrock	Ldig	23
None	No biotope assigned due to insufficient fauna and flora	Bare rock	12
LR.MLR.BF.FvesB	*Fucus vesiculosus* and barnacle mosaics on moderately exposed mid eulittoral rock	FvesB	10
LR.MLR.BF.Fser.R	*Fucus serratus* and red seaweeds on moderately exposed lower eulittoral rock	Fser.R	9
LR.FLR.Eph.Ent	*Enteromorpha* spp. on freshwater-influenced and/or unstable upper eulittoral rock	Eph.Ent	7
LR.FLR.Rkp.Cor.Cor	Coralline crusts and *Corallina officinalis* in shallow eulittoral rockpools	Cor	6
LR.FLR.Rkp.FK	Fucoids and kelp in deep eulittoral rockpools	Rkp.FK	4
LR.MLR.BF.FSpiB	*Fucus spiralis* on exposed to moderately exposed upper eulittoral rock	FSpiB	2
	Total number of samples:		264

Percentage cover of seaweed species, barnacles and bare rock was recorded using a 0.25m^2 quadrat for the samples collected in 2015. Hierarchical cluster analysis was applied to these data based on a Bray-Curtis similarity matrix using PRIMER v.7 (Clarke *et al.*, 2014). The resulting cluster dendrogram and non-metric MDS plot produced habitat classes that were very closely correlated with the biotopes assigned to the samples, so the classes created through cluster analysis were not used in the mapping process. The coordinates of every sample were recorded using a Leica Viva GS10 high-precision receiver (Leica Geosystems), which recorded one observation per second for three minutes. The logged coordinates were differentially corrected in Leica Geo Office software (Leica Geosystems) using reference data from the Global Navigation Satellite System (GNSS) base station network downloaded from

Leica's SmartNet website (http://uk.smartnet-eu.com/) in RINEX format. The processed coordinates had a horizontal and vertical accuracy of between 0.001m and 0.003m.

Aerial imagery

Aerial imagery was collected during low spring tides on the 3rd July and 1st September 2017 using a senseFly eBee UAV (www.sensefly.com/drones/ebee). As in the previous chapter, flights were pre-programmed to collect imagery at 0.04m ground sampling distance with 60% lateral overlap and 75% forward overlap between images. Perpendicular intersecting flight lines maximised image overlap and reduced the impact of crosswinds on image acquisition. Two flights were conducted on each date, one using a Canon IXUS 127 HS 16.1 megapixels camera to capture red-green-blue (RGB) imagery (390nm to 700nm) and one using a Canon Powershot ELPH 110 HS 16.1 megapixels camera to capture red edge imagery (680nm to 750nm). Seven ground control points (GCPs) were placed within the survey area during all flights and their coordinates logged and post-processed as described above. A summary of image acquisition is provided in Table 4.2. There was no cloud cover during any of the flights.

Table 4.2: Flight and imagery details of UAV surveys conducted on 3rd July and 1st September 2015

Date	Camera	Flight times (GMT+1)	Tide height above Chart Datum (m)	Number of images	Survey Area (km^2)	Mean Ground Sampling Distance (m)
3/7/2017	RGB	11:49 – 12:00	0.78 – 0.79	113	0.2246	0.0392
3/7/2017	Red Edge	12:23 – 12:34	0.88 – 0.97	133	0.1988	0.0346
1/9/2017	RGB	12:50 – 12:55	0.26 – 0.28	53	0.0946	0.0380
1/9/2017	Red Edge	13:24 – 13:29	0.46 – 0.52	56	0.0827	0.0380

The images were processed using PostFlight Terra 3D software [senseFly] to create orthomosaics and digital elevation models (DEMs) for all four flights at 0.04m resolution. The georeferencing RMS error was 0.011m for the RGB orthomosaic and 0.006m for the red edge orthomosaic. ArcGIS v10.3 [ESRI] was used to clip and align the imagery, to derive slope layers from the DEMs, and to create normalised difference vegetation index (NDVI) layers from the red and red edge bands using the formula:

$$\frac{\text{Red edge} - \text{Red}}{\text{Red edge} + \text{Red}}$$

4.2.3 OBIA workflows

Workflows were created in eCognition Developer v9.0.3 [Trimble] to create habitat maps from both sets of imagery. The first stage of the workflow classified cliffs, sea and shadow to

remove these objects from further classification. eCognition's multi-resolution segmentation algorithm was applied to the DEM using a scale parameter of 120 with homogeneity criteria which weighted shape (0.1) versus colour (0.9) and object compactness (0.5) versus smoothness (0.5), and objects were classified as 'cliff' based on a threshold mean elevation value. A further segmentation was carried out on unclassified objects at scale parameter 90 with homogeneity criteria weighting shape (0.1) versus colour (0.9) and compactness (0.9) versus smoothness (0.1), following which objects were classified as 'sea' based on threshold values of shore height, NDVI and red/green band ratio and as 'shadow' based on threshold values of border contrast with slope, border to cliffs, NDVI, blue and red/blue band ratio.

Three different classification methods were then applied and compared to create habitat maps using a broadscale classification (red, green and brown algae and barnacle/rock) and a classification consisting of the biotopes shown in Table 4.1. The methods evaluated were the Standard Nearest Neighbour (SNN) and Random Forests (RF) algorithms which classify objects based on their similarity to training samples, and a hierarchical knowledge-based rule set which used combinations of Boolean thresholds and membership functions to classify objects. The hierarchical rule-set first classified objects as broadscale habitats, then re-classified red and brown algae as species, then created a new level with larger objects which were classified as biotopes based on the proportion of species within them. eCognition's Sample Editor tool was used with objects selected from the imagery to inform feature selection and the definition of thresholds and membership functions in the knowledge-based rules.

The SNN and RF classifiers were trained using reference data. The samples assigned to each habitat class were divided randomly into two equal subsets, each of which was used in turn for training the classifier, so two maps were produced using each method. eCognition's Feature Space Optimisation tool was used to identify the best combination of ten features for distinguishing habitats using the SNN classifier. The lowest separation distance between habitat classes calculated by Feature Space Optimisation ranged from 3.56 to 4.92 for broadscale habitats and from 2.11 to 2.89 for biotopes. The RF classifier was queried to generate 'importance values' for the features used in the classification, and the classification re-run using the features with a value greater than 0. The feature space used by the SNN and RF classifiers comprised mean (including brightness), mode, standard deviation,

skewness and border contrast of all layers, grey level co-occurrence matrices (GLCM) of the DEM, NDVI and slope layers, and customised features of band ratios.

Segmentation was carried out at scale parameter 10 with a weighting of shape (0.1) versus colour (0.9) and compactness (0.9) versus smoothness (0.1) to produce broadscale habitat maps, and at scale parameter 120 with the same homogeneity criteria weightings to produce biotope maps. A finer segmentation was used for broadscale habitats than for biotopes because there was fine scale heterogeneity of the classes red, green and brown algae and rock, whereas biotopes can comprise a mosaic of algae and rock and should be at least 25m^2 (Connor *et al.*, 2004) so a larger segmentation scale was appropriate for biotope classification.

The OBIA workflows are summarised in Figure 4.1 and the knowledge-based rule set is shown in detail in Appendix 2.

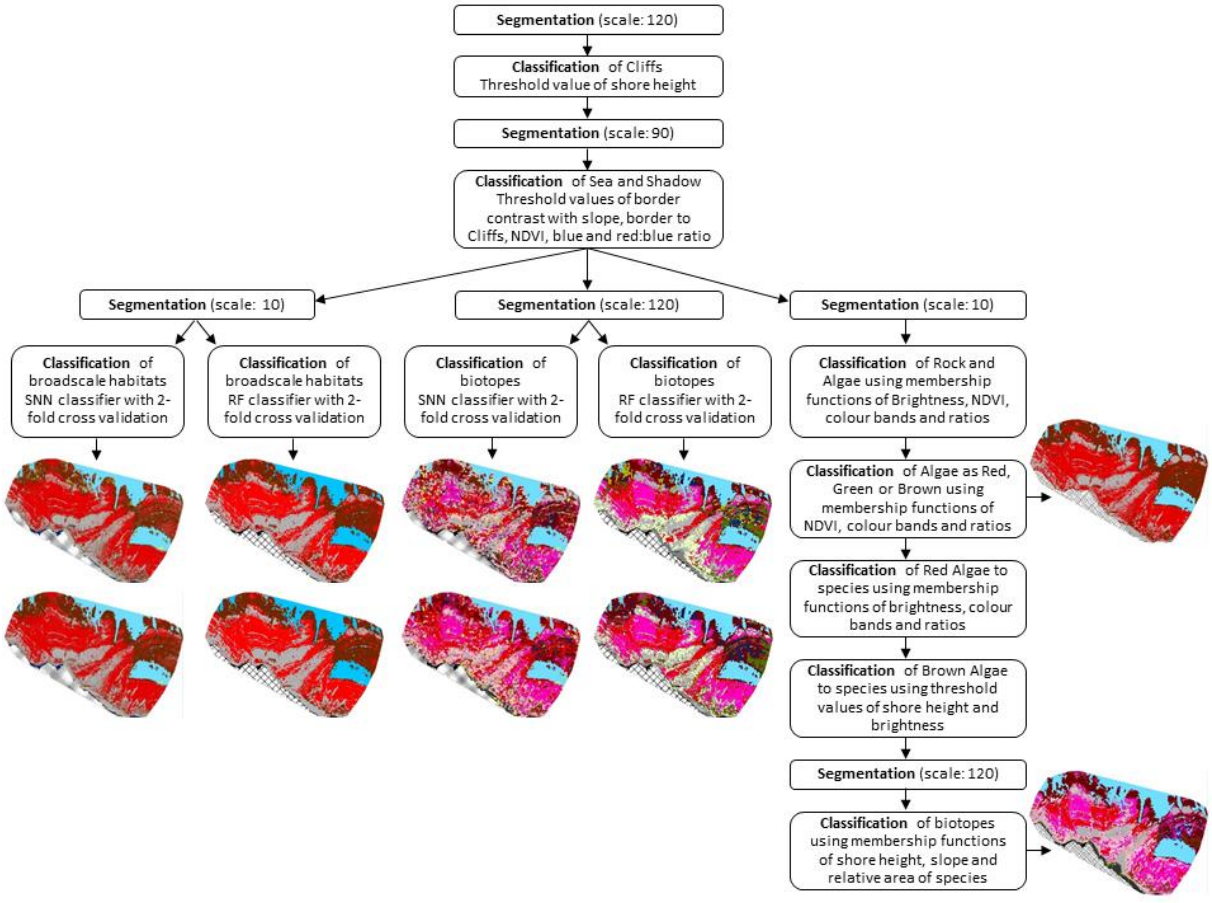

Figure 4.1: Summary of OBIA workflows to produce habitat maps using SNN and RF classifiers and a knowledge-based rule set

4.2.4 Evaluation methods

Overall accuracy, user's and producer's accuracy, Kappa coefficient and balanced error rate were calculated for each map through comparison with the reference data. Classification stability assessments were performed for the maps produced using the SNN classifier. The consistency of the outputs produced by the same classifier using different training data was assessed by calculating the percentage area with the same classification in each pair of maps.

4.3 Results

4.3.1 Broadscale Habitat Maps

Overall accuracy of the broadscale habitat maps ranged from 67.7% ± 8.6% to 94.5% ± 4.5% using the RF classifier, from 80.0% ± 7.1% to 87% ± 10.1 using the SNN classifier, and from 80.6% ± 13.0% to 84.8% ± 14.5% using the knowledge-based rules (Figure 4.2). The Kappa coefficient was largely correlated with overall accuracy. Balanced error rate was not simply inversely correlated with overall accuracy because of the uneven number of samples per habitat class. Maps produced using the SNN classifier with training samples B from the July and September imagery had very similar overall accuracy of 79.7% and 80.0% respectively but balanced error rates of 44.5% and 25.7%. The July validation dataset contained only one sample of green algae and this intersected an object which had been left unclassified, while the September dataset contained two samples, both of which intersected objects classified as green algae resulting in a lower balanced error rate. The 90% confidence intervals ranged from ± 4.8% to ± 7.8% for maps derived from the July imagery and from ± 8.6% to ± 14.5% for maps derived from the September imagery, because fewer ground truth samples were available for the area covered by the September imagery. In all but one case, overall accuracy was lower for broadscale maps derived from September imagery than from July imagery, although the difference was smaller than the 90% confidence interval range.

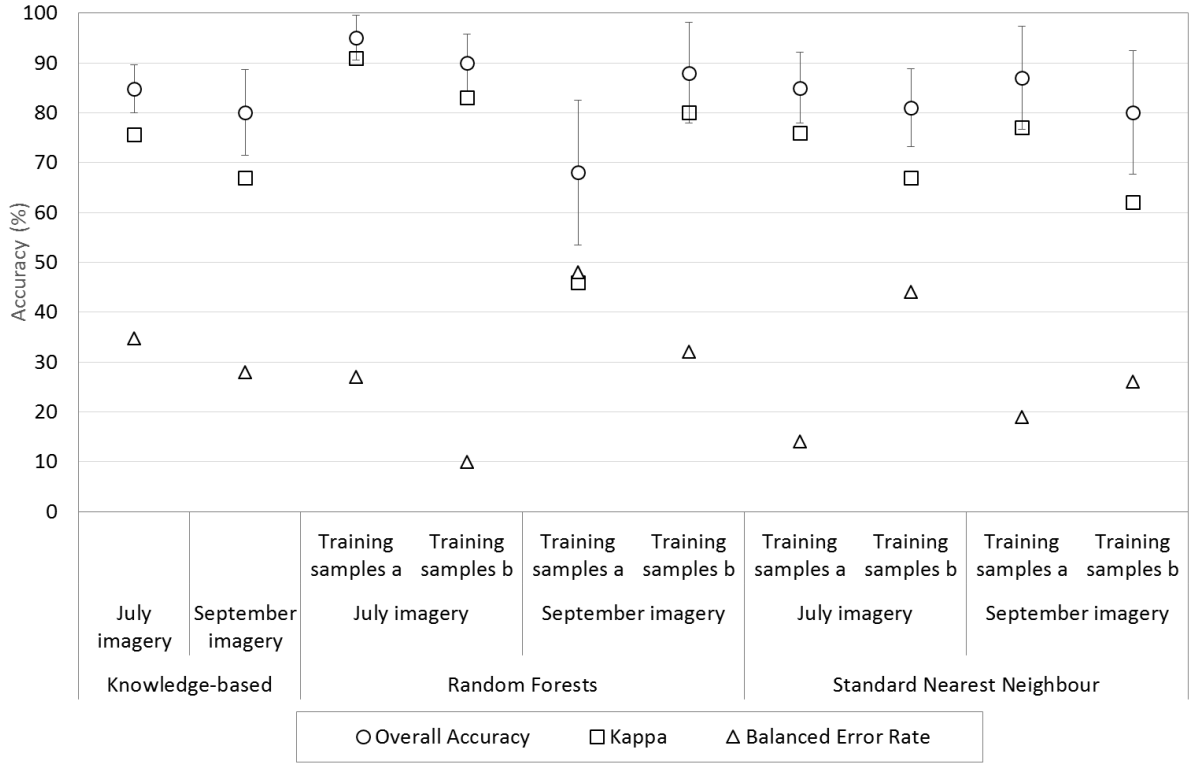

Figure 4.2: Overall accuracy, Kappa coefficient and Balanced Error Rate for broadscale habitat maps produced using the knowledge-based rule set, RF and SNN classifiers. Error bars on overall accuracy represent 90% confidence intervals.

Calculation of user's and producer's accuracy gave further insight into classifier performance (Figure 4.3 and Figure 4.4). Maps produced by the knowledge-based rules had high producer's accuracy for red and brown algae, and high user's accuracy for barnacle/rock, showing that this rule set over-predicted red and brown algae and under-predicted barnacle/rock. The performance of the SNN and RF classifiers varied with training samples. The map produced using the SNN classifier and training samples A from July imagery had high errors of commission for brown algae, while that produced using training samples B had high errors of commission for red algae. Each habitat class in the map produced from July imagery using the RF classifier with training samples A had similar user's and producer's accuracy, indicating an equal level of errors of commission and omission per habitat class. In contrast, the map produced from the same dataset and classifier using training samples B had high errors of commission for red algae and high errors of omission for brown algae. The 90% confidence interval values were very large for some classes, particularly on the maps derived from the September imagery, indicating an insufficient number of ground truth samples.

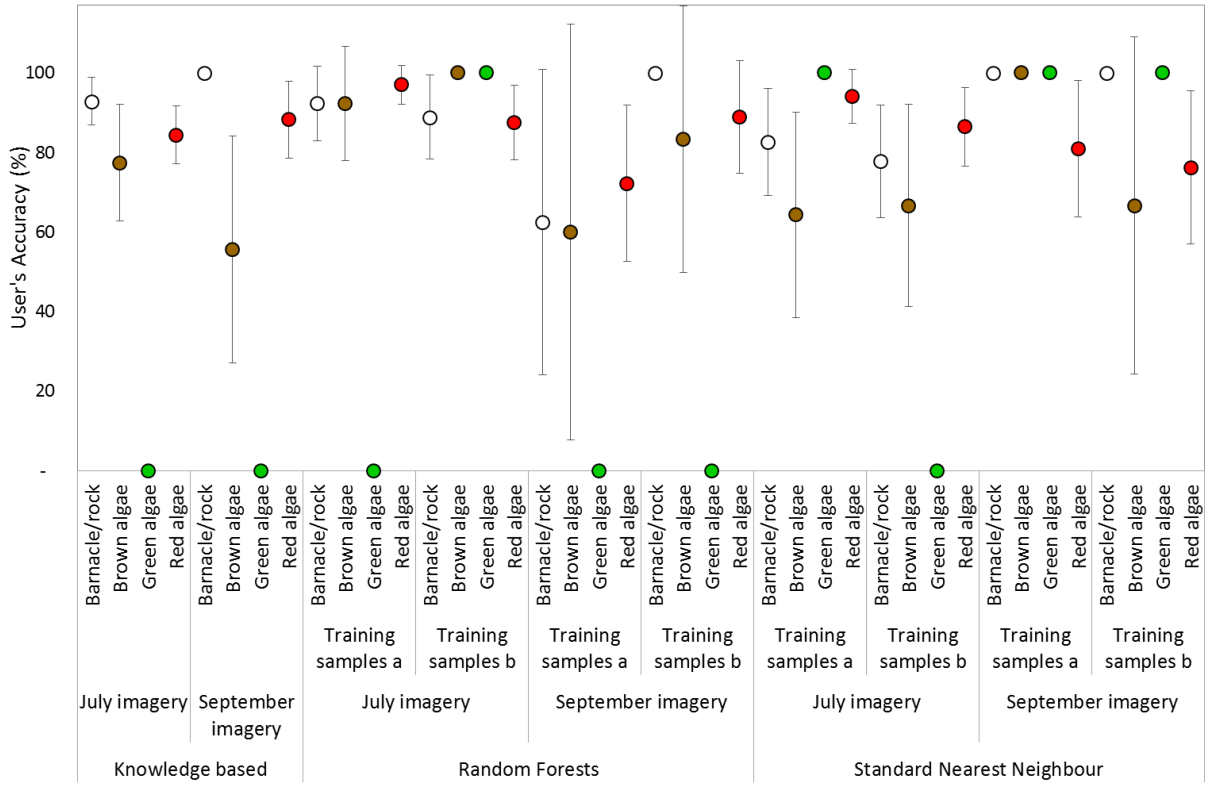

Figure 4.3: User's accuracy for broadscale habitat maps produced using the knowledge-based rule set, RF and SNN classifiers. Error bars represent 90% confidence intervals.

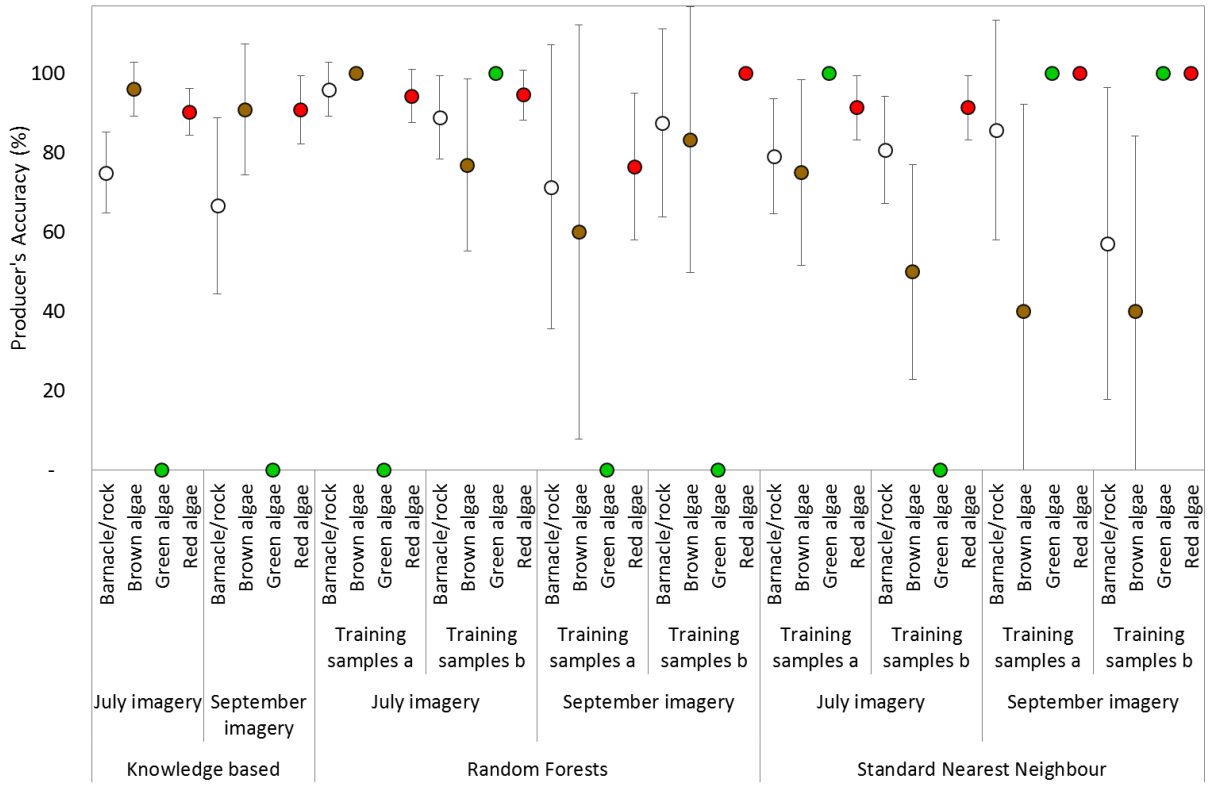

Figure 4.4: Producer's accuracy for broadscale habitat maps produced using the knowledge-based rule set, RF and SNN classifiers. Error bars represent 90% confidence intervals.

The most important features for distinguishing broadscale habitat classes using the RF classifier were the mean and mode of band ratios, DEM and single bands, and standard deviation of band ratios and slope (Figure 4.5).

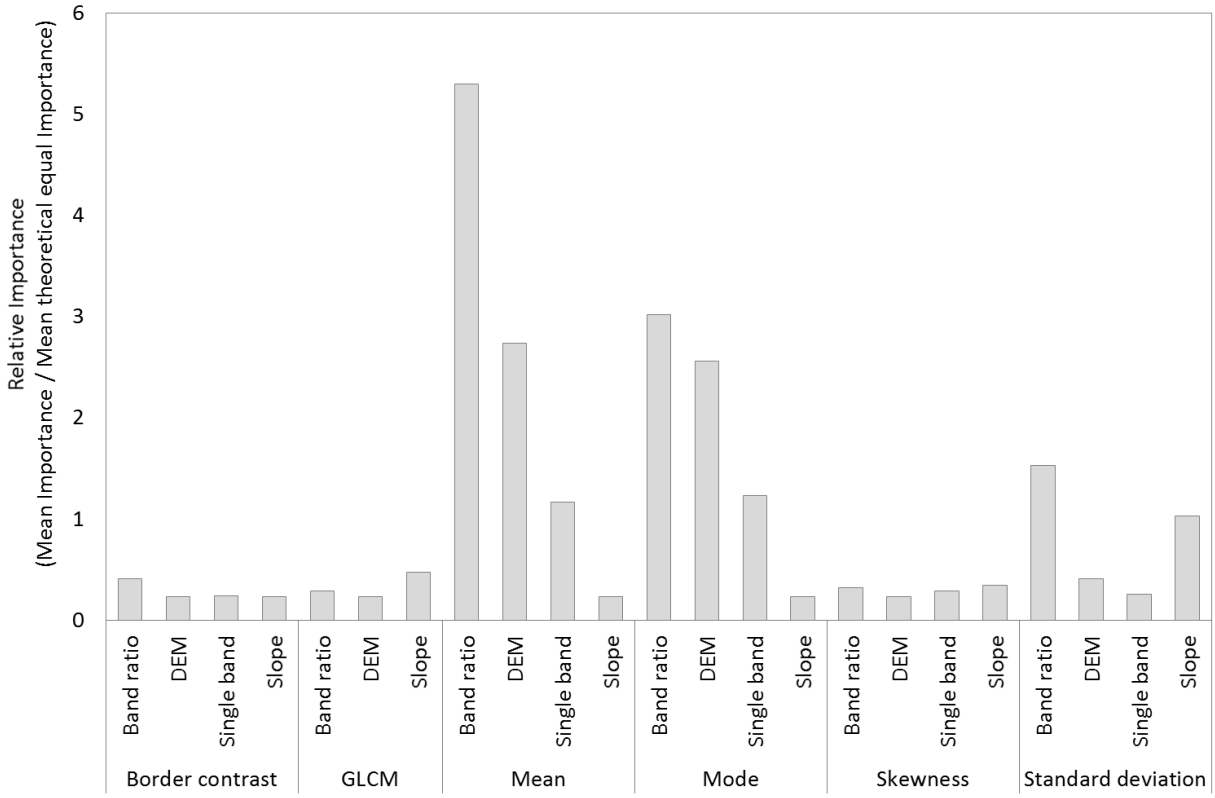

Figure 4.5: Relative importance values of features used in RF classification of broadscale habitat maps (mean importance / mean theoretical equal importance).

Figure 4.6 shows the range of sample values for the three features with the highest importance value used by the RF classifier, illustrating a good level of class separability, particularly when these features were used in combination.

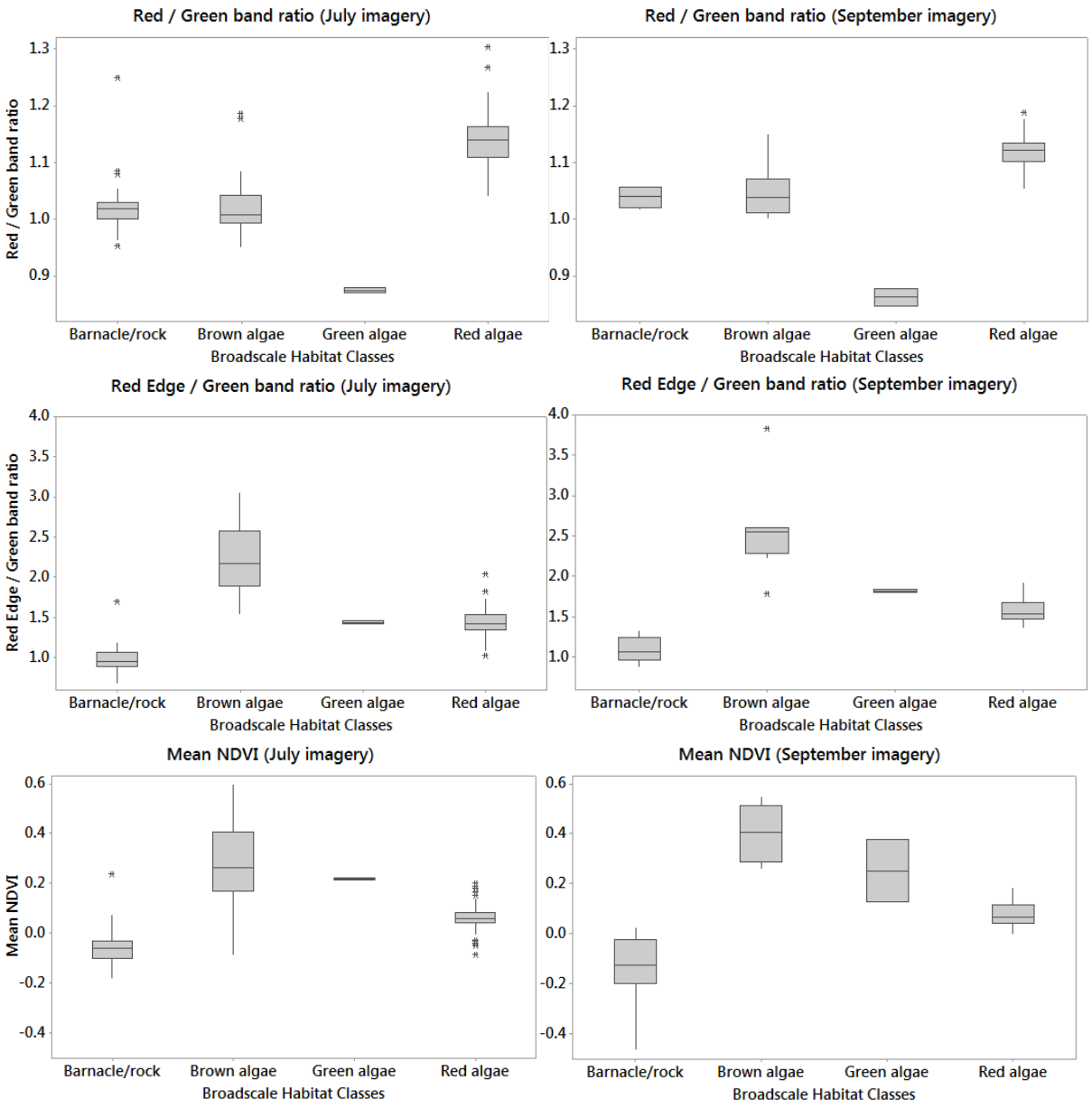

Figure 4.6: Sample values for the three features with highest importance used to create biotope maps using the RF classifier

Figure 4.7 shows the features predominantly selected by Feature Space Optimisation for distinguishing broadscale habitats using the SNN classifier. Some features selected by Feature Space Optimisation also had high importance when used with the RF classifier, notably the mean, mode and standard deviation of band ratios and mean DEM. In contrast, skewness of DEM, single bands and slope were frequently selected by Feature Space Optimisation but had very low importance values when used with the RF classifier. The range of sample values for the three features most frequently selected by Feature Space Optimisation are shown in Figure 4.8, illustrating that mean DEM (which also had high importance value with the RF classifier) provided good class separability, while skewness

DEM and skewness red edge had considerable overlap in the range of sample values for all classes.

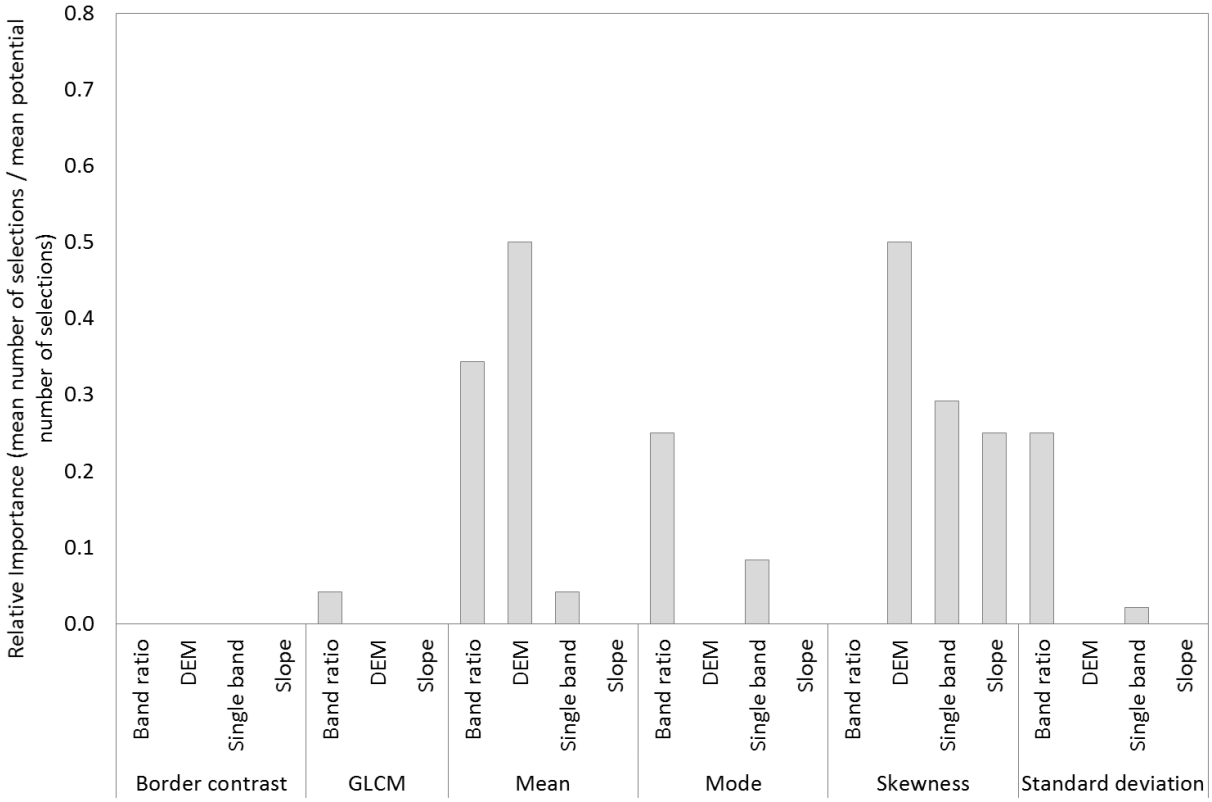

Figure 4.7: Relative importance values of features used to create broadscale maps using the SNN classifier (mean number of selections by Feature Space Optimisation / mean potential number of selections by Feature Space Optimisation).

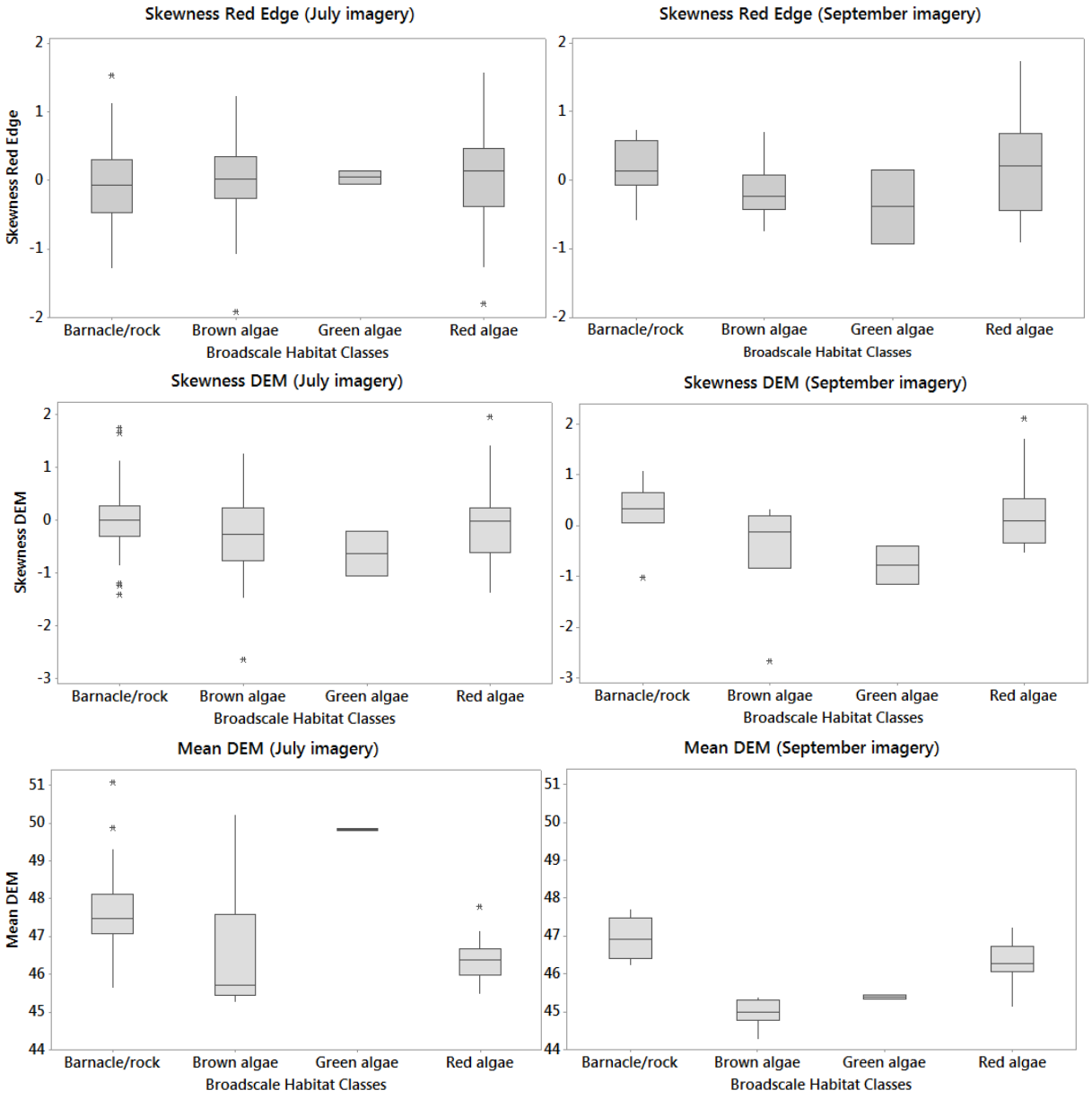

Figure 4.8: Sample values for the three features most frequently selected by Feature Space Optimisation to create broadscale habitat maps using the SNN classifier

Classification stability is the difference between an object's membership value to its assigned class and to the second most similar class. Mean classification stability of broadscale habitats ranged from 0.17 ± 0.14 to 0.36 ± 0.19 (Table 4.3). The mean values suggested a reasonably stable classification (Benz, 2004) but the standard deviation values indicated high variability, showing that for many objects the SNN classifier with this feature space did not provided clear separation of broadscale classes.

Table 4.3: Mean and standard deviation classification stability derived from all classified objects in broadscale habitat maps created using the Standard Nearest Neighbour classifier

Imagery	**July**				**September**			
Training samples	**A**		**B**		**A**		**B**	
Classification stability	Mean	St dev	Mean	St dev	Mean	St dev	Mean	St dev
Red algae	0.27	0.18	0.36	0.23	0.33	0.19	0.29	0.19
Brown algae	0.20	0.14	0.25	0.15	0.30	0.18	0.19	0.13
Barnacle/rock	0.19	0.13	0.23	0.16	0.19	0.14	0.21	0.14
Green algae	0.17	0.14	0.23	0.12	0.21	0.18	0.18	0.16

4.3.2 Biotope maps

There was far greater variability in classifier performance when applied to biotope mapping than broadscale habitat mapping (Figure 4.9). The overall accuracy of the map produced by the knowledge-based rule set from the July imagery was 70.2% ± 13.1% but only 30.9% ± 11.7% for the map produced from the September imagery using the same rule set. Overall accuracy for maps produced by the RF classifier ranged from 53.7% ± 12.1% to 65.6% ± 10.2%, and from 26.8% ± 10.6 to 55.6% ± 8.5% for maps produced by the SNN classifier.

The Kappa coefficient was less closely correlated with overall accuracy than was the case with the broadscale habitat maps; Kappa values were low relative to overall accuracy for the maps derived from September imagery because the ground truth dataset for the September imagery was smaller and contained fewer classes, so the probability of correct classification happening by chance was greater for maps produced from the September imagery. As with the broadscale maps, balanced error rate values were not simply inversely correlated with accuracy, due to the uneven number of samples per habitat class. For example, the two maps created from July imagery using the RF classifier had similar levels of overall accuracy but the map produced using training samples B had a disproportionately high balanced error rate due to misclassification of locally rare habitats. The validation dataset for this map contained only one sample each of the rockpool biotopes Cor and Rkp.FK, both of which intersected objects which have been incorrectly classified. In contrast, the validation dataset for the map produced from training samples A contained two samples of Cor, both of which intersected correctly classified objects, and two samples of Rkp.FK, one of which intersected a correctly classified object.

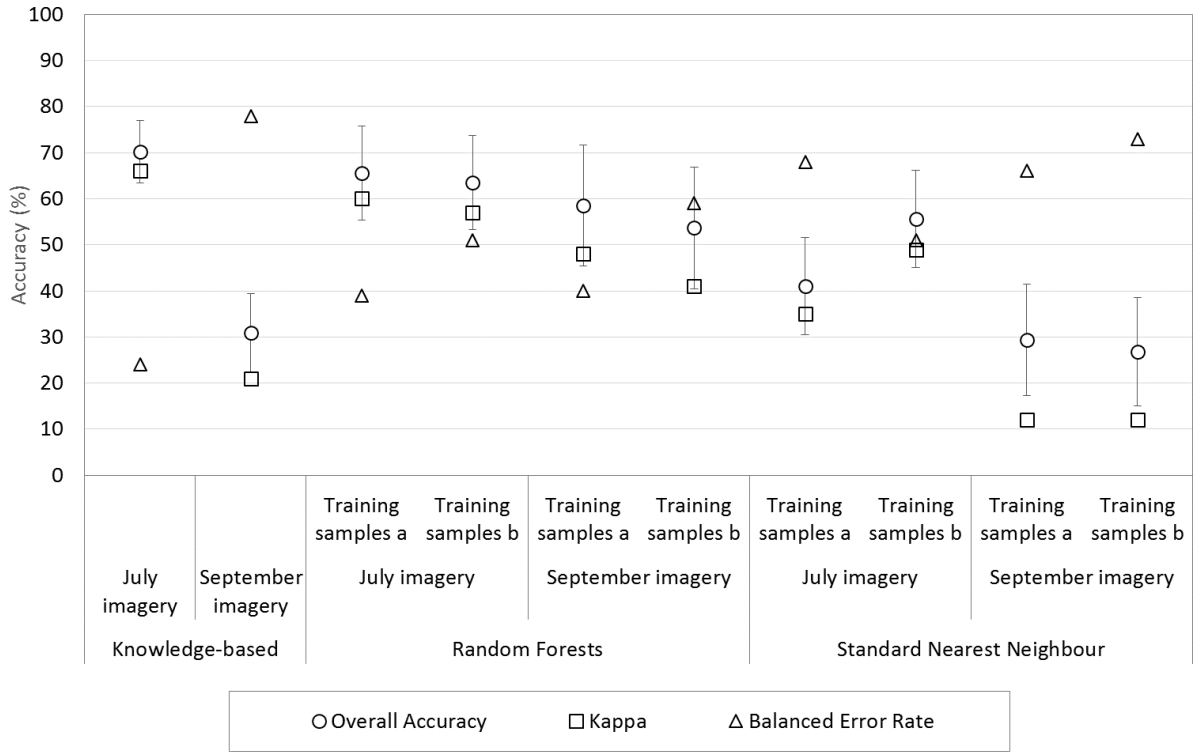

Figure 4.9: Overall accuracy, Kappa and Balanced Error Rate for biotope maps produced from UAV imagery using the knowledge-based rule set, SNN and RF classifiers

User's and producer's accuracy for biotope maps are shown in Table 4.4 and Table 4.5. Due to the low number of ground truth samples for some habitat classes, these values only provided insight into classifier performance with regard to the dominant biotopes Coff, FvesR, Ldig, Osm and Sem (emphasised in bold type in both tables). The RF classifier tended to over-predict the red seaweed dominated biotopes Osm and Coff, while the knowledge-based rule set tended to over-predict the kelp biotope Ldig and the red seaweed biotope Coff, but to under-predict the red seaweed biotope Osm.

Table 4.4: User's accuracy for biotope maps produced using the knowledge-based rule set, RF and SNN classifiers. Empty cells indicate that no objects of that class intersected ground truth points of any class. Grey cells indicate that the class was not mapped due to absence of ground truth samples.

Classifier	**Random Forests**				**Standard Nearest Neighbour**				**Knowledge based**	
Imagery	July		September		July		September		July	Sept
Training samples	A	B	A	B	A	B	A	B		
bare rock	0.67	0.33			0.00	0.50			1.00	
Coff	**0.78**	**0.82**	**0.43**	**0.43**	**0.43**	**0.54**	**0.00**	**0.20**	**0.70**	**0.35**
Cor	1.00					0.33			0.33	0.00
Eph.Ent	1.00	1.00	1.00	1.00			0.00		0.67	
Fser.R				0.00	0.17	0.00	0.00	0.00	0.25	
FspiB						0.00			1.00	
FvesB	1.00	0.60			0.33	0.60			0.86	
FvesR	**0.40**	**0.46**	**0.50**	**1.00**	**0.44**	**0.54**	**0.00**	**0.13**	**0.61**	**0.30**
Ldig	**1.00**	**0.43**	**0.75**	**0.60**	**1.00**	**0.25**	**0.33**	**0.00**	**0.78**	**0.39**
Osm	**0.73**	**0.71**	**0.59**	**0.56**	**0.60**	**0.70**	**0.40**	**0.60**	**0.89**	**0.33**
Rkp.FK	1.00		1.00		1.00	0.50	1.00	1.00	1.00	
Sem	**0.50**	**0.78**	**0.50**	**0.56**	**0.50**	**0.88**	**0.30**	**0.22**	**0.67**	**0.67**

Table 4.5: Producer's accuracy for biotope maps produced using the knowledge-based rule set, RF and SNN classifiers. Empty cells indicate that no validation samples existed for that class. Grey cells indicate that the class was not mapped due to absence of ground truth samples.

Classifier	**Random Forests**				**Standard Nearest Neighbour**				**Knowledge based**	
Imagery	July		September		July		September		July	Sept.
Training samples	A	B	A	B	A	B	A	B		
bare rock	0.50	0.25			0.00	0.25			0.63	
Coff	**0.88**	**1.00**	**0.43**	**0.38**	**0.38**	**0.78**	**0.00**	**0.13**	**0.94**	**0.53**
Cor	1.00	0.00			0.00	1.00			1.00	0.00
Eph.Ent	1.00	1.00	1.00	0.50	0.00	0.00	0.00	0.00	1.00	0.00
Fser.R	0.00	0.00	0.00	0.00	0.50	0.00	0.00	0.00	0.25	0.00
FspiB	0.00	0.00			0.00	0.00			1.00	0.00
FvesB	0.75	0.75			0.50	0.75			0.75	
FvesR	**0.36**	**0.50**	**0.17**	**0.25**	**0.36**	**0.58**	**0.00**	**0.25**	**0.48**	**0.33**
Ldig	**0.75**	**1.00**	**0.75**	**0.75**	**0.25**	**0.33**	**0.25**	**0.00**	**1.00**	**0.88**
Osm	**0.80**	**0.91**	**0.77**	**0.69**	**0.60**	**0.64**	**0.46**	**0.46**	**0.76**	**0.04**
Rkp.FK	0.50	0.00	1.00	0.00	0.50	1.00	1.00	1.00	0.67	0.00
Sem	**0.75**	**0.50**	**0.67**	**0.71**	**0.58**	**0.50**	**0.60**	**0.29**	**0.62**	**0.46**

The extremely low producer's accuracy for the Osm biotope in the map produced by the knowledge-based rules from the September imagery is the main contributing factor to the low overall accuracy of this map. The validation dataset contained 26 samples of Osm, 10 of

which intersected objects misclassified as Coff and 13 of which intersected objects misclassified as Cor. The dominant species of the Osm biotope, *Osmundea pinnatifida* (Hudson) Stackhouse 1809, is known to change frond colour from dark red to pale yellow due to UV exposure (Wells, 2007). The features used to distinguish the Osm, Cor and Coff biotopes in the knowledge-based rules were the green/blue band ratio, red/blue band ratio, mean green, mean blue, mean red edge, mode green, mode blue, mode red edge and brightness. Figure 4.10 shows the range of values for those features in the July and September imagery based on objects overlying ground truth sampling points. For each feature, the range of values for each biotope changed from the July to September imagery, and while the values taken from the July imagery showed good separation of Osm from the Coff and/or Cor biotopes, the values taken from the September imagery showed considerable overlap in value ranges between the Osm and the Coff and/or Cor biotopes. This explains how the changed spectral signature of *Osmundea pinnatifida* between July and September led to misclassification of this locally abundant biotope by the knowledge-based rules and low overall accuracy of the resultant biotope map. The accuracy of the broadscale habitat maps produced by the knowledge-based rules was not affected by this change in spectral signature because both *Osmundea pinnatifida* and *Corallina officinilis* are in the class 'red algae'.

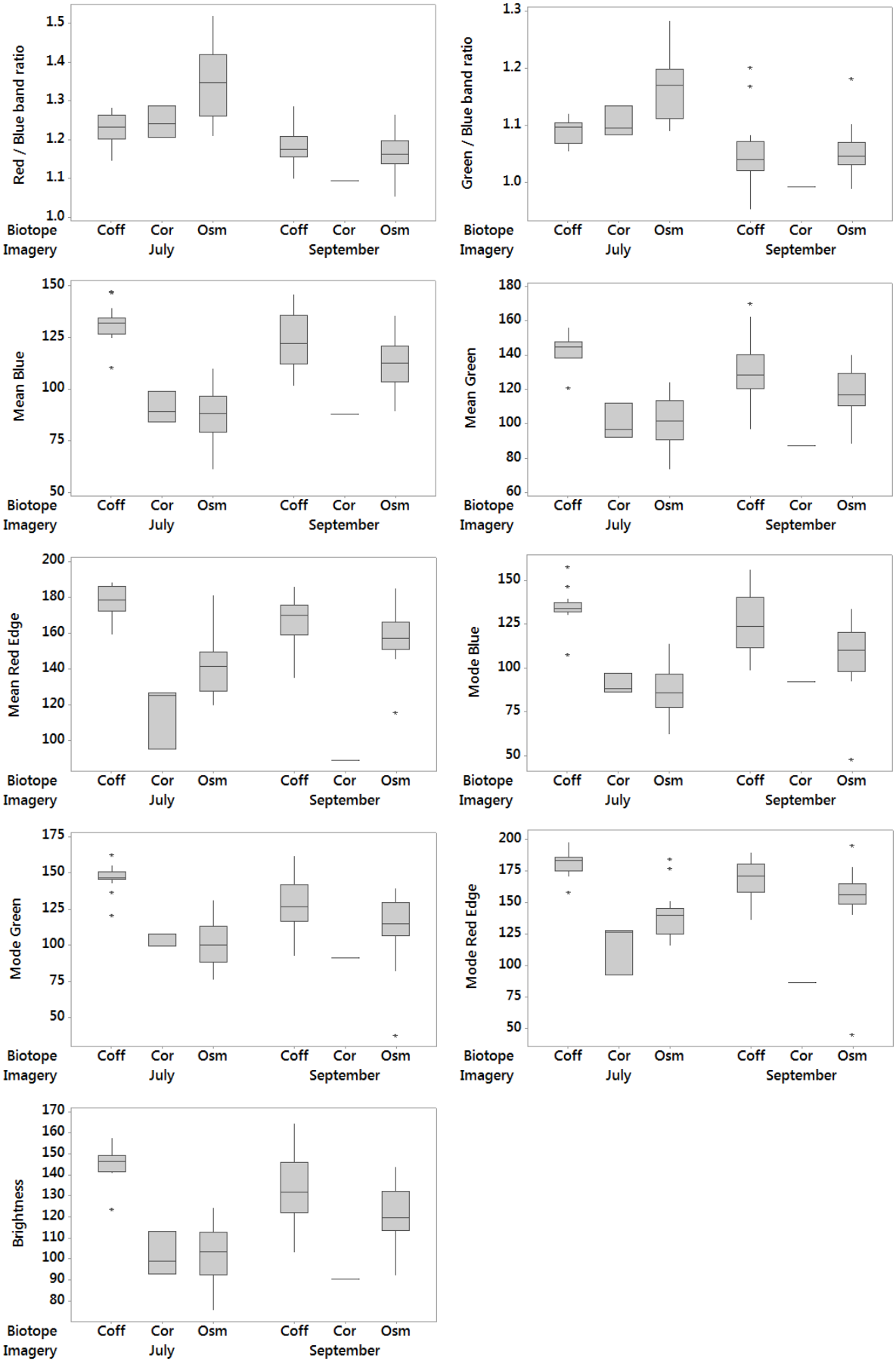

Figure 4.10: Sample values from UAV imagery collected in July and September 2015 for the biotopes Coff, Cor and Osm.

The four most important types of feature for distinguishing biotopes using the RF classifier were mean band ratios, mean single band values, and mean and mode DEM values (Figure 4.11), all of which were also important for distinguishing broadscale habitat classes (Figure 4.5). In contrast, mode band ratios and single band values were important for distinguishing broadscale habitats but not biotopes.

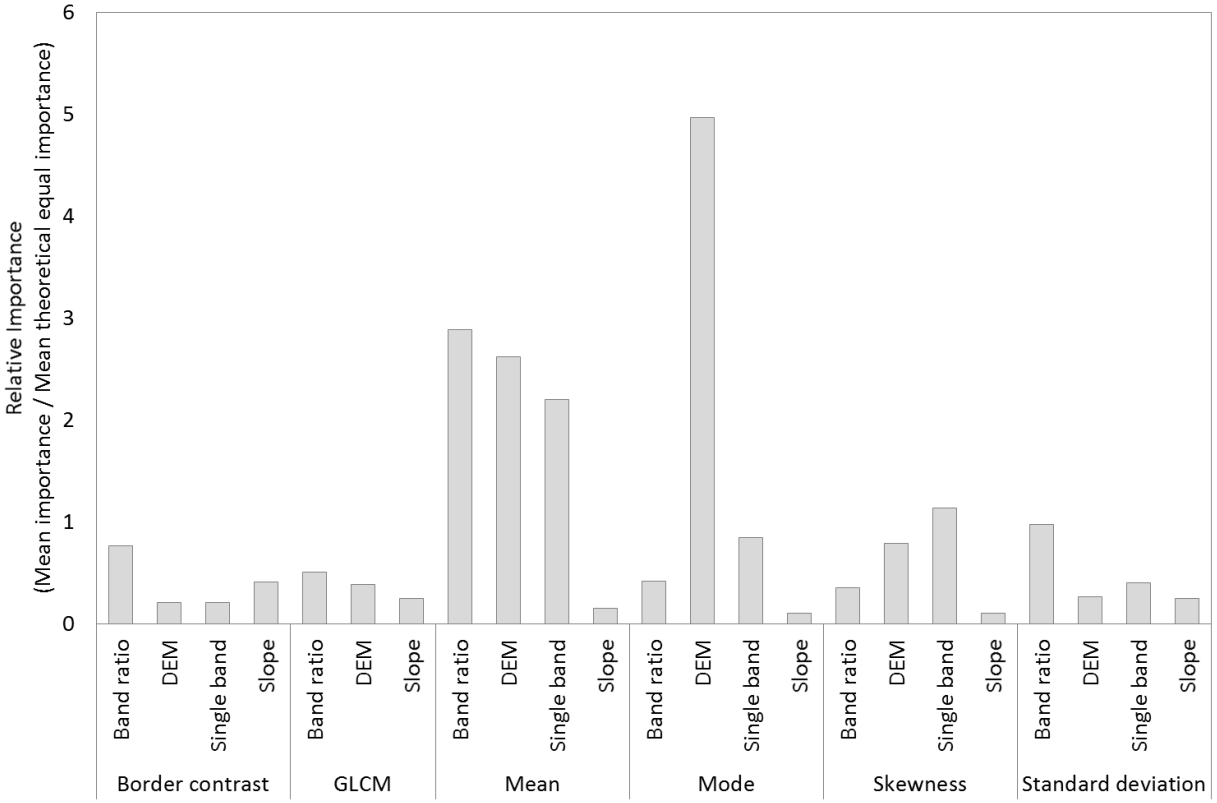

Figure 4.11: Relative importance values of features used to create biotope maps from UAV imagery using the RF classifier (mean importance / mean theoretical equal importance)

The range of sample values for the three features with the highest importance values used by the RF classifier are shown in Figure 4.12, illustrating that while no single feature could be used to separate all twelve classes, each feature provided good separability of some classes. For example, FSer.R could be separated from FVesR using mode DEM but not using brightness, while Coff could be separated from Cor using brightness but not using mode DEM.

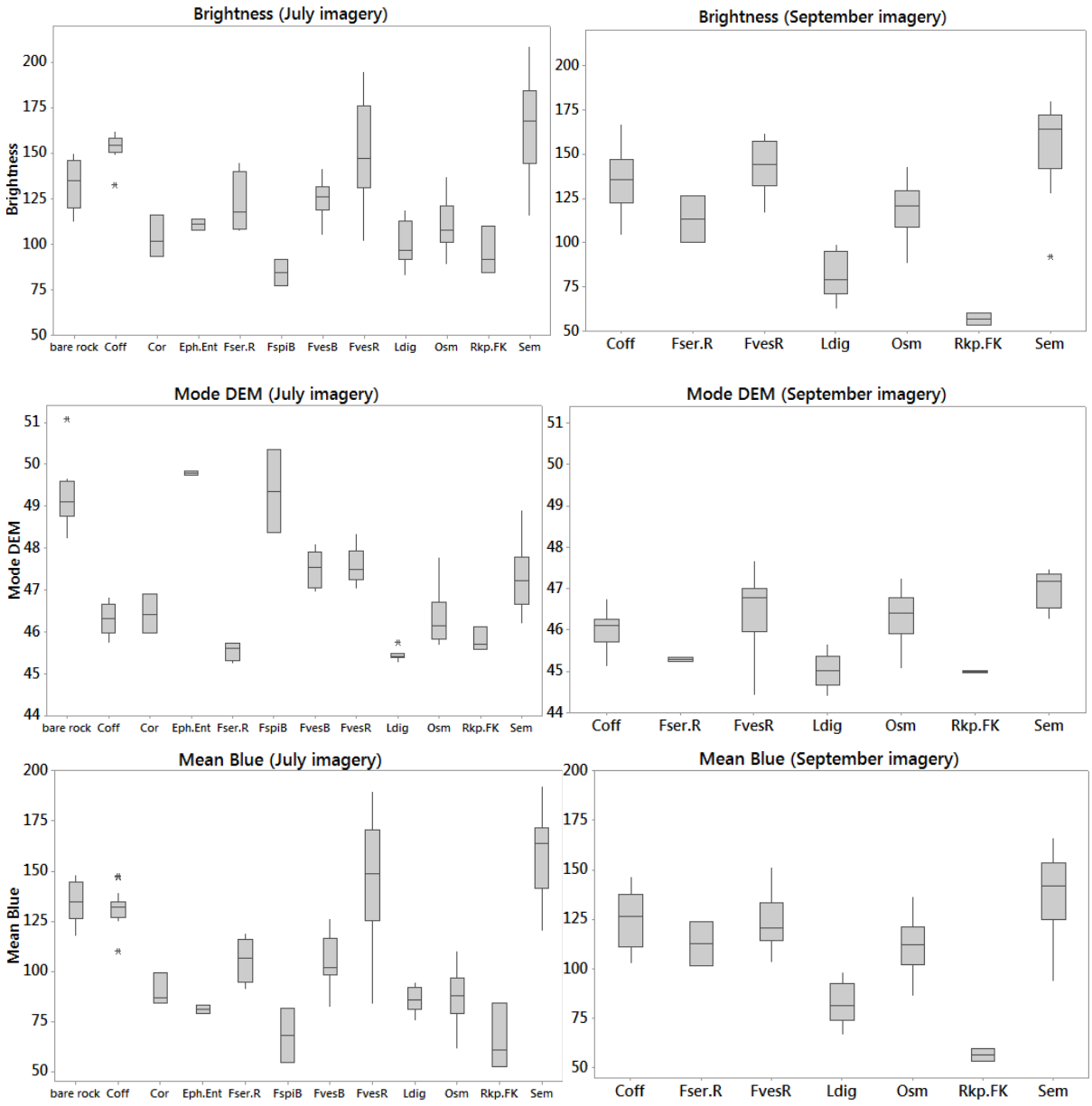

Figure 4.12: Sample values for the three features with highest importance used to create biotope maps from UAV imagery using the RF classifier

Figure 4.13 shows the features predominantly selected by Feature Space Optimisation for classifying biotopes using SNN. The only feature to have high importance with both the RF and SNN classifiers was mean DEM; the features most frequently selected by Feature Space Optimisation were border contrast of band ratios, GLCM of band ratios, DEM and slope and Skewness of band ratios, DEM and single bands.

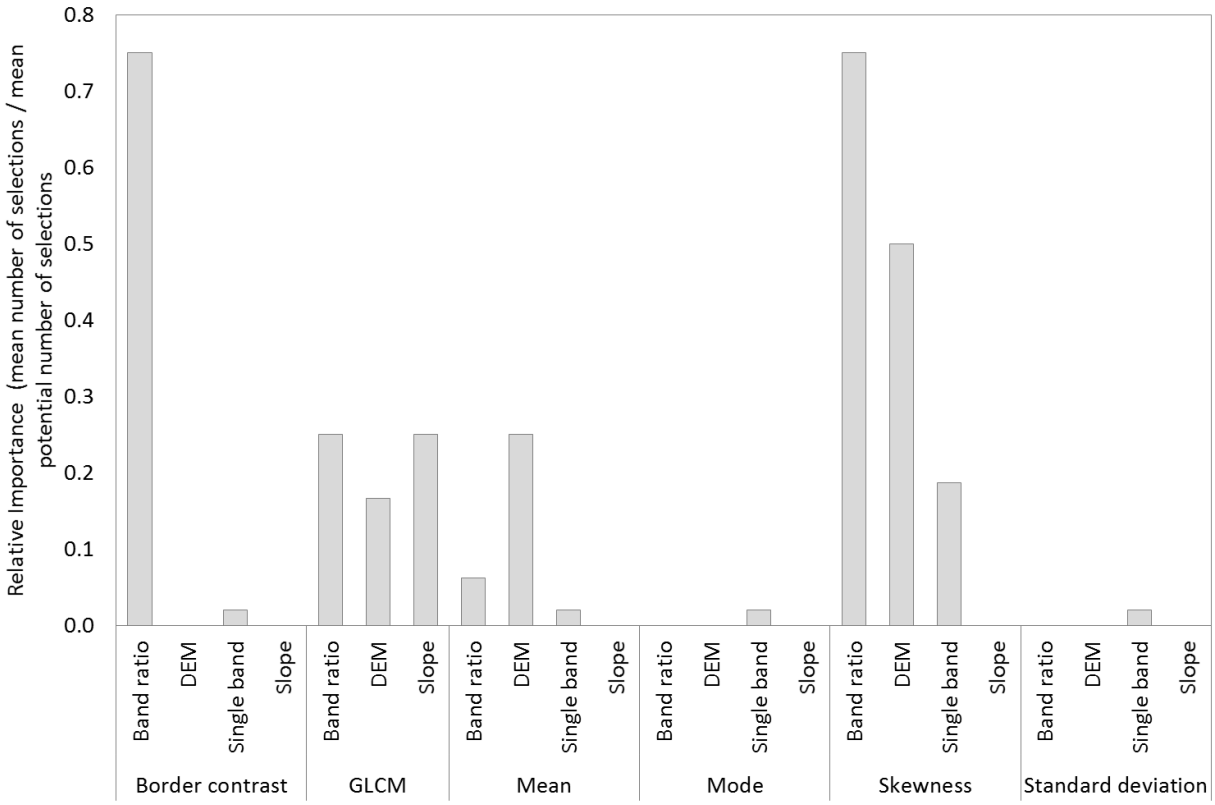

Figure 4.13: Relative importance values of features used to create biotope maps from UAV imagery using the SNN classifier (mean number of selections / mean potential number of selections by Feature Space Optimisation)

The range of sample values for the three features most frequently selected by Feature Space Optimisation for biotope classification are shown in Figure 4.14, illustrating that these features provided low class separability due to the considerable overlap in sample value ranges for most biotopes.

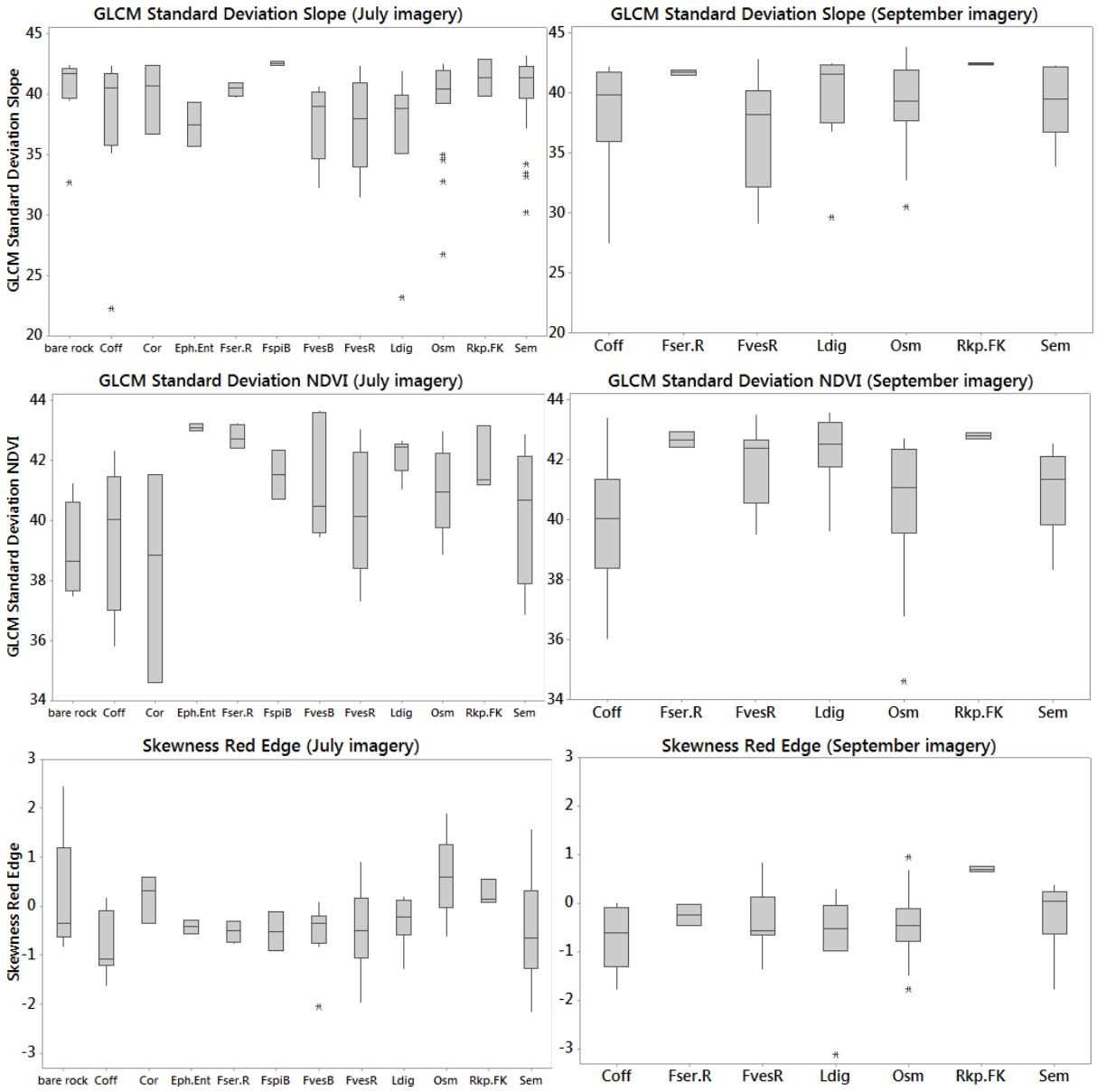

Figure 4.14: Sample values for the three features most frequently selected by Feature Space Optimisation to create biotope maps from UAV imagery using the SNN classifier

Mean classification stability of biotope objects ranged from 0.06 ± 0.05 to 0.17 ± 0.12 (Table 4.6). The low mean values show that the classification was not very stable, suggesting that the SNN classifier with this feature space did not provide clear separation of biotopes.

Table 4.6: Mean and standard deviation classification stability derived from all classified objects in biotope maps created from UAV imagery using the Standard Nearest Neighbour classifier. Grey cells indicate that the biotope was not predicted due to lack of training samples for this class.

Imagery	**July**				**September**			
Training samples	**A**		**B**		**A**		**B**	
Classification stability	Mean	St dev	Mean	St dev	Mean	St dev	Mean	St dev
Bare rock	0.10	0.10	0.11	0.08				
Coff	0.12	0.11	0.13	0.11	0.12	0.11	0.13	0.13
Cor	0.17	0.12	0.15	0.14				
Eph.Ent	0.00	0.00	0.00	0.00	0.08	0.08	0.09	0.07
Fser.R	0.13	0.11	0.15	0.12	0.10	0.08	0.06	0.05
FspiB	0.08	0.06	0.14	0.12				
FvesB	0.09	0.08	0.15	0.12				
FvesR	0.13	0.11	0.13	0.10	0.13	0.11	0.11	0.08
Ldig	0.13	0.10	0.11	0.10	0.11	0.10	0.12	0.09
Osm	0.13	0.11	0.14	0.11	0.12	0.10	0.10	0.09
Rkp.FK	0.10	0.08	0.14	0.11	0.13	0.11	0.08	0.08
Sem	0.15	0.13	0.11	0.10	0.12	0.10	0.13	0.10

4.3.3 Consistency of outputs

The consistency of outputs was evaluated by measuring the proportion of total area with the same classification in maps produced from the same imagery using the same classifier with different training samples. The results are shown in Table 4.7, illustrating that the RF classifier produced more consistent results than the SNN classifier in all cases and that broadscale habitat maps had a higher level of consistency than biotope maps. The knowledge-based rules were not included in this analysis because although ground truth data were used to inform the establishment of thresholds and membership functions, these data were not used to train a classification algorithm so two-fold cross validation was not applied to this method.

Table 4.7: Proportion of total area with the same classification in two maps produced from the same imagery using the same classifier with different training samples.

		Proportion of total area with the same classification in both maps	
Imagery	**Thematic scale**	**Standard Nearest Neighbour**	**Random Forests**
July	Broadscale	0.79	0.92
September	Broadscale	0.74	0.83
July	Biotopes	0.32	0.62
September	Biotopes	0.23	0.72

4.4 Discussion

The aim of this study was to evaluate the accuracy, consistency and reproducibility of OBIA methods for mapping temperate intertidal rock habitats from high resolution UAV imagery at broad and fine thematic scales. The results show that application of OBIA to UAV imagery has great potential for habitat mapping in this highly spatially heterogeneous environment, but that thematic scale, ground truth sampling protocol and classification algorithm all have considerable impact on the accuracy and consistency of outputs.

Broadscale habitat maps had greater accuracy and consistency than biotope maps regardless of the choice of classifier or training samples, which concurs with the findings of other studies that accuracy increases as the number of habitat classes decreases, for example through aggregation into parent classes in a hierarchical classification system (White *et al.*, 2003; Lucieer, 2008; Lyons *et al.*, 2012). The accuracy metrics for the broadscale maps showed that OBIA of UAV imagery can produce accurate and reproducible habitat maps at this thematic scale, but they provided little insight to inform classifier choice because the difference in values for maps produced by different classifiers was small. Only the calculation of percentage area agreement between maps produced from different training samples provided information to aid classifier choice, suggesting that RF produces more consistent results than SNN. In contrast, the accuracy metrics for biotope maps showed far greater variability in response to choice of classifier. The knowledge-based method produced the biotope map with the highest overall accuracy, corroborating other habitat mapping studies that used membership functions with a multi-scale hierarchical approach informed by ecological knowledge (de Oliveira *et al.*, 2006; Lucas *et al.*, 2011; Ouyang *et al.*, 2011). However, the low accuracy of the map produced by the knowledge-based rules from the September imagery showed that the model was over-fitted to the data used to develop

it. However, this should not be taken as an indication that the knowledge-based method is unsuitable; other studies have acknowledged that manual intervention may be necessary to change thresholds and membership function value ranges when applying a knowledge-based rule set to imagery from a different location or season (Lucas *et al.*, 2011; Lucas *et al.*, 2015). An important advantage of the RF classifier is its ability to avoid over-fitting by training each tree using a bootstrapped sample of the training data and randomly selected features (Breiman, 2001), but Juel *et al.* (2015) report a significant reduction in classification accuracy when RF models are applied to imagery that they were not trained on. In this study, the RF classifier was not expected to be sensitive to seasonal changes in spectral signature because it was trained using sample values taken from the relevant imagery, and indeed the accuracy of the RF biotope maps was reasonably consistent for both sets of imagery and training samples.

Although the SNN classifier performed comparably with the RF classifier and knowledge-based rules at the broad thematic scale, it performed noticeably worse than the other classifiers at the biotope scale, producing maps with low overall accuracy, high balanced error rate, low consistency (% area agreement between maps produced from different training samples) and low classification stability. Feature space is a key factor affecting classifier performance; reduction of data dimensionality is crucial for decreasing processing time and improving map accuracy, but there are many possible feature selection methods (Laliberte *et al.*, 2012; Canovas-Garcia and Alonso-Sarria, 2015; Diesing *et al.*, 2016; Gregorutti *et al.*, 2017). In this study, dimensionality was reduced by using Feature Space Optimisation with the SNN classifier, 'importance' metrics with the RF classifier and the Sample Editor tool with the knowledge-based rules. All three methods produced a reduced feature space that nevertheless included correlated features, for example the use of both mean and mode blue, green and red edge values to separate the Osm, Coff and Cor biotopes in the knowledge-based rules. The inclusion of correlated features is counter-intuitive, but Guyon and Elisseeff (2003) demonstrate that in many research areas, better class separation can be achieved by including variables that are so highly correlated they appear to be redundant.

At the broad thematic scale, there was some consistency between features used by the RF and SNN classifiers, notably mean and mode band ratios and DEM values, and analysis of sample value ranges showed that these features provide good separation of classes,

especially when used in combination. At the biotope scale, the RF classifier used similar features to those used for broadscale mapping and, again, analysis of sample values showed that these provided good separation of classes. In contrast, feature space for the SNN classifier was dominated by skewness, GLCM and border contrast features, and analysis of sample values for these features showed poor class separation. This is likely to be a key contributing factor to the poor performance of the SNN classifier at creating biotope maps, consistent with the findings of Laliberte *et al.* (2012) that although eCognition's Feature Space Optimisation tool is a rapid and convenient method for reducing data dimensionality, it frequently generates a feature space that results in relatively low classification accuracy.

At both thematic scales, Kappa is largely correlated with overall accuracy, consistent with the assertion by Pontius and Millones (2011) that Kappa does not reveal information that is different from overall accuracy in a way that could inform decision-making, and is thus redundant. In contrast, balanced error rate was not correlated with overall accuracy and did provide a useful additional measure of classifier performance, consistent with other studies that have attempted classifier comparison with an uneven number of ground truth samples per class (e.g. Diesing and Stephens, 2015).

While accuracy is likely to be the main driver for classifier choice, there are other considerations. A disadvantage of RF is that the decision rules are hidden from the user (Gomez *et al.*, 2016), whereas this study demonstrates that the transparency of the knowledge-based approach enables the user to determine the cause of classification errors. The RF and SNN classifiers offer the speed, convenience and relative objectivity of an 'off the shelf' solution. In contrast, a knowledge-based rule set takes longer to develop (around 40 hours in this study), but the ability to integrate ecological expertise is a valuable benefit (Adamo *et al.*, 2016) and once developed, knowledge-based rule sets may be built upon or adapted to new sites and imagery (Medcalf *et al.*, 2014b; Medcalf *et al.*, 2015). Although the rules developed in this study proved to be over-fitted to the data derived from the July imagery, the transparency of the classification rules should enable thresholds and membership function value ranges to be adjusted to improve classification accuracy of the September imagery, or indeed imagery from another site or season.

4.4.1 Sources of error and uncertainty

Regardless of classifier choice, reference data to train and validate a supervised classification

should be statistically independent and large enough to represent the entire study area and to adequately characterise each habitat class (Congalton, 1991; Foody and Mathur, 2004; Millard and Richardson, 2015). The main limitation of this study was that the stratified random sampling protocol based on shore height provided too few samples of some habitat classes for effective training and validation, as illustrated by the variation in balanced error rate, user's and producer's accuracy. Despite the high sampling density of 1,122 samples km^{-2}, some classes were under-represented in the reference data due to the high number and unequal proportions of habitats in the study area. This was particularly problematic at the biotope scale, leading to the omission of some classes from the maps, but even at the broad thematic scale the locally rare class of green algae was under-sampled. Furthermore, random sampling produced several samples were not good representatives of their class, for example located in a non-homogeneous area in an ecotone between two habitats. In an attempt to mitigate these problems, the dataset was augmented with samples which had been collected for the primary purpose of measuring rugosity (Chapter 3). These supplementary samples occurred in pairs located less than 5m apart, but even at segmentation scale parameter 120 these paired points occurred in different objects and frequently in different habitats due to the high spatial heterogeneity of the site. Nevertheless, due to the high sampling density, there is likely to be spatial autocorrelation between some training and reference data points. Reference data should be collected contemporaneously with remote sensing data where possible, but due to time constraints the reference data in this study were collected between April 2015 and March 2016 and used to train and validate imagery collected in July and September 2015. This relies on the assumption that the dominant community at each sample point did not change during that time period; this assumption is supported by visual assessment of the UAV imagery and knowledge of the site. Although the shortcomings of the stratified random sampling protocol do not detract from this study's findings, they do highlight an area where methodological improvements could be introduced.

4.4.2 Methodological improvements

Stratified sampling of reference data based on shore height was used in this pilot study to ensure objectivity and independence of ground truth samples from remote sensing data. A benefit of this approach was that it enabled ground truth data collection to start before UAV imagery collection, thus maximising use of low spring tides which are a critical limiting factor

in intertidal fieldwork. However, in future applications a two-stage methodology could be adopted in which unsupervised classification of the UAV imagery could inform a stratified random sampling protocol to collect reference data from areas of homogeneous spectral signature, which would then be used for supervised classification of the imagery. This two-stage methodology is commonly used in broadscale benthic surveys (Anderson *et al.*, 2008) and has the benefit of ensuring an even number of samples per habitat class and possibly increasing the spectral separability of habitat classes (Franklin and Wulder, 2002; Clements *et al.*, 2010).

As hierarchical cluster analysis of the ground truth data produced classes that were closely correlated with the biotopes assigned to the samples, future applications could omit the recording of species percentage cover and simply record the biotope or broadscale habitat class. This would increase efficiency and enable the collection of a far larger reference dataset.

An alternative way of increasing ground truth sample size and ensuring all classes are adequately represented is to augment the reference dataset with samples selected through expert interpretation of the imagery (Corcoran *et al.*, 2013); this would certainly be possible at the broad thematic scale but it is unlikely that all biotopes could be distinguished through visual assessment of UAV imagery.

Truly random sampling is likely to generate samples which are not good representatives of their class, potentially resulting in reduced accuracy when used as training data in a supervised classification. Corcoran *et al.* (2013) demonstrated how this problem can be overcome by following a random sampling protocol but using discretion during field survey to collect data from the most homogeneous area in the vicinity of each target sample location and also later eliminating training samples that were not representative of their habitat class.

In this study, equipment limitations required collection of RGB and red edge imagery on two separate flights, introducing potential inconsistency due to changes in lighting, tide height or other environmental conditions between flights. A methodological improvement would be to use a multispectral camera to collect data from all bands simultaneously, thus improving consistency and increasing the amount of data that can be captured during a single low tide. Future research should evaluate the effect on accuracy of using near infrared (750nm to

950nm) rather than red edge imagery (680nm to 750nm), as studies based on satellite or hyperspectral aerial imagery have shown the near infrared band to be useful in distinguishing seaweed species (Zacharias *et al.*, 1992; Guillaumont *et al.*, 1993; Bajjouk *et al.*, 1996; Siddiqui and Zaidi, 2015).

Feature selection was shown to be an important factor affecting the accuracy of maps created by the RF and SNN classifiers; further research could investigate other data dimensionality reduction methods such as principal component analysis or feature ranking conducted outside the classification software, or simply using expert judgement and analysis of sample values rather than Feature Space Optimisation to select features for the SNN classifier.

4.4.3 Future implications

The recent upsurge of interest in UAVs for ecological surveillance and monitoring is likely to continue due to ongoing innovation in platform and sensor design coupled with reductions in cost (Anderson and Gaston, 2013; Colomina and Molina, 2014). UAVs are a particularly attractive option for intertidal survey due to the inaccessibility, high spatial heterogeneity and dynamic nature of this environment (Burrows *et al.*, 2014). The findings of this study can help to inform adoption of UAV and OBIA technology for intertidal habitat mapping at both broad and fine thematic scales, particularly decisions on classifier choice and ground truth sampling protocol.

The ability to produce intertidal habitat maps in a rapid, repeatable way has positive implications for intertidal MPA planning, management and monitoring. Even at the broad thematic scale, maps derived from UAV surveillance can provide useful insight into rocky shore dynamics. For example, the shape and size of areas of bare rock has been shown to influence recruitment and recovery after disturbance (Airoldi, 2003); this study demonstrated that OBIA of UAV imagery was an efficient and reliable method of measuring shape and extent of bare and vegetated patches on intertidal reef. UAV surveillance only captures dominant species such as canopy-forming macroalgae or sessile fauna such as barnacles, it cannot capture information on understorey algae or small, mobile species (Konar and Iken, 2017; Murfitt *et al.*, 2017). However, other studies have demonstrated that understorey species can be predicted from macroalgal canopy composition (Irving and Connell, 2006; Cardenas *et al.*, 2016), and the classification system used in this study was

created through statistical analysis of empirical data (Connor *et al.* 2004) so correlation is expected between dominant species and associated communities.

The evaluation of consistency by two-fold cross validation and of reproducibility by applying the methods to a second dataset from a different season and partially different area of the site have important implications for the adoption of these methods for monitoring change. At the broad thematic scale, all the OBIA methods had a good level of reproducibility and consistency, although RF was less affected by changing the training samples than SNN. At the biotope scale, only the RF classifier performed consistently in response to changing training samples and datasets, and is therefore likely to be a better choice of classifier for change detection. Further research into within-class spectral variability and the effect of seasonal change on seaweed spectral signatures could inform the establishment of feature value ranges for thresholds and membership functions, enabling the application of the knowledge-based rule set for intertidal monitoring. Although this pilot study was conducted in one region, the findings regarding the accuracy, consistency and reproducibility of OBIA methods are broadly applicable and could inform the adoption of these methods for surveillance and monitoring on intertidal reefs in any temperate region.

4.5 Conclusions

This study demonstrated the great potential of OBIA and UAV imagery for intertidal habitat mapping and provided valuable insight to help inform choice of classifier, sampling protocol and thematic scale.

The accuracy, consistency and reproducibility of outputs were higher at the broad thematic scale than at the biotope scale. Of the two sample-trained classifiers, RF performed better than SNN, largely due to its superior feature selection method and its ability to avoid over-fitting to training data. The performance of both the RF and SNN classifiers could likely be improved by collecting training samples from homogeneous areas stratified by spectral signature to ensure a sufficiently high number of samples per habitat class. The knowledge-based rule set shows promise for both broadscale habitat and biotope mapping, but further research into within-class spectral variability is recommended to improve its reproducibility at the biotope scale.

A great benefit of UAV technology is the ability to target surveys to sites of interest at optimal times, such as low spring tides, and to capture imagery at sub-decimetre and even

sub-centimetre resolution. A disadvantage is that UAVs can only cover small areas, typically less than 1km^2 per flight, due to technical and operational restrictions such as battery duration and regulations on flying within visual line-of-sight (VLOS). It is possible to cover the landward to seaward extent of a typical UK rocky shore on a low spring tide without flying outside VLOS, but surveying a linear stretch of coastline would require several flights from different take-off points, which could not all be completed on a single low tide. This study demonstrated the ability of OBIA to produce single-date intertidal habitat maps of a small area using UAV imagery. Further research will evaluate the scalability of these methods through application to other types of data in order to cover larger areas, and test the change-detection capability of OBIA through application to multi-temporal imagery. If successful, the OBIA and UAV surveillance methods evaluated in this study could form an integral part of a cost-effective monitoring protocol for temperate intertidal habitats.

Chapter 5: Using OBIA with multi-temporal aerial and LiDAR data to monitor change in intertidal habitats

5.1 Introduction

Coastal ecosystems are naturally dynamic, exhibiting high levels of temporal and spatial change (Hartnoll and Hawkins, 1980). However, in addition to these natural seasonal and cyclical fluctuations, the distribution of species and habitats can be affected by anthropogenic factors, including ocean warming and acidification (Brodie *et al.*, 2014), non-native species (Molnar *et al.*, 2008), pollution (Islam and Tanaka, 2004) and coastal development (Bulleri and Chapman, 2010). Several studies provide evidence of long term change in extent and distribution of habitat-forming macroalgae on temperate rocky shores, possibly influenced by climate change (Davies *et al.*, 2007; Fernandez, 2011; Yesson *et al.*, 2015). It is predicted that canopy-forming fucoids will decline as the climate continues to warm, with consequent reduction of biodiversity and primary productivity (Hawkins *et al.*, 2009). Surveillance and monitoring of coastal ecosystems within and outside MPAs is required under national and international legislation (for example EC, 1992; EC, 2000; EC, 2008) and must seek to distinguish anthropogenic changes from natural fluctuations in order to inform management of anthropogenic pressures.

Multi-decadal marine time-series datasets, for example on plankton (Reid *et al.*, 2003), seabird populations (Paleczny *et al.*, 2015), rocky shore communities (Hawkins *et al.*, 2008) or physical oceanography (Mackenzie and Schiedek, 2007), are a valuable resource for monitoring environmental change, providing insight into the impact of anthropogenic activities on marine ecosystems and predicting future trends (Ducklow *et al.*, 2009; Mieszkowska *et al.*, 2014). Remote sensing does not provide datasets of comparable duration, nor can it be used for monitoring detailed change in species communities, but it can be used to detect change in land use, land cover or habitats at coarse thematic scales over large areas (Singh, 1989). Automated interpretation of remote sensing data offers several advantages for monitoring change in land use, land cover or habitats for conservation purposes; it is non-invasive and can be applied at different temporal and spatial scales to provide quantitative outputs (Willis, 2015). Although remote sensing is a relatively new field compared to the long-term marine monitoring methods mentioned above, a growing number of systems and sensors provide data with high temporal frequency over many years, for example Landsat imagery which dates back to 1972 (Lyons *et al.*, 2012).

The increasing availability of remote sensing data has given rise to many change detection methods, but despite a number of comparative studies there is no agreement as to the 'best' technique (Tewkesbury *et al.*, 2015). This proliferation of methods has arisen in response to the particular challenges presented by multi-temporal data (Lu *et al.*, 2004; Gomez *et al.*, 2016), namely that inaccurate spatial registration can lead to spurious change detection caused by image misalignment; there may be considerable spectral variability between datasets, for example due to sensor calibration, off-nadir angle or weather conditions; imagery acquired under different phenological conditions may cause natural seasonal fluctuation to be confounded with meaningful ecological change; and the acquisition of reference data to train models and validate outputs can be difficult, especially for historical imagery. These challenges influence the decisions taken at every stage in the change detection process, from selecting and pre-processing imagery, defining units of analysis, choosing a comparison method, determining the magnitude and type of change to be detected, to assessing the accuracy of the final output (Tewkesbury *et al.*, 2015).

The most widely used approach to change detection is bi-temporal comparison, which entails comparing two sets of imagery collected on different dates, most commonly on anniversary dates in different years (Lambin, 1996; Coppin *et al.*, 2004). However, comparison of two dates gives no insight into the rate or persistence of change, and techniques have been developed to analyse multi-temporal imagery to detect longer term trends in phenology and landscape dynamics (Gillanders *et al.*, 2008; Melaas *et al.*, 2013). Whether comparing imagery from two or multiple dates, efforts must be made to reduce or compensate for spectral variability between images; the most common approach with satellite data is to pre-process the imagery, for example using methods outlined by Lu *et al.* (2004).

The simplest unit of analysis in remote sensing change detection is the pixel, but as spatial resolution of data has increased, object-based methods of producing change detection maps have become more popular. These avoid the 'salt and pepper' classification of pixel-based methods, enable the use of a wider range of features such as texture and geometric properties (Chen *et al.*, 2012; Hussain *et al.*, 2013) and have been shown to produce more accurate results than pixel-based approaches (Im *et al.*, 2008; Robertson and King, 2011). However, segmenting two or more sets of imagery separately can cause 'sliver' objects resulting in spurious change detection (McDermid *et al.*, 2008), and some studies have

overcome this by using hybrid approaches between pixel- and object-based methods (Aguirre-Gutierrez *et al.*, 2012; Duro *et al.*, 2013).

Change detection comparison methods fall into two broad categories, pre- and post-classification. Pre-classification techniques involve combining imagery from two or more dates in a single stack and identifying areas of change through simple layer arithmetic or by applying a classification algorithm trained by reference samples, while post-classification methods involve creating a map for each date and comparing them to classify areas of change using transitional 'from-to' classes (Manandhar *et al.*, 2010). Areas of change identified through pre-classification methods may subsequently be classified according to transition type using a classification algorithm or knowledge-based rules (Doxani *et al.*, 2012; Bruzzone and Bovolo, 2013). Post-classification methods overcome the problem of spectral variability due to atmospheric conditions or sensor differences (Fan *et al.*, 2007) and provide information on the direction of change, but the potentially large number of transition classes can be computationally expensive and confusing to end users, and classification errors in the interim maps are perpetuated in the final change maps (Tewkesbury *et al.*, 2015). An advantage of pre-classification techniques is that only one classification stage is required, although the generation of training samples can be challenging and time-consuming (Schneider, 2012). Although several reviews discuss the advantages and disadvantages of both approaches (Coppin *et al.*, 2004; Lu *et al.*, 2004; Tewkesbury *et al.*, 2015), only two studies to our knowledge have compared pre- and post-classification methods directly by applying both techniques to the same data and quantifying the accuracy of the results (Mas, 1999; Conchedda *et al.*, 2008). Both of these studies found post-classification to be more accurate than pre-classification methods when applied to low resolution satellite imagery, but no comparative study has yet been carried out using high resolution imagery.

Methods for quantifying the accuracy of single-date predictive maps through comparison with reference data, such as the error matrix (Congalton, 1991), Kappa coefficient (Cohen, 1960) and balanced error rate (Stephens and Diesing, 2014), may be used in change detection studies but the selection of reference data presents challenges when working with multi-temporal data. In some cases, reference data may be available from ground sampling that was carried out over the same period as remote sensing data collection, but it is more common that reference data will need to be sourced from remote sensing data (Duro *et al.*, 2013; Gomez *et al.*, 2016). The key principle is that the reference classification must be of

higher quality than the map classification. If ground truth data or higher resolution remote sensing data are not available, reference data may be obtained from the same source material used to create the map, provided that the method of classifying the validation samples is more accurate than the method used to classify the map they will be used to evaluate (Olofsson *et al.*, 2014).

Most remote sensing change detection studies, including those cited above, developed methods using satellite imagery. Satellite imagery has been the focus of change detection research because it is available, often free of charge, over decadal time periods with frequent revisit times and its spectral and spatial resolution is suitable for detecting landscape-scale changes such as deforestation, desertification or urban expansion. However, satellite imagery might not be suitable for change detection in marine and coastal environments, particularly in areas with turbid water, frequent cloud cover or fine-scale habitat heterogeneity (Thomson *et al.*, 2003). More recent studies have started to apply established change detection methods to a wider range of remote sensing data for marine and coastal monitoring, such as sonar (Rattray *et al.*, 2013), UAV (Goncalves and Henriques, 2015; Ierodiaconou *et al.*, 2016), LiDAR and aerial imagery (Anderson *et al.*, 2016), but no study has yet compared the accuracy and consistency of object-based pre- and post-classification change detection methods.

Preceding chapters developed and evaluated OBIA methods for creating habitat maps using data collected specifically for that purpose, but an important benefit of remote sensing is that data can be used for multiple purposes. In this chapter, data which were originally collected to monitor coastal erosion and inform shoreline management plans are repurposed for habitat mapping and change detection. This chapter aims to evaluate the application of OBIA to high resolution, freely available aerial and LiDAR multi-temporal imagery to detect short-term change in extent and distribution of temperate intertidal habitats. Specific objectives are (1) to ascertain whether OBIA of aerial and LiDAR multi-temporal data can detect change in extent and distribution of broadscale intertidal habitats, (2) to gain insight into the type, magnitude and spatial distribution of change within the study site over the eight year period, (3) to compare the accuracy of random forests and membership function classifiers as means of producing habitat maps from aerial and LiDAR data, (4) to compare the accuracy and consistency of pre- and post-classification change detection methods, and (5) to evaluate the impact on map accuracy of different thresholds

for defining 'change'. Some challenges of using multi-temporal data are explored and their impact on the accuracy and consistency of output maps is quantified.

5.2 Methodology

5.2.1 Study site

This study was conducted on the south coast of Flamborough Head in the East Riding of Yorkshire, 54° 6.20 N, 0° 8.50 W. Flamborough Head was designated a Special Area of Conservation in April 2005 to protect and monitor features of conservation importance under the Habitats Directive (EC, 1992), including intertidal and subtidal chalk reefs. Under Article 17 of the Directive, the condition and conservation status of designated features must be assessed and reported every six years. Prior to designation, a baseline survey was carried out to map intertidal biotopes and establish eight monitoring transects (Howson, 2000) to be resurveyed at intervals to monitor change in extent or distribution of biotopes along each transect (Musk *et al.*, 2010).

The coastline from Sewerby to Danes Dyke on the south of the headland (Figure 5.1) was established as the North Sea's first No Take Zone (NTZ) in July 2010 under a local bylaw. The NTZ covers 1km^2, of which approximately 80% is subtidal and 20% intertidal, the intertidal area composed predominantly of chalk bedrock and boulder reef.

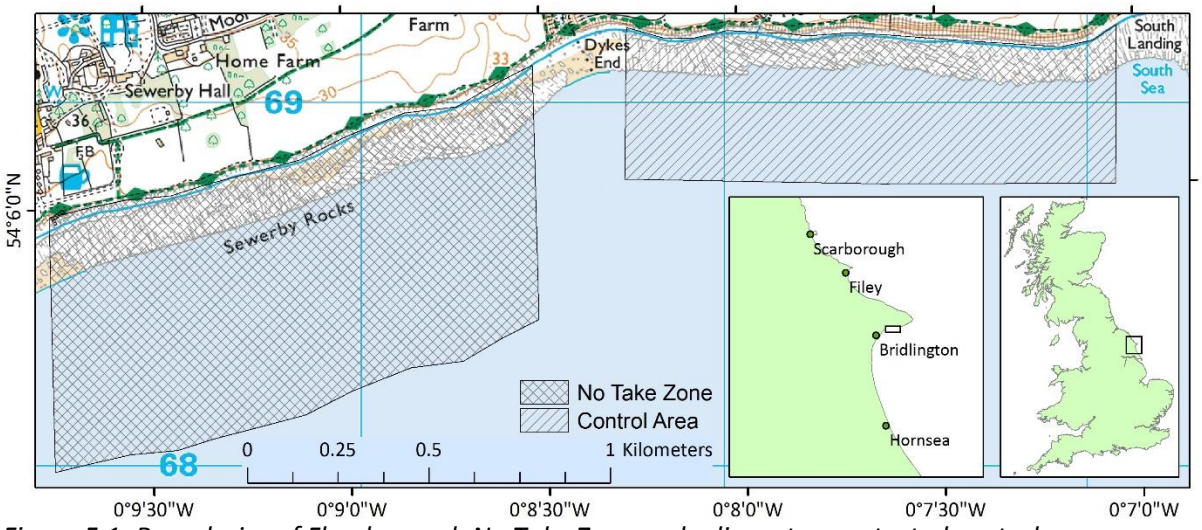

Figure 5.1: Boundaries of Flamborough No Take Zone and adjacent unprotected control area. Contains Ordnance Survey data © Crown copyright and database right (2018)

A criterion of establishment was that the NTZ would be monitored for an experimental period of five years. Current monitoring activity comprises surveys by the North Eastern Inshore Fisheries and Conservation Authority (NE IFCA) to monitor the extent of *Mytilus*

edulis beds and carapace sizes of *Cancer pagurus* and *Homarus gammarus*, and annual surveys by the University of York to monitor intertidal species communities through direct sampling in the NTZ and an adjacent unprotected control area (Figure 5.1).

A full-coverage swath bathymetry survey was conducted from Flamborough Head to Spurn Point in 2011 and expert visual interpretation of the data used to produce subtidal broadscale (EUNIS level 3) and substratum maps (Colenutt and Kinnear, 2014), but to date no use has been made of remote sensing data to map or monitor change in intertidal habitats at this site.

5.2.2 Aerial and LiDAR data

Aerial and LiDAR surveys of the East Riding coast have been conducted every spring and autumn since September 2008 to monitor coastal erosion and inform the maintenance of coastal defence structures. These surveys were commissioned by East Riding of Yorkshire Council and carried out by the Environment Agency, producing 1m resolution LiDAR and 0.2m resolution aerial imagery which is freely available for re-use under the UK's Open Government License. LiDAR and aerial tiles overlapping the study area were downloaded from the Channel Coast Observatory website [http://www.channelcoast.org/] with metadata for each set of imagery. The RMS error for image alignment of the aerial imagery ranged from 0.19m to 0.50m which is in accordance with guidelines set by the Royal Institution of Chartered Surveyors (RICS, 2010; Environment Agency, 2016).

The data collection period runs from spring 2009 to spring 2016; no data were available for autumn 2008 because the flight did not fully cover the study area, and no flight was conducted in autumn 2016 due to bad weather. Table 5.1 shows metadata for each set of imagery, demonstrating variation in flight month and sensor within the eight year dataset.

Table 5.1: Aerial and LiDAR data collected by the Environment Agency for East Riding of Yorkshire Council from 2009 to 2016, showing date of collection, sensor used and area covered within the study site. Data courtesy of Channel Coast Observatory.

Flight year	Flight month	Camera	LiDAR system	Coverage of study area (km^2)
2009	April	Rollei P45+	Optech ALTM Gemini 06SEN191	0.366
	September	Rollei P45+	Optech ALTM Gemini 06SEN191	0.541
2010	April	Rollei P45+	Optech ALTM Gemini 07SEN206	0.402
	October	Rollei P45+	Optech ALTM Gemini 06SEN191	0.514
2011	April	Rollei P45+	Optech ALTM Gemini 06SEN191	0.500
	September	Rollei Metric AIC	Optech ALTM Gemini 167	0.580
2012	March	Leica RCD30	Optech ALTM Gemini 06SEN191	0.361
	September	Leica RCD30	Optech ALTM Gemini 08SN230	0.513
2013	April	Leica RCD30	Optech ALTM Gemini 06SEN191	0.435
	October	Leica RCD30	Optech ALTM Gemini 06SEN191	0.359
2014	May	Leica RCD30	Optech ALTM Gemini 06SEN191	0.445
	November	Leica RCD30	Optech ALTM Gemini 06SEN191	0.479
2015	April	Leica RCD30	Optech ALTM Gemini 06SEN191	0.536
	September	Leica RCD30	Optech Orion 13SEN330	0.526
2016	March	Leica RCD30	Optech ALTM Orion 14SEN342	0.463

Each set of flight imagery was processed by the Environment Agency to produce orthorectified mosaics (Environment Agency, 2016). Radiometric adjustments were applied using inPho Orthovista (Trimble) to compensate for intensity, contrast or colour differences between adjacent or overlapping images, sun glint was removed and the individual images were mosaicked to produce 1km tiles. These were adjusted for white balance, contrast and exposure in Photoshop CC (Adobe). An atmospheric sharpening filter was applied and the geotiffs were compressed to Enhanced Compression Wavelet (ECW) format using Erdas Imagine (Hexagon Geospatial). No further processing was conducted to compensate for variability between datasets, for example due to different atmospheric conditions on different flight dates.

ArcGIS v.10.3 (ESRI) was used to mosaic the image tiles, define the coordinate system as OSGB36 and clip the imagery to the intertidal zone of the NTZ and control area. The area covered varies because of differences in tidal height at the time of data capture, ranging from 0.359km^2 to 0.580km^2 (Table 5.1). ArcGIS was also used to create slope rasters from the LiDAR imagery and normalised band indices from the aerial imagery. Identification and

comparison of landmarks in the aerial imagery ensured that each dataset was accurately aligned with the others. Visual assessment of the imagery determined that change of substratum and algal cover did occur during the eight year period and is detectable from the imagery. Some examples of change are shown in Figure 5.2, Figure 5.3 and Figure 5.4.

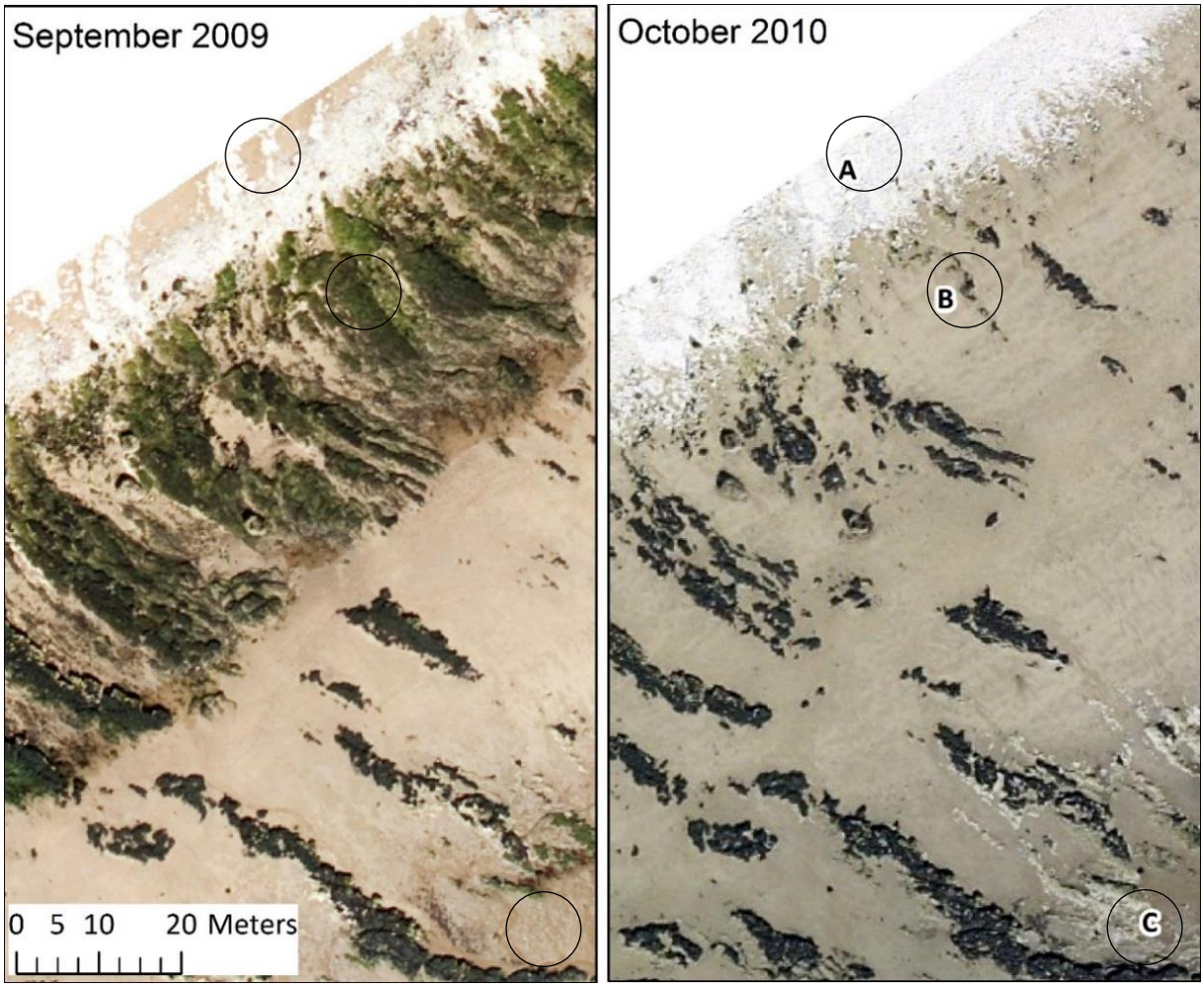

Figure 5.2: Examples of change from sand to chalk cobbles (A), green algae to sand (B) and sand to rock (C) seen in aerial imagery of Flamborough Head collected in September 2009 and October 2010

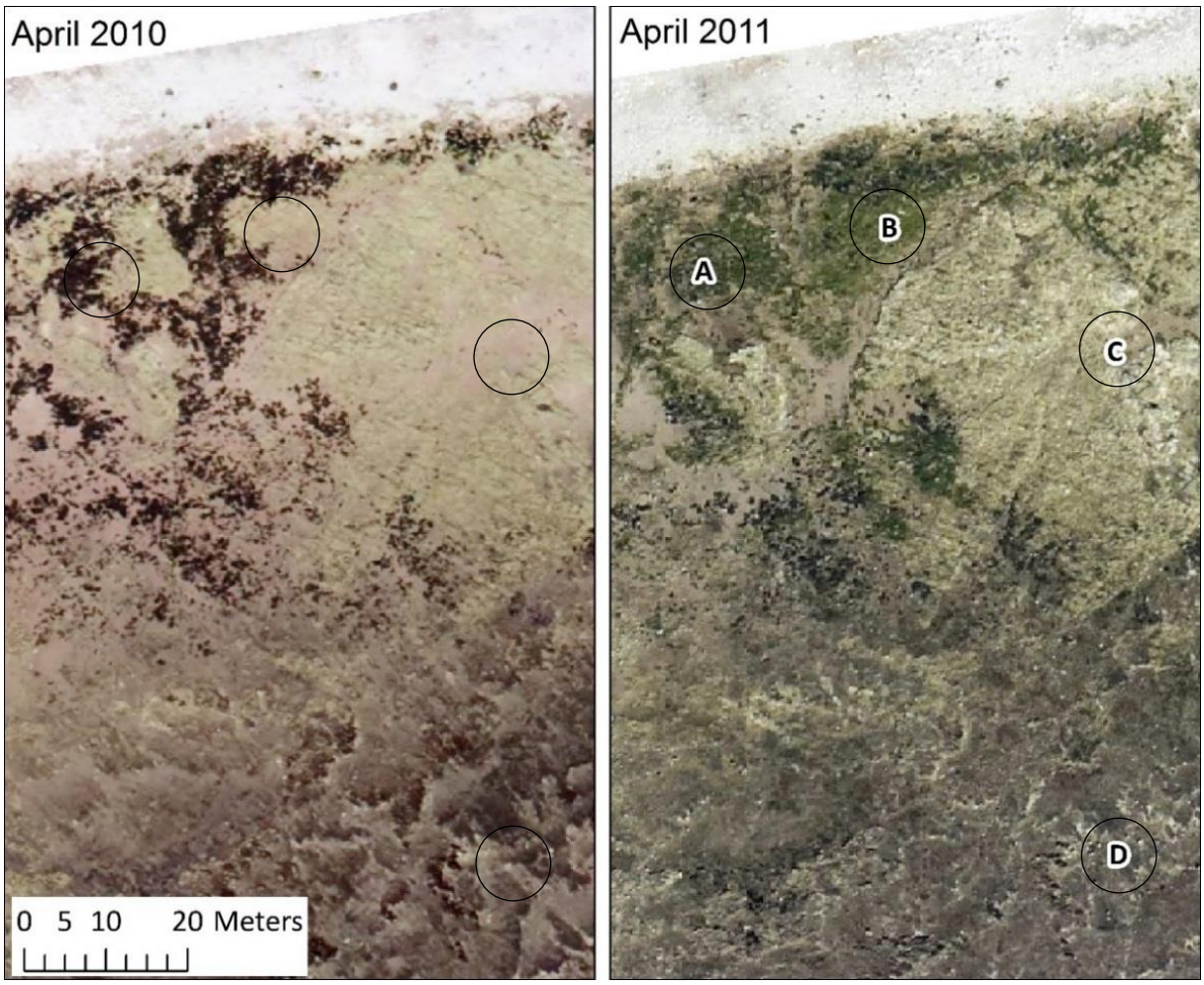

Figure 5.3: Examples of change from brown algae to green algae (A), rock to green algae (B), sand to rock (C) and red algae to rock (D) seen in aerial imagery of Flamborough Head collected in April 2010 and April 2011

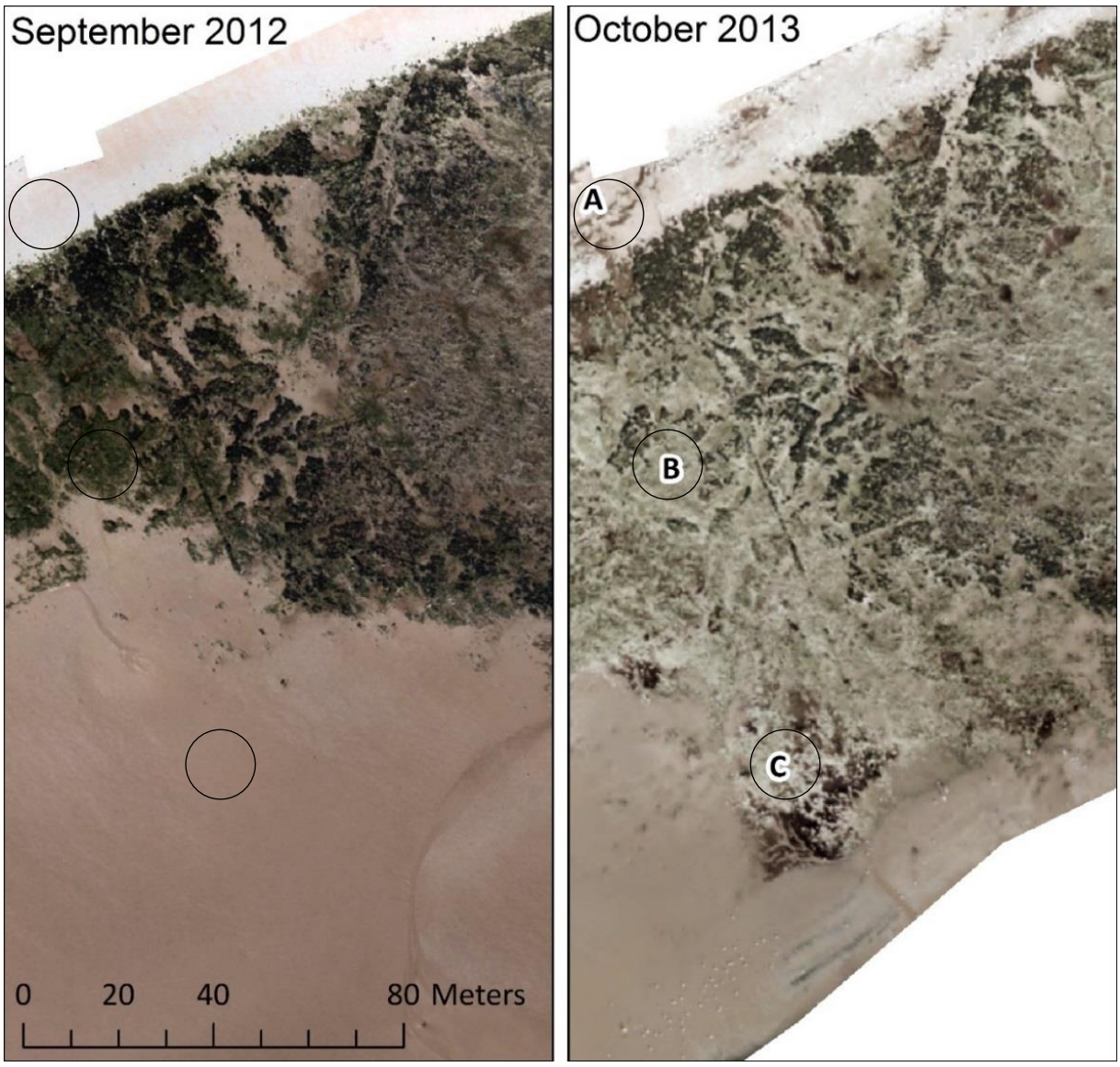

Figure 5.4: Examples of change from chalk cobbles to strandline (A), green algae to rock (B) and sand to rock (C) seen in aerial imagery of Flamborough Head collected in September 2012 and October 2013

5.2.3 Creation and validation of habitat maps

Workflows were created in eCognition Developer v9.0.3 [Trimble] to create habitat maps from each dataset. A broadscale habitat classification was defined for the study area through visual interpretation of the imagery and reference to survey reports (Howson, 2000; Musk *et al.*, 2010). The classification comprised eight classes: red algae, green algae, brown algae, barnacle-covered rock, bare chalk cobbles and sand, plus classes of shadow and strandline to remove these objects from further classification.

Segmentation was performed by applying eCognition's multi-resolution segmentation algorithm to the red, green and blue layers at scale parameter 22 with homogeneity criteria weighting shape (0.1) versus colour (0.9) and object compactness (0.9) versus smoothness

(0.1). These parameters were selected by starting from scale 30 and trialling progressively smaller scales with different combinations of shape and compactness parameters, evaluating each output by visual comparison with the imagery. Scale parameter 22 created separate objects for different algal communities, while larger scales produced objects containing a mixture of brown and green algae.

The site's topography consists of low bedrock ridges which cast narrow linear shadows, so objects were classified as shadow if they met the criteria of brightness <= 50 and length/width >= 4. The strandline consists of dried fucoid algae on the upper shore, so objects were classified as strandline if they met the criteria of brightness <= 100 and mean elevation >= 2m or brightness <= 150 and mean elevation >= 2.4m.

Training samples for the remaining six classes were created for each set of imagery through manual non-random selection to provide around 100 samples per dataset, divided as evenly as possible between habitat classes. Validation samples were created through systematic random sampling by creating an evenly spaced grid of points. In both cases, habitat classes were assigned to the points through visual inspection of the imagery. Examples are shown in Figure 5.5.

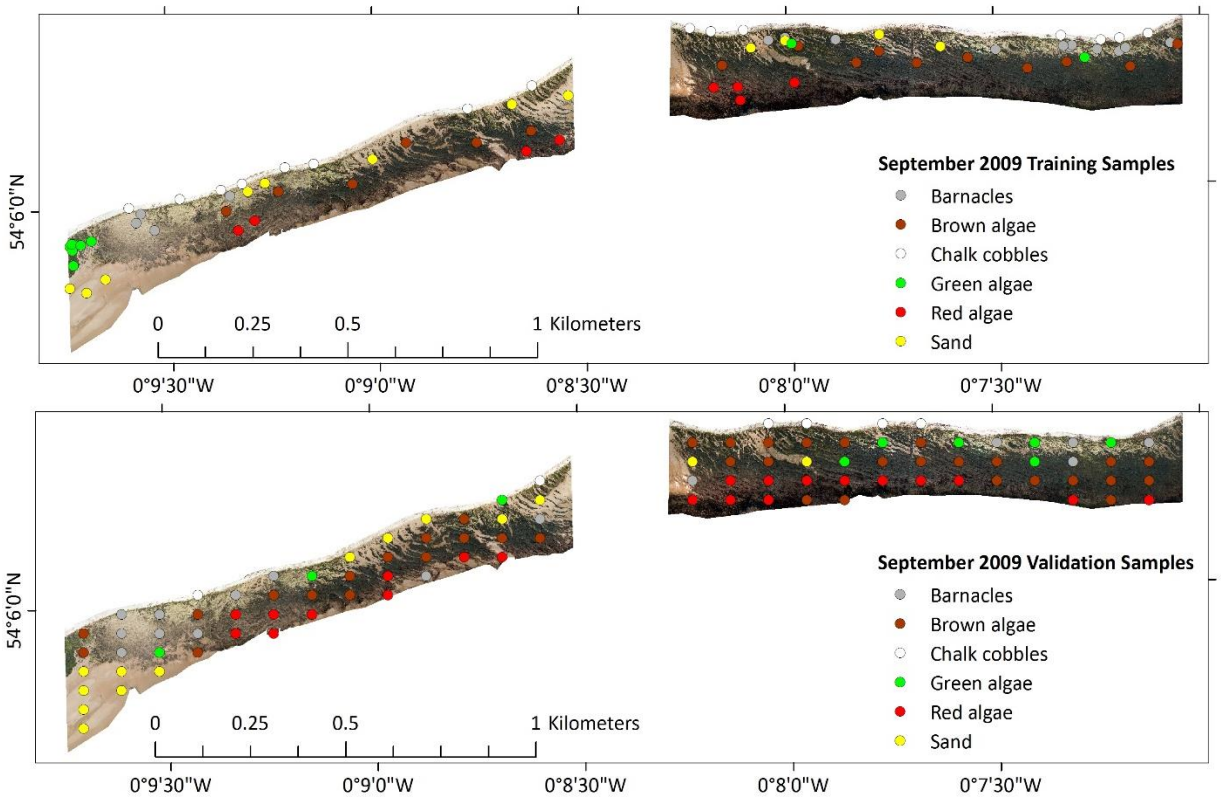

Figure 5.5: Training and validation samples created through visual inspection of aerial imagery collected in September 2009

Unclassified objects were then classified as red, brown or green algae, barnacles, chalk cobbles or sand using two supervised classification methods in turn: random forests (RF) and membership functions (MF).

Random Forests

Objects overlying points in the training dataset were defined as training samples. eCognition's Random Trees classifier was trained using these samples with a set of 45 feature values for 2009-2014 imagery and 65 feature values for 2014-2016 imagery which includes near infrared (NIR) (Table 5.2). All other training parameters in the Random Trees classifier were kept at their default values.

Table 5.2: Feature values used to train Random Trees classifier in eCognition to produce habitat maps from each set of combined aerial and LiDAR imagery. Spectral layers which were only available from 2014 onwards are shown in italics.

Feature	**Spectral layers**	**Topographic layers**
Mean	Brightness, Maximum difference, Red, Green, Blue, Blue/Green Band Ratio, Red/Blue Band Ratio, Red/Green Band Ratio, Normalised Blue Green Index, Normalised Blue Red Index, Normalised Green Red Index, *NIR, NDVI, Normalised NIR Blue Index, Normalised NIR Green Index*	Elevation, Slope
Mode	Red, Green, Blue, Normalised Blue Green Index, Normalised Blue Red Index, Normalised Green Red Index *NIR, NDVI, Normalised NIR Blue Index, Normalised NIR Green Index*	Elevation, Slope
Standard deviation	Red, Green, Blue, Normalised Blue Green Index, Normalised Blue Red Index, Normalised Green Red Index *NIR, NDVI, Normalised NIR Blue Index, Normalised NIR Green Index*	Elevation, Slope
Skewness	Red, Green, Blue, Normalised Blue Green Index, Normalised Blue Red Index, Normalised Green Red Index *NIR, NDVI, Normalised NIR Blue Index, Normalised NIR Green Index*	Elevation, Slope
GLCM Homogeneneity (all directions)	Red, Green, Blue, Normalised Blue Green Index, Normalised Blue Red Index, Normalised Green Red Index *NIR, NDVI, Normalised NIR Blue Index, Normalised NIR Green Index*	Elevation, Slope

The trained classifier was applied to all unclassified objects to produce a habitat map. The classifier was then queried to generate 'importance values' for the features used in the classification, and the classification re-run using the subset of features with an importance value greater than the mean importance value for the whole set of features.

Membership Functions (MF)

Membership functions define an object's degree of membership (from 0 to 1) to a class by applying fuzzy logic. Samples were created from objects overlying points in the training dataset. eCognition's Sample Editor tool was used to compare histograms of sample values for pairs of classes to select the best subset of features for defining membership to each class. eCognition's basic classification algorithm was used to evaluate every unclassified object's degree of membership to each class based on these features, assigning the object to the class with the highest membership value. The classification was run twice for each dataset; first the same set of 'fixed' value ranges was applied to each dataset, then value ranges specific to each dataset were computed from the samples for that dataset. Table 5.3 shows the features and the 'fixed' value ranges used to define membership to each class.

Table 5.3: Membership functions used to define the degree of membership to habitat classes. Features which were only available for data from 2014 onwards are shown in italics. See Appendix 2 for an explanation of function forms.

Habitat class	Feature	Value range	Function form
Barnacles	Brightness	70 – 255	About range
	Standard deviation Red	0.85 – 29	About range
	Red/Green Band Ratio	0.8 – 1.2	Linear range (triangle)
	Mean NDVI	*-0.19 – 0.18*	*About range*
Chalk cobbles	Brightness	150 – 255	Full range
	Mean LiDAR (x3 weighting)	1.2 – 15	Full range
Browns	Mean Normalised Blue Red Index	-0.1 – 0.2	Approximate Gaussian
	Mean Normalised Blue Green Index	-0.1 – 0.08	About range
	Brightness	28 – 88	About range
	Mean NDVI	*-0.3 – 0.85*	*Approximate Gaussian*
Greens	Brightness	0 – 105	Approximate Gaussian
	Red/Green Band Ratio	0.7 – 1.1	About range
	Mean Normalised Blue Green Index	-0.15 – 0.01	About range
	Mean Normalised NIR Green Index	*0.04 – 0.37*	*About range*
Reds	Mean Normalised Green Red Index	-0.08 – 0.07	About range
	Brightness	20 – 120	Approximate Gaussian
	Mean Normalised Blue Red Index	-0.18 – 0.18	About range
	Red/Blue Band Ratio	0.5 – 1.5	About range
	Mean Normalised NIR Blue Index	*-0.25 – 0.33*	*About range*
Sand	Maximum difference	0.2 – 1.8	Greater than
	Red/Green Band Ratio	0.9 – 1.17	Linear range (triangle)
	Standard deviation Red	0 – 18	About range
	Mean NDVI	*-0.49 – 0.11*	*About range*

The overall accuracy of each map generated by the RF and MF classifiers was calculated through comparison with validation samples, which were created from objects overlying the grid of points as exemplified in Figure 5.5.

5.2.4 Post-classification change detection

Maps created using the RF classifier were converted to 0.2m resolution rasters with habitat class names reclassified as numeric values as follows:

Strandline	1
Shadow	2
Barnacle/rock	3
Chalk cobbles	4
Sand	5
Brown algae	6
Red algae	7
Green algae	8

Pairs of maps from the same season in consecutive years were imported to eCognition and a chessboard segmentation carried out at scale 1 to create objects consisting of single pixels. Habitat classes and membership thresholds were created to classify change at three levels of sensitivity by comparing the classification of each single-pixel object in the two maps (Table 5.4). The term 'sensitivity' is used in this context to describe each map's thresholds for defining change, it is not a reference to ecological sensitivity. 'High' sensitivity classifies change as any difference in classification between the two maps except for change to or from shadow or strandline; 'medium' sensitivity classifies change as any difference in classification except change to or from shadow or strandline or from one algal class to another; 'low' sensitivity classifies change as a transition from any algal class to any unvegetated class or vice versa.

Table 5.4: Habitat classes and membership thresholds for creating change-detection maps at three levels of sensitivity, showing the transitions in either direction between pairs of habitat classes classified by each rule.

Class	Membership thresholds	Transition in either direction between classes
Change (high)	Year 1 <> Year 2 and Year 1 > 2 and Year 2 > 2	3-4, 3-5, 3-6, 3-7, 3-8, 4-5, 4-6, 4-7, 4-8, 5-6, 5-7, 5-8, 6-7, 6-8, 7-8
No change (high)	Year 1 = Year 2	1-1, 2-2, 3-3, 4-4, 5-5, 6-6, 7-7, 8-8
Change (medium)	Year 1 <> Year 2 and Year 1 > 2 and Year 2 > 2 and Year 1 < 6 or Year 1 <> Year 2 and Year 1 > 2 and Year 2 > 2 and Year 2 < 6	3-4, 3-5, 4-5, 3-6, 3-7, 3-8, 4-6, 4-7, 4-8, 5-6, 5-7, 5-8
No change (medium)	Year 1 = Year 2 or Year 1 >=6 and Year 2 >= 6	1-1, 2-2, 3-3, 4-4, 5-5, 6-6, 7-7, 8-8, 6-7, 6-8, 7-8
Change (low)	Year 1 >= 6 and Year 2 <= 5 and Year 2 >= 3 or Year 2 >=6 and Year 1 <= 5 and Year 1 >=3	3-6, 3-7, 3-8, 4-6, 4-7, 4-8, 5-6, 5-7, 5-8
No change (low)	Year 1 = Year 2 or Year 1 >=6 and Year 2 >= 6 or Year 1 <=5 and Year 1 >=3 and Year 2 <=5 and Year 2 >=3	1-1, 2-2, 3-3, 4-4, 5-5, 6-6, 7-7, 8-8, 3-4, 3-5, 4-5, 6-7, 6-8, 7-8

5.2.5 Pre-classification change detection

Rasters were created from the normalised index between the same band in two consecutive images using the formula:

$$\frac{\text{Year 2 Band x} - \text{Year 1 Band x}}{\text{Year 2 Band x} + \text{Year 1 Band x}} \times 100$$

The index is multiplied by 100 to enable the layers to be used in segmentation; differences in values from -1 to 1 are too small to be detected by eCognition's multi-resolution region growing segmentation algorithm.

Spectral layers for pairs of imagery were imported to eCognition, creating projects with 15 image layers for years with RGB imagery and 24 image layers for years with RGB and NIR imagery (Table 5.5). LiDAR data was not included because comparison of consecutive images showed that difference in elevation was less than the vertical accuracy of the imagery (0.15m) for between 80-90% of the total area, and change in elevation greater than 0.15m was restricted to areas of sand and the base of cliffs, rather than intertidal reef which was the focus of this study.

Table 5.5: Image layers used in the creation of pre-classification change detection maps. Layers only available from 2014 onwards are shown in italics.

Year 1	Red, Green, Blue, *NIR*, Normalised Blue Green Index, Normalised Blue Red Index, Normalised Green Red Index, *Normalised NIR Blue Index, Normalised NIR Green Index, NDVI*
Year 2	Red, Green, Blue, *NIR*, Normalised Blue Green Index, Normalised Blue Red Index, Normalised Green Red Index, *Normalised NIR Blue Index, Normalised NIR Green Index, NDVI*
Difference	Normalised Year 2 Year 1 Red Index, Normalised Year 2 Year 1 Green Index, Normalised Year 2 Year 1 Blue Index, *Normalised Year 2 Year 1 NIR Index*

A class hierarchy was created with the following classes:

Change	**No change**
Algae to Rock	Algae to Algae
Algae to Sand	Rock to Rock
Rock to Algae	Sand to Sand
Rock to Sand	
Sand to Algae	
Sand to Rock	

Segmentation was carried out at scale parameter 22 with homogeneity criteria weighting shape (0.1) versus colour (0.9) and compactness (0.9) versus smoothness (0.1) using the three normalised year 1 year 2 band index layers. Points were created at the centroid of each object, and a training dataset was created for each pair of images by manually selecting at least 100 points, distributed as evenly as possible between the above habitat classes, and classifying them through visual interpretation of both images. Supervised classification was carried out using both RF and standard nearest neighbour (SNN) classifiers with reference to sample object values of mean, mode, standard deviation, skewness and GLCM homogeneity

for all image layers. Feature Space Optimisation was carried out prior to SNN classification, to select the best ten features for separating classes with each pair of images.

Objects were then reclassified as 'change' or 'no change' to produce medium or low sensitivity change maps as shown in Table 5.6:

Table 5.6: Transition types included in 'low' and 'medium' sensitivity pre-classification change maps

	Change	**No change**
Medium sensitivity	Algae to Rock, Algae to Sand, Rock to Sand, Sand to Rock, Rock to Algae, Sand to Algae	Algae to Algae, Rock to Rock, Sand to Sand
Low sensitivity	Algae to Rock, Algae to Sand, Rock to Algae, Sand to Algae	Algae to Algae, Rock to Rock, Rock to Sand, Sand to Rock, Sand to Sand

Validation datasets were created by randomly selecting equal numbers of points within areas classified as 'change' and areas classified as 'no change' and classifying them through visual assessment of the imagery. Overall accuracy, user's accuracy and producer's accuracy of each map was calculated through comparison with the validation datasets. Finally, the Combine tool in ArcGIS was used to calculate the percentage area with the same classification in pairs of change maps produced from the same data using different methods.

5.3 Results

5.3.1 Habitat maps

Validation of the habitat maps produced from each dataset showed that the RF classifier produced maps with the highest and most consistent level of mean accuracy (71.4% ± 1.6%). Limiting the number of features used with the RF classifier to those with a high importance value did not increase the mean accuracy of the output maps (67.5% ± 2.0%). Maps produced using the MF classifier had a mean overall accuracy of 64.9% ± 3.6% when value ranges were derived from the image being used to create the map, but a mean overall accuracy of 41.8% ± 7.0% when the same value ranges were applied to all datasets.

Examination of feature values of training samples showed a high degree of within-class spectral variability during the multi-temporal dataset as exemplified in Figure 5.6. This variability explains the low accuracy of maps produced using the MF classifier with fixed values and could be caused by changes in atmospheric conditions, sun angle, sensor and image processing methods during the eight year period.

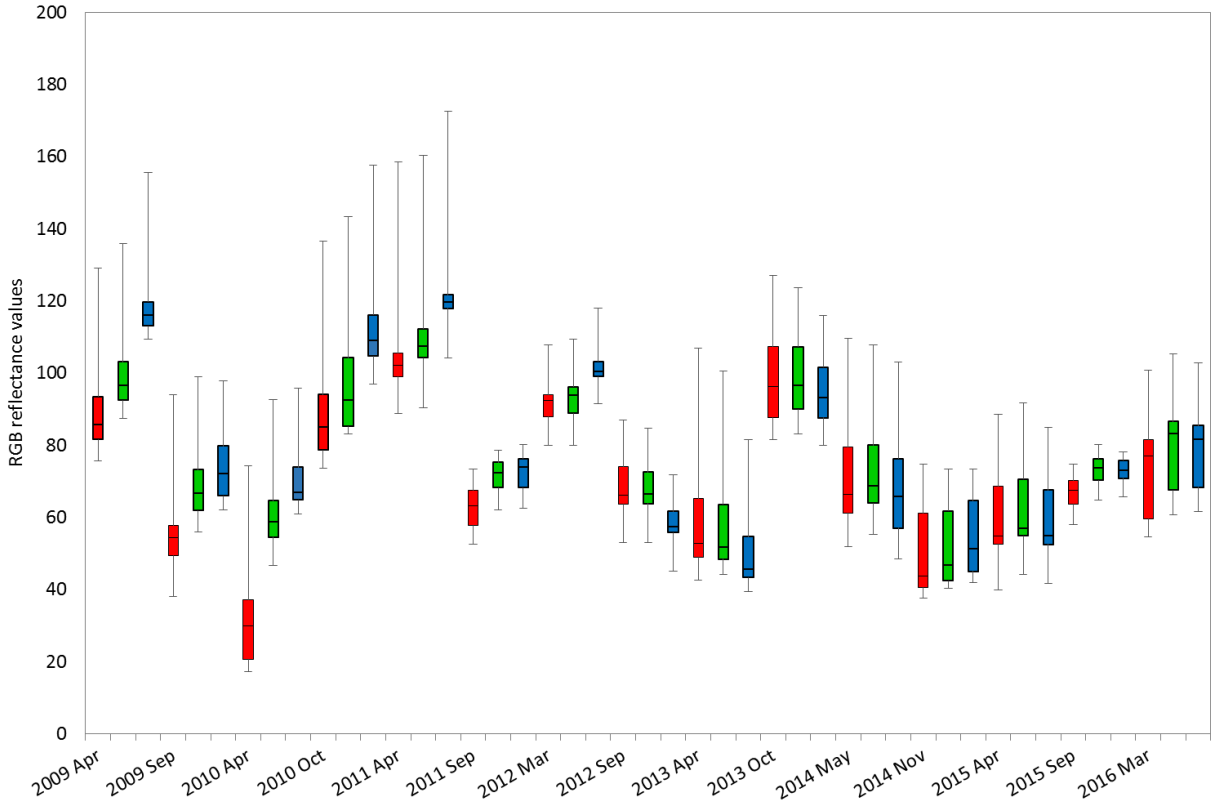

Figure 5.6: Mean red, mean green and mean blue values for training samples in the brown algae habitat class (n = 16).

Examination of training sample values showed that the best features for separating classes were band ratios, normalised band indices, brightness and shore height. However, no single feature could separate all six classes and the ability of spectral features to distinguish habitat classes varied from one dataset to another. For example, the normalised blue red index (blue – red / blue + red) was used by both the MF and RF classifiers, but Figure 5.7 illustrates the variability in the range of values defining each class and in the ability of this feature to separate classes. Some plots showed a clear separation of values for brown and red algae, while others showed overlap in the range of values for these two classes.

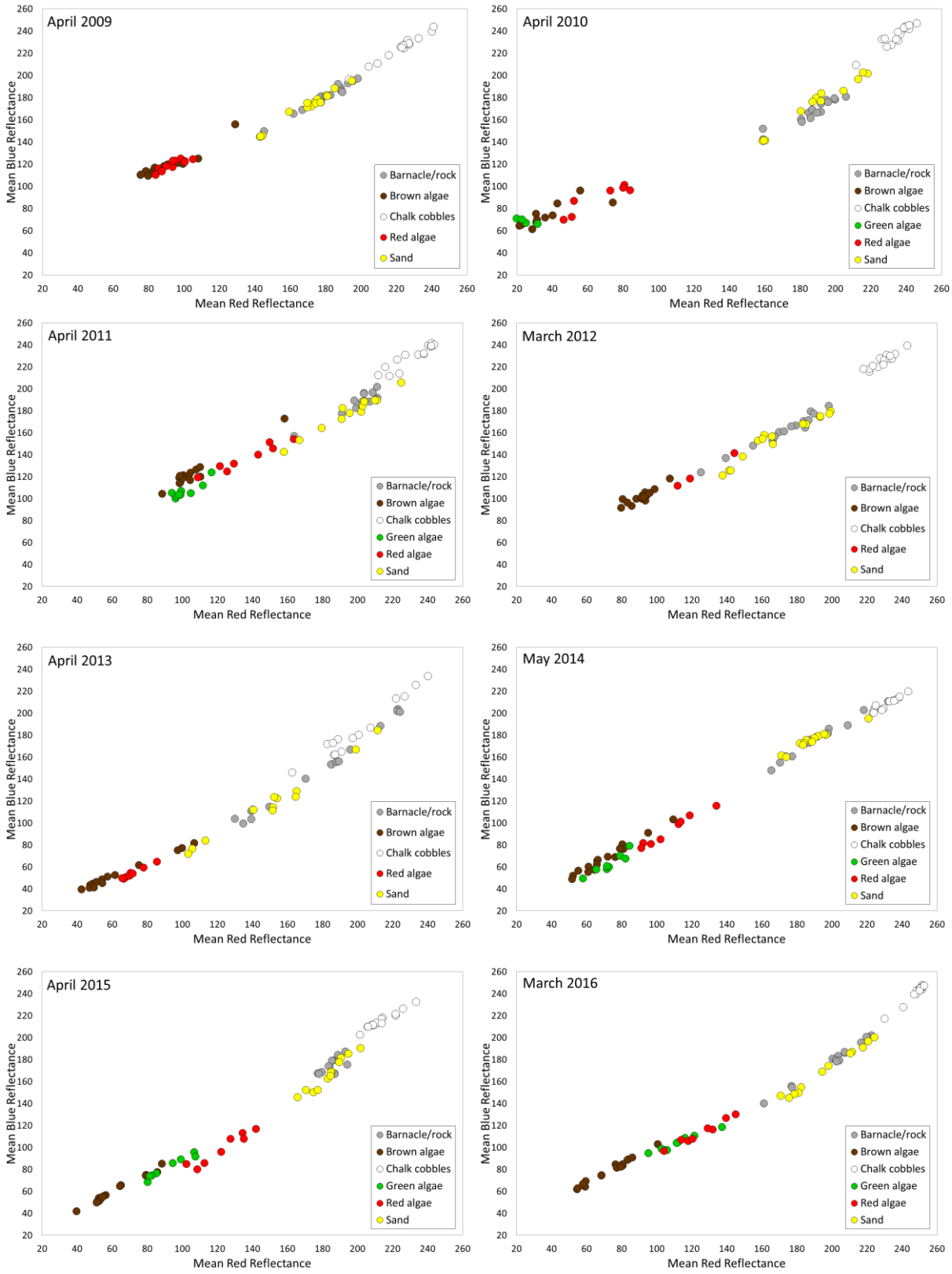

Figure 5.7: Mean red and mean blue reflectance values of training samples used to create habitat maps from spring aerial imagery. Green algae training samples were not created for some datasets because the habitat class was not detectable in the imagery.

For each method, the mean accuracy was slightly higher for maps created using RGB and NIR imagery (2014-2016, *n* = 5) than for those created using only RGB imagery (2009-2013, *n* =

10), but in each case the difference between the means was smaller than the standard deviation (Figure 5.8).

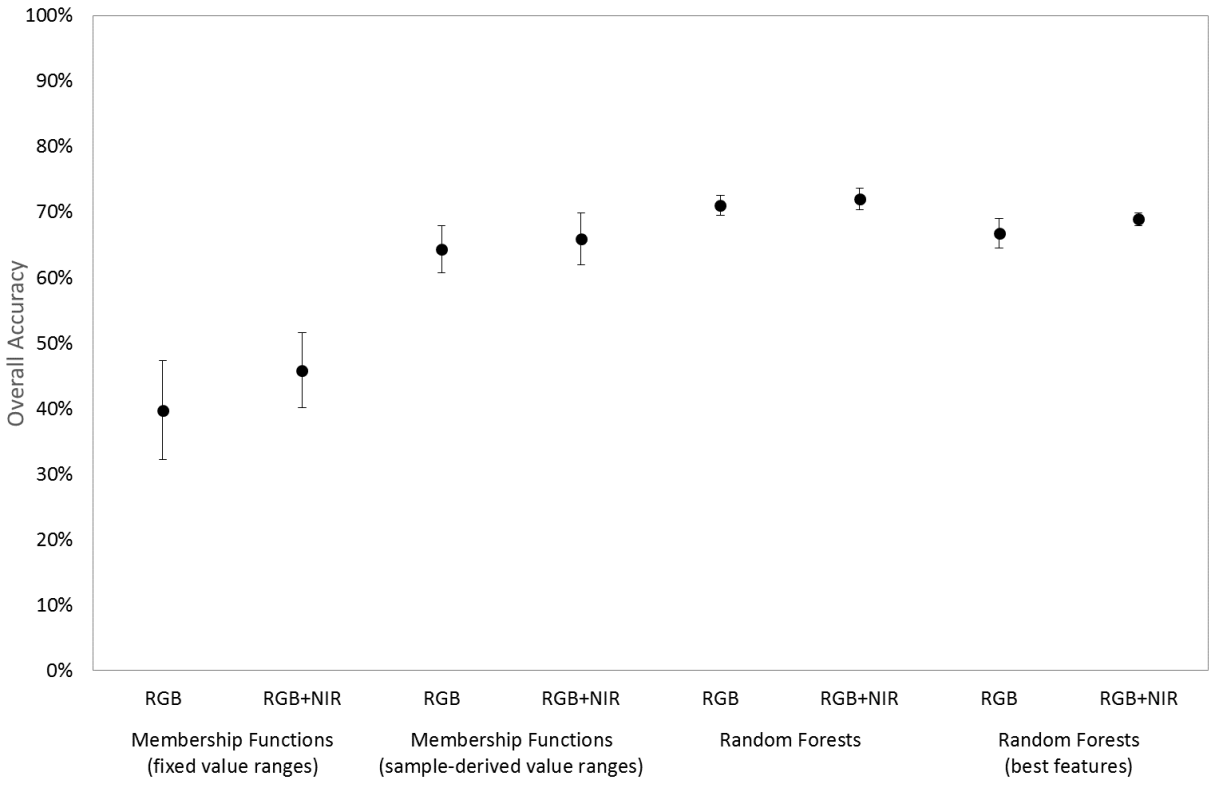

Figure 5.8: Mean overall accuracy of habitat maps created through object-based analysis of multi-temporal aerial and LiDAR imagery (n = 15). Error bars represent standard deviation.

Classification accuracy varied with habitat class; chalk cobbles, sand and brown algae had high levels of accuracy compared to barnacle/rock, red algae and green algae (Figure 5.9). User's accuracy was higher than producer's accuracy for all habitat classes except for red and green algae, showing that errors of omission were more prevalent than errors of commission in classifying these habitats. Red and green algae classes had particularly low user's accuracy, meaning that errors of commission were more prevalent for these habitat classes, which were less abundant and more transient than the other habitat classes.

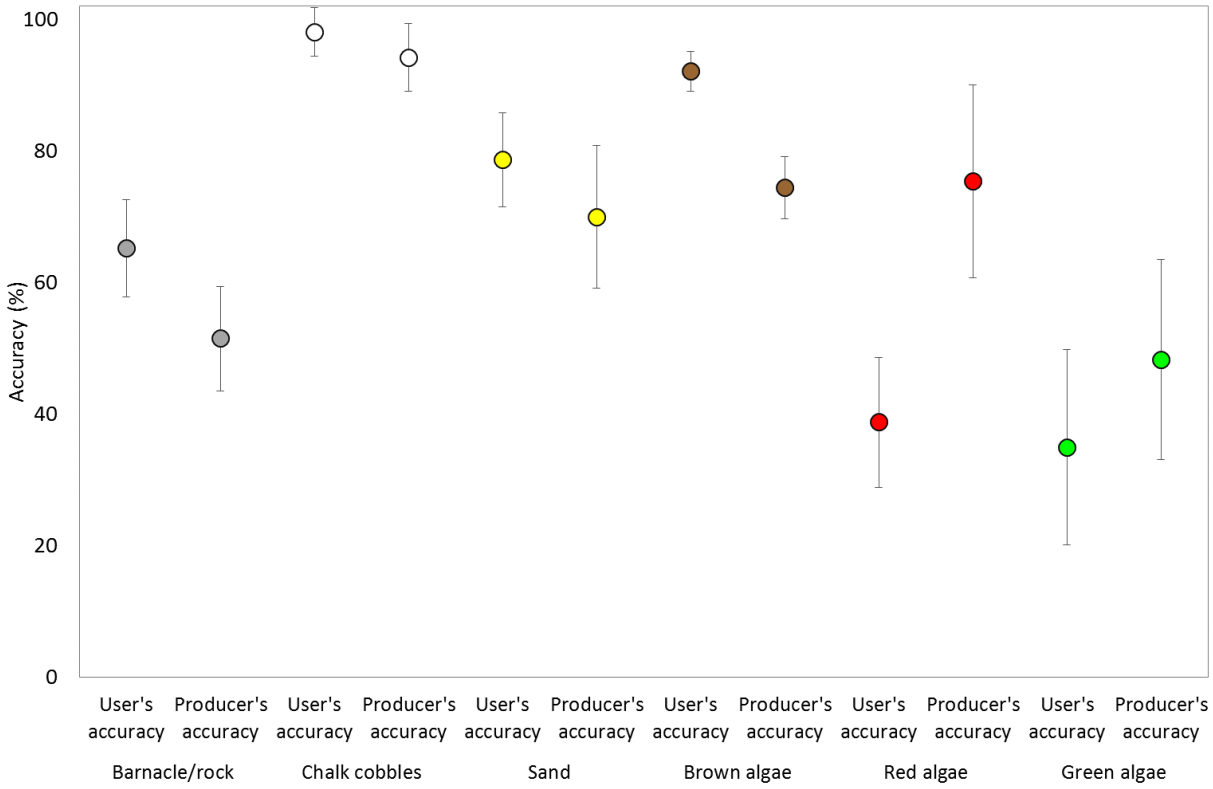

Figure 5.9: User's and Producer's accuracy per class for the habitat maps produced using the RF classifier. Error bars represent standard deviation. (n = 15)

The relatively low accuracy of the barnacle/rock category could be due to the presence of sparsely vegetated rock with a different spectral signature to fully vegetated and unvegetated rock, and indeed Figure 5.10 shows evidence of misclassification between rock and all three algal classes. Figure 5.10 shows that equally high levels of misclassification occurred between algal classes (mean proportion of total map inaccuracy of 11.5% ± 2.3%) and between algal and bare substratum classes (11.6% ± 2.2%).

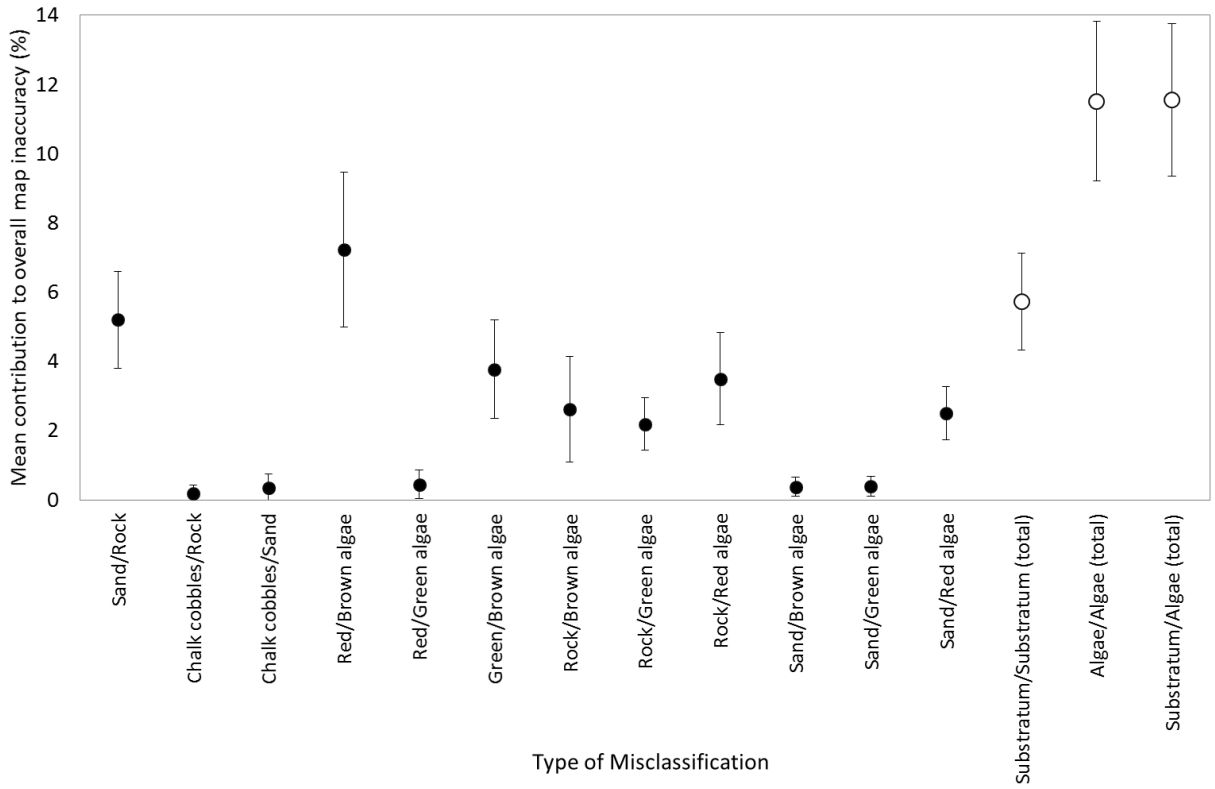

Figure 5.10: Mean contribution of each misclassification type to overall map inaccuracy for habitat maps produced using the RF classifier. Error bars represent standard deviation. (n = 15).

This has implications for the production of change detection maps; medium and low sensitivity maps ignore change from one algal class to another, so could have higher accuracy than the habitat maps from which they are produced, but misclassification errors between algal and bare substratum classes will impact the accuracy of change detection maps even at low sensitivity. The highest levels of misclassification occurred between sand and rock and between red and brown algae, classes which have similar spectral signatures and, in the case of red and brown algae, phase into each other on the shore rather than having distinct boundaries. Rock is likely to have higher rugosity than sand, but this may not be detectable from LiDAR imagery at 1m resolution.

Despite overall inaccuracy levels of around 30%, visual assessment of habitat maps produced using the RF classifier showed that areas of change visible in the aerial imagery are also visible in the habitat maps, for example the transition from algae-covered rock to sand shown in Figure 5.11.

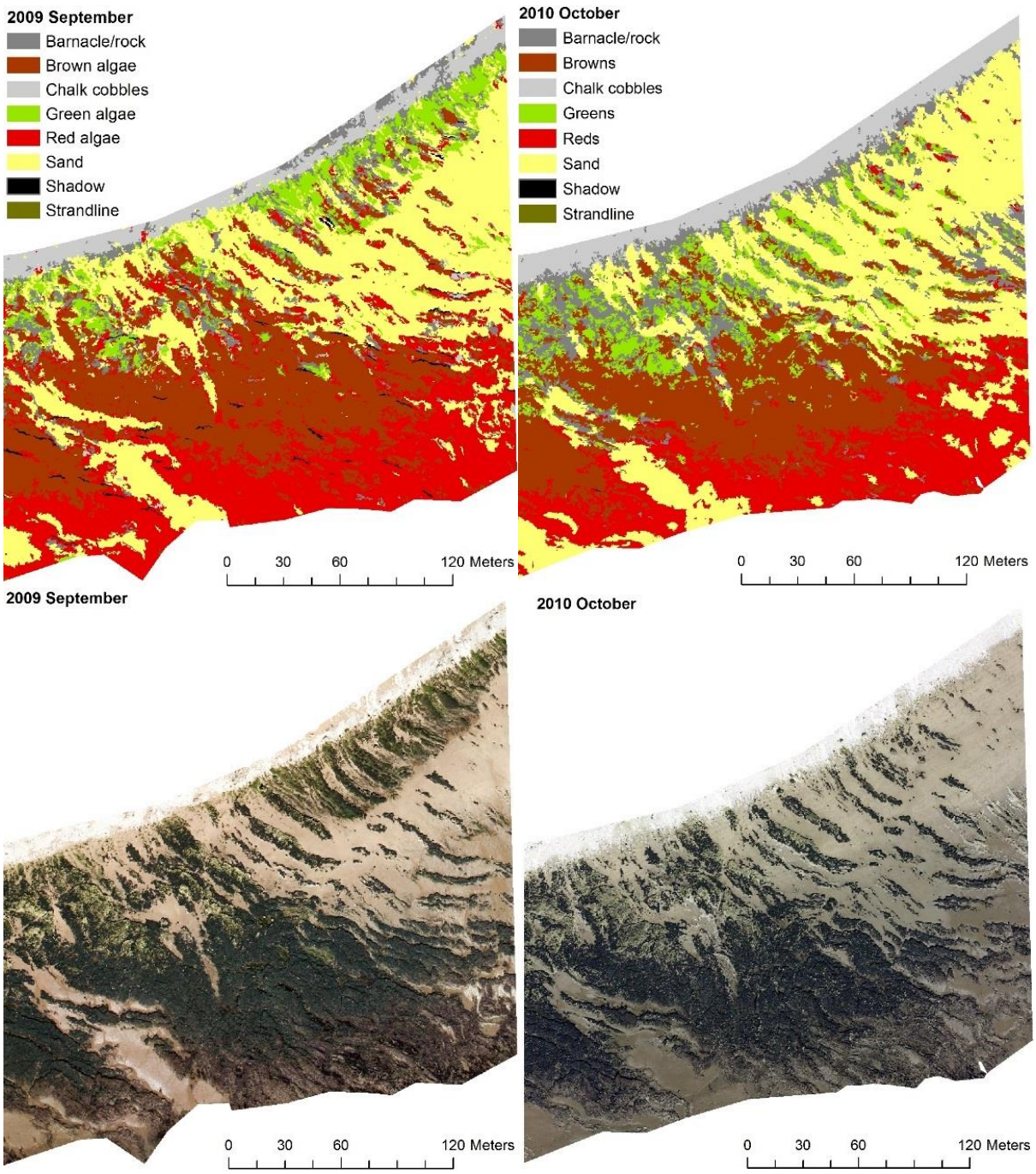

Figure 5.11: Habitat maps for September 2009 (72.5% accuracy) and October 2010 (71.0% accuracy) produced using a RF classifier (top) and the aerial imagery from which they were produced (bottom), showing a transition from algae-covered rock to sand in the north east of the map.

5.3.2 Change detection maps

Mean overall accuracy of the change detection maps ranged from 70.5% ± 2.9% to 82.6% ± 3.3%, with the RF and post-classification methods producing more accurate results than the SNN classifier (Figure 5.12). Both RF and post-classification methods showed a slight inverse correlation between accuracy and sensitivity.

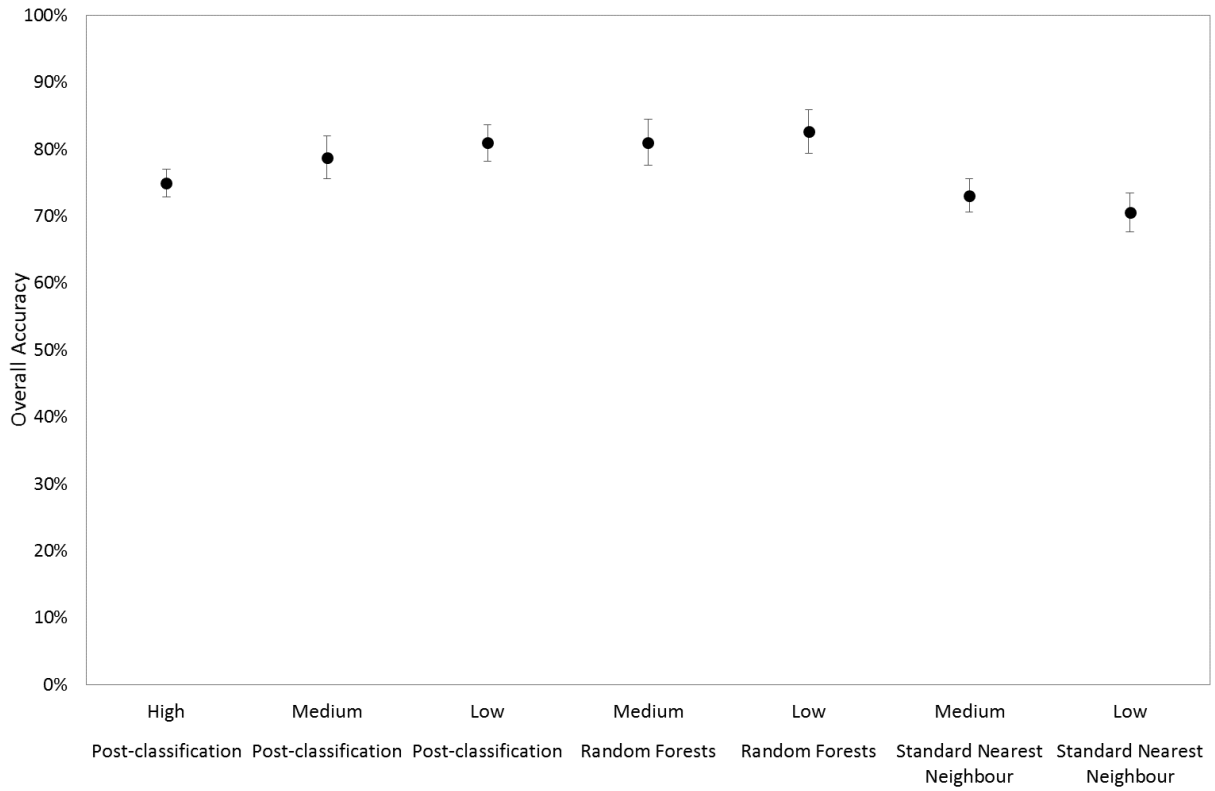

Figure 5.12: Mean overall accuracy of high, medium and low sensitivity change detection maps created by object-based analysis of multi-temporal aerial and LiDAR imagery (n = 13). Error bars represent standard deviation.

Mean user's accuracy for the 'change' class ranged from 58.8% ± 3.1% to 75.7% ± 3.0% and was consistently lower than mean user's accuracy for the 'no change' class which ranged from 80.3% ± 2.3% to 93.5% ± 2.6% (Figure 5.13).

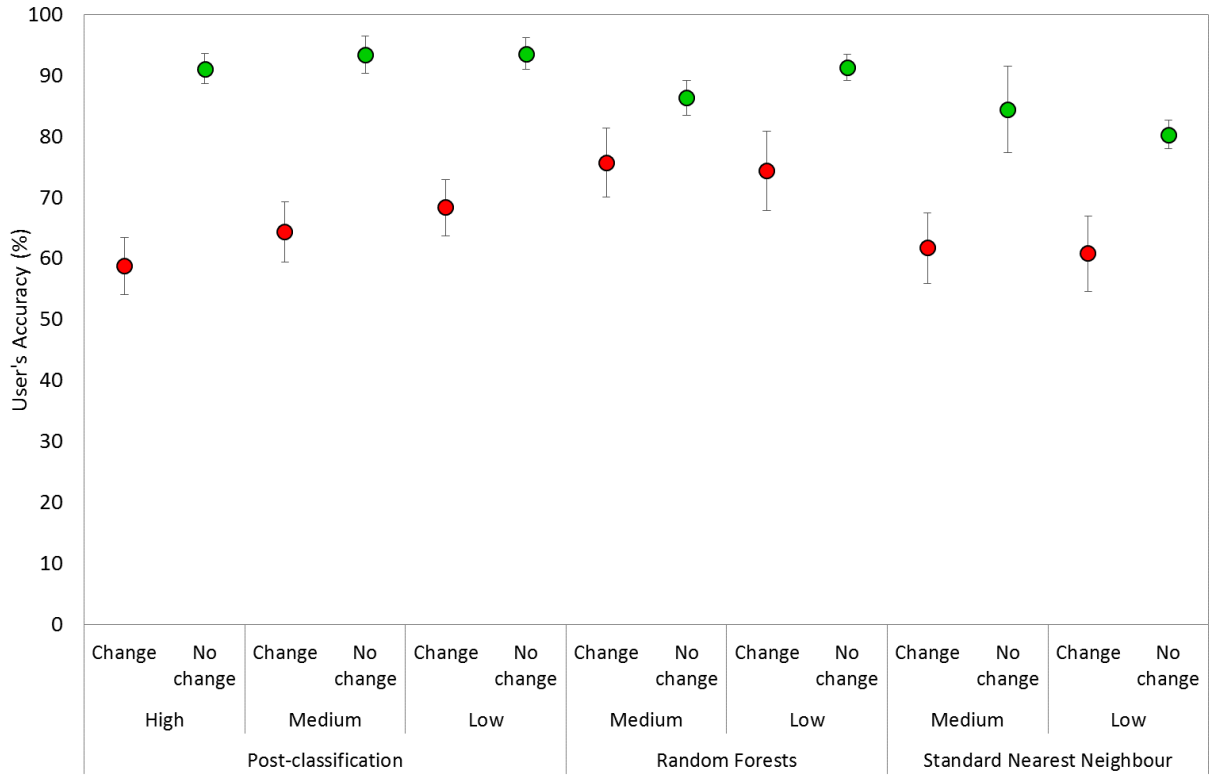

Figure 5.13: Mean user's accuracy for the 'change' and 'no change' classes (n = 13). Error bars represent standard deviation.

Mean producer's accuracy for the 'change' class ranged from 75.3% ± 2.4% to 91.6% ± 3.1% and was consistently higher than mean producer's accuracy for the 'no change' class which ranged from 67.9% ± 3.3% to 78.9% ± 4.5% (Figure 5.14).

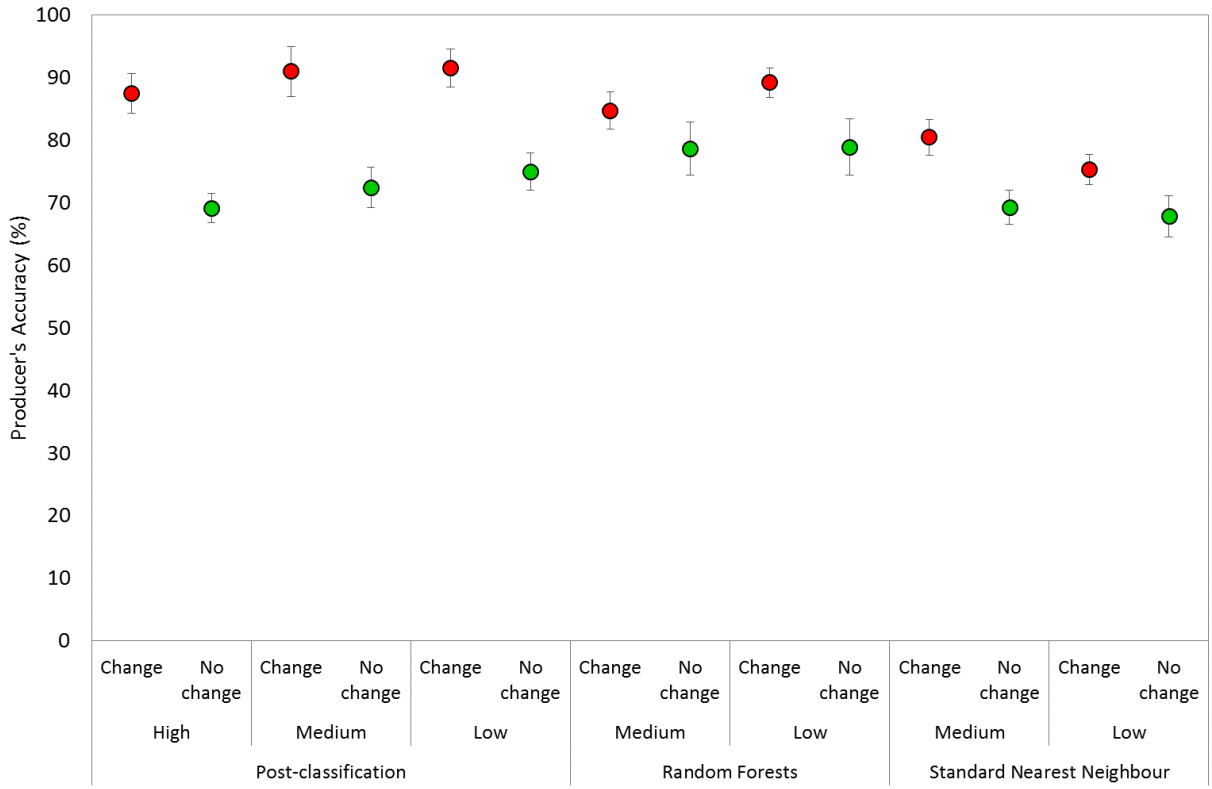

Figure 5.14: Mean Producer's accuracy for the 'change' and 'no change' classes (n = 13). Error bars represent standard deviation

Figure 5.13 and Figure 5.14 show that the main cause of map inaccuracy with all three classification methods and all levels of sensitivity was errors of commission in the 'change' class and errors of omission in the 'no change' class. Although mean overall accuracy was comparable between the post-classification and RF methods, the post-classification approach produced maps with a higher producer's accuracy for 'change' and higher user's accuracy for 'no change', showing that this method had greater tendency to over-predict change than the RF pre-classification method.

The mean proportion of total area classified as 'change' was 39.5% ± 1.3% for the high sensitivity maps, and ranged from 16.7% ± 3.7% to 22.8% ± 2.0% for medium sensitivity maps and from 13.8% ± 3.3% to 16.2% ± 3.4% for low sensitivity maps (Figure 5.15).

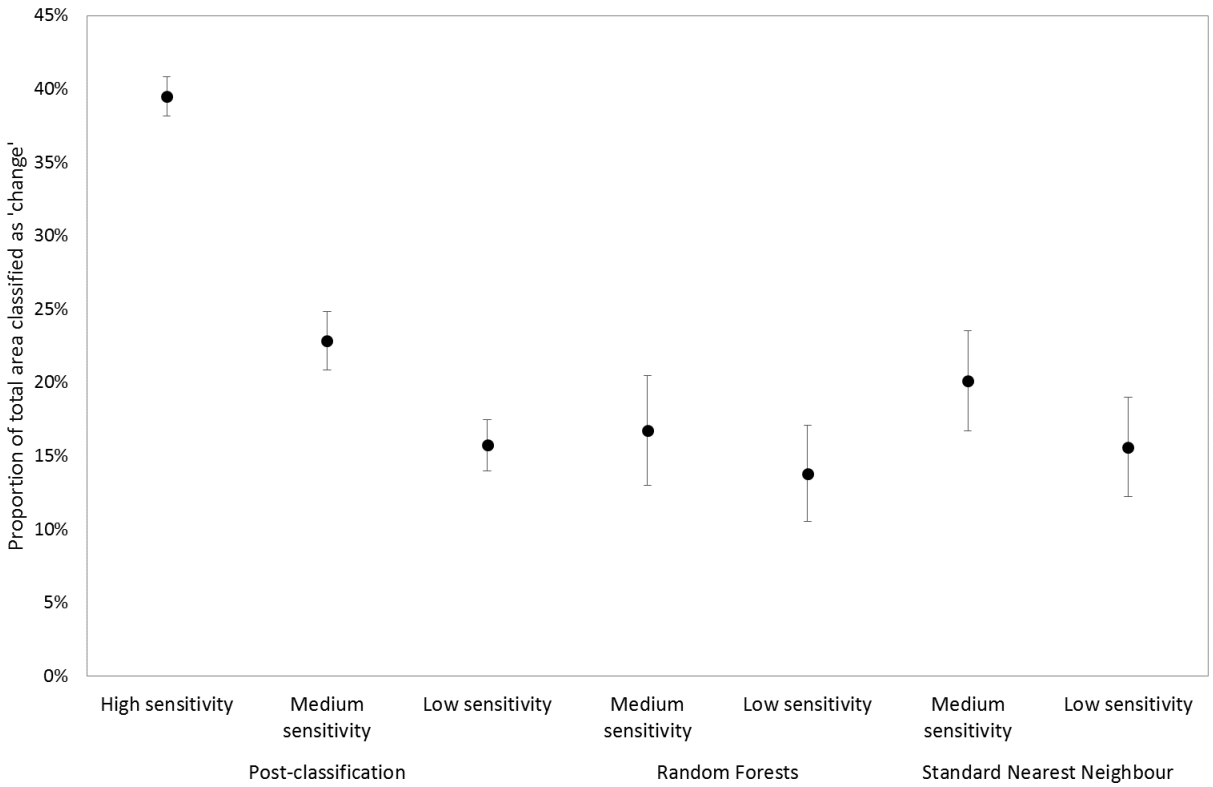

Figure 5.15: Mean proportion of total area classified as 'change' in change detection maps created by object-based analysis of multi-temporal aerial and LiDAR imagery (n = 13). Error bars represent standard deviation.

Comparison of the proportion of total area occupied by each change class in consecutive maps provided no evidence of directional change within the 8-year period but was suggestive of cyclical fluctuation (Figure 5.16 and Figure 5.17). For example, an increase in rock in autumn 2010 was followed by an increase in algae in the following two years, then by another increase in rock in 2013 and another increase in algae in the following two years (Figure 5.17). In some years there was no single dominant change class, but similar sized losses and gains in different parts of the shore. For example, in spring 2011-12, 4% of the total area was classified as changing from algae to rock while 3.7% was classified as changing from rock to algae, and in autumn 2011-12, 3.9% of the total area was classified as changing from algae to sand while 4.5% was classified as changing from sand to algae.

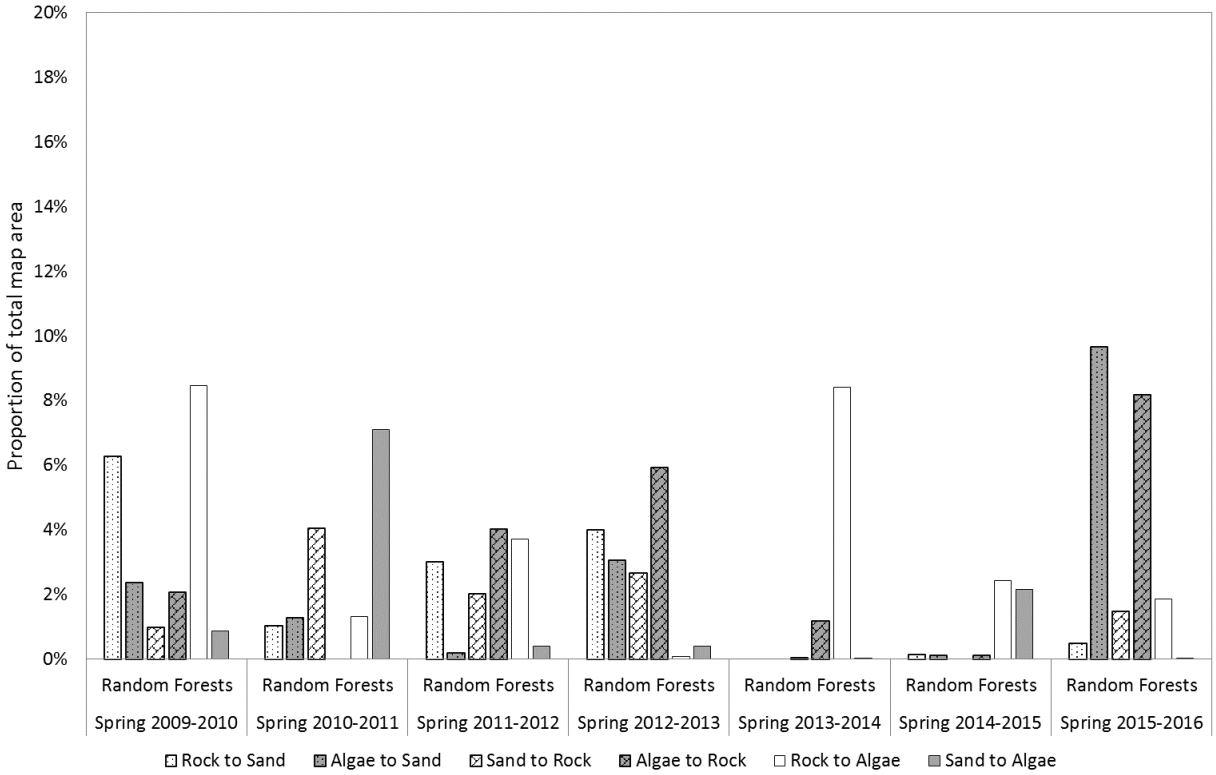

Figure 5.16: Proportion of total area classified as each change category from bi-temporal comparisons of spring imagery using a RF classification

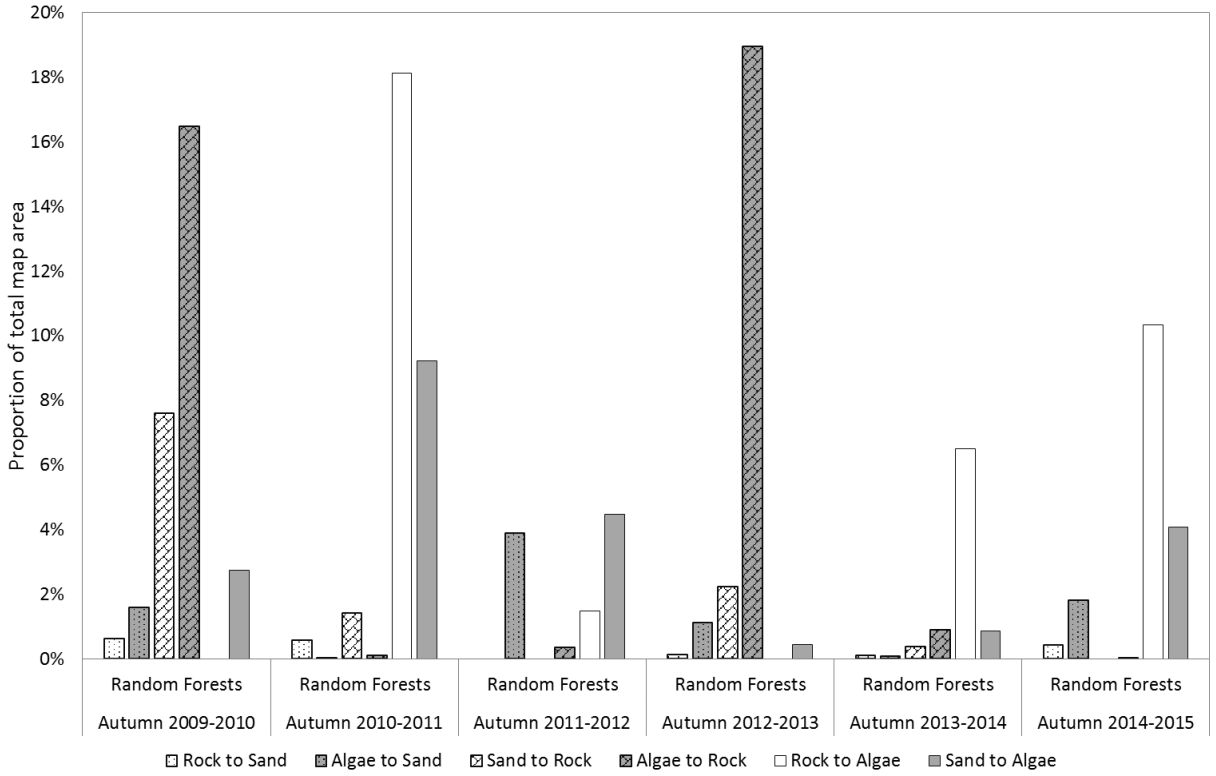

Figure 5.17: Proportion of total area classified as each change category from bi-temporal comparisons of autumn imagery using a RF classification

Although the amount and type of change varied from year to year, change consistently occurred predominantly at the reef edges where there is an interface between bedrock and sand or between bedrock and chalk cobbles on the upper shore. Figure 5.18 shows consecutive spring aerial images of the edge of the reef at the western boundary of the NTZ, again suggesting cyclical fluctuations rather than directional change, with algal coverage decreasing in 2010, 2012 and 2016, increasing in 2011 and 2013 and remaining stable in 2014 and 2015. Sand covered much of the reef in 2010, then receded over subsequent years to expose increasing amounts of bare rock, but covered much of the reef again in 2015 and 2016.

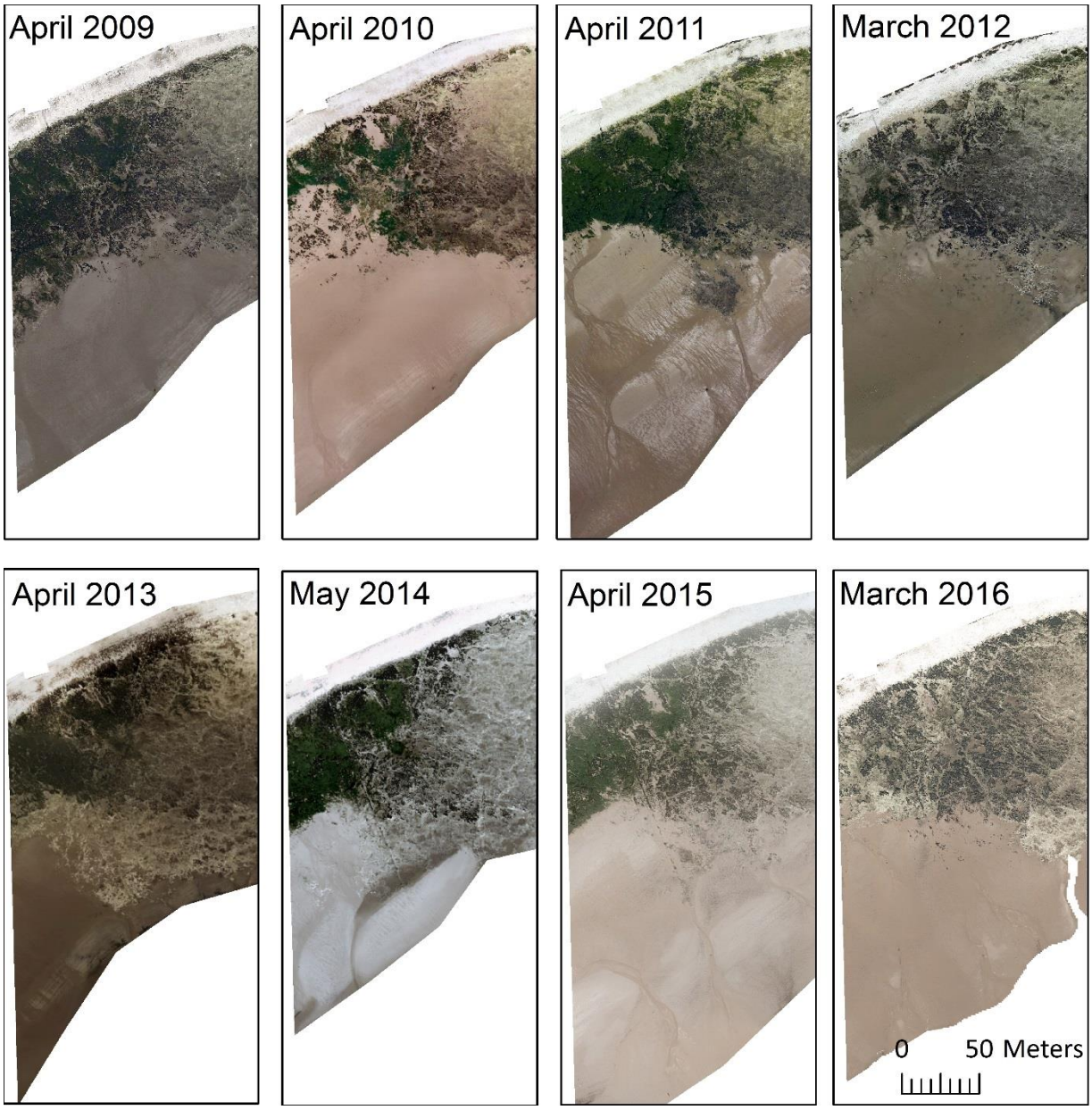

Figure 5.18: Spring aerial imagery from the western end of the No Take Zone showing fluctuations in algae, sand and bare rock at the reef edge

Figure 5.19 shows a low sensitivity change detection map produced using the RF classification as a typical example of the spatial distribution of change at the reef edges; reference to the aerial imagery shows change from algae to sand on the lower shore of both the NTZ and the control zone, from algae to rock at the western end of the NTZ, from algae to sand at the eastern end of the NTZ and from algae to rock along the upper shore, all of which have been classified as 'change' by the RF classification.

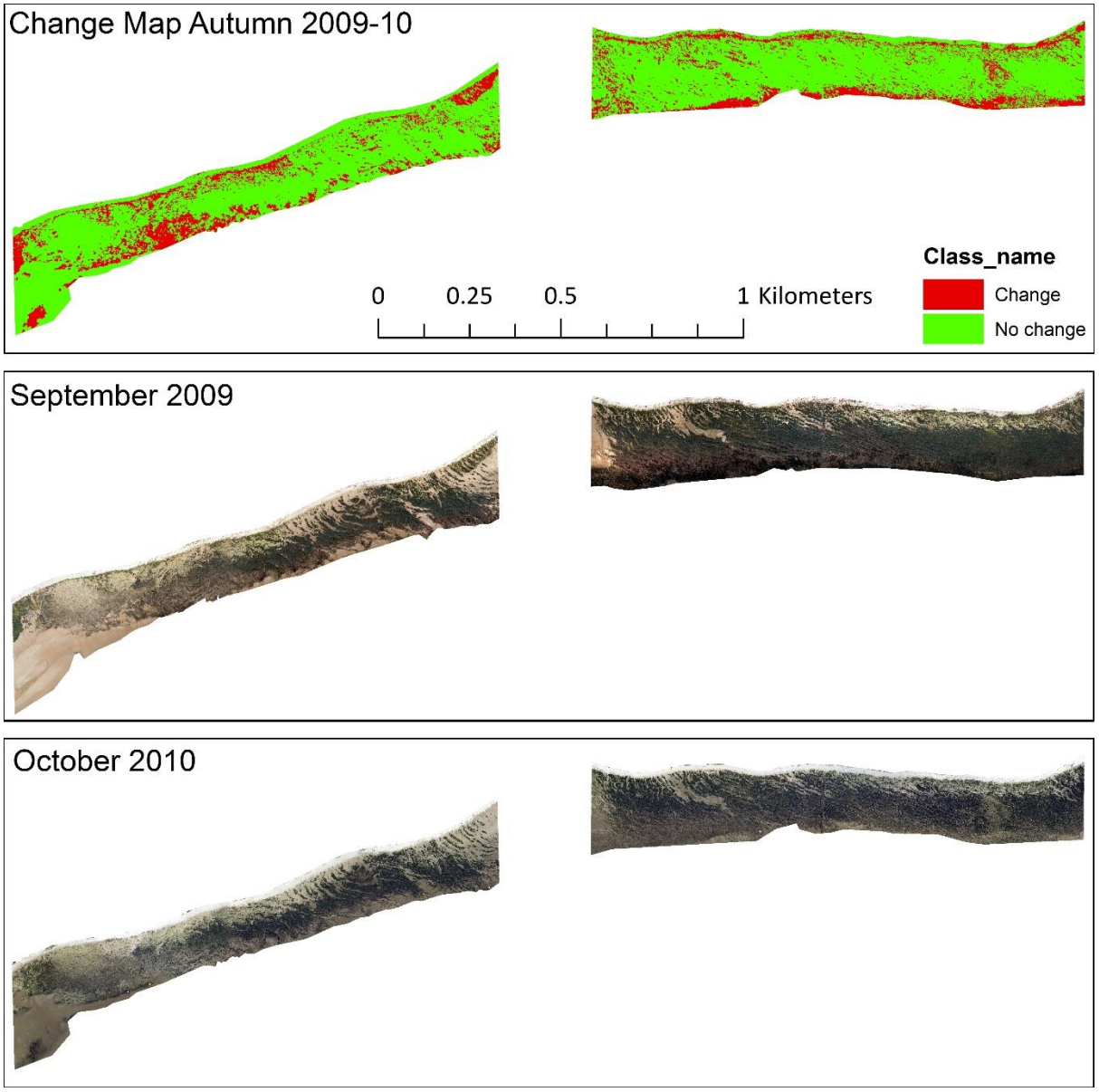

Figure 5.19: Low sensitivity change map produced using the RF classifier and the two sets of aerial imagery collected in September 2009 and October 2010 from which it was produced.

The mean proportion of total area with the same classification in pairs of maps produced from the same imagery using different methods ranged from 70.0% ± 2.3% to 83.1% ± 1.7% (Figure 5.20). The level of consistency was lowest between maps produced by the post-

classification and SNN methods. With all three pairs of methods there was a slight inverse correlation between consistency and sensitivity.

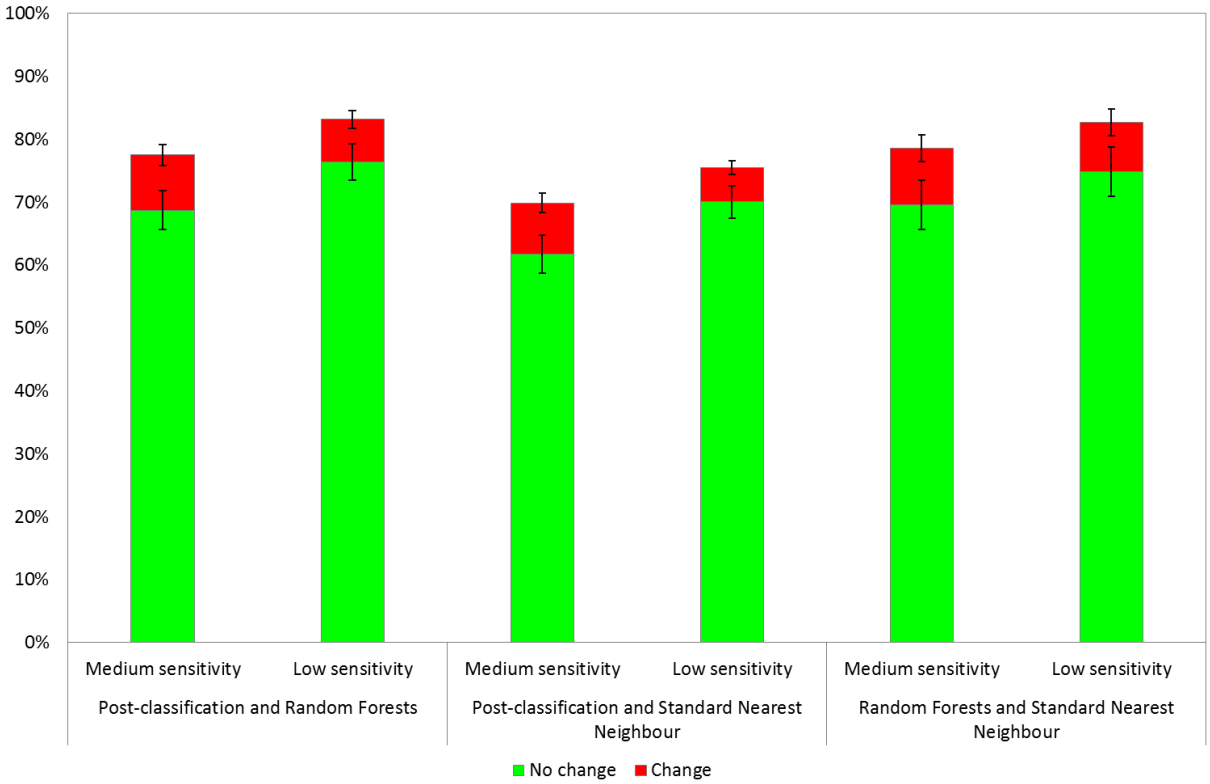

Figure 5.20: Consistency between change detection maps produced by different OBIA methods calculated as mean % of total area with the same classification in pairs of maps produced from the same data using different methods (n = 13). Error bars represent standard deviation.

5.4 Discussion

5.4.1 Accuracy of habitat maps

This study set out to evaluate whether freely available aerial and LiDAR imagery could be used to detect change in the extent and distribution of intertidal habitats, and to compare the accuracy and consistency of different OBIA change detection methods. The results showed that despite considerable within-class spectral variability, OBIA methods can be applied to these data to produce habitat maps with overall accuracy >70% and change detection maps with overall accuracy > 80%.

This was the first study to map temperate intertidal habitats from aerial and LiDAR imagery using an object-based approach, but for comparison overall accuracy achieved by pixel-based supervised classification in similar environments range from 53%-68% (Hunter and Power, 2002), 64%-71% (Thomson et al., 2003), 76% (Hennig et al., 2007), >80% (Lucas et al., 2011), 77%-85% (Oppelt et al., 2012) to 85% (Bajjouk et al., 1996). The low accuracy of

habitat maps created using the MF classifier with 'fixed' values is to be expected due to variability in the data. Signature extension, the process of training a classifier with reference values from one set of imagery then applying it to imagery of another place or time (Sexton et al., 2013), is only likely to be successful if radiometric correction is first applied to improve the consistency of imagery (Gomez et al., 2016). However, even when the MF classifier was applied using value ranges derived from each set of imagery, it produced habitat maps with lower mean accuracy and greater variability in accuracy than the RF classifier. Several comparative studies have shown RF to have higher accuracy than other classifiers, particularly when multi-dimensional or multi-source data are used (Ghimire *et al.*, 2012; Ghosh and Joshi, 2014; Shang and Chisholm, 2014; Xu *et al.*, 2014; Han *et al.*, 2015; Belgiu and Dragut, 2016), so these findings regarding the performance of the RF classifier at producing both habitat maps and change detection maps from combined aerial and LiDAR imagery are consistent with these studies. The low user's accuracy indicating high errors of commission of the red and green algae classes may be explained by the sampling design which aimed to create an equal number of training samples per habitat class. Other studies have shown that the RF classifier is sensitive to the proportions of different classes in the training samples (Colditz, 2015; Millard and Richardson, 2015) so given that some habitat classes (e.g. red and green algae) are less abundant than others (e.g. fucoid algae) at this study site, an area-proportional sampling strategy might have produced more accurate results. It would have been possible to create a multi-level classification rule set similar to the one developed in chapter 4, first to separate rock, sand, algae and chalk cobbles and then to separate algae into red, green and brown classes. The simpler approach of classifying all classes simultaneously using Random Forests or Membership Functions was adopted here because of the larger number of datasets involved, but future studies could assess the impact on accuracy of applying multi-level classification to these types of data.

5.4.2 Accuracy of change-detection methods

The accuracy of post-classification change detection maps usually cannot exceed the accuracy of the contributing single-date habitat maps, and for this reason some studies provide an accuracy assessment only for the single-date maps (Anderson et al., 2016) while others estimate change detection accuracy by multiplying the overall accuracies (Serra et al., 2003) or the Kappa coefficients (Prenzel and Treitz, 2006) for each single-date map. However, the decision to create maps at different sensitivity levels which combine some

transitions into a single class enabled the accuracy of the post-classification change maps to differ from the single-date maps, making a separate validation necessary. The stratified random validation of the change maps showed little difference in accuracy between the post-classification and RF pre-classification methods, with mean accuracy around 80% for the low and medium sensitivity maps produced by both approaches. This contrasts with the findings of Mas (1999) and Conchedda et al. (2008) who found post-classification more accurate than pre-classification methods for detecting change in coastal environments, although those studies both used low resolution satellite imagery, the former with a pixel-based and the latter with an object-based approach, so are not directly comparable with this study.

While some studies have found a SNN classifier to produce change detection maps with a good level of accuracy (Conchedda et al., 2008; Son et al., 2015), in some cases outperforming support vector machine and decision tree classifiers (Tehrany et al., 2014) and membership function classifiers (Stow et al., 2008), to our knowledge this is the first study to compare SNN and RF classifiers for change detection, finding the SNN classifier to be less accurate than the RF classifier.

The main source of inaccuracy with all three approaches consisted of false positives, i.e. areas that had not changed being incorrectly classified as having changed. The relative importance of errors of commission and omission depends on the map's intended use. A slight tendency to over-predict change, to 'err on the side of caution', may be preferable if the map is to be used as a decision-support tool to highlight areas of potential change for further investigation.

5.4.3 Defining change

In addition to evaluating different methods of producing change detection maps from aerial and LiDAR imagery, this study provided insight into the types of change occurring at the study site, identified the areas most susceptible to change and strongly suggested that this is cyclical fluctuation rather than directional change. While other studies have used multi-temporal remotely sensed data to detect coastal change, many have focussed on periods with severe directional change due to weather events (Anderson *et al.*, 2016) or anthropogenic impacts (Manson *et al.*, 2003); this was the first study to our knowledge that identified a baseline level of change in temperate intertidal habitats from aerial and LiDAR

multi-temporal data. Further research would be needed to assess whether this is representative of other temperate intertidal systems with similar physical characteristics, but this insight into the baseline level of fluctuation at the site is crucial information for the development of monitoring protocols, whether using remote sensing or ground-based survey methods or a combination.

This study compared three different thresholds for defining change, finding that the high sensitivity maps produced by classifying every possible transition as change had lower overall accuracy than the medium and low sensitivity maps, and classified around 40% of the total area as change. This corroborates the statement by Olofsson et al. (2014) that it might not be advisable to define every possible transition as change due to the large number of potential classes this can create. A change detection map that classifies almost half of the total area as change is likely to be of little use as a decision-support tool to aid monitoring, and classifying every transition as change is not justified in this case by the accuracy of the contributing habitat maps.

The methods developed and evaluated here detected change in the extent and distribution of simple broadscale habitats. Further development and application of these methods should involve consultation with the responsible monitoring authorities to identify particular types of change of relevance to conservation targets and management decisions and to ascertain whether these can be detected through OBIA of remote sensing data. These could include reduction in area of conservation priority habitats, such as seagrass, saltmarsh or biogenic reefs, increase in area of non-native algal canopy species such as *Sargassum muticum,* or change in intertidal algal communities potentially indicative of climate change and ocean acidification (Brodie *et al.*, 2014).

5.4.4 Sources of error and uncertainty

The creation of training and validation data through visual interpretation of the imagery is unavoidable when neither ground truth data nor higher quality remote sensing data are available. Change is often clearly detectable using this approach, as was the case in this study, but this introduced operator-mediated selection into an otherwise automated process and could therefore be a source of bias or even error. Imperfect reference data have been shown to affect the outcome of quality assessments (Foody, 2010). Future research could quantify the impact of this by collecting ground truth data to compare with

samples derived from contemporary imagery and/or conducting a study to quantify between-operator consistency in classifying samples derived from historic imagery. Operator bias or error can affect classifications made *in situ* as well as classifications derived from imagery, although this is more likely to be a factor with complex classifications based on identification and abundance of species than with the simple classification used in this study.

The main sources of error in the habitat classification maps were the within-class variability in spectral signature throughout the multi-temporal dataset and the between-class overlap in object feature values for any given year. Remote sensing can only be used for change detection when the change in land cover produces a change in spectral signature which is larger than changes caused by other factors such as atmospheric conditions or sun angle (Singh, 1989). Although the aerial imagery was processed to reduce differences in contrast and colour between adjacent images, no further processing was carried out to attempt to reduce variability between imagery collected on different dates; instead the impact of within-class spectral variability on accuracy was reduced by using training samples taken from each set of imagery. The accuracy of OBIA supervised classifications is greatly affected by feature selection, including the removal of redundant or correlated features (Laliberte *et al.*, 2010; Diesing *et al.*, 2016). This study attempted to optimise feature selection through analysis of sample values using box plots, eCognition's Sample Editor tool and 'importance values' derived from RF classifications. Further research might determine better features for separating classes, but some habitats remain inherently difficult to separate due to the similarity of their spectral signatures, e.g. red and brown algae, or sand and rock.

The decision to investigate change using data collected biannually for eight years was determined by data availability rather than ecological rationale. This study demonstrated that cyclical habitat fluctuations occurred during this period and that they were concentrated at the reef edges. There was no evidence of directional change; analysis of multi-decadal time-series imagery, possibly with more frequent observations, would be necessary to investigate this question.

5.4.5 Methodological improvements

The aerial and LiDAR imagery used in this study were not collected with the purpose of detecting change in the extent and distribution of intertidal habitats, and a key aim of the

study was to evaluate what could be achieved with pre-existing freely available data. Nevertheless, methodological improvements could be introduced to future data collection to improve suitability for habitat monitoring, namely collecting data on low spring tides and in the same seasons each year. Collection of LiDAR data at sub-metre resolution could also improve classification accuracy by enabling the use of texture features, such as grey level co-occurrence matrix or standard deviation, to aid the separation of classes that are difficult to separate on spectral signature alone.

These methods only defined change from one habitat class to another, they did not consider potential indicators of habitat quality, such as density of algal coverage or diversity of habitat types in a given area. Future methodological developments could include monitoring change in algal density by creating additional classes, and monitoring the patchiness/continuity of intertidal habitats by evaluating change in object size, shape and relation to neighbouring objects, but at present this level of analysis is not justified by the accuracy of initial classifications that can be achieved from these data.

This study made a series of bi-temporal comparisons of the same season in consecutive years. Bi-temporal comparison is the most widely used approach to change-detection (Lu *et al.*, 2004; Hussain *et al.*, 2013; Tewkesbury *et al.*, 2015) but it is also the most simplistic. Temporal trajectory analysis would give more insight into whether continuous change is occurring and in which direction (Coppin *et al.*, 2004; Czerwinski *et al.*, 2014; Thonfeld *et al.*, 2015). This approach was not used in this study because the timespan of the dataset was too short to expect to see continuous change, phenological conditions are not comparable between images, and the study area would be reduced to the area of the imagery captured at the highest tide. Nevertheless this approach might be a methodological improvement where suitable data are available, especially if directional change is suspected.

5.4.6 Future implications

The use of remote sensing and OBIA for mapping and monitoring habitats in the UK is likely to increase rapidly in the next few years (Medcalf *et al.*, 2014a; Medcalf *et al.*, 2014b; Medcalf *et al.*, 2015). The results of this study can contribute considerably to the understanding of remote sensing methods by the responsible monitoring authorities, enabling more robust use of information derived from remote sensing data and more confident communication with stakeholders. Despite the cost of aerial surveys and the

increasing availability of free satellite imagery, regular multi-spectral and LiDAR coastal surveys are likely to continue in the UK because only these methods provide data at the coverage and resolution necessary to inform shoreline management plans. This study demonstrated that OBIA of these freely publicly available datasets can detect change in the extent and distribution of broadscale intertidal habitats and provided insight into the type, magnitude and spatial distribution of natural cyclical change that occurred in the study area over the eight year period. OBIA of remote sensing data could provide regular coarse-scale rapid assessments of large areas of coastline. This could act as an 'early warning system' to direct more detailed UAV or ground-based surveys to areas where ecologically relevant change has been detected. Coppin *et al.* (2004) recommend such a "multi-scale, nested approach" in which different change detection methods are applied at spatial and temporal scales relevant to the type of change observed. The insight into cyclical change and its detectability by OBIA provided by this study could inform the establishment of such an approach.

The broad cycle of change observed at the study site consisted of sand being washed away to reveal bare rock at the reef edges; the bare rock was then colonised by brown/green algae; the sand then re-covered the rock and the algae was removed, presumably due to scouring or smothering. A sudden or gradual change in environmental conditions could affect the background pattern of cyclical change at the study site in various ways, for example the cycle could speed up or slow down, steps in the cycle could be omitted or new steps added, the spatial distribution of change could alter, or the cycle could be disrupted and a particular state could become permanent or at least last for several decades (Masselink *et al.*, 2016; Hawkins *et al.*, 2017; O'Brien *et al.*, 2018).

Understanding the baseline level of natural fluctuation in intertidal broadscale habitats could act as a trigger for further investigation if OBIA of remote sensing data detects change above the baseline level. The knowledge that change occurs predominantly at the reef edges could prompt investigation if change is detected in different areas. Awareness of the expected cyclical pattern of fluctuation could prompt investigation if change occurs out of sequence or if a different type of change is detected, for example a large growth of green algae could indicate a change in salinity or nutrient levels (Fong *et al.*, 1996; Arevalo *et al.*, 2007). Finally, understanding the baseline level of natural fluctuation can help monitoring authorities know when investigation is not necessary and to reassure stakeholders that

cyclical change or sediment movement due to longshore drift is expected in the dynamic intertidal environment and is not a cause for concern. This is valuable information at a time when resources for monitoring and surveillance are limited.

The study also provided quantitative evaluation to inform choice of change detection method, classification algorithm, sample selection protocol and change definition thresholds. Both the pre- and post-classification methods based on the RF classifier showed great potential for detecting change in the extent and distribution of intertidal habitats from aerial and LiDAR imagery. Both methods had a similar level of accuracy, so the choice may be determined by other factors, for example the pre-classification approach required less processing time, but post-classification produced single-date habitat maps which may be useful for other purposes. The two methods produced fairly consistent results, but the post-classification approach had a slightly higher tendency to over-predict change. The MF classifier is not recommended for intertidal habitat mapping as part of a post-classification change detection approach; even when using feature values derived from samples from the relevant year to compensate for between-year spectral variability, it produced less accurate results than the RF classifier. The SNN classifier is not recommended for pre-classification change detection as it produced less accurate results than the RF classifier.

The temporal scale of observations should match that of the type of change being monitored (Lambin, 1996; Nagendra *et al.*, 2013). Biannual data as used in this study could be suitable for repeated coarse-scale rapid assessments as described above, but frequent observations over several weeks or months would be needed to monitor the impact of a pollution incident or severe storm, while a multi-decadal time-series would be needed to monitor the response of intertidal communities to climate change. Future studies could explore adaptation of the methods developed and evaluated here for use on different temporal scales where suitable data are available.

5.5 Conclusions

This study provided insight into both the background level of change in temperate intertidal habitats and the accuracy of different approaches to intertidal habitat mapping and change detection. The results are of direct practical relevance; they can inform the adoption of suitable methods by monitoring authorities and improve their understanding and communication about remote sensing. Despite considerable within-class variability in

spectral signature and overlap in the spectral values of different classes, freely available aerial and LiDAR imagery can be used to detect change in intertidal habitats on a coarse thematic scale with a good degree of accuracy. Although the 'best' change detection algorithm has been shown to vary from case to case (Lu *et al.*, 2004), these findings suggests that a RF classifier is a better choice than SNN or MF classifiers for producing intertidal habitat or change detection maps from aerial and LiDAR imagery. Defining every possible transition as 'change' reduces classification accuracy and classifies a high proportion of the total area as change; raising thresholds for defining change by combining transition types produces more accurate maps, but the classification should be developed based on ecological rationale and user requirements. Ecologically significant change in intertidal habitats can sometimes only be detected by expert ground survey (Wells *et al.*, 2007; Konar and Iken, 2017), but the approaches developed and evaluated in this chapter have great potential for adoption, in combination with other remote sensing and ground-survey methods, as part of a multi-scale monitoring strategy to ensure the most effective use of resources.

Chapter 6: Thesis overview, limitations and wider implications

This thesis has examined the potential of object-based image analysis (OBIA) and remote sensing for mapping and monitoring temperate marine and coastal habitats in the North Sea. A variety of sensors and platforms were used to provide imagery at different spectral and spatial resolutions, which was interpreted using photogrammetry to create topographic models and OBIA to produce habitat and change-detection maps. Outputs were validated using ground truth data, enabling direct comparison of methods. As the first study of its kind in the North Sea, this work provides novel and timely insight into the applicability of these methods in the temperate marine environment. This chapter provides an overview of the thesis, highlights key findings and their wider implications, discusses the limitations of the study, and suggests areas for future research.

6.1 Key findings and contribution to knowledge

Globally, interest in remote sensing for nature conservation is growing, fuelled by rapid advances in sensors, platforms and software and the increasing need to monitor pressures and impacts that occur at large spatial scales (Lucas *et al.*, 2017). In the marine environment, remote sensing has become a "keystone technology" for monitoring fragile habitats (Purkis, 2018) and a critical component of robust extrapolation from fine-scale ecological sampling to broad-scale ecosystem assessments (Strong and Elliott, 2017). Both optical and acoustic remote sensing are promising tools for marine monitoring at an ecosystem scale, with potential for integration with other novel methods such as genomic tools and species distribution modelling (Borja *et al.*, 2016). Remote sensing could thus aid the monitoring of climate-driven changes that are already being observed in marine ecosystems and expected to increase rapidly in future (Mieszkowska and Sugden, 2016; Henson *et al.*, 2017), potentially providing cost-effective solutions at a time when a growing need for monitoring coincides with reduced availability of resources (Borja and Elliott, 2013).

However, remote sensing is still not as widely used for nature conservation as it could be, partly because the increasing choice of remote sensing data products is potentially overwhelming and the responsible organisations often lack the time, skills or staff to access and interpret remotely sensed data to inform their operations (Lucas *et al.*, 2017). Lack of transferability of methods, caused by variability of data, ground truthing protocols, interpretation techniques and user requirements, also presents a significant barrier to the

application of remote sensing for habitat monitoring in both terrestrial and marine environments (Lillis *et al.*, 2016; Borre *et al.*, 2017). Even where remote sensing is being used for marine habitat mapping, it is not always applied effectively or consistently, with consequent negative implications for marine management and decision making (Diesing *et al.*, 2016; Lecours, 2017).

In the UK, the new framework for marine spatial planning and the recent increase in the number and extent of MPAs create a pressing need to maximise the potential of remote sensing and ensure its robust use to inform decision making. This must be underpinned by understanding of the current limitations as well as potential benefits of different approaches. Comparative evaluation of methods in the temperate marine environment is therefore crucial, but prior to this thesis no such studies had been conducted in the North Sea or applied to such a wide range of data. The novel achievements of this thesis lie in the rigorous evaluation of the consistency, accuracy and repeatability of photogrammetry and OBIA for mapping and monitoring temperate marine habitats using a variety of remote sensing data. These achievements provide new insight, outlined in the following sections of this chapter, to inform the choices that analysts make throughout the process of data collection, interpretation and validation.

6.1.1 Sensors and platforms

This study developed and applied photogrammetry and OBIA methods for the interpretation of data collected by several sensors and platforms, with spectral resolution ranging from one to five bands and spatial resolution ranging from 0.04m to 1m (Table 6.1).

Table 6.1: Spectral and spatial resolution of data used in this thesis

Platform	Sensor	Spectral resolution		Spatial resolution (m)
UAV	RGB camera	3 bands	(Combined to give 5 bands: R,G,B,RE + DEM)	0.04
UAV	Red edge camera	3 bands		0.04
Aeroplane	RGB camera	3 bands		0.20
Aeroplane	RGB-NIR camera	4 bands		0.20
Aeroplane	LiDAR	1 band		1.00
Boat	Multibeam echosounder	2 bands		1.00

Most remote sensing habitat mapping studies to date have focussed on satellite imagery, which has higher spectral resolution and lower spatial resolution than the sensors studied here. The optimal spatial resolution of remotely sensed data is determined by the scale of

features being observed, in this case the size of habitat patches and three dimensional topographic features. The present study demonstrated that both aerial and UAV imagery can be interpreted using OBIA to produce reliable broadscale habitat maps of temperate intertidal sites, which are characteristically highly spatially heterogeneous. Broadscale intertidal habitat maps produced from 0.04m resolution imagery at Runswick Bay using a Random Forests (RF) classifier had higher mean overall accuracy (85.3% ± 5.9%) than those produced from 0.2m resolution aerial imagery at Flamborough using the same classifier (71.4% ± 1.6%). Spatial resolution might be a contributing factor to this observed difference in accuracy, but it could also be influenced by ecological differences between the two sites, e.g. Runswick Bay is dominated by red algae while Flamborough is dominated by fucoids, or by methodological differences, e.g. the validation samples for Runswick Bay were collected by field survey using stratified random sampling while those for Flamborough were selected from the imagery using systematic sampling. The aim of the study was to evaluate the OBIA approach and compare different classifiers, rather than to evaluate the influence of spatial resolution on classification accuracy, but the results suggest a possible correlation between accuracy and spatial resolution in temperate intertidal habitat mapping that could be tested in future studies. Research in highly heterogeneous tropical marine environments has shown that classification accuracy of pixel-based habitat maps is improved by using higher spatial resolution imagery, although this is less cost-effective than using lower resolution imagery (Capolsini *et al.*, 2003; Mumby and Edwards, 2003). Terrestrial OBIA studies have shown that the accuracy of habitat maps in heterogeneous environments can be improved by using high resolution aerial or UAV imagery to supplement lower resolution satellite imagery, but working with such high resolution imagery in OBIA can result in over-segmentation and increased processing time (Medcalf *et al.*, 2015; Medcalf *et al.*, 2017).

Spectral resolution may also influence classification accuracy; a greater number of spectral bands typically increases the ability to distinguish habitats based on subtle differences in spectral response (Medcalf *et al.*, 2014a). The majority of intertidal mapping studies to date have used hyperspectral aerial imagery, which enables the detection of seagrass and algal classes due to its high number of narrow bands, but these sensors are expensive and data interpretation requires considerable expertise (Garono *et al.*, 2008; Oppelt *et al.*, 2012; Valle *et al.*, 2015). Thus the availability of the red edge band may be another factor which contributed to the higher accuracy of the habitat maps produced for Runswick Bay. While

the Runswick Bay imagery consisted of four colour bands, the aerial imagery for Flamborough consisted mainly of three bands, with a fourth near-infrared (NIR) band available for five of the fifteen images. The inclusion of the NIR band did not significantly improve classification accuracy of the Flamborough habitat maps produced using a RF classifier (mean overall accuracy 71.0% ± 1.6% with three bands, 72.0% ± 1.7% with four bands). Nevertheless, analysis of the feature importance values generated by the RF classifier showed that the Normalised Difference Vegetation Index (NDVI) and other features derived from NIR and red edge were consistently important features for separating broadscale habitats at both Runswick Bay and Flamborough.

Evaluation of topographic models produced by photogrammetry from 0.04m resolution imagery demonstrated high vertical accuracy (mean RMSE 0.07m ± 0.01m for the models produced without compressing the imagery) and the ability to detect decimetre scale topographic features. The inclusion of topographic information alongside spectral information aided the predictive mapping of intertidal habitats. Mean and mode elevation values derived from the digital elevation model (DEM) were assigned a high importance value by the RF classifier, and mean elevation was used at many stages of the knowledge-based workflow to aid the classification of broadscale habitats and biotopes. However, the photogrammetric models lacked sufficient accuracy to detect sub-decimetre scale features and to measure the fine-scale rugosity that is known to influence species distributions in this environment, and it is possible that increasing the spatial resolution of the imagery by flying at a lower altitude could generate more accurate results (Kung *et al.*, 2011).

The circalittoral study demonstrated that OBIA of 1m resolution multibeam echosounder data can be used to produce substratum maps with a high degree of accuracy. Although this sensor produces only two bands of imagery (bathymetry and backscatter), the data were enriched through the production of bathymetric derivatives. These aided the classification process, for example slope was used in combination with backscatter to separate rock from sediment through iterative cycles of threshold based rules. Comparative studies have found that the inclusion of secondary acoustic features improves classification accuracy (Calvert *et al.*, 2015), although predictive power is decreased by the indiscriminate inclusion of all available derivatives (Stephens and Diesing, 2014). The only derivative layers created and used in this study were slope and bathymetric position index (BPI) at a range of scales. Additional derivatives could be explored in future studies to evaluate their influence on

accuracy in OBIA mapping of temperate marine habitats, for example eastness, northness, Moran's I, topographic roughness index, vector rugosity measure and curvature (Rattray *et al.*, 2009; Elvenes *et al.*, 2014).

Even when supplemented by derivative layers, habitat mapping from acoustic data is challenging, particularly on sediment seabeds. The majority of studies that have obtained high accuracy in distinguishing sediment grades overcame the low spectral resolution of acoustic data by using specialist software such as RoxAnn or QTC-Multiview to detect subtle variations in backscatter data (McGonigle *et al.*, 2009; Brown *et al.*, 2011b; Brown *et al.*, 2012) or by analysing the backscatter angular response curve (Hamilton and Parnum, 2011; Lamarche *et al.*, 2011). In the present study, the successful discrimination of sand and mud using OBIA of acoustic layers and derivatives owed much to the correlation between sediment type and depth in the study site. Were it not for this correlation, it is unlikely that a Standard Nearest Neighbour OBIA approach could distinguish sediments using the available data with an acceptable degree of accuracy. However, improvements to acoustic data collection, as discussed in chapter 2, could produce bathymetry and backscatter data with fewer artefacts. Future studies could apply the OBIA methods that were tested in later chapters, such as Random Forests or membership functions, to 'cleaner' acoustic data and derivatives, to evaluate the capability of distinguishing sediments without relying on correlation with depth.

OBIA of acoustic imagery was found by the present study to be unsuitable for mapping temperate circalittoral reef communities, but this was primarily due to the characteristics of the study site than to shortcomings of the sensor. Other studies have successfully mapped benthic biota from acoustic data in areas where broadly defined species communities have distinct environmental niches defined by environmental parameters which have a wide spectrum of values in the study site (Holmes *et al.*, 2008; Ierodiaconou *et al.*, 2011; Hasan *et al.*, 2012a; Mielck *et al.*, 2014). The low accuracy of biotope maps in this study was largely due to the similarity of the circalittoral rock communities in terms of species composition and environmental parameters. In the classification system used, each habitat class in the study area has the same set of characterising species, all of which tolerate a wide range of conditions, and the differences between habitats are defined by differences in the relative abundance of each species. The classification of subtly different sub-biotopes was based on interpretation of seabed photographs with the assumption that a photograph is

representative of the surrounding area, an assumption which is likely to be a source of error (Rattray *et al.*, 2014). The spectral and spatial resolution of acoustic data are likely to be too low to detect such subtle differences in habitat composition, regardless of the interpretation methods used. However, fine-scale seabed habitat maps could be produced for areas of interest through application of the photogrammetric and OBIA methods developed in chapters 2 and 3 if suitable optical imagery could be obtained; this is discussed in section 6.3.

Variability of data within habitats is an issue with all sensors and platforms, but the use of satellite imagery for habitat and land cover mapping over several decades has led to increased standardisation of collection and calibration procedures to reduce variability. In contrast, aerial and UAV platforms are subject to less standardisation, and their smaller coverage means that data for a large area may need to be collected over several days, the final image being a composite of multiple dates (Medcalf *et al.*, 2015). Chapter 5 demonstrated that the considerable within-class spectral variability of aerial imagery collected on different dates can severely impact classification accuracy but can be overcome by defining habitat classes using feature value ranges specific to each set of imagery. In chapter 4, the main cause of inaccuracy when OBIA rules were applied to imagery from a different season was a change in spectral signature caused by actual environmental change (seaweed bleaching) rather than by data variability. However, variability in UAV imagery is also to be expected, particularly as the sensors were not calibrated for difference in lighting conditions on different flights. There was no opportunity in this study to compare acoustic data collected from the same site at different times, but variability in acoustic data is well documented and research is underway to address this through development of standardised protocols for collection and processing (Lamarche and Lurton, 2017).

This study has demonstrated the potential of each of the platforms and sensors tested for mapping temperate marine habitats using OBIA. With their ability to collect high resolution topographic and spectral information simultaneously on demand, UAVs seem an ideal platform for surveying the intertidal environment due to its dynamic nature and high spatial and spectral heterogeneity. However, UAV coverage is typically limited to <1km^2 per flight due to regulations that require the craft to remain within the operator's visual line of sight. An aeroplane may collect colour imagery simultaneously with LiDAR data, covering several kilometres of coastline within a single low tide. This study suggests that the lower spectral

and spatial resolution of aerial imagery compared to UAV imagery may result in reduced classification accuracy, but this might be an acceptable trade-off for more extensive coverage. In subtidal environments where turbidity prevents use of optical data from aerial platforms, acoustic data and derivatives can be interpreted using OBIA to provide reliable maps of seabed substrata.

None of the sensors studied produced data that enabled habitats to be separated based on single features or simple threshold values. Even the separation of rock from sediment in chapter 2 required the use of two features (mean slope and mean backscatter intensity) and an iterative cycle of classification with different threshold combinations, because the range of values for both of these features overlapped between the two classes. Overlap in the acoustic signature of different seabed substrata has been documented by other subtidal studies (Lucieer *et al.*, 2011; Diesing *et al.*, 2014; Stephens and Diesing, 2014; Calvert *et al.*, 2015), but chapters 4 and 5 also demonstrated considerable overlap in spectral signature of intertidal habitat classes derived from optical imagery, even when working at a coarse thematic scale. This highlights the challenge of habitat mapping in the temperate marine environment from relatively low spectral resolution data and shows that an OBIA approach can help to overcome this challenge by increasing the number of features available and enabling creation of workflows based on knowledge of the site and of the data.

6.1.2 OBIA workflows

Several OBIA approaches were developed and evaluated in this thesis. The approach adopted in the initial subtidal study was relatively simple, consisting of rule sets based on thresholds and a Standard Nearest Neighbour (SNN) classifier. No further algorithms or rule based approaches were tested in this chapter because of the limitations imposed by the nature of the study site and the data, as discussed in the previous section. However, subsequent chapters explored more sophisticated OBIA approaches including multi-level classification, the RF classifier and rule sets based on membership functions.

A key finding of chapters 4 and 5 was that the RF classifier produced more accurate and consistent results than SNN. SNN is a popular choice of classifier due to its simplicity and the fact that it is better documented than other classifiers in software literature (Trimble, 2014) so this study has been valuable in highlighting its weaknesses. An important weakness, demonstrated in chapters 2 and 4, was the failure of the Feature Space Optimisation tool to

select the best features for separating habitat classes. The main reasons for the superior performance of the RF classifier were the avoidance of over-fitting to training data and the potential to improve classification accuracy by using features with high importance values to train the classifier. These benefits of RF have been discussed in other studies (Belgiu and Dragut, 2016), but this was the first study to demonstrate the benefits in this environment with these types of data.

The 2-fold and 4-fold cross validation applied in these studies highlighted the considerable influence of sample selection on model output when using classifiers trained by samples. Changing the training dataset led to inconsistent results in both intertidal and subtidal maps, the level of inconsistency being far greater with the SNN classifier than with the RF classifier. This is a crucial point for practitioners to be aware of, because such inconsistency of outputs could create the illusion of change in extent or distribution of habitats (Frost *et al.*, 2013). It may be desirable to use standard classification algorithms for marine or coastal habitat mapping, particularly where there is insufficient prior knowledge of the study site to develop a rule-based workflow, or where speed and ease of use are primary concerns. The most statistically robust outputs are likely to be achieved by applying several classifiers to the same data with the same training samples and combining the results through ensemble analysis (Diesing and Stephens, 2015; Zhang, 2015), but this approach is complex and requires greater technical expertise than the application of a single classification algorithm. RF is itself an ensemble approach combining the outputs of multiple decision trees, and is a reliable choice provided that care is taken to ensure that sample selection adequately represents the range of habitats present, and that feature selection is informed by previous research and by the importance values generated by the classifier (Ma *et al.*, 2015; Millard and Richardson, 2015).

Chapter 4 demonstrated both the benefits and risks of a knowledge-based OBIA approach. The transparent, sequential workflow enabled the rules to be adjusted, resulting in a higher classification accuracy than was achieved by the RF or SNN classifiers. However, this approach has been criticised by other studies for its subjectivity (Arvor *et al.*, 2013; Belgiu *et al.*, 2014). The present study clearly demonstrated the risk, especially when working with high resolution imagery, of creating overly intricate rules to achieve the desired result. The low classification accuracy that arose from application of the knowledge-based rules to another set of imagery showed that the rules were over-fitted to the imagery for which they

were originally developed, leading to misclassification of habitats whose spectral signature had altered due to seasonal change. This study's findings suggest that knowledge-based rules should be considered for wider implementation for intertidal habitat mapping due to their potential to achieve high classification accuracy without the need for training samples, but workflows should be kept as simple as possible and value ranges will need to be adjusted when rules are applied to new imagery.

This study did not directly compare object-based with pixel-based approaches through application to the same data, but nevertheless demonstrated several benefits of the object-based approach, notably the use of a wider range of features than would be possible with pixel-based mapping, simultaneous interpretation of multiple layers and, in chapter 4, the ability to classify a scene on multiple hierarchical levels. However, it did not use contextual data, which is a great potential benefit of the OBIA approach (Lucas *et al.*, 2007; Medcalf *et al.*, 2014b). Contextual data, for example on exposure and currents, were not available for the North Sea at sufficient resolution for use in this study, but this is an important potential benefit of the OBIA approach and should be explored in future studies where such data can be made available through survey or modelling.

6.1.3 Classification system and thematic resolution

This study used existing standard classification systems in chapters 2 and 4, a classification derived from cluster analysis of species abundance data in chapter 2 and a classification derived from visual analysis of imagery in chapter 5. The thematic resolution of habitat maps ranged from purely physical classes of seabed substrata in chapter 2, to broad community classes in chapters 4 and 5, and highly detailed biological communities (biotopes) in chapters 2 and 4.

The thematic resolution of habitat maps must be justified by the spatial and spectral resolution of the remote sensing data (discussed in 6.1.1) and, if training samples are used, by the taxonomic resolution of the ground truth data. This study showed that biotopes could be assigned with confidence to ground truth data collected through intertidal field survey in chapter 4, but the allocation of biotopes or sub-biotopes to seabed photographs in chapter 2 was fraught with uncertainty. Visual interpretation of aerial imagery in chapter 5 enabled classification of broad community classes with a reasonable degree of confidence, but did not enable the classification of detailed biological communities.

Using a site-specific classification produced by cluster analysis of subtidal species abundance data produced no improvement in classification accuracy compared to a standard classification system, while cluster analysis of intertidal species abundance data produced habitat classes that were so closely aligned with the standard classification that there was no justification for their use in habitat mapping. However, creation of a broad community classification based on analysis of aerial imagery in chapter 5 enabled intertidal habitats to be mapped at higher thematic resolution than would have been possible if using a standard classification. In the UK's standard classification system, even broad community types are defined by species-level classification, for example requiring the separation of fucoid algae species which are not spectrally distinct, or by the presence of sub-canopy species such as barnacles or mussels, which cannot be detected by remote sensing (Connor *et al.*, 2004; Parry, 2014). Using aerial imagery it would therefore only be possible to classify intertidal habitats at the higher 'habitat complex' level, in which classes are defined only by substratum and energy. The creation of classes such as red, green and brown algae thus enabled production of more useful habitat maps from the available data than if the standard classification system had been used. It is recommended that a standard marine habitat classification system is used where possible because of the practical benefits of being widely understood by marine managers and facilitating comparison between sites and over time. However, site-specific classifications should be used if they enable production of maps at higher thematic resolution, as these may be of greater use for monitoring or spatial planning.

Standard marine habitat classifications are based on ecological knowledge of the environmental factors that influence the distribution of species communities, while site-specific classifications created for remote sensing studies are based on what can be detected by sensors. In some cases, the latter approach may be the only approach justified by the spectral and spatial resolution of the imagery. Ground truth sampling is needed to ascertain the ecological relevance of a classification based on what sensors can detect, i.e. whether there is correlation between features detected by the sensor and the ecological communities present on the ground. Habitat or change detection maps based on a simple site-specific classification can provide useful information to aid site management or to direct survey effort, provided that the relationship between benthic biodiversity and detectable features is understood.

6.1.4 Ground truth sampling protocols and quality assessment

The stratified random ground truth sampling protocols adopted in chapters 2 and 4 led to the under-sampling of locally rare habitat classes and consequent inability to map and validate those habitats reliably. Chapter 5 used manual non-random selection of training samples to ensure that all classes were adequately represented, and systematic selection of validation samples (i.e. using an evenly spaced grid of points) to ensure that the validation approach was objective. Although systematic sampling was effective for the quality assessment of habitat maps, it proved inadequate for validating the change detection maps because these consisted of just two classes, of which 'no change' occupied a far greater proportion of the map than 'change'. Validation samples for the change detection maps were therefore selected using random sampling stratified by class, generating an equal number of validation points per class and enabling the calculation of meaningful user's and producer's accuracy values for both 'change' and 'no change' classes.

Chapter 2 demonstrated that random sampling generated some samples which were not good representatives of their class, for example occurring on a boundary between two habitats. It has generally been widely assumed in remote sensing studies that ground truth samples should be taken from homogeneous areas and that the use of mixed pixels or mixed objects would reduce mapping accuracy, although a recent study has challenged this assumption and shown that the inclusion of mixed samples in a training set can actually improve classification accuracy (Costa *et al.*, 2017). Further research would be necessary to evaluate whether these findings are applicable to other classifiers and environments, but although mixed samples may prove viable as training samples, validation samples should consist of pure objects to avoid ambiguity in accuracy metrics.

Random sampling is recommended for its objectivity, but should be based on unsupervised classification of the remote sensing imagery where possible to ensure that all classes are adequately represented and that samples are taken from homogeneous areas with a pure spectral signature. When this is not possible, for example if ground truth data are collected before or during the remote sensing survey as in chapter 4, a random sampling protocol could be modified to ensure adequate representative samples of each habitat while retaining an element of objectivity (Corcoran *et al.*, 2013).

Evaluation and clear communication of map accuracy is crucial if maps are to be used as a basis for environmental decision making. This is particularly true in the UK, where "the data and information we use to make our decisions will be available for others to scrutinise and challenge us" under the Defra Open Data Strategy, and data are often given a confidence rating (Defra, 2013a). Validation assessment in this study was carried out in accordance with best practice recommendations drawn from the literature and outlined in chapter 1. Overall accuracy was calculated as a useful headline figure, but was insufficient on its own to evaluate model performance. Balanced Error Rate was found to be a useful additional measure, particularly in chapters 2 and 4 where there was an uneven number of ground truth samples per class. The Kappa statistic proved less useful in this study as it was correlated with overall accuracy, but there was justification for considering it as some seabed mapping studies have found Kappa to be a more useful measure than overall accuracy for comparing performance of different approaches (Stephens and Diesing, 2014).

The most useful measures were user's and producer's accuracy, which provided valuable insight into model performance in terms of tendency to over- or under-predict particular classes, and the error matrix which illustrates where classification errors occur between habitats, enabling users to judge whether some misclassifications are more acceptable than others. This study also demonstrated that user's and producer's accuracy cannot be generated reliably for classes with a very low number of samples, but this could be overcome by adopting a more representative sampling protocol as described above. Calculation of the percentage of total area with the same classification in maps produced from the same data using different methods, as used in chapters 2, 4 and 5, was a valuable measure of consistency. Where classifications were based on fuzzy membership, the measures of separation distance and classification stability used in chapters 2 and 4 provided a useful evaluation of the reliability of the output maps. Although overall accuracy has the appeal of offering 'at a glance' comparison between outputs, the more detailed insight provided by these additional measures should always be considered when conducting comparative evaluation to inform choice of mapping method.

Root Mean Square Error (RMSE) is a standard method for evaluating horizontal and vertical accuracy of remote sensing data and thus has the benefit of being intuitive and widely understood. It was a reliable measure of the vertical accuracy of topographic models produced in chapter 3 because the measurements taken through field survey had a very high

degree of accuracy and precision. In contrast, the manual measurements of rugosity contained many sources of error which are discussed in chapter 3, so in this instance the ground truth data do not represent perfect accuracy, and RMSE can only be interpreted as a measure of consistency between manual and photogrammetric measurements rather than a measure of the accuracy of the model output.

The quality assessments applied in these studies could not be made spatially explicit due to insufficient data density, but a geographically weighted approach to validation has considerable benefits and should be considered in future studies (Comber, 2013). This would be a useful addition to the above measures of accuracy and could significantly aid communication between decision makers and stakeholders.

6.2 Limitations

This study was subject to several limitations imposed by the timeframe of the research and the cost and logistic constraints of collecting data in the North Sea. The spatial extent of the study was limited to one large subtidal site and two small intertidal sites. Findings are likely to be applicable to other temperate marine and coastal areas, but this cannot be assumed and further field studies are recommended to test the transferability of these methods.

The UAV and sensors available for this study also imposed certain limitations. The lightweight (0.7 kg) UAV offered logistical and cost benefits, but could only carry one camera per flight, thus reducing the amount of data that could be collected during a low tide and increasing the likelihood of changes in atmospheric conditions during the survey. The UAV was not equipped with a downwelling light sensor to measure ambient light during the flight and enable image correction for changes in lighting. The consumer-grade compact cameras used did not capture RAW imagery, thus some spectral and spatial detail is likely to have been lost through compression. The make and model of the camera used to collect the aerial imagery in chapter 5 was changed during the eight year time period, which could have contributed to the observed within-class variability of spectral signature. Different LiDAR systems were also used during the study period.

The study was also subject to several temporal limitations. The temporal coverage of the acoustic and UAV data consisted of one acoustic survey conducted in 2014 and two UAV surveys conducted in 2015, which limited the potential for testing the reproducibility of methods with these sensors. However, the availability of biannual aerial and LiDAR data for

an eight year period enabled exploration of issues of data variability, method reproducibility and the dynamic nature of intertidal environment. Survey timing is also likely to have affected the quality of outputs. The acoustic survey was not conducted at the optimal time of year, which led to artefacts in the data with consequent negative impacts on segmentation and classification. The aerial and LiDAR data were not always collected on the lowest spring tides, thus limiting their usefulness for intertidal habitat mapping. Logistic constraints meant that subtidal ground truth data were not collected at the same time as the acoustic survey, and that only part of the intertidal ground truth data was collected at the same time as the UAV survey. Due to budgetary constraints, the majority of circalittoral ground truth data consisted of seabed photographs rather than grab samples, which is a potential source of error particularly in the classification of sediments.

These limitations do not detract from the study's findings, but demonstrate what can be achieved with the available equipment and have helped to highlight specific methodological improvements which are outlined in each of the preceding chapters. Improved coordination of data collection, for example collecting aerial or LiDAR imagery on low spring tides, could increase the number of potential uses of a dataset.

6.3 Wider implications

The findings presented here have immediate practical relevance and potential to inform wider adoption of these methods for mapping and monitoring temperate marine habitats. This study has demonstrated that OBIA can be applied to imagery from a range of sensors to record the extent and distribution of subtidal and intertidal habitats. Mapping at high thematic resolution with a reasonable degree of accuracy requires higher spectral and spatial resolution imagery, but there is a trade-off between extent of coverage and spatial resolution of data. Furthermore, survey costs per area tend to increase with increasing spatial resolution. In the UK, an individual MPA may cover several hundred square kilometres, and surveillance is required outside as well as within MPAs to inform wider marine spatial planning.

Choice of appropriate thematic resolution is therefore influenced by the level of detail required to inform decision-making, the acceptable minimum level of accuracy or confidence in output maps and the level of detail justified by the remote sensing data and ground truth data. Individually, each of the methods and levels of spatial and thematic resolution

explored in this thesis have potential for practical application. Detailed species community maps can be used for local-scale site monitoring, while broadscale habitat maps can inform MPA designation and management, for example ensuring that targets for the representativity and replication of habitats are met (JNCC and Natural England, 2010) or underpinning site-specific risk-based management measures (Defra, 2013b).

However, the most promising opportunity lies in the potential to develop an integrated mapping and monitoring protocol, in which multiple remote sensing platforms and sensors collect data at different spatial resolutions. OBIA methods would be applied to the imagery at each level of resolution to create habitat or change-detection maps, which would then be used to identify areas of interest for surveillance using higher resolution, and therefore more costly, survey methods (Figure 6.1).

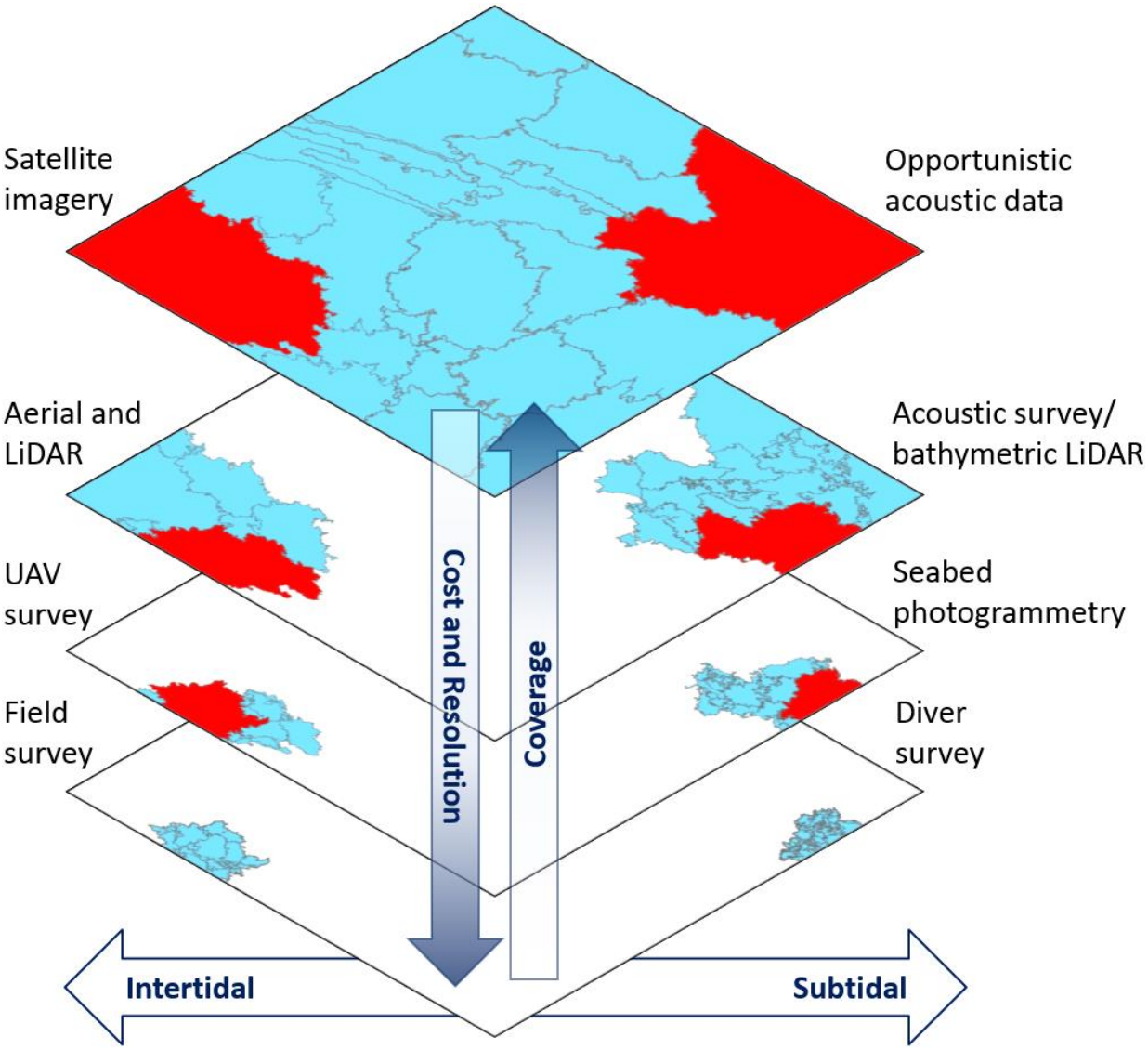

Figure 6.1: Diagrammatic illustration of a multi-scale OBIA and remote sensing protocol for intertidal and subtidal habitat monitoring. Intertidal survey methods are shown on the left and subtidal methods on the right. The coloured area represents the spatial coverage of the survey at each level. Methods at the top of the diagram have high spatial coverage but low spatial resolution, while those at the bottom of the diagram have high spatial resolution but low spatial coverage. The grey boundaries represent interpretation of survey data to create ecologically meaningful objects, such as habitats or other features, at each level of resolution. The red area at each level represents the area of interest targeted for more detailed survey in the level below. Survey costs per equivalent area are higher for the methods shown at the bottom of the diagram than for those shown at the top of the diagram. Detailed costs are provided in Table 6.2

In this hierarchy, the greatest coverage but lowest spatial resolution data would be provided by satellite imagery for the intertidal environment and by opportunistic acoustic data for the subtidal environment. Freely available satellite imagery, such as that provided by the LandSat or Sentinel platforms, has lower spatial resolution than imagery from commercial platforms such as WorldView but higher spectral resolution than aerial imagery. Studies have demonstrated that such imagery can be used for mapping coastal habitats at very coarse spatial and thematic scales with extensive coverage and a good degree of accuracy

(Larsen *et al.*, 2004; Lyons *et al.*, 2012). In the subtidal environment, full-coverage acoustic survey is expensive, but vessels fitted with acoustic equipment can become platforms of opportunity, collecting data while performing other tasks. The most affordable systems are single-beam echosounders. Single-beam data tend to be lower spatial resolution than data generated by multi-beam or sidescan sonar systems, fine-scale variation in the seabed is lost through interpolation between tracks, and performance instability can lead to inconsistent results (Kenny *et al.*, 2003). Nevertheless, studies have demonstrated that single-beam data can be used effectively for benthic mapping either alone (Foster-Smith and Sotheran, 2003) or 'blended' with higher resolution multibeam data (Serpetti *et al.*, 2011). Data collected opportunistically rather than by targeted survey are likely to be patchy and biased, but Elvenes *et al.* (2014) demonstrated that compiled single-beam data can be interpreted to create benthic maps for management purposes where full coverage multibeam data are not available. Recent development of more affordable multibeam systems could lead to opportunistic generation of multibeam imagery (ENL Group, 2016), and there would be benefit in developing and testing OBIA methods for interpreting such imagery in future.

At the next level in the hierarchy, medium resolution imagery can be provided by aerial and LiDAR surveys in the intertidal environment and by targeted acoustic survey or bathymetric LiDAR in the subtidal environment. In particular, bathymetric or topobathymetric LiDAR could provide solutions for mapping the shallow turbid sublittoral areas inaccessible to acoustic or optical survey (Zavalas *et al.*, 2014; Parrish *et al.*, 2016). Automated interpretation of these data using the methods outlined in chapters 2 and 5 could identify areas of interest for higher resolution remote sensing survey, for example areas where change appears to be occurring above a natural baseline level. Chapter 5 provides insight into the type and level of natural fluctuation occurring at a temperate intertidal site, as well as into the 'noise' caused by variability in the data. This information could be used to define site-specific minimum detectable change values, i.e. the percentage change in extent that can be detected against a background of natural variation within the limits of confidence associated with the survey method (Strong, 2015).

The highest resolution remote sensing imagery for the intertidal environment could be provided by UAV surveillance or by more affordable solutions such as balloons or kites (Bryson *et al.*, 2013; Fonstad *et al.*, 2013). Fine-scale subtidal habitat mapping could be achieved by collecting optical imagery using a remotely operated underwater vehicle (ROV),

autonomous underwater vehicle (AUV) or by SCUBA divers. AUVs are an increasingly reliable and flexible platform due to their ability to operate independently from the surface vessel for up to several days, to carry a range of sensors and to fly relatively close to the seabed (Wynn *et al.*, 2014; Lucieer and Forrest, 2016). High resolution two- or three-dimensional mosaics could then be created from the imagery using the photogrammetric methods demonstrated with UAV imagery in chapter 3, and OBIA methods could be applied to interpret spectral and topographic information simultaneously, as demonstrated in chapter 4. In common with UAV surveillance, the time and cost of conducting such detailed surveys make this method suitable for smaller areas of interest where maps are needed at fine spatial and thematic resolution. A recent study on the Great Barrier Reef demonstrated effective use of an AUV to collect hyperspectral and stereo imagery simultaneously to create highly detailed spectral and topographic maps for a small area (Bongiorno *et al.*, 2017).

In situ surveillance by divers or intertidal ecologists will always be necessary to achieve high levels of taxonomic resolution which cannot be detected even by the finest resolution remote sensing data (Wells *et al.*, 2007; Konar and Iken, 2017; Murfitt *et al.*, 2017). Field surveys are costly, but automated OBIA interpretation of remote sensing imagery could identify priority areas for more detailed surveillance, thus making the most efficient use of scarce resources. Table 6.2 provides a comparison of data collection and data processing costs, spatial coverage and spatial resolution for the methods discussed above and illustrated in *Figure* 6.1. This comparison considers the direct costs of data collection and preliminary processing, such as digitising field data or producing orthomosaics from aerial imagery. Ancillary costs such as travel and subsistence for surveyors, pre-survey planning and preparation, risk assessment and report writing are not included in the comparison as there is likely to be great variability in these costs depending on the site and the scope of the survey. Similarly, the costs of recruiting or developing staff skills in field survey and/or data processing methods and the costs of purchasing and maintaining hardware for data processing are not included in the comparison as these vary from one organisation to another due to differences in company size, assets and staff retention. Although like-for-like comparison between such different survey methods is challenging, the information provided in Table 6.2 and throughout Section 6.3 provides insight into the costs and benefits of each approach which could aid greater integration of these methods for marine and coastal monitoring.

Table 6.2: Comparison of data collection and data processing costs, spatial coverage and spatial resolution for different sensors and survey methods.

Data collection method	Purchase of platform/ sensor	Cost to end-user of one day's data collection	Area covered by one day's survey	Cost to end-user of data processing	Resolution of processed imagery	References
INTERTIDAL OR SHALLOW SUBTIDAL IN CLEAR WATER						
Satellite	n/a	**Free** (Sentinel, Landsat) **£3,820** for 4-band data and **£3,975** for 8-band data collected on demand (GeoEye, WorldView, QuickBird) **£193** to **£367** per 25km^2 archive imagery (GeoEye, WorldView, Quickbird, IKONOS, Pleiades)	Swath width: **84,100km^2** (Sentinel 2) **34,225km^2 (**Landsat 8) **272km^2** (WorldView 2) **269km^2** (QuickBird) **225km^2** (GeoEye)	**None** if using analysis ready data. Otherwise, staff time **~1 day** plus software e.g. one of the following: ENVI **£6,200 to £8,040** perpetual ArcGIS **£5,592** per year ERDAS IMAGINE **£2,150** per year MATLAB **£1,800** perpetual If using free software e.g. R, QGIS, GRASS GIS, Sentinel Toolbox, Google Earth Engine or MultiSpec the only cost is staff time.	**30m** (Landsat 8) **10m** (Sentinel 2) **4m** (IKONOS) **2.4m** (QuickBird) **2m** (Pleiades) **1.84m** (GeoEye 1, WorldView 2)	Thierry Büttel, European Space Imaging (pers. comm.) (Young *et al.*, 2017) https://sentinel.esa.int/web/sentinel/toolboxes https://store.esriuk.com/products/#business https://www.hexagongeospatial.com/ Gareth Kirby, Harris Geospatial (pers.comm.)
Aerial and LiDAR	n/a	Archive imagery in England is **free to end users** under Open Government License. The cost of data collection and initial processing (orthorectification and radiometric adjustments) is **£123 per km^2** for aerial imagery and **£265 per km^2** for LiDAR. The minimum starting cost for one flight is **£5,500**.	**50 – 60km^2**	Minimal processing required by end-user, e.g. mosaicking tiles. Staff time **<1 day** plus software costs if using commercial software e.g. ArcGIS (see above)	**0.1m – 0.2m** (Aerial) **0.25m – 2m** (LiDAR)	http://environment.data.gov.uk/ds/survey/#/survey https://www.channelcoast.org/ Samuel Pitman, Channel Coast Observatory (pers. comm.) Suzanne Winch, Environment Agency (pers. comm.)
UAV	**~£1,000** to **£25,000**	**£350 - £500**	**1km^2** to **4km^2** depending on shape of coastline and desired spatial resolution	Staff time **<1 day** plus specialist software e.g. one of the following: Pix4D Mapper: **£2,320** per year DroneDeploy: **£2,309** per year Agisoft Photoscan Pro: **£2,703** perpetual	**<0.1m**	https://cloud.pix4d.com/store/ https://www.dronedeploy.com/pricing.html http://www.agisoft.com/buy/online-store/
Field survey Phase 1 biotope survey by 2 intertidal ecologists	n/a	**£600**	**0.3km^2** (complex bedrock platform) to **0.5km^2** (mixed shores)	Staff time **1-2 days** to process field data plus software costs if using specialist software e.g. ArcGIS (see above)	n/a	Paul Brazier, Natural Resources Wales (pers. comm.) (Wyn *et al.*, 2006) Liz Morris-Webb, Marine EcoSol (pers.comm.)

Data collection method	Purchase of platform/ sensor	Cost to end-user of one day's data collection	Area covered by one day's survey	Cost to end-user of data processing	Resolution of processed imagery	References
SUBTIDAL						
Opportunistic acoustic data	WASSP S3 multibeam **£11,650** (includes software) Single beam echosounder **£3,000** to **£6,000**	n/a – opportunistic data collection	**6.5km²** to **13km²** (WASSP) **0.07km²** to **0.14km²** (Olex single beam) based on 8 hours at depth of ~30m	Staff time **2 days** plus software e.g. Olex software and hardware: **£4,984** perpetual WASSP interface for Olex: **£3,000** perpetual WASSP software: included with purchase of sensor (£11,650)	**0.25m - 4m** (WASSP) **5m** (Olex single beam)	http://www.olex.no/produkter_e.html Mark Southerton, Northumberland Inshore Fisheries Conservation Authority (pers. comm.) Arlene Hardacre, Echomaster Marine (pers. comm.)
Acoustic survey	Reson Seabat **£16,000 to £25,000** WASSP (see above)	**£3,000 – £3,500**	**8km²** to **9km²** based on 8 hours at depth of ~30m. Area covered varies with shape of survey area and number of line turns needed.	Staff time **2 days** plus software: Teledyne CARIS HIPS and SIPS Professional software **£14,680** perpetual	**1m**	Alison Pettafor, Cefas (pers. comm.) Mark Southerton, NIFCA (pers. comm.) Tony Cran, Seatronics Ltd (pers. comm.)
AUV survey	From **£580,000** for a small AUV e.g. Teledyne GAVIA	**£800 - £4,000** (small UAV) **or £1,800 - £5,800** (large UAV) plus technician fees, boat costs and insurance	**1km²** for a small UAV with a single battery.	Staff time **1 day** plus specialist software e.g. one of the following: Teledyne CARIS HIPS & SIPS Professional **£14,680** perpetual QPS Fledermaus 7, FM Geocoder Toolbox and FM GIS add-on: **£3,460** per year	**0.1m** to **0.5m** side scan **0.5m** to **1m** bathymetry and backscatter	Karen Boswarva, Scottish Association for Marine Science (pers. comm.) (Tillin *et al.*, 2018) QPS BV (pers. comm.)
Diver survey Phase 1 biotope survey by 2 - 4 scientific divers	n/a	**£1,760 - £2,440**	**0.0003km² – 0.0009km²** (2 to 6 x 150m² transects) The number of transects completed in a single day is site-specific, depends on tides and current.	Staff time **~1 day** per two 150m² transects to process field data plus software costs if using specialist software e.g. ArcGIS (see above)	n/a	Paul Brazier, Natural Resources Wales (pers. comm.) Liz Morris-Webb, Marine EcoSol (pers.comm.)

All of the above methods are already being used, or at least starting to be explored, for marine habitat mapping, but they are not yet integrated into a coherent multi-resolution 'nested' strategy for monitoring marine biodiversity at different spatial scales (van Rein *et al.*, 2009; Lecours *et al.*, 2015). Although such 'nested' approaches are sometimes used to collect benthic data at different scales within a single survey (Ferrini *et al.*, 2007; Yoerger *et al.*, 2007; Paull *et al.*, 2013), there is scope to develop this idea further into a regional or national monitoring protocol. The OBIA methods developed and tested in this thesis could play a key role within this protocol, enabling automated interpretation of imagery with low resolution and wide coverage to direct higher resolution survey effort towards areas of interest or change. Achievement of this goal would require progress in a number of areas: data collection and calibration protocols should be developed to reduce data variability, particularly for platforms other than satellites (Held *et al.*, 2015; Lillis *et al.*, 2016; Lamarche and Lurton, 2017); remote sensing data should be made more widely accessible, particularly pre-processed 'analysis-ready' data, (Turner *et al.*, 2015; Giuliani *et al.*, 2017); data interpretation methods should be standardised and, where possible, developed for open source software (Kilcoyne *et al.*, 2017) and, finally, marine ecological research must continue to improve our understanding of the relationships between species communities and abiotic variables detectable from remotely sensed data to produce maps at a scale relevant to management (Diesing *et al.*, 2016). Progress in these areas could ultimately enable direct comparison of outputs derived from different sensors and potentially seamless habitat mapping from the intertidal to the subtidal to inform marine and coastal spatial planning.

6.4 Future considerations

This study addressed several key questions but has also highlighted new areas of interest. In order to fulfil the potential of OBIA within a multi-scale monitoring strategy, further research should be undertaken in the following areas:

- The effect of spatial resolution on map accuracy should be quantified by creating habitat maps for the same site using the same method with different data, for example, satellite, aerial and UAV imagery for an intertidal site.
- UAV data collection methods must be optimised to improve the accuracy of topographic models and habitat maps. This thesis posits suggestions in chapters 3 and 4 as to how this may be achieved, but field tests must be conducted in temperate

intertidal environments to quantify the influence on accuracy of variables such as ground sampling distance, ground control point density, image density and use of oblique imagery.

- The transferability and scalability of methods described in this thesis must be assessed through applications in other temperate areas. Aerial and LiDAR imagery are available for most of the English coastline, providing an opportunity for wider testing of the methods developed in chapter 5.
- Research into OBIA for temperate marine habitat mapping needs to keep pace with rapid developments in sensor technology. OBIA methods should be developed and tested in temperate marine and coastal areas using multispectral acoustic data (Hughes Clarke, 2015), multibeam data collected by a cost-effective sensor (ENL Group, 2016), bathymetric or topobathymetric LiDAR, and acoustic and optical data collected by AUV.
- Methods for topographic modelling through photogrammetry of seabed imagery collected by ROV or AUV need to be developed and tested in temperate seas. The methods described in chapter 3 could be applied to evaluate the accuracy and feature detection capability of seabed terrain models. Ecological research should be conducted to identify relationships between benthic biodiversity and features detectable through photogrammetric modelling, to inform use of topographic models as proxies for habitat condition.
- The recent ability to apply OBIA to point cloud data (Blaschke and Tomljenovic, 2017) should be tested in the marine and coastal environment, for example using topographic models derived from sonar or LiDAR surveys or from photogrammetry of optical imagery.
- Knowledge-based OBIA rule sets for intertidal and subtidal mapping should be refined by defining ranges of threshold or membership function values for habitat classes to aid the transferability of these methods. Appropriate sources of contextual data should be integrated into the workflow if possible, and their impact on classification accuracy assessed.
- A wider range of OBIA machine learning classifiers should be tested in temperate marine and coastal environments, such as Bayesian neural networks, support vector

machines and CART decision trees, followed by evaluation of ensemble approaches to combine the results of the best performing classifiers.

- To facilitate wider uptake and testing of these methods, the OBIA and photogrammetry approaches developed and evaluated in this thesis using commercial software should be adapted to open source software and the outputs compared (da Costa *et al.*, 2007; Christophe and Inglada, 2009; Clewley *et al.*, 2014; Kilcoyne *et al.*, 2017).

6.5 Concluding remarks

This thesis was the first study to evaluate OBIA methods with a variety of remote sensing data in the North Sea. It greatly improved our knowledge of the distribution of habitats at the study sites, which in the case of Coquet to St Mary's Island informed the site's designation and subsequent management as an MPA. It offered novel insight into the potential benefits of remote sensing, photogrammetry and OBIA for mapping temperate intertidal and subtidal habitats. The current limitations and opportunities for future research outlined here highlight the need for continued collaboration and knowledge exchange between researchers and practitioners.

At a time of increased demand for marine habitat maps and decreased resources for surveillance and monitoring, key findings from this work will help to inform the adoption of these methods. This will help user organisations to make more robust use of information derived from remote sensing data, enabling more cost-effective use of limited resources, more confident communication with stakeholders and most importantly improved environmental decision making. It is hoped that these findings, and those arising from the future research recommended here, will help to inform the development of a well-integrated, multi-scale monitoring protocol for temperate seas.

References

ABP Marine Environmental Research Ltd (2008) *Atlas of UK Marine Renewable Energy Resources: Technical Report*. Southampton: Department for Business, Enterprise and Regulatory Reform.

Adamo, M., Tarantino, C., Tomaselli, V., Veronico, G., Nagendra, H. and Blonda, P. (2016) 'Habitat mapping of coastal wetlands using expert knowledge and Earth observation data', *Journal of Applied Ecology*, 53(5), pp. 1521-1532.

Addink, E.A., de Jong, S.M. and Pebesma, E.J. (2007) 'The importance of scale in object-based mapping of vegetation parameters with hyperspectral imagery', *Photogrammetric Engineering and Remote Sensing*, 73(8), pp. 905-912.

Agisoft LLC (2017) 'Agisoft Photoscan User Manual: Professional Edition, Version 1.3'. St Petersburg, Russia: Agisoft.

Aguirre-Gutierrez, J., Seijmonsbergen, A.C. and Duivenvoorden, J.F. (2012) 'Optimizing land cover classification accuracy for change detection, a combined pixel-based and object-based approach in a mountainous area in Mexico', *Applied Geography*, 34, pp. 29-37.

Airoldi, L. (2003) 'Effects of patch shape in intertidal algal mosaics: roles of area, perimeter and distance from edge', *Marine Biology*, 143(4), pp. 639-650.

Airoldi, L., Balata, D. and Beck, M.W. (2008) 'The Gray Zone: Relationships between habitat loss and marine diversity and their applications in conservation', *Journal of Experimental Marine Biology and Ecology*, 366, pp. 8-15.

Airoldi, L. and Beck, M.W. (2007) 'Loss, status and trends for coastal marine habitats of Europe', *Oceanography and Marine Biology*, 45, pp. 345-405.

Allard, A. (2017) 'NILS - A Nationwide Inventory Program for Monitoring the Conditions and Change of the Swedish Landscape', in Diaz-Delgado, R., Lucas, R. and Hurford, C. (eds.) *The Roles of Remote Sensing in Nature Conservation: A Practical Guide and Case Studies*. Switzerland: Springer, pp. 79-90.

Anderson, C.P., Carter, G.A. and Funderburk, W.R. (2016) 'The Use of Aerial RGB Imagery and LIDAR in Comparing Ecological Habitats and Geomorphic Features on a Natural versus Man-Made Barrier Island', *Remote Sensing*, 8(7), pp. 1-17.

Anderson, J.T., Van Holliday, D., Kloser, R., Reid, D.G. and Simard, Y. (2008) 'Acoustic seabed classification: current practice and future directions', *ICES Journal of Marine Science*, 65(6), pp. 1004-1011.

Anderson, K. and Gaston, K.J. (2013) 'Lightweight unmanned aerial vehicles will revolutionise spatial ecology', *Frontiers in Ecology and the Environment*, 11(3), pp. 138-146.

Aplin, P. (2005) 'Remote sensing: ecology', *Progress in Physical Geography*, 29(1), pp. 104-113.

Arevalo, R., Pinedo, S. and Ballesteros, E. (2007) 'Changes in the composition and structure of Mediterranean rocky-shore communities following a gradient of nutrient enrichment: Descriptive study and test of proposed methods to assess water quality regarding macroalgae', *Marine Pollution Bulletin*, 55(1-6), pp. 104-113.

Arvor, D., Durieux, L., Andres, S. and Laporte, M.A. (2013) 'Advances in Geographic Object-Based Image Analysis with ontologies: A review of main contributions and limitations from a remote sensing perspective', *ISPRS Journal of Photogrammetry and Remote Sensing*, 82, pp. 125-137.

Baatz, M. and Schape, A. (2000) 'Multiresolution Segmentation: an optimization approach for high quality multi-scale image segmentation', *Angewandte Geographische Informationzverarbeitung XII. Beitrage sum AGIT-Symposium*. Salzburg. Herbert Wichmann Verlag, pp. 12-23.

Baily, B., Collier, P., Farres, P., Inkpen, R. and Pearson, A. (2003) 'Comparative assessment of analytical and digital photogrammetric methods in the construction of DEMs of geomorphological forms', *Earth Surface Processes and Landforms*, 28(3), pp. 307-320.

Bajjouk, T., Guillaumont, B. and Populus, J. (1996) 'Application of airborne imaging spectrometry system data to intertidal seaweed classification and mapping', *Hydrobiologia*, 327, pp. 463-471.

Baker, E.K. and Harris, P.T. (2012) 'Habitat Mapping and Marine Management', in Harris, P.T. and Baker, E.K. (eds.) *Seafloor Geomorphology as Benthic Habitat: GeoHAB Atlas of Seafloor Geomorphic Features and Benthic Habitats*. London: Elsevier, pp. 23-38.

Bangdiwala, S.I. and Shankar, V. (2013) 'The Agreement Chart', *BMC Medical Research Methodology*, 13, pp. 1-7.

Banks, S.A. and Skilleter, G.A. (2007) 'The importance of incorporating fine-scale habitat data into the design of an intertidal marine reserve system', *Biological Conservation*, 138(1-2), pp. 13-29.

Barbier, E.B. (2012) 'Progress and Challenges in Valuing Coastal and Marine Ecosystem Services', *Review of Environmental Economics and Policy*, 6(1), pp. 1-19.

Baumstark, R., Duffey, R. and Pu, R.L. (2016) 'Mapping seagrass and colonized hard bottom in Springs Coast, Florida using WorldView-2 satellite imagery', *Estuarine Coastal and Shelf Science*, 181, pp. 83-92.

Beck, M.W. (1998) 'Comparison of the measurement and effects of habitat structure on gastropods in rocky intertidal and mangrove habitats', *Marine Ecology Progress Series*, 169, pp. 165-178.

Beck, M.W. (2000) 'Separating the elements of habitat structure: independent effects of habitat complexity and structural components on rocky intertidal gastropods', *Journal of Experimental Marine Biology and Ecology*, 249(1), pp. 29-49.

Bejarano, S., Mumby, P.J., Hedley, J.D. and Sotheran, I. (2010) 'Combining optical and acoustic data to enhance the detection of Caribbean forereef habitats', *Remote Sensing of Environment*, 114(11), pp. 2768-2778.

Belgiu, M. and Dragut, L. (2016) 'Random forest in remote sensing: A review of applications and future directions', *ISPRS Journal of Photogrammetry and Remote Sensing*, 114, pp. 24-31.

Belgiu, M., Dragut, L. and Strobl, J. (2014) 'Quantitative evaluation of variations in rule-based classifications of land cover in urban neighbourhoods using WorldView-2 imagery', *ISPRS Journal of Photogrammetry and Remote Sensing*, 87, pp. 205-215.

Bellec, V.K., Dolan, M.F.J., Boe, R., Thorsnes, T., Rise, L., Buhl-Mortensen, L. and Buhl-Mortensen, P. (2009) 'Sediment distribution and seabed processes in the Troms II area - offshore North Norway', *Norwegian Journal of Geology*, 89(1-2), pp. 29-40.

Benfield, S.L., Guzman, H.M., Mair, J.M. and Young, J.A.T. (2007) 'Mapping the distribution of coral reefs and associated sublittoral habitats in Pacific Panama: a comparison of optical satellite sensors and classification methodologies', *International Journal of Remote Sensing*, 28(22), pp. 5047-5070.

Benz, U.C. (2004) 'Multi-resolution, object-oriented fuzzy analysis of remote sensing data for GIS-ready information', *ISPRS Journal of Photogrammetry and Remote Sensing*, 58, pp. 239–258.

Biondo, M. and Bartholoma, A. (2017) 'A multivariate analytical method to characterize sediment attributes from high-frequency acoustic backscatter and ground-truthing data (Jade Bay, German North Sea coast)', *Continental Shelf Research*, 138, pp. 65-80.

Blaschke, T. (2010) 'Object based image analysis for remote sensing', *ISPRS Journal of Photogrammetry and Remote Sensing*, 65(2), pp. 2-16.

Blaschke, T., Hay, G.J., Kelly, M., Lang, S., Hofmann, P., Addink, E., Feitosa, R.Q., van der Meer, F., van der Werff, H., van Coillie, F. and Tiede, D. (2014) 'Geographic Object-Based Image Analysis - Towards a new paradigm', *ISPRS Journal of Photogrammetry and Remote Sensing*, 87, pp. 180-191.

Blaschke, T., Lang, S., Lorup, E., Strobl, J. and Zeil, P. (2000) 'Object-Oriented Image Processing in an Integrated GIS/Remote Sensing Environment and Perspectives for Environmental Applications', in Cremers, A. and Greve, K. (eds.) *Environmental Information for Planning, Politics and the Public*. Marburg: Metropolis Verlag, pp. 555-570.

Blaschke, T. and Strobl, J. (2001) 'What's wrong with pixels? Some recent developments interfacing remote sensing and GIS', *Geoinformationssysteme*, 14(6), pp. 12-17.

Blaschke, T. and Tomljenovic, I. (2017) 'OBIA and Point Clouds', *GIM International - the Worldwide Magazine for Geomatics*, 31(11), pp. 16-19.

Bongiorno, D.L., Bryson, M., Bridge, T.C.L., Dansereau, D.G. and Williams, S.B. (2017) 'Coregistered Hyperspectral and Stereo Image Seafloor Mapping from an Autonomous Underwater Vehicle', *Journal of Field Robotics*.

Borja, A. and Elliott, M. (2013) 'Marine monitoring during an economic crisis: The cure is worse than the disease', *Marine Pollution Bulletin*, 68(1-2), pp. 1-3.

Borja, A., Elliott, M., Andersen, J.H., Berg, T., Carstensen, J., Halpern, B.S., Heiskanen, A.-S., Korpinen, S., Lowndes, J.S.S., Martin, G. and Rodriguez-Ezpeleta, N. (2016) 'Overview of Integrative Assessment of Marine Systems: The Ecosystem Approach in Practice', *Frontiers in Marine Science*, 3(20).

Borre, J., Spanhove, T. and Haest, B. (2017) 'Towards a Mature Age of Remote Sensing for Natura 2000 Habitat Conservation: Poor Method Transferability as a Prime Obstacle', in Diaz-Delgado, R., Lucas, R. and Hurford, C. (eds.) *The Roles of Remote Sensing in Nature Conservation: A Practical Guide and Case Studies*. Switzerland: Springer.

Borsje, B.W., van Wesenbeeck, B.K., Dekker, F., Paalvast, P., Bouma, T.J., van Katwijk, M.M. and de Vries, M.B. (2011) 'How ecological engineering can serve in coastal protection', *Ecological Engineering*, 37(2), pp. 113-122.

Bradter, U., Thom, T.J., Altringham, J.D., Kunin, W.E. and Benton, T.G. (2011) 'Prediction of National Vegetation Classification communities in the British uplands using environmental data at multiple spatial scales, aerial images and the classifier random forest', *Journal of Applied Ecology*, 48(4), pp. 1057-1065.

Brander, K., Botsford, L.W., Ciannelli, L., Fogarty, M.J., Heath, M.R., Planque, B., Shannon, L.J. and Wieland, K. (2010) 'Human impacts on marine ecosystems', in Barange, M., Field, J.G., Harris, R.P., Hofmann, E.E., Perry, R.I., Werner, F.E., Ashby, D.M. (ed.) *Marine Ecosystems and Global Change*. Oxford: Oxford University Press, pp. 41-71.

Brazier, D.P., Davies, J., Holt, R.H.F. and Murray, E. (1998) *Marine Nature Conservation Review Sector 5. South-east Scotland and north-east England: area summaries*. Peterborough: Joint Nature Conservation Committee.

Breiman, L. (2001) 'Random forests', *Machine Learning*, 45(1), pp. 5-32.

Breyer, J., Pike, S., Medcalf, K. and Parker, J. (2016) 'Making Earth Observation Work (MEOW) for UK Biodiversity Monitoring and Surveillance, Phase 4: Testing applications in habitat condition assessment. A report to the Department for Environment, Food and Rural Affairs, prepared by Environment Systems Ltd'.

Brodie, J., Williamson, C.J., Smale, D.A., Kamenos, N.A., Mieszkowska, N., Santos, R., Cunliffe, M., Steinke, M., Yesson, C., Anderson, K.M., Asnaghi, V., Brownlee, C., Burdett, H.L., Burrows, M.T., Collins, S., Donohue, P.J.C., Harvey, B., Foggo, A., Noisette, F., Nunes, J., Ragazzola, F., Raven, J.A., Schmidt, D.N., Suggett, D., Teichberg, M. and Hall-Spencer, J.M. (2014) 'The future of the northeast Atlantic benthic flora in a high CO2 world', *Ecology and Evolution*, 4(13), pp. 2787-2798.

Brown, C.J. and Blondel, P. (2009) 'Developments in the application of multibeam sonar backscatter for seafloor habitat mapping', *Applied Acoustics*, 70(10), pp. 1242-1247.

Brown, C.J. and Collier, J.S. (2008) 'Mapping benthic habitat in regions of gradational substrata: An automated approach utilising geophysical, geological, and biological relationships', *Estuarine Coastal and Shelf Science*, 78(1), pp. 203-214.

Brown, C.J., Sameoto, J.A. and Smith, S.J. (2012) 'Multiple methods, maps, and management applications: Purpose made seafloor maps in support of ocean management', *Journal of Sea Research*, 72, pp. 1-13.

Brown, C.J., Smith, S.J., Lawton, P. and Anderson, J.T. (2011a) 'Benthic habitat mapping: A review of progress towards improved understanding of the spatial ecology of the seafloor using acoustic techniques', *Estuarine Coastal and Shelf Science*, 92(3), pp. 502-520.

Brown, C.J., Todd, B.J., Kostylev, V.E. and Pickrill, R.A. (2011b) 'Image-based classification of multibeam sonar backscatter data for objective surficial sediment mapping of Georges Bank, Canada', *Continental Shelf Research*, 31(2), pp. S110-S119.

Bruzzone, L. and Bovolo, F. (2013) 'A Novel Framework for the Design of Change-Detection Systems for Very-High-Resolution Remote Sensing Images', *Proceedings of the IEEE*, 101(3), pp. 609-630.

Bryson, M., Johnson-Roberson, M., Murphy, R.J. and Bongiorno, D. (2013) 'Kite Aerial Photography for Low-Cost, Ultra-high Spatial Resolution Multi-Spectral Mapping of Intertidal Landscapes', *PLOS ONE*, 8(9).

Buchanan, G.M., Brink, A.B., Leidner, A.K., Rose, R. and Wegmann, M. (2015) 'Advancing terrestrial conservation through remote sensing', *Ecological Informatics*, 30, pp. 318-321.

Buhl-Mortensen, L., Buhl-Mortensen, P., Dolan, M.J.F. and Gonzalez-Mirelis, G. (2015) 'Habitat mapping as a tool for conservation and sustainable use of marine resources: Some perspectives from the MAREANO Programme, Norway', *Journal of Sea Research*, 100, pp. 46-61.

Bulleri, F. and Chapman, M.G. (2010) 'The introduction of coastal infrastructure as a driver of change in marine environments', *Journal of Applied Ecology*, 47(1), pp. 26-35.

Bunker, F., Foster-Smith, R. and Perrins, J. (2001) 'Procedural Guideline 1-1: Intertidal resource mapping using aerial photographs', in Davies, J., Baxter, J., Bradley, M., Connor, D., Khan, J., Murray, E., Sanderson, W., Turnbull, C. and Vincent, M. (eds.) *Marine Monitoring Handbook*. Peterborough: JNCC, pp. 165-174.

Burns, J.H.R., Delparte, D., Gates, R.D. and Takabayashi, M. (2015) 'Integrating structure-from-motion photogrammetry with geospatial software as a novel technique for quantifying 3D ecological characteristics of coral reefs', *PeerJ*, 3.

Burrows, M.T. (2012) 'Influences of wave fetch, tidal flow and ocean colour on subtidal rocky communities', *Marine Ecology Progress Series*, 445, pp. 193-207.

Burrows, M.T., Mieszkowska, N. and Hawkins, S.J. (2014) *Marine Strategy Framework Directive Indicators for UK Rocky Shores. Part 1: Defining and validating the indicators* (Report Number 522). Peterborough: JNCC.

Caldow, C., Monaco, M.E., Pittman, S.J., Kendall, M.S., Goedeke, T.L., Menza, C., Kinlan, B.P. and Costa, B.M. (2015) 'Biogeographic assessments: A framework for information synthesis in marine spatial planning', *Marine Policy*, 51, pp. 423-432.

Calvert, J., Strong, J.A., Service, M., McGonigle, C. and Quinn, R. (2015) 'An evaluation of supervised and unsupervised classification techniques for marine benthic habitat mapping using multibeam echosounder data', *ICES Journal of Marine Science*, 72(5), pp. 1498-1513.

Cameron, A., & Askew, N. (eds.). (2011) 'EUSeaMap - Preparatory Action for development and assessment of a European broad-scale seabed habitat map final report. Available at http://jncc.gov.uk/euseamap'.

Canovas-Garcia, F. and Alonso-Sarria, F. (2015) 'Optimal Combination of Classification Algorithms and Feature Ranking Methods for Object-Based Classification of Submeter Resolution Z/I-Imaging DMC Imagery', *Remote Sensing*, 7(4), pp. 4651-4677.

Capolsini, P., Andrefouet, S., Rion, C. and Payri, C. (2003) 'A comparison of Landsat ETM+, SPOT HRV, Ikonos, ASTER, and airborne MASTER data for coral reef habitat mapping in south pacific islands', *Canadian Journal of Remote Sensing*, 29(2), pp. 187-200.

Cardenas, C.A., Davy, S.K. and Bell, J.J. (2016) 'Influence of a canopy-forming algae on temperate sponge assemblages', *Journal of the Marine Biological Association of the United Kingdom*, 96(2), pp. 351-362.

Caveen, A.J., Fitzsimmons, C., Pieraccini, M., Dunn, E., Sweeting, C.J., Johnson, M.L., Bloomfield, H., Jones, E.V., Lightfoot, P., Gray, T.S., Stead, S.M. and Polunin, N.V.C. (2014) 'Diverging Strategies to Planning an Ecologically Coherent Network of MPAs in the North Sea: The Roles of Advocacy, Evidence and Pragmatism in the Face of Uncertainty', in Johnson, M.L. and Sandell, J. (eds.) *Advances in Marine Biology*. Oxford: Elsevier Ltd Academic Press, pp. 325-369.

Chen, G., Hay, G.J., Carvalho, L.M.T. and Wulder, M.A. (2012) 'Object-based change detection', *International Journal of Remote Sensing*, 33(14), pp. 4434-4457.

Christophe, E. and Inglada, J. (2009) 'Open Source Remote Sensing: Increasing the Usability of Cutting-Edge Algorithms', *IEEE Geoscience and Remote Sensing Society Newsletter*, March 2009, pp. 9-15.

Chust, G., Galparsoro, I., Borja, A., Franco, J. and Uriarte, A. (2008) 'Coastal and estuarine habitat mapping, using LIDAR height and intensity and multi-spectral imagery', *Estuarine Coastal and Shelf Science*, 78(4), pp. 633-643.

Clarke, K.R., Gorley, R.N., Somerfield, P.J. and Warwick, R.M. (2014) 'Change in marine communities: an approach to statistical analysis and interpretation 3rd Edition'. Plymouth: PRIMER-E Ltd.

Clements, A.J., Strong, J.A., Flanagan, C. and Service, M. (2010) 'Objective stratification and sampling-effort allocation of ground-truthing in benthic-mapping surveys', *ICES Journal of Marine Science*, 67(4), pp. 628-637.

Clewley, D., Bunting, P., Shepherd, J., Gillingham, S., Flood, N., Dymond, J., Lucas, R., Armston, J. and Moghaddam, M. (2014) 'A Python-Based Open Source System for Geographic Object-Based Image Analysis (GEOBIA) Utilizing Raster Attribute Tables', *Remote Sensing*, 6(7), pp. 6111-6135.

Cogan, C.B., Todd, B.J., Lawton, P. and Noji, T.T. (2009) 'The role of marine habitat mapping in ecosystem-based management', *ICES Journal of Marine Science*, 66(9), pp. 2033-2042.

Coggan, R. and Diesing, M. (2011) 'The seabed habitats of the central English Channel: A generation on from Holme and Cabioch, how do their interpretations match-up to modern mapping techniques?', *Continental Shelf Research*, 31(2), pp. S132-S150.

Coggan, R.C., Mitchell, A.Q., White, J.M. and Golding, N.J. (2007) *Recommended operating guidelines (ROG) for underwater video and photographic imaging techniques*. Mapping European Seabed Habitats (MESH) Video Working Group. [Online]. Available at: http://www.emodnet-seabedhabitats.eu/Default.aspx?page=1915.

Cohen, J. (1960) 'A coefficient of agreement for nominal scales', *Educational and Psychological Measurement*, 20, pp. 37-46.

Colditz, R.R. (2015) 'An Evaluation of Different Training Sample Allocation Schemes for Discrete and Continuous Land Cover Classification Using Decision Tree-Based Algorithms', *Remote Sensing*, 7(8), pp. 9655-9681.

Colenutt, A. and Kinnear, R. (2014) *Seabed Mapping: Flamborough Head to Spurn Point. Report TR47 produced for East Riding of Yorkshire Council*. Southampton: Channel Coast Observatory, National Oceanography Centre, Southampton.

Collier, J.S. and McGonigle, C.D. (2011) *Examining the relationship between acoustic backscatter and physical properties of the seabed* (Report Number MEPF/09/P80). London: Marine Aggregate Levy Sustainability Fund.

Collin, A., Archambault, P. and Long, B. (2011) 'Predicting Species Diversity of Benthic Communities within Turbid Nearshore Using Full-Waveform Bathymetric LiDAR and Machine Learners', *PLOS ONE*, 6(6).

Colomina, I. and Molina, P. (2014) 'Unmanned aerial systems for photogrammetry and remote sensing: A review', *ISPRS Journal of Photogrammetry and Remote Sensing*, 92, pp. 79-97.

Comber, A., Fisher, P., Brunsdon, C. and Khmag, A. (2012) 'Spatial analysis of remote sensing image classification accuracy', *Remote Sensing of Environment*, 127, pp. 237-246.

Comber, A.J. (2013) 'Geographically weighted methods for estimating local surfaces of overall, user and producer accuracies', *Remote Sensing Letters*, 4(4), pp. 373-380.

Conchedda, G., Durieux, L. and Mayaux, P. (2008) 'An object-based method for mapping and change analysis in mangrove ecosystems', *ISPRS Journal of Photogrammetry and Remote Sensing*, 63(5), pp. 578-589.

Congalton, R.G. (1991) 'A Review of Assessing the Accuracy of Classifications of Remotely Sensed Data', *Remote Sensing of Environment*, 37(1), pp. 35-46.

Congalton, R.G. and Green, K. (2009) *Assessing the Accuracy of Remotely Sensed Data: Principles and Practices*. 2nd edn. Florida, USA: CRC Press Taylor and Francis Group.

Connor, D., Gilliland, P., Golding, N., Robinson, P., Todd, D. and Verling, E. (2006) *UKSeaMap: the mapping of seabed and water column features of UK seas.* Peterborough: JNCC.

Connor, D.W., Allen, J.H., Golding, N., Howell, K.L., Lieberknecht, L.M., Northen, K.O. and Reker, J.B. (2004) *The Marine Habitat Classification for Britain and Ireland Version 04.05*. Peterborough: JNCC.

Coppin, P., Jonckheere, I., Nackaerts, K., Muys, B. and Lambin, E. (2004) 'Digital change detection methods in ecosystem monitoring: a review', *International Journal of Remote Sensing*, 25(9), pp. 1565-1596.

Corbane, C., Lang, S., Pipkins, K., Alleaume, S., Deshayes, M., Milian, V.E.G., Strasser, T., Vanden Borre, J., Spanhove, T. and Foerster, M. (2015) 'Remote sensing for mapping natural habitats and their conservation status - New opportunities and challenges', *International Journal of Applied Earth Observation and Geoinformation*, 37, pp. 7-16.

Corcoran, J.M., Knight, J.F. and Gallant, A.L. (2013) 'Influence of Multi-Source and Multi-Temporal Remotely Sensed and Ancillary Data on the Accuracy of Random Forest Classification of Wetlands in Northern Minnesota', *Remote Sensing*, 5(7), pp. 3212-3238.

Costa, B.M. and Battista, T.A. (2013) 'The semi-automated classification of acoustic imagery for characterizing coral reef ecosystems', *International Journal of Remote Sensing*, 34(18), pp. 6389-6422.

Costa, H., Foody, G.M. and Boyd, D.S. (2017) 'Using mixed objects in the training of object-based image classifications', *Remote Sensing of Environment*, 190, pp. 188-197.

Courtney, L.A., Fisher, W.S., Raimondo, S., Oliver, L.M. and Davis, W.P. (2007) 'Estimating 3-dimensional colony surface area of field corals', *Journal of Experimental Marine Biology and Ecology*, 351(1-2), pp. 234-242.

Cracknell, A.P. (1999) 'Remote sensing techniques in estuaries and coastal zones - an update', *International Journal of Remote Sensing*, 20(3), pp. 485-496.

Crowder, L. and Norse, E. (2008) 'Essential ecological insights for marine ecosystem-based management and marine spatial planning', *Marine Policy*, 32(5), pp. 772-778.

Curtis, M., Mitchell, P. and Jenkins, C. (2015) *Skerries Bank and Surrounds MCZ Post-survey Site Report. Marine Protected Areas Data and Evidence Co-ordination Programme Report No. 43. Defra Project Code: MB0120*. London: Defra.

Czerwinski, C.J., King, D.J. and Mitchell, S.W. (2014) 'Mapping forest growth and decline in a temperate mixed forest using temporal trend analysis of Landsat imagery, 1987-2010', *Remote Sensing of Environment*, 141, pp. 188-200.

da Costa, G.A.O.P., de Pinho, C.M.D., Feitosa, R.Q., de Almeida, C.M., Kux, H.J.H., Fonseca, L.M.G. and Oliveira, D.A.B. (2007) 'Interimage: an open source platform for automatic image interpretation', *II Simposio Brasileiro de Geomatica e V Colquio Brasileiro de Ciencias Geodesicas*. Presidente Prudente, Sao Paolo, 24-27 July 2007.

Dartnell, P. and Gardner, J.V. (2004) 'Predicting Seafloor Facies from Multibeam Bathymetry and Backscatter Data', *Photogrammetric Engineering and Remote Sensing*, 70(9), pp. 1081-1091.

Davies, A.J., Johnson, M.P. and Maggs, C.A. (2007) 'Limpet grazing and loss of Ascophyllum nodosum canopies on decadal time scales', *Marine Ecology Progress Series*, 339, pp. 131-141.

Davies, J., Baxter, J., Bradley, M., Connor, D., Khan, J., Murray, E., Sanderson, W., Turnbull, C. and Vincent, M. (2001) *Marine Monitoring Handbook*. Peterborough: JNCC.

de Oliveira, E., Populus, J. and Guillaumont, B. (2006) 'Predictive modelling of coastal habitats using remote sensing data and fuzzy logic: A case for seaweed in Brittany (France)', *EARSeL eProceedings, 5(2), 208-223*.

Defra (2010) *The Government's strategy for contributing to the delivery of a UK network of Marine Protected Areas*. London.

Defra (2012) *Marine Conservation Zones: Consultation on proposals for designation in 2013. Annex A.4 - Net Gain sites requiring further consideration*. London: Defra.

Defra (2013a) *Defra Open Data Strategy*. London: Defra.

Defra (2013b) *Revised Approach to the Management of Commercial Fisheries in European Marine Sites - Overarching Policy and Delivery Document*. Defra. [Online]. Available at: http://www.marinemanagement.org.uk/protecting/conservation/documents/ems_fisheries/policy_and_delivery.pdf.

Degraer, S., Moerkerke, G., Rabaut, M., Van Hoey, G., Du Four, I., Vincx, M., Henriet, J.P. and Van Lancker, V. (2008) 'Very-high resolution side-scan sonar mapping of biogenic reefs of the tube-worm Lanice conchilega', *Remote Sensing of Environment*, 112(8), pp. 3323-3328.

Dekavalla, M. and Argialas, D. (2017) 'Object-based classification of global undersea topography and geomorphological features from the SRTM30_PLUS data', *Geomorphology*, 288, pp. 66-82.

Dey, V., Zhang, Y. and Zhong, M. (2010) 'A Review on Image Segmentation Techniques with Remote Sensing Perspective', *100 Years ISPRS Advancing Remote Sensing Science, Pt 1*, 38, pp. 31-42.

Diaz, R.J., Solan, M., Valente, R. M. (2004) 'A review of approaches for classifying benthic habitats and evaluating habitat quality', *Journal of Environmental Management*, 73(3), pp. 165-181.

Diesing, M., Coggan, R. and Vanstaen, K. (2009) 'Widespread rocky reef occurrence in the central English Channel and the implications for predictive habitat mapping', *Estuarine Coastal and Shelf Science*, 83(4), pp. 647-658.

Diesing, M., Green, S.L., Stephens, D., Lark, R., M., Stewart, H.A. and Dove, D. (2014) 'Mapping seabed sediments: Comparison of manual, geostatistical, object-based image analysis and machine learning approaches', *Continental Shelf Research*, 84, pp. 107-119.

Diesing, M., Mitchell, P. and Stephens, D. (2016) 'Image-based seabed classification: what can we learn from terrestrial remote sensing?', *ICES Journal of Marine Science*, 73(10), pp. 2425-2441.

Diesing, M. and Stephens, D. (2015) 'A multi-model ensemble approach to seabed mapping', *Journal of Sea Research*, 100, pp. 62-69.

Dolan, M.F.J. and Lucieer, V.L. (2014) 'Variation and Uncertainty in Bathymetric Slope Calculations Using Geographic Information Systems', *Marine Geodesy*, 37(2), pp. 187-219.

Doxani, G., Karantzalos, K. and Tsakiri-Strati, M. (2012) 'Monitoring urban changes based on scale-space filtering and object-oriented classification', *International Journal of Applied Earth Observation and Geoinformation*, 15, pp. 38-48.

Dragut, L., Tiedec, D. and Levick, S.R. (2010) 'ESP: a tool to estimate scale parameter for multiresolution image segmentation of remotely sensed data', *International Journal of Geographical Information Science*, 24(6), pp. 859-871.

Du Preez, C. (2015) 'A new arc-chord ratio (ACR) rugosity index for quantifying three-dimensional landscape structural complexity', *Landscape Ecology*, 30(1), pp. 181-192.

Ducklow, H.W., Doney, S.C. and Steinberg, D.K. (2009) 'Contributions of Long-Term Research and Time-Series Observations to Marine Ecology and Biogeochemistry', *Annual Review of Marine Science*, 1, pp. 279-302.

Duffy, J.P., Pratt, L., Anderson, K., Land, P.E. and Shutler, J.D. (2018) 'Spatial assessment of intertidal seagrass meadows using optical imaging systems and a lightweight drone', *Estuarine Coastal and Shelf Science*, 200, pp. 169-180.

Duro, D.C., Franklin, S.E. and Dube, M.G. (2012) 'Multi-scale object-based image analysis and feature selection of multi-sensor earth observation imagery using random forests', *International Journal of Remote Sensing*, 33(14), pp. 4502-4526.

Duro, D.C., Franklin, S.E. and Dube, M.G. (2013) 'Hybrid Object-based Change Detection and Hierarchical Image Segmentation for Thematic Map Updating', *Photogrammetric Engineering and Remote Sensing*, 79(3), pp. 259-268.

EC (1992) *COUNCIL DIRECTIVE 92 / 43 / EEC of 21 May 1992 on the conservation of natural habitats and of wild fauna and flora*. [Online]. Available at: http://eur-lex.europa.eu/legal-content/EN/TXT/HTML/?uri=CELEX:31992L0043&from=EN (Accessed: November 2014).

EC (2000) *DIRECTIVE 2000/60/EC OF THE EUROPEAN PARLIAMENT AND OF THE COUNCIL of 23 October 2000 establishing a framework for Community action in the field of water policy*.

[Online]. Available at: http://eur-lex.europa.eu/legal-content/EN/TXT/HTML/?uri=CELEX:32000L0060&from=EN (Accessed: November 2014).

EC (2008) *DIRECTIVE 2008/56/EC OF THE EUROPEAN PARLIAMENT AND OF THE COUNCIL of 17 June 2008 establishing a framework for community action in the field of marine environmental policy (Marine Strategy Framework Directive)*. [Online]. Available at: http://eur-lex.europa.eu/legal-content/EN/TXT/HTML/?uri=CELEX:32008L0056&from=EN (Accessed: November 2014).

Ehler, C. and Douvere, F. (2007) *Visions for a Sea Change. Report of the First International Workshop on Marine Spatial Planning*. Paris: UNESCO.

Ehler, C. and Douvere, F. (2009) *Marine Spatial Planning: a step-by-step approach towards ecosystem-based management*. Paris: UNESCO.

Eisenbeiss, H. and Sauerbier, M. (2011) 'Investigation of UAV systems and flight modes for photogrammetric applications', *Photogrammetric Record*, 26(136), pp. 400-421.

Ekebom, J. and Erkkila, A. (2003) 'Using aerial photography for identification of marine and coastal habitats under the EU's Habitats Directive', *Aquatic Conservation-Marine and Freshwater Ecosystems*, 13(4), pp. 287-304.

Elvenes, S., Dolan, M.F.J., Buhl-Mortensen, P. and Bellec, V.K. (2014) 'An evaluation of compiled single-beam bathymetry data as a basis for regional sediment and biotope mapping', *ICES Journal of Marine Science*, 71(4), pp. 867-881.

Elvidge, C.D., Zhizhin, M., Baugh, K. and Hsu, F.C. (2015) 'Automatic Boat Identification System for VIIRS Low Light Imaging Data', *Remote Sensing*, 7(3), pp. 3020-3036.

ENL Group (2016) *Wide Angle Sonar Seafloor Profiler (WASSP)*. Available at: www.wassp.com (Accessed: January 2018).

Environment Agency (2014) *Coquet to St. Mary's rMCZ Survey Cruise Report*. York: Environment Agency.

Environment Agency (2016) *Ortho-rectified Aerial Photography Project Report*. Bath, UK: Environment Agency.

Estomata, M.T.L., Blanco, A.C., Nadaoka, K. and Tomoling, E.C.M. (2012) 'Extraction of Benthic Cover Information from Video Tows and Photographs Using Object-Based Image Analysis', *xxii ISPRS Congress, Technical Commission viii*, 39-B8, pp. 539-544.

EUNIS (2012) *European Nature Information System Habitat Classification*. Available at: http://eunis.eea.europa.eu/habitats/1 (Accessed: November 2014).

Evans, J.L., Peckett, F. and Howell, K.L. (2015) 'Combined application of biophysical habitat mapping and systematic conservation planning to assess efficiency and representativeness of the existing High Seas MPA network in the Northeast Atlantic', *ICES Journal of Marine Science*, 72(5), pp. 1483-1497.

Fan, F.L., Weng, Q.H. and Wang, Y.P. (2007) 'Land use and land cover change in Guangzhou, China, from 1998 to 2003, based on Landsat TM/ETM+ imagery', *Sensors*, 7(7), pp. 1323-1342.

Fernandez, C. (2011) 'The retreat of large brown seaweeds on the north coast of Spain: the case of Saccorhiza polyschides', *European Journal of Phycology*, 46(4), pp. 352-360.

Ferrini, V.L., Fornari, D.J., Shank, T.M., Kinsey, J.C., Tivey, M.A., Soule, S.A., Carbotte, S.M., Whitcomb, L.L., Yoerger, D. and Howland, J. (2007) 'Submeter bathymetric mapping of volcanic and hydrothermal features on the East Pacific Rise crest at 9°50'N', *Geochemistry, Geophysics, Geosystems*, 8(1).

Figueira, W., Ferrari, R., Weatherby, E., Porter, A., Hawes, S. and Byrne, M. (2015) 'Accuracy and Precision of Habitat Structural Complexity Metrics Derived from Underwater Photogrammetry', *Remote Sensing*, 7(12), pp. 16883-16900.

Firth, L.B., Thompson, R.C., Bohn, K., Abbiati, M., Airoldi, L., Bouma, T.J., Bozzeda, F., Ceccherelli, V.U., Colangelo, M.A., Evans, A., Ferrario, F., Hanley, M.E., Hinz, H., Hoggart, S.P.G., Jackson, J.E., Moore, P., Morgan, E.H., Perkol-Finkel, S., Skov, M.W., Strain, E.M., van Belzen, J. and Hawkins, S.J. (2014) 'Between a rock and a hard place: Environmental and engineering considerations when designing coastal defence structures', *Coastal Engineering*, 87, pp. 122-135.

Fitzgerald, R.W. and Lees, B.G. (1994) 'Assessing the Classification Accuracy of Multisource Remote-Sensing Data', *Remote Sensing of Environment*, 47(3), pp. 362-368.

Fitzsimmons, C., Lightfoot, P. and Stephenson, F. (2015a) *Coquet to St Mary's rMCZ post-survey site report. Report for Defra as part of the Marine Protected Areas Data and Evidence Co-ordination Programme 2013-14* (Report number 36). London: Defra.

Fitzsimmons, C., Lightfoot, P. and Stephenson, F. (2015b) *Runswick Bay rMCZ post-survey site report. Report for Defra as part of the Marine Protected Areas Data and Evidence Co-ordination Programme 2013-14* (Report Number 32). London: Defra.

Fletcher, S., Jefferson, R., Glegg, G., Rodwell, L. and Dodds, W. (2014) 'England's evolving marine and coastal governance framework', *Marine Policy*, 45, pp. 261-268.

Foden, J., Rogers, S.I. and Jones, A.P. (2011) 'Human pressures on UK seabed habitats: a cumulative impact assessment', *Marine Ecology Progress Series*, 428, pp. 33-47.

Fong, P., Boyer, K.E., Desmond, J.S. and Zedler, J.B. (1996) 'Salinity stress, nitrogen competition and facilitation: what controls seasonal succession of two opportunistic green macroalgae?', *Journal of Experimental Marine Biology and Ecology*, 206(1-2), pp. 203-221.

Fonseca, L., Brown, C., Calder, B., Mayer, L. and Rzhanov, Y. (2009) 'Angular range analysis of acoustic themes from Stanton Banks Ireland: A link between visual interpretation and multibeam echosounder angular signatures', *Applied Acoustics*, 70(10), pp. 1298-1304.

Fonseca, L. and Mayer, L. (2007) 'Remote estimation of surficial seafloor properties through the application of angular range analysis to multibeam sonar data', *Marine Geophysical Researches*, 28(2), pp. 119-126.

Fonstad, M.A., Dietrich, J.T., Courville, B.C., Jensen, J.L. and Carbonneau, P.E. (2013) 'Topographic structure from motion: a new development in photogrammetric measurement', *Earth Surface Processes and Landforms*, 38(4), pp. 421-430.

Foody, G.M. (1992) 'On the Compensation for Chance Agreement in Image Classification Accuracy Assessment', *Photogrammetric Engineering and Remote Sensing*, 58(10), pp. 1459-1460.

Foody, G.M. (2003) 'Geographical weighting as a further refinement to regression modelling: An example focused on the NDVI-rainfall relationship', *Remote Sensing of Environment*, 88(3), pp. 283-293.

Foody, G.M. (2005) 'Local characterization of thematic classification accuracy through spatially constrained confusion matrices', *International Journal of Remote Sensing*, 26(6), pp. 1217-1228.

Foody, G.M. (2008) 'Harshness in image classification accuracy assessment', *International Journal of Remote Sensing*, 29(11), pp. 3137-3158.

Foody, G.M. (2010) 'Assessing the accuracy of land cover change with imperfect ground reference data', *Remote Sensing of Environment*, 114(10), pp. 2271-2285.

Foody, G.M. and Mathur, A. (2004) 'Toward intelligent training of supervised image classifications: directing training data acquisition for SVM classification', *Remote Sensing of Environment*, 93(1-2), pp. 107-117.

Foster-Smith, R.L. and Sotheran, I.S. (2003) 'Mapping marine benthic biotopes using acoustic ground discrimination systems', *International Journal of Remote Sensing*, 24(13), pp. 2761-2784.

Franklin, S.E. and Wulder, M.A. (2002) 'Remote sensing methods in medium spatial resolution satellite data land cover classification of large areas', *Progress in Physical Geography*, 26(2), pp. 173-205.

Fraschetti, S., Terlizzi, A. and Boero, F. (2008) 'How many habitats are there in the sea (and where)?', *Journal of Experimental Marine Biology and Ecology*, 366, pp. 109-115.

Freitas, R., Ricardo, F., Pereira, F., Sampaio, L., Carvalho, S., Gaspar, M., Quintino, V. and Rodrigues, A.M. (2011) 'Benthic habitat mapping: Concerns using a combined approach (acoustic, sediment and biological data)', *Estuarine Coastal and Shelf Science*, 92(4), pp. 598-606.

Freitas, R., Rodrigues, A.M. and Quintino, V. (2003) 'Benthic biotopes remote sensing using acoustics', *Journal of Experimental Marine Biology and Ecology*, 285, pp. 339-353.

Fretwell, P.T., Staniland, I.J. and Forcada, J. (2014) 'Whales from Space: Counting Southern Right Whales by Satellite', *PLOS ONE*, 9(2), pp. 1-9.

Friedman, A., Pizarro, O., Williams, S.B. and Johnson-Roberson, M. (2012) 'Multi-Scale Measures of Rugosity, Slope and Aspect from Benthic Stereo Image Reconstructions', *PLOS ONE*, 7(12).

Frost, M., Sanderson, W.G., Vina-Herbon, C. and Lowe, R.J. (2013) *The potential use of mapped extent and distribution of habitats as indicators of Good Environmental Status. Healthy and Biologically Diverse Seas Evidence Group Workshop Report*. London: Defra.

Frost, N.J., Burrows, M.T., Johnson, M.P., Hanley, M.E. and Hawkins, S.J. (2005) 'Measuring surface complexity in ecological studies', *Limnology and Oceanography-Methods*, 3, pp. 203-210.

Galparsoro, I., Borja, A., Bald, J., Liria, P. and Chust, G. (2009) 'Predicting suitable habitat for the European lobster (Homarus gammarus), on the Basque continental shelf (Bay of Biscay), using Ecological-Niche Factor Analysis', *Ecological Modelling*, 220(4), pp. 556-567.

Galparsoro, I., Connor, D.W., Borja, A., Aish, A., Amorim, P., Bajjouk, T., Chambers, C., Coggan, R., Dirberg, G., Ellwood, H., Evans, D., Goodin, K.L., Grehan, A., Haldin, J., Howell, K., Jenkins, C., Michez, N., Mo, G., Buhl-Mortensen, P., Pearce, B., Populus, J., Salomidi, M., Sanchez, F., Serrano, A., Shumchenia, E., Tempera, F. and Vasquez, M. (2012a) 'Using EUNIS habitat classification for benthic mapping in European seas: present concerns and future needs', *Marine Pollution Bulletin*, 64(12), pp. 2630-8.

Galparsoro, I., Connor, D.W., Borja, A., Aish, A., Amorim, P., Bajjouk, T., Chambers, C., Coggan, R., Dirberg, G., Ellwood, H., Evans, D., Goodin, K.L., Grehan, A., Haldin, J., Howell, K., Jenkins, C., Michez, N., Mo, G., Buhl-Mortensen, P., Pearce, B., Populus, J., Salomidi, M., Sanchez, F., Serrano, A., Shumchenia, E., Tempera, F. and Vasquez, M. (2012b) 'Using EUNIS habitat classification for benthic mapping in European seas: present concerns and future needs', *Mar Pollut Bull*, 64(12), pp. 2630-8.

Galparsoro, I., Rodriguez, J.G., Menchaca, I., Quincoces, I., Garmendia, J.M. and Borja, A. (2015) 'Benthic habitat mapping on the Basque continental shelf (SE Bay of Biscay) and its application to the European Marine Strategy Framework Directive', *Journal of Sea Research*, 100, pp. 70-76.

Gao, J. (2009) 'Bathymetric mapping by means of remote sensing: methods, accuracy and limitations', *Progress in Physical Geography*, 33(1), pp. 103-116.

Gao, Y. and Mas, J.F. (2008) 'A Comparison of the Performance of Pixel Based and Object Based Classifications over Images wtih Various Spatial Resolutions', *Online Journal of Earth Sciences*, 2(1), pp. 27-35.

Gao, Y., Mas, J.F., Kerle, N. and Pacheco, J.A.N. (2011) 'Optimal region growing segmentation and its effect on classification accuracy', *International Journal of Remote Sensing*, 32(13), pp. 3747-3763.

Garono, R.J., Simenstad, C.A., Robinson, R. and Ripley, H. (2004) 'Using high spatial resolution hyperspectral imagery to map intertidal habitat structure in Hood Canal, Washington, USA', *Canadian Journal of Remote Sensing*, 30(1), pp. 54-63.

Garono, R.J., Simenstad, C.A., Robinson, R., Weller, C. and Todd, S. (2008) 'Mapping Intertidal Eelgrass Landscapes in Hood Canal (WA) Using High Spatial Resolution Compact Airborne Spectrographic Imager (CASI) Imagery', *PNAMP Special Session at the 2008 American Society*

for Photogrammetry and Remote Sensing Annual Meeting. Portland, Oregon, USA, 28 April - 2 May 2008.

Gavazzi, G.M., Madricardo, F., Janowski, L., Kruss, A., Blondel, P., Sigovini, M. and Foglini, F. (2016) 'Evaluation of seabed mapping methods for fine-scale classification of extremely shallow benthic habitats - Application to the Venice Lagoon, Italy', *Estuarine Coastal and Shelf Science*, 170, pp. 45-60.

Geldsetzer, T., Arkett, M., Zagon, T., Charbonneau, F., Yackel, J.J. and Scharien, R.K. (2015) 'All-Season Compact-Polarimetry C-band SAR Observations of Sea Ice', *Canadian Journal of Remote Sensing*, 41(5), pp. 485-504.

Georganos, S., Grippa, T., Vanhuysse, S., Lennert, M., Shimoni, M., Kalogirou, S. and Wolff, E. (2017) 'Less is more: optimizing classification performance through feature selection in a very-high-resolution remote sensing object-based urban application', *GI Science & Remote Sensing*, Online.

George, D.A. and Hill, P.S. (2008) 'Wave climate, sediment supply and the depth of the sand-mud transition: A global survey', *Marine Geology*, 254(3-4), pp. 121-128.

Ghimire, B., Rogan, J., Galiano, V.R., Panday, P. and Neeti, N. (2012) 'An Evaluation of Bagging, Boosting, and Random Forests for Land-Cover Classification in Cape Cod, Massachusetts, USA', *Giscience & Remote Sensing*, 49(5), pp. 623-643.

Ghosh, A. and Joshi, P.K. (2014) 'A comparison of selected classification algorithms for mapping bamboo patches in lower Gangetic plains using very high resolution WorldView 2 imagery', *International Journal of Applied Earth Observation and Geoinformation*, 26, pp. 298-311.

Gilbertson, J.K. and van Niekerk, A. (2017) 'Value of dimensionality reduction for crop differentiation with multi-temporal imagery and machine learning', *Computers and Electronics in Agriculture*, 142, pp. 50-58.

Gillanders, S.N., Coops, N.C., Wulder, M.A., Gergel, S.E. and Nelson, T. (2008) 'Multitemporal remote sensing of landscape dynamics and pattern change: describing natural and anthropogenic trends', *Progress in Physical Geography*, 32(5), pp. 503-528.

Giuliani, G., Chatenoux, B., De Bono, A., Rodila, D., Richard, J.-P., Allenbach, K., Dao, H. and Peduzzi, P. (2017) 'Building an Earth Observations Data Cube: lessons learned from the Swiss Data Cube (SDC) on generating Analysis Ready Data (ARD)', *Big Earth Data*, 1(1-2), pp. 100-117.

Gomez, C., White, J.C. and Wulder, M.A. (2016) 'Optical remotely sensed time series data for land cover classification: A review', *ISPRS Journal of Photogrammetry and Remote Sensing*, 116, pp. 55-72.

Goncalves, J.A. and Henriques, R. (2015) 'UAV photogrammetry for topographic monitoring of coastal areas', *ISPRS Journal of Photogrammetry and Remote Sensing*, 104, pp. 101-111.

Gonzalez-Mirelis, G., Bergstrom, P. and Lindegarth, M. (2011) 'Interaction between classification detail and prediction of community types: implications for predictive modelling of benthic biotopes', *Marine Ecology Progress Series*, 432, pp. 31-44.

Goodman, J.A., Purkis, S.J. and Phinn, S.R. (2013) *Coral Reef Remote Sensing: A Guide for Mapping, Monitoring and Management*. Dordrecht: Springer.

Graham, N.A.J. and Nash, K.L. (2013) 'The importance of structural complexity in coral reef ecosystems', *Coral Reefs*, 32(2), pp. 315-326.

Gratwicke, B. and Speight, M.R. (2005) 'The relationship between fish species richness, abundance and habitat complexity in a range of shallow tropical marine habitats', *Journal of Fish Biology*, 66(3), pp. 650-667.

Gregorutti, B., Michel, B. and Saint-Pierre, P. (2017) 'Correlation and variable importance in random forests', *Statistics and Computing*, 27(3), pp. 659-678.

Guichard, F., Bourget, E. and Agnard, J.P. (2000) 'High-resolution remote sensing of intertidal ecosystems: A low-cost technique to link scale-dependent patterns and processes', *Limnology and Oceanography*, 45(2), pp. 328-338.

Guillaumont, B., Callens, L. and Dion, P. (1993) 'Spatial distribution and quantification of Fucus species and Ascophyllum nodosum beds in intertidal zones using SPOT imagery', *Hydrobiologia*, 260(261), pp. 297-305.

Guyon, I. and Elisseeff, A. (2003) 'An Introduction to Variable and Feature Selection', *Journal of Machine Learning Research*, 3, pp. 1157-1182.

Hall, O., Hay, G.J., Bouchard, A. and Marceau, D.J. (2004) 'Detecting dominant landscape objects through multiple scales: An integration of object-specific methods and watershed segmentation', *Landscape Ecology*, 19(1), pp. 59-76.

Halpern, B.S., Frazier, M., Potapenko, J., Casey, K.S., Koenig, K., Longo, C., Lowndes, J.S., Rockwood, R.C., Selig, E.R., Selkoe, K.A. and Walbridge, S. (2015) 'Spatial and temporal changes in cumulative human impacts on the world's ocean', *Nature Communications*, 6, pp. 1-7.

Halpern, B.S., Lester, S.E. and McLeod, K.L. (2010) 'Placing marine protected areas onto the ecosystem-based management seascape', *Proceedings of the National Academy of Sciences of the United States of America*, 107(43), pp. 18312-18317.

Halpern, B.S., Walbridge, S., Selkoe, K.A., Kappel, C.V., Micheli, F., D'Agrosa, C., Bruno, J.F., Casey, K.S., Ebert, C., Fox, H.E., Fujita, R., Heinemann, D., Lenihan, H.S., Madin, E.M.P., Perry, M.T., Selig, E.R., Spalding, M., Steneck, R. and Watson, R. (2008) 'A global map of human impact on marine ecosystems', *Science*, 319(5865), pp. 948-952.

Hamilton, L.J. and Parnum, I. (2011) 'Acoustic seabed segmentation from direct statistical clustering of entire multibeam sonar backscatter curves', *Continental Shelf Research*, 31, pp. 138-148.

Han, H., Lee, S., Im, J., Kim, M., Lee, M.I., Ahn, M.H. and Chung, S.R. (2015) 'Detection of Convective Initiation Using Meteorological Imager Onboard Communication, Ocean, and Meteorological Satellite Based on Machine Learning Approaches', *Remote Sensing*, 7(7), pp. 9184-9204.

Haralick, R.M. (1979) 'Statistical and Structural Approaches to Texture', *Proceedings of the IEEE*, 67(5), pp. 786-804.

Haralick, R.M., Shanmugam, K. and Dinstein, I. (1973) 'Textural features for image classification', *IEEE Transactions Systems, Man and Cybernetics*, 3, pp. 610-621.

Harris, P.T., Macmillan-Lawler, M., Rupp, J. and Baker, E.K. (2014) 'Geomorphology of the oceans', *Marine Geology*, 352, pp. 4-24.

Harris, P.T. and Whiteway, T. (2009) 'High seas marine protected areas: Benthic environmental conservation priorities from a GIS analysis of global ocean biophysical data', *Ocean & Coastal Management*, 52(1), pp. 22-38.

Hartnoll, R.G. and Hawkins, S.J. (1980) 'Monitoring Rocky-Shore Communities - a Critical-Look at Spatial and Temporal Variation', *Helgolander Meeresuntersuchungen*, 33(1-4), pp. 484-494.

Harwin, S. and Lucieer, A. (2012) 'Assessing the Accuracy of Georeferenced Point Clouds Produced via Multi-View Stereopsis from Unmanned Aerial Vehicle (UAV) Imagery', *Remote Sensing*, 4(6), pp. 1573-1599.

Hasan, R.C., Ierodiaconou, D. and Laurenson, L. (2012a) 'Combining angular response classification and backscatter imagery segmentation for benthic biological habitat mapping', *Estuarine Coastal and Shelf Science*, 97, pp. 1-9.

Hasan, R.C., Ierodiaconou, D., Laurenson, L. and Schimel, A. (2014) 'Integrating Multibeam Backscatter Angular Response, Mosaic and Bathymetry Data for Benthic Habitat Mapping', *PLOS ONE*, 9(5), pp. 1-14.

Hasan, R.C., Ierodiaconou, D. and Monk, J. (2012b) 'Evaluation of Four Supervised Learning Methods for Benthic Habitat Mapping Using Backscatter from Multi-Beam Sonar', *Remote Sensing*, 4, pp. 3427-3443.

Hawkins, S.J., Evans, A.J., Moore, J., Whittington, M., Pack, K., Firth, L.B., Adams, L.C., Moore, P.J., Masterson-Algar, P., Mieszkowska, N. and Southward, E.C. (2017) 'From the Torrey Canyon to today: A 50-year retrospective of recovery from the oil spill and interaction with climate-driven fluctuations on Cornish rocky shores.', *International Oil Spill Conference*. Long Beach, California.

Hawkins, S.J., Moore, P.J., Burrows, M.T., Poloczanska, E., Mieszkowska, N., Herbert, R.J.H., Jenkins, S.R., Thompson, R.C., Genner, M.J. and Southward, A.J. (2008) 'Complex interactions in a rapidly changing world: responses of rocky shore communities to recent climate change', *Climate Research*, 37(2-3), pp. 123-133.

Hawkins, S.J., Sugden, H.E., Mieszkowska, N., Moore, P.J., Poloczanska, E., Leaper, R., Herbert, R.J.H., Genner, M.J., Moschella, P.S., Thompson, R.C., Jenkins, S.R., Southward, A.J.

and Burrows, M.T. (2009) 'Consequences of climate-driven biodiversity changes for ecosystem functioning of North European rocky shores', *Marine Ecology Progress Series*, 396, pp. 245-259.

Hay, G.J. and Castilla, G. (2006) 'Geographic Object-Based Image Analysis (GEOBIA): A new name for a new discipline', in Blaschke, T., Lang, S. and Hay, G.J. (eds.) *Object-based Image Analysis: spatial concepts for knowledge-driven remote sensing applications*. Berlin and Heidelberg: Springer Verlag.

Hay, G.J., Castilla, G., Wulder, M.A. and Ruiz, J.R. (2005) 'An automated object-based approach for the multiscale image segmentation of forest scenes', *International Journal of Applied Earth Observation and Geoinformation*, 7(4), pp. 339-359.

Hay, G.J., Marceau, D.J., Dube, P. and Bouchard, A. (2001) 'A multiscale framework for landscape analysis: Object-specific analysis and upscaling', *Landscape Ecology*, 16(6), pp. 471-490.

He, H., Ferrari, R., McKinnon, D., Roff, G.A., Smith, R., Mumby, P.J. and Upcroft, B. (2012) 'Measuring reef complexity and rugosity from monocular video bathymetric reconstruction', *12th International Coral Reef Symposium*. Cairns, Australia, 9-13 July 2012.

Heap, A.D., Harris, P.T. (2011) 'Geological and biological mapping and characterisation of benthic marine environments—Introduction to the special issue', *Continental Shelf Research*, 31(2), pp. 1-3.

Hedley, J.D., Roelfsema, C.M., Chollett, I., Harborne, A.R., Heron, S.F., Weeks, S.J., Skirving, W.J., Strong, A.E., Eakin, C.M., Christensen, T.R.L., Ticzon, V., Bejarano, S. and Mumby, P.J. (2016) 'Remote Sensing of Coral Reefs for Monitoring and Management: A Review', *Remote Sensing*, 8(2), pp. 1-40.

Held, A., Phinn, S., Soto-Berelov, M. and Jones, S. (2015) *AusCover Good Practice Guidelines: A technical handbook supporting calibration and validation activities of remotely sensed data products. Version 1.1.* Queensland, Australia: Terrestrial Ecosystem Research Network, University of Queensland.

Hennig, B.D., Cogan, C.B. and Bartsch, I. (2007) 'Hyperspectral remote sensing and analysis of intertidal zones: A contribution to monitor coastal biodiversity', *First Geoinformatics Forum*. Salzburg. Wichman Verlag, Heidelberg.

Henriques, V., Mendes, B., Pinheiro, L.M., Gonçalves, D. and Long, D. (2013) *Recommended Operating Guidelines (ROG) for sidescan sonars*. MESHAtlantic Working Group. [Online]. Available at: http://www.emodnet-seabedhabitats.eu/Default.aspx?page=1915.

Henson, S.A., Beaulieu, C., Ilyina, T., John, J.G., Long, M., Seferian, R., Tjiputra, J. and Sarmiento, J.L. (2017) 'Rapid emergence of climate change in environmental drivers of marine ecosystems', *Nature Communications*, 8.

Heumann, B.W. (2011) 'An Object-Based Classification of Mangroves Using a Hybrid Decision Tree-Support Vector Machine Approach', *Remote Sensing*, 3(11), pp. 2440-2460.

Hill, J. and Wilkinson, C. (2004) *Methods for ecological monitoring of coral reefs: a resource for managers*. Townsville MC, Australia: Australian Institute of Marine Science.

Hill, N.A., Lucieer, A., Barrett, N.S., Anderson, T.J. and Williams, S.B. (2014) 'Filling the gaps: Predicting the distribution of temperate reef biota using high resolution biological and acoustic data', *Estuarine Coastal and Shelf Science*, 147, pp. 137-147.

Hladik, C. and Alber, M. (2012) 'Accuracy assessment and correction of a LiDAR-derived salt marsh digital elevation model', *Remote Sensing of Environment*, 121(Supplement C), pp. 224-235.

Hodgson, M.E. and Bresnahan, P. (2004) 'Accuracy of airborne LiDAR-derived elevation: Empirical assessment and error budget', *Photogrammetric Engineering and Remote Sensing*, 70(3), pp. 331-339.

Holmes, K.W., Van Niel, K.P., Radford, B., Kendrick, G.A. and Grove, S.L. (2008) 'Modelling distribution of marine benthos from hydroacoustics and underwater video', *Continental Shelf Research*, 28(14), pp. 1800-1810.

Hopkins, A. (2007) *Recommended operating guidelines (ROG) for swath bathymetry*. Mapping European Seabed Habitats (MESH),. [Online]. Available at: http://www.emodnet-seabedhabitats.eu/Default.aspx?page=1915.

Howson, C.M. (2000) *Flamborough Head cSAC Intertidal Survey*. York: English Nature.

Hsieh, Y.T., Chen, C.T. and Chen, J.C. (2017) 'Applying object-based image analysis and knowledge-based classification to ADS-40 digital aerial photographs to facilitate complex forest land cover classification', *Journal of Applied Remote Sensing*, 11, pp. 1-16.

Huang, Z., Brooke, B.P. and Harris, P.T. (2011) 'A new approach to mapping marine benthic habitats using physical environmental data', *Continental Shelf Research*, 31(2), pp. S4-S16.

Hugenholtz, C.H., Whitehead, K., Brown, O.W., Barchyn, T.E., Moorman, B.J., LeClair, A., Riddell, K. and Hamilton, T. (2013) 'Geomorphological mapping with a small unmanned aircraft system (sUAS): Feature detection and accuracy assessment of a photogrametically-derived digital terrain model', *Geomorphology*, 194, pp. 16-24.

Hughes Clarke, J.E. (2015) 'Multispectral Acoustic Backscatter from Multibeam, Improved Classification Potential', *United States Hydrographic Conference*. Maryland, USA.

Hunter, E.L. and Power, C.H. (2002) 'An assessment of two classification methods for mapping Thames Estuary intertidal habitats using CASI data', *International Journal of Remote Sensing*, 23(15), pp. 2989-3008.

Hunter, W.R. and Sayer, M.D.J. (2009) 'The comparative effects of habitat complexity on faunal assemblages of northern temperate artificial and natural reefs', *ICES Journal of Marine Science*, 66(4), pp. 691-698.

Hussain, M., Chen, D.M., Cheng, A., Wei, H. and Stanley, D. (2013) 'Change detection from remotely sensed images: From pixel-based to object-based approaches', *ISPRS Journal of Photogrammetry and Remote Sensing*, 80, pp. 91-106.

Husson, E., Ecke, F. and Reese, H. (2016) 'Comparison of Manual Mapping and Automated Object-Based Image Analysis of Non-Submerged Aquatic Vegetation from Very-High-Resolution UAS Images', *Remote Sensing*, 8(9).

Ierodiaconou, D., Burq, S., Reston, M. and Laurenson, L. (2007) 'Marine benthic habitat mapping using multibeam data, georeferenced video and image classification techniques in Victoria, Australia', *Journal of Spatial Science*, 52(1), pp. 93-104.

Ierodiaconou, D., Monk, J., Rattray, A., Laurenson, L. and Versace, V.L. (2011) 'Comparison of automated classification techniques for predicting benthic biological communities using hydroacoustics and video observations', *Continental Shelf Research*, 31(2), pp. S28-S38.

Ierodiaconou, D., Schimel, A.C.G. and Kennedy, D.M. (2016) 'A new perspective of storm bite on sandy beaches using Unmanned Aerial Vehicles', *Zeitschrift Fur Geomorphologie*, 60, pp. 123-137.

Im, J., Jensen, J.R. and Tullis, J.A. (2008) 'Object-based change detection using correlation image analysis and image segmentation', *International Journal of Remote Sensing*, 29(2), pp. 399-423.

Irving, A.D. and Connell, S.D. (2006) 'Predicting understorey structure from the presence and composition of canopies: an assembly rule for marine algae', *Oecologia*, 148(3), pp. 491-502.

Islam, M.S. and Tanaka, M. (2004) 'Impacts of pollution on coastal and marine ecosystems including coastal and marine fisheries and approach for management: a review and synthesis', *Marine Pollution Bulletin*, 48(7-8), pp. 624-649.

Javernick, L., Brasington, J. and Caruso, B. (2014) 'Modeling the topography of shallow braided rivers using Structure-from-Motion photogrammetry', *Geomorphology*, 213, pp. 166-182.

Jecock, M., Dunn, C., Carter, A. and Clowes, M. (2003) *The Alum Works and other industries at Kettleness, North Yorkshire: an archaeological and historical survey* (Report Number AI/24/2003). English Heritage. [Online]. Available at: http://research.historicengland.org.uk/.

Jenness, J.S. (2004) 'Calculating landscape surface area from digital elevation models', *Wildlife Society Bulletin*, 32(3), pp. 829-839.

Jhonnerie, R., Siregar, V.P., Nababan, B., Prasetyo, L.B. and Wouthuyzen, S. (2015) 'Random forest classification for mangrove land cover mapping using Landsat 5 TM and ALOS PALSAR imageries', *1st International Symposium on Lapan-Ipb Satellite (Lisat) for Food Security and Environmental Monitoring*, 24, pp. 215-221.

JNCC (2004) *Common Standards Monitoring Guidance for Littoral Rock and Inshore Sublittoral Rock Habitats*. Peterborough: JNCC.

JNCC (2013) *The UK Approach to Asssessing Conservation Status for the 2013 EU Habitats Directive Article 17 Reporting*. Peterborough: JNCC.

JNCC and Natural England (2010) *MCZ Project Ecological Network Guidance*. Peterborough: JNCC.

JNCC and Natural England (2012) *JNCC and Natural England's advice to Defra on recommended Marine Conservation Zones*. Peterborough: JNCC and Natural England.

Johnson, M.P., Burrows, M.T., Hartnoll, R.G. and Hawkins, S.J. (1997) 'Spatial structure on moderately exposed rocky shores: patch scales and the interactions between limpets and algae', *Marine Ecology Progress Series*, 160, pp. 209-215.

Johnson, M.P., Frost, N.J., Mosley, M.W., Roberts, M.F. and Hawkins, S.J. (2003) 'The area-independent effects of habitat complexity on biodiversity vary between regions', *Ecology Letters*, 6, pp. 126-132.

Jones, G., Bunting, P. and Hurford, C. (2017) 'Mapping Coastal Habitats in Wales', in Diaz-Delgado, R., Lucas, R. and Hurford, C. (eds.) *The Roles of Remote Sensing in Nature Conservation: A Practical Guide and Case Studies*. Switzerland: Springer.

Jordan, A., Lawler, M., Halley, V. and Barrett, N. (2005) 'Seabed habitat mapping in the Kent Group of islands and its role in marine protected area planning', *Aquatic Conservation-Marine and Freshwater Ecosystems*, 15(1), pp. 51-70.

Juel, A., Groom, G.B., Svenning, J.C. and Ejrnaes, R. (2015) 'Spatial application of Random Forest models for fine-scale coastal vegetation classification using object based analysis of aerial orthophoto and DEM data', *International Journal of Applied Earth Observation and Geoinformation*, 42, pp. 106-114.

Kenny, A.J., Cato, I., Desprez, M., Fader, G., Schuttenhelm, R.T.E. and Side, J. (2003) 'An overview of seabed-mapping technologies in the context of marine habitat classification', *ICES Journal of Marine Science*, 60(2), pp. 411-418.

Kerr, J.T. and Ostrovsky, M. (2003) 'From space to species: ecological applications for remote sensing', *Trends in Ecology & Evolution*, 18(6), pp. 299-305.

Kilcoyne, A.M., Alexander, R., Cox, P. and Brownett, J. (2017) *Living Maps: Satellite-based Habitat Classification. Evidence Project SD1705*. London: Natural England.

Kilpatrick, K.A., Podesta, G., Walsh, S., Williams, E., Halliwell, V., Szczodrak, M., Brown, O.B., Minnett, P.J. and Evans, R. (2015) 'A decade of sea surface temperature from MODIS', *Remote Sensing of Environment*, 165, pp. 27-41.

Klemas, V. (2011) 'Beach Profiling and LIDAR Bathymetry: An Overview with Case Studies', *Journal of Coastal Research*, 27(6), pp. 1019-1028.

Klemas, V.V. (2015) 'Coastal and Environmental Remote Sensing from Unmanned Aerial Vehicles: An Overview', *Journal of Coastal Research*, 31(5), pp. 1260-1267.

Kloser, R.J., Penrose, J.D. and Butler, A.J. (2010) 'Multi-beam backscatter measurements used to infer seabed habitats', *Continental Shelf Research*, 30, pp. 1772-1782.

Kohler, K.E. and Gill, S.M. (2006) 'Coral Point Count with Excel extensions (CPCe): A Visual Basic program for the determination of coral and substrate coverage using random point count methodology', *Computers & Geosciences*, 32(9), pp. 1259-1269.

Konar, B. and Iken, K. (2017) 'The use of unmanned aerial vehicle imagery in intertidal monitoring', *Deep-Sea Research Part II (Online http://www.sciencedirect.com/science/article/pii/S0967064516301333)*.

Kostylev, V.E., Erlandson, J., Ming, M.Y. and Williams, G.A. (2005) 'The relative importance of habitat complexity and surface area in assessing biodiversity: fractal application on rocky shores', *Ecological Complexity*, 2, pp. 272-286.

Kotta, J., Remm, K., Vahtmae, E., Kutser, T. and Orav-Kotta, H. (2014) 'In-air spectral signatures of the Baltic Sea macrophytes and their statistical separability', *Journal of Applied Remote Sensing*, 8.

Kovalenko, K.E., Thomaz, S.M. and Warfe, D.M. (2012) 'Habitat complexity: approaches and future directions', *Hydrobiologia*, 685(1), pp. 1-17.

Kuenzer, C., Bluemel, A., Gebhardt, S., Quoc, T.V. and Dech, S. (2011) 'Remote Sensing of Mangrove Ecosystems: A Review', *Remote Sensing*, 3(5), pp. 878-928.

Kung, O., Strecha, C., Beyeler, A., Zufferey, J.C., Floreano, D., Fua, P. and Gervaix, F. (2011) 'The Accuracy of Automatic Photogrammetric Techniques on Ultra-Light UAV Imagery', *International Conference on Unmanned Aerial Vehicle in Geomatics (UAV-G)*, 38-1(C22), pp. 125-130.

Lacharite, M., Metaxas, A. and Lawton, P. (2015) 'Using object-based image analysis to determine seafloor fine-scale features and complexity', *Limnology and Oceanography-Methods*, 13(10), pp. 553-567.

Laliberte, A.S., Browning, D.M. and Rango, A. (2010) 'Feature Selection Methods for Object-Based Classification of Sub-Decimeter Resolution Digital Aerial Imagery', *Geobia 2010: Geographic Object-Based Image Analysis*. Ghent, Belgium, 29 June to 2 July 2010.

Laliberte, A.S., Browning, D.M. and Rango, A. (2012) 'A comparison of three feature selection methods for object-based classification of sub-decimeter resolution UltraCam-L imagery', *International Journal of Applied Earth Observation and Geoinformation*, 15, pp. 70-78.

Laliberte, A.S. and Rango, A. (2009) 'Texture and Scale in Object-Based Analysis of Subdecimeter Resolution Unmanned Aerial Vehicle (UAV) Imagery', *IEEE Transactions on Geoscience and Remote Sensing*, 47(3), pp. 761-770.

Lamarche, G. and Lurton, X. (2017) 'Recommendations for improved and coherent acquisition and processing of backscatter data from seafloor-mapping sonars', *Marine Geophysical Research (Online https://link.springer.com/journal/11001/onlineFirst/page/1)*.

Lamarche, G., Lurton, X., Verdier, A.L. and Augustin, J.M. (2011) 'Quantitative characterisation of seafloor substrate and bedforms using advanced processing of multibeam backscatter-Application to Cook Strait, New Zealand', *Continental Shelf Research*, 31(2), pp. 93-109.

Lambert, G.I., Jennings, S., Hinz, H., Murray, L.G., Lae, P., Kaiser, M.J. and Hiddink, J.G. (2012) 'A comparison of two techniques for the rapid assessment of marine habitat complexity', *Methods in Ecology and Evolution*, 4(3), pp. 226-235.

Lambin, E.F. (1996) 'Change detection at multiple temporal scales: Seasonal and annual variations in landscape variables', *Photogrammetric Engineering and Remote Sensing*, 62(8), pp. 931-938.

Lang, S., Albrecht, F., Kienberger, S. and Tiede, D. (2010) 'Object validity for operational tasks in a policy context', *Journal of Spatial Science*, 55(1), pp. 9-22.

Larsen, P.F., Barker, S., Wright, J. and Erickson, C.B. (2004) 'Use of cost effective remote sensing to map and measure marine intertidal habitats in support of ecosystem modeling efforts: Cobscook Bay, Maine', *Northeastern Naturalist*, 11, pp. 225-242.

Lathrop, R.G., Montesano, P. and Haag, S. (2006) 'A multi-scale segmentation approach to mapping seagrass habitats using airborne digital camera imagery', *Photogrammetric Engineering and Remote Sensing*, 72(6), pp. 665-675.

Lavy, A., Eyal, G., Neal, B., Keren, R., Loya, Y. and Ilan, M. (2015) 'A quick, easy and non-intrusive method for underwater volume and surface area evaluation of benthic organisms by 3D computer modelling', *Methods in Ecology and Evolution*, 6(5), pp. 521-531.

Lawrence, E., Hayes, K.R., Lucieer, V.L., Nichol, S.L., Dambacher, J.M., Hill, N.A., Barrett, N., Kool, J. and Siwabessy, J. (2015) 'Mapping Habitats and Developing Baselines in Offshore Marine Reserves with Little Prior Knowledge: A Critical Evaluation of a New Approach', *PLOS ONE*, 10(10).

Le Bas, T.P. and Huvenne, V.A.I. (2009) 'Acquisition and processing of backscatter data for habitat mapping - Comparison of multibeam and sidescan systems', *Applied Acoustics*, 70(10), pp. 1248-1257.

Lecours, V. (2017) 'On the Use of Maps and Models in Conservation and Resource Management (Warning: Results May Vary)', *Frontiers in Marine Science*, 4(288).

Lecours, V., Devillers, R., Edinger, E.N., Brown, C.J. and Lucieer, V.L. (2017) 'Influence of artefacts in marine digital terrain models on habitat maps and species distribution models: a multiscale assessment', *Remote Sensing in Ecology and Conservation*, 3(4), pp. 232-246.

Lecours, V., Devillers, R., Schneider, D.C., Lucieer, V.L., Brown, C.J. and Edinger, E.N. (2015) 'Spatial scale and geographic context in benthic habitat mapping: review and future directions', *Marine Ecology Progress Series*, 535, pp. 259-284.

Leon, J. and Woodroffe, C.D. (2011) 'Improving the synoptic mapping of coral reef geomorphology using object-based image analysis', *International Journal of Geographical Information Science*, 25(6), pp. 949-969.

Leon, J.X., Roelfsema, C.M., Saunders, M.I. and Phinn, S.R. (2015) 'Measuring coral reef terrain roughness using 'Structure-from-Motion' close-range photogrammetry', *Geomorphology*, 242, pp. 21-28.

Levin, N., Coll, M., Fraschetti, S., Gal, G., Giakoumi, S., Goke, C., Heymans, J.J., Katsanevakis, S., Mazor, T., Ozturk, B., Rilov, G., Gajewski, J., Steenbeek, J. and Kark, S. (2014) 'Biodiversity data requirements for systematic conservation planning in the Mediterranean Sea', *Marine Ecology Progress Series*, 508, pp. 261-281.

Li, M.C., Ma, L., Blaschke, T., Cheng, L. and Tiede, D. (2016) 'A systematic comparison of different object-based classification techniques using high spatial resolution imagery in agricultural environments', *International Journal of Applied Earth Observation and Geoinformation*, 49, pp. 87-98.

Lillesand, T., Kiefer, R.W. and Chipman, J. (2015) *Remote Sensing and Image Interpretation (7th Edition)*. USA: Wiley.

Lillis, H., Strong, J., Diesing, M. and Green, S. (2016) *Standardising the production of habitat maps in the UK. Seabed Mapping Working Group workshop November 2015. JNCC Report No. 596.* Peterborough: JNCC.

Limpenny, D.S., Foster-Smith, R.L., Edwards, T.M., Hendrick, V.J., Diesing, M., Eggleton, J.D., Meadows, W.J., Crutchfield, Z., Pfeifer, S. and Reach, I.S. (2010) *Best methods for identifying and evaluating Sabellaria spinulosa and cobble reef*. [Online]. Available at: www.alsf-mepf.org.uk (Accessed: September 2017).

Lindenbaum, C., Bennell, J.D., Rees, E.L.S., Mcclean, D., Cook, W., Wheeler, A.J. and Sanderson, W.G. (2008) 'Small-scale variation within a Modiolus modiolus (Mollusca : Bivalvia) reef in the Irish Sea: I. Seabed mapping and reef morphology', *Journal of the Marine Biological Association of the United Kingdom*, 88(1), pp. 133-141.

Liu, C.R., Frazier, P. and Kumar, L. (2007) 'Comparative assessment of the measures of thematic classification accuracy', *Remote Sensing of Environment*, 107(4), pp. 606-616.

Loisel, H., Mangin, A., Vantrepotte, V., Dessailly, D., Dinh, D.N., Garnesson, P., Ouillon, S., Lefebvre, J.P., Meriaux, X. and Phan, T.M. (2014) 'Variability of suspended particulate matter concentration in coastal waters under the Mekong's influence from ocean color (MERIS) remote sensing over the last decade', *Remote Sensing of Environment*, 150, pp. 218-230.

Lu, D., Mausel, P., Brondizio, E. and Moran, E. (2004) 'Change detection techniques', *International Journal of Remote Sensing*, 25(12), pp. 2365-2407.

Lucas, R., Blonda, P., Bunting, P., Jones, G., Inglada, J., Arias, M., Kosmidou, V., Petrou, Z.I., Manakos, I., Adamo, M., Charnock, R., Tarantino, C., Mucher, C.A., Jongman, R.H.G., Kramer, H., Arvor, D., Honrado, J.P. and Mairota, P. (2015) 'The Earth Observation Data for Habitat Monitoring (EODHaM) system', *International Journal of Applied Earth Observation and Geoinformation*, 37, pp. 17-28.

Lucas, R., Díaz-Delgado, R. and Hurford, C. (2017) 'Expected Advances in a Rapidly Developing Work Area', in Díaz-Delgado, R., Lucas, R. and Hurford, C. (eds.) *The Roles of Remote Sensing in Nature Conservation: A Practical Guide and Case Studies*. Switzerland: Springer International Publishing, pp. 309-318.

Lucas, R., Medcalf, K., Brown, A., Bunting, P., Breyer, J., Clewley, D., Keyworth, S. and Blackmore, P. (2011) 'Updating the Phase 1 habitat map of Wales, UK, using satellite sensor data', *ISPRS Journal of Photogrammetry and Remote Sensing*, 66(1), pp. 81-102.

Lucas, R., Rowlands, A., Brown, A., Keyworth, S. and Bunting, P. (2007) 'Rule-based classification of multi-temporal satellite imagery for habitat and agricultural land cover mapping', *ISPRS Journal of Photogrammetry and Remote Sensing*, 62(3), pp. 165-185.

Lucieer, A., Turner, D., King, D.H. and Robinson, S.A. (2014) 'Using an Unmanned Aerial Vehicle (UAV) to capture micro-topography of Antarctic moss beds', *International Journal of Applied Earth Observation and Geoinformation*, 27, pp. 53-62.

Lucieer, V. (2007) 'Morphometric characterisation of rocky reef using multibeam acoustic bathymetric data', *IGARSS: 2007 IEEE International Geoscience and Remote Sensing Symposium, Vols 1-12*, pp. 905-909.

Lucieer, V., Hill, N., Barrett, N. and Nichol, S. (2011) 'Spatial analysis of multi-beam acoustic data for the prediction of marine substrates and benthic communities in temperate coastal waters', *34th International Symposium on Remote Sensing of Environment*. Sydney, Australia.

Lucieer, V., Hill, N.A., Barrett, N.S. and Nichol, S. (2013) 'Do marine substrates 'look' and 'sound' the same? Supervised classification of multibeam acoustic data using autonomous underwater vehicle images', *Estuarine Coastal and Shelf Science*, 117, pp. 94-106.

Lucieer, V. and Lamarche, G. (2011) 'Unsupervised fuzzy classification and object-based image analysis of multibeam data to map deep water substrates, Cook Strait, New Zealand', *Continental Shelf Research*, 31(11), pp. 1236-1247.

Lucieer, V. and Pederson, H. (2008) 'Linking morphometric characterisation of rocky reef with fine scale lobster movement', *ISPRS Journal of Photogrammetry and Remote Sensing*, 63(5), pp. 496-509.

Lucieer, V.L. (2008) 'Object-oriented classification of sidescan sonar data for mapping benthic marine habitats', *International Journal of Remote Sensing*, 29(3), pp. 905-921.

Lucieer, V.L. and Forrest, A.L. (2016) 'Emerging Mapping Techniques for Autonomous Underwater Vehicles (AUVs)', in Finkl, C.W. and Makowski, C. (eds.) *Seafloor Mapping along Continental Shelves: Research and Techniques for Visualizing Benthic Environments*. Cham: Springer International Publishing, pp. 53-67.

Luckhurst, B.E. and Luckhurst, K. (1978) 'Analysis of Influence of Substrate Variables on Coral-Reef Fish Communities', *Marine Biology*, 49(4), pp. 317-323.

Lyons, M.B., Phinn, S.R. and Roelfsema, C.M. (2012) 'Long term land cover and seagrass mapping using Landsat and object-based image analysis from 1972 to 2010 in the coastal environment of South East Queensland, Australia', *ISPRS Journal of Photogrammetry and Remote Sensing*, 71, pp. 34-46.

Lyons, M.B., Roelfsema, C.M. and Phinn, S.R. (2013) 'Towards understanding temporal and spatial dynamics of seagrass landscapes using time-series remote sensing', *Estuarine Coastal and Shelf Science*, 120, pp. 42-53.

Ma, L., Cheng, L., Li, M.C., Liu, Y.X. and Ma, X.X. (2015) 'Training set size, scale, and features in Geographic Object-Based Image Analysis of very high resolution unmanned aerial vehicle imagery', *ISPRS Journal of Photogrammetry and Remote Sensing*, 102, pp. 14-27.

Ma, L., Fu, T.Y., Blaschke, T., Li, M.C., Tiede, D., Zhou, Z.J., Ma, X.X. and Chen, D.L. (2017) 'Evaluation of Feature Selection Methods for Object-Based Land Cover Mapping of Unmanned Aerial Vehicle Imagery Using Random Forest and Support Vector Machine Classifiers', *ISPRS International Journal of Geo-Information*, 6(2).

Mackenzie, B.R. and Schiedek, D. (2007) 'Daily ocean monitoring since the 1860s shows record warming of northern European seas', *Global Change Biology*, 13(7), pp. 1335-1347.

MacKenzie, R.A. and Cormier, N. (2012) 'Stand structure influences nekton community composition and provides protection from natural disturbance in Micronesian mangroves', *Hydrobiologia*, 685(1), pp. 155-171.

Mairota, P., Cafarelli, B., Didham, R.K., Lovergine, F.P., Lucas, R.M., Nagendra, H., Rocchini, D. and Tarantino, C. (2015) 'Challenges and opportunities in harnessing satellite remote-sensing for biodiversity monitoring', *Ecological Informatics*, 30, pp. 207-214.

Malthus, T.J. and Mumby, P.J. (2003) 'Remote sensing of the coastal zone: an overview and priorities for future research', *International Journal of Remote Sensing*, 24(13), pp. 2805-2815.

Manandhar, R., Odeh, I.O.A. and Pontius, R.G. (2010) 'Analysis of twenty years of categorical land transitions in the Lower Hunter of New South Wales, Australia', *Agriculture Ecosystems & Environment*, 135(4), pp. 336-346.

Mancini, F., Dubbini, M., Gattelli, M., Stecchi, F., Fabbri, S. and Gabbianelli, G. (2013) 'Using Unmanned Aerial Vehicles (UAV) for High-Resolution Reconstruction of Topography: The Structure from Motion Approach on Coastal Environments', *Remote Sensing*, 5(12), pp. 6880-6898.

Manson, F.J., Loneragan, N.R. and Phinn, S.R. (2003) 'Spatial and temporal variation in distribution of mangroves in Moreton Bay, subtropical Australia: a comparison of pattern metrics and change detection analyses based on aerial photographs', *Estuarine Coastal and Shelf Science*, 57(4), pp. 653-666.

Marsh, I. and Brown, C. (2009) 'Neural network classification of multibeam backscatter and bathymetry data from Stanton Bank (Area IV)', *Applied Acoustics*, 70, pp. 1269-1276.

Mas, J.F. (1999) 'Monitoring land-cover changes: a comparison of change detection techniques', *International Journal of Remote Sensing*, 20(1), pp. 139-152.

Masselink, G., Scott, T., Poate, T., Russell, P., Davidson, M. and Conley, D. (2016) 'The extreme 2013/2014 winter storms: hydrodynamic forcing and coastal response along the southwest coast of England', *Earth Surface Processes and Landforms*, 41(3), pp. 378-391.

Matias, M.G., Underwood, A.J., Hochuli, D.F. and Coleman, R.A. (2010) 'Independent effects of patch size and structural complexity on diversity of benthic macroinvertebrates', *Ecology*, 91(7), pp. 1908-1915.

Mayer, L.A. (2006) 'Frontiers in seafloor mapping and visualization', *Marine Geophysical Researches*, 27, pp. 7-17.

McArthur, M.A., Brooke, B.P., Przeslawski, R., Ryan, D.A., Lucieer, V.L., Nichol, S., McCallum, A.W., Mellin, C., Cresswell, I.D. and Radke, L.C. (2010) 'On the use of abiotic surrogates to describe marine benthic biodiversity', *Estuarine Coastal and Shelf Science*, 88(1), pp. 21-32.

McBreen, F., Askew, N., Cameron, A., Connor, D., Ellwood H., & Carter, A. (2011) *UK SeaMap 2010 Predictive mapping of seabed habitats in UK waters*. Peterborough: JNCC.

McCormick, M.I. (1994) 'Comparison of Field Methods for Measuring Surface-Topography and Their Associations with a Tropical Reef Fish Assemblage', *Marine Ecology Progress Series*, 112(1-2), pp. 87-96.

McDermid, G.J., Linke, J., Pape, A.D., Laskin, D.N., McLane, A.J. and Franklin, S.E. (2008) 'Object-based approaches to change analysis and thematic map update: challenges and limitations', *Canadian Journal of Remote Sensing*, 34(5), pp. 462-466.

McGonigle, C., Brown, C., Quinn, R. and Grabowski, J. (2009) 'Evaluation of image-based multibeam sonar backscatter classification for benthic habitat discrimination and mapping at Stanton Banks, UK', *Estuarine Coastal and Shelf Science*, 81(3), pp. 423-437.

McGonigle, C., Brown, C.J. and Quinn, R. (2010) 'Operational Parameters, Data Density and Benthic Ecology: Considerations for Image-Based Classification of Multibeam Backscatter', *Marine Geodesy*, 33(1), pp. 16-38.

McGonigle, C., Grabowski, J.H., Brown, C.J., Weber, T.C. and Quinn, R. (2011) 'Detection of deep water benthic macroalgae using image-based classification techniques on multibeam backscatter at Cashes Ledge, Gulf of Maine, USA', *Estuarine Coastal and Shelf Science*, 91(1), pp. 87-101.

McIntyre, K., McLaren, K. and Prospere, K. (2018) 'Mapping shallow nearshore benthic features in a Caribbean marine-protected area: assessing the efficacy of using different data types (hydroacoustic versus satellite images) and classification techniques', *International Journal of Remote Sensing*, 39(4), pp. 1117-1150.

Meager, J.J., Schlacher, T.A. and Green, M. (2011) 'Topographic complexity and landscape temperature patterns create a dynamic habitat structure on a rocky intertidal shore', *Marine Ecology Progress Series*, 428, pp. 1-12.

Medcalf, K., Parker, J., Bell, G., Robinson, P., Neal, S., Horlock, M. and Breyer, J. (2017) 'Integrated Monitoring for Biodiversity Using Remote Sensing: From Local to Regional - A Case Study from Norfolk', in Diaz-Delgado, R., Lucas, R. and Hurford, C. (eds.) *The Roles of Remote Sensing in Nature Conservation: A Practical Guide and Case Studies*. Switzerland: Springer International Publishing AG.

Medcalf, K., Parker, J., Breyer, J. and Turton, N. (2015) *MEOW Phase 3: Cost effective methods to measure extent and condition of habitats. A report produced by Environment Systems Ltd for Defra and the JNCC*. Peterborough: JNCC.

Medcalf, K., Parker, J.A., Turton, N. and Bell, G. (2014a) *Making Earth Observation Work for UK Biodiversity Conservation Phase 1*. Peterborough: JNCC.

Medcalf, K., Parker, J.A., Turton, N. and Bell, G. (2014b) *Making Earth Observation Work for UK Biodiversity Conservation Phase 2*. Peterborough: JNCC.

Medeiros, P.R., Rosa, R.S. and Francini, R.B. (2011) 'Dynamics of fish assemblages on a continuous rocky reef and adjacent unconsolidated habitats at Fernando de Noronha Archipelago, tropical western Atlantic', *Neotropical Ichthyology*, 9(4), pp. 869-879.

Melaas, E.K., Friedl, M.A. and Zhu, Z. (2013) 'Detecting interannual variation in deciduous broadleaf forest phenology using Landsat TM/ETM plus data', *Remote Sensing of Environment*, 132, pp. 176-185.

Menard, A., Turgeon, K., Roche, D.G., Binning, S.A. and Kramer, D.L. (2012) 'Shelters and Their Use by Fishes on Fringing Coral Reefs', *PLOS ONE*, 7(6).

Menderes, A., Erener, A. and Sarp, G. (2015) 'Automatic Detection of Damaged Buildings after Earthquake Hazard by Using Remote Sensing and Information Technologies', *World Multidisciplinary Earth Sciences Symposium, WMESS 2015*. Prague, Czech Republic, 7 - 11 September 2015.

MESH (2010) *The MESH Confidence Assessment Scheme*. Available at: http://www.emodnet-seabedhabitats.eu/default.aspx?page=1693 (Accessed: 20/12/2017).

Micheletti, N., Chandler, J.H. and Lane, S.N. (2015) 'Structure from Motion (SfM) Photogrammetry', in Cook, S., Clarke, L. and Nield, J. (eds.) *Geomorphological Techniques (online edition)*. London, UK: British Society for Geomorphology.

Mielck, F., Bartsch, I., Hass, H.C., Wolfl, A.C., Burk, D. and Betzler, C. (2014) 'Predicting spatial kelp abundance in shallow coastal waters using the acoustic ground discrimination system RoxAnn', *Estuarine Coastal and Shelf Science*, 143, pp. 1-11.

Mieszkowska, N., Sugden, H., Firth, L. and Hawkins, S.J. (2014) 'The role of sustained observations in tracking impacts of environmental change on marine biodiversity and ecosystems', *Philosophical Transactions of the Royal Society A*, 372.

Mieszkowska, N. and Sugden, H.E. (2016) 'Chapter Seven - Climate-Driven Range Shifts Within Benthic Habitats Across a Marine Biogeographic Transition Zone', in Dumbrell, A.J., Kordas, R.L. and Woodward, G. (eds.) *Advances in Ecological Research*. Academic Press, pp. 325-369.

Millard, K. and Richardson, M. (2015) 'On the Importance of Training Data Sample Selection in Random Forest Image Classification: A Case Study in Peatland Ecosystem Mapping', *Remote Sensing*, 7(7), pp. 8489-8515.

Millenium Ecosystem Assessment (2005) *Ecosystems and human well-being: synthesis*. Washington DC: Island Press.

Miller, I.E. (2002) *Steeped in History - The Alum Industry of North-East Yorkshire*. Helmsley: North York Moors National Park Authority.

Mitchell, P. and McIlwaine, P. (2015) *Inner Bank rMCZ Post-survey Site Report. Marine Protected Areas Data and Evidence Co-ordination Programme Report No. 48*. London: Defra.

Mlambo, R., Woodhouse, I., Gerard, F. and Anderson, K. (2017) 'Structure from Motion (SfM) Photogrammetry with Drone Data: A Low Cost Method for Monitoring Greenhouse Gas Emissions from Forests in Developing Countries', *Forests*, 8(68), p. 20.

MMO (2014a) *East Inshore and East Offshore Marine Plans*. London: Defra.

MMO (2014b) *East Inshore and East Offshore Marine Plans. Annex 1: Supporting information on the production of maps*. London: Defra.

Moller, M., Lymburner, L. and Volk, M. (2007) 'The comparison index: A tool for assessing the accuracy of image segmentation', *International Journal of Applied Earth Observation and Geoinformation*, 9(3), pp. 311-321.

Molnar, J.L., Gamboa, R.L., Revenga, C. and Spalding, M.D. (2008) 'Assessing the global threat of invasive species to marine biodiversity', *Frontiers in Ecology and the Environment*, 6(9), pp. 485-492.

Moore, J.J., van Rein, H. and Bunker, F. (2014) *Methodological trials: Recording subtidal epibiota in-situ and in photographs, Portrush, August 2013*. Cosheston, Pembrokeshire: A report to JNCC from Aquatic Survey & Monitoring Ltd.

Mountrakis, G., Im, J. and Ogole, C. (2011) 'Support vector machines in remote sensing: A review', *ISPRS Journal of Photogrammetry and Remote Sensing*, 66(3), pp. 247-259.

Mucher, C.A., Roupioz, L., Kramer, H., Bogers, M.M.B., Jongman, R.H.G., Lucas, R.M., Kosmidou, V.E., Petrou, Z., Manakos, I., Padoa-Schioppa, E., Adamo, M. and Blonda, P. (2015) 'Synergy of airborne LiDAR and Worldview-2 satellite imagery for land cover and habitat mapping: A BIO_SOS-EODHaM case study for the Netherlands', *International Journal of Applied Earth Observation and Geoinformation*, 37, pp. 48-55.

Mucher, S., Roupioz, L., Kramer, H., Wolters, M., Bogers, M., Lucas, R., Bunting, P., Petrou, Z., Kosmidou, V., Manakos, I., Padoa-Schioppa, E., Ficetola, G.F., Bonardi, A., Adamo, M. and Blonda, P. (2013) 'LiDAR as a Valuable Information Source for Habitat Mapping', *GI Forum 2013: Creating the GI society*, pp. 520-523.

Mumby, P.J. and Edwards, A.J. (2003) 'Mapping marine environments with IKONOS imagery: enhanced spatial resolution can deliver greater thematic accuracy', *Remote Sensing of Environment*, 84(2), pp. 320-320.

Murfitt, S.L., Allan, B.M., Bellgrove, A., Rattray, A., Young, M.A. and Ierodiaconou, D. (2017) 'Applications of unmanned aerial vehicles in intertidal reef monitoring ', *Nature (Online https://www.nature.com/articles/s41598-017-10818-9)*.

Murray, S.N., Ambrose, R.F. and Dethier, M.N. (2001) *Methods for performing monitoring, impact and ecological studies on rocky shores. MMS OCS Study 2001-070*. Santa Barbara, California: Coastal Research Center, Marine Science Institute, University of California.

Musk, W.A., Smith, T. and Thomson, S. (2010) *Biotope Mapping of the Intertidal Reef Features of Flamborough Head Special Area of Conservation* (ZBB739-2010). Hull: Institute of Estuarine and Coastal Studies (IECS).

Na, X.D., Zang, S.Y., Wu, C.S. and Li, W.L. (2015) 'Mapping forested wetlands in the Great Zhan River Basin through integrating optical, radar, and topographical data classification techniques', *Environmental Monitoring and Assessment*, 187(11).

Nagendra, H., Lucas, R., Honrado, J.P., Jongman, R.H.G., Tarantino, C., Adamo, M. and Mairota, P. (2013) 'Remote sensing for conservation monitoring: Assessing protected areas, habitat extent, habitat condition, species diversity, and threats', *Ecological Indicators*, 33, pp. 45-59.

Net Gain (2011) *Net Gain Final Recommendations Submission to Natural England and JNCC v.1.2*. Hull: Net Gain Project Team.

Newman, S.P., Meesters, E.H., Dryden, C.S., Williams, S.M., Sanchez, C., Mumby, P.J. and Polunin, N.V.C. (2015) 'Reef flattening effects on total richness and species responses in the Caribbean', *Journal of Animal Ecology*, 84(6), pp. 1678-1689.

O'Brien, L., Renzi, E., Dudley, J.M., Clancy, C. and Dias, F. (2018) 'Catalogue of extreme wave events in Ireland: revised and updated for 14 680 BP to 2017', *Natural Hazards and Earth System Sciences*, 18(3), pp. 729-758.

Olofsson, P., Foody, G.M., Herold, M., Stehman, S.V., Woodcock, C.E. and Wulder, M.A. (2014) 'Good practices for estimating area and assessing accuracy of land change', *Remote Sensing of Environment*, 148, pp. 42-57.

Onojeghuo, A.O. and Onojeghuo, A.R. (2017) 'Object-based habitat mapping using very high spatial resolution multispectral and hyperspectral imagery with LiDAR data', *International Journal of Applied Earth Observation and Geoinformation*, 59, pp. 79-91.

Oppelt, N., Schulze, F., Bartsch, I., Doernhoefer, K. and Eisenhardt, I. (2012) 'Hyperspectral classification approaches for intertidal macroalgae habitat mapping: a case study in Heligoland', *Optical Engineering*, 51(11).

OSPAR (1992) *Convention for the Protection of the Marine Environment of the North-East Atlantic*. Paris: Oslo and Paris Commissions.

Ouedraogo, M.M., Degre, A., Debouche, C. and Lisein, J. (2014) 'The evaluation of unmanned aerial system-based photogrammetry and terrestrial laser scanning to generate DEMs of agricultural watersheds', *Geomorphology*, 214, pp. 339-355.

Ouyang, Z.T., Zhang, M.Q., Xie, X., Shen, Q., Guo, H.Q. and Zhao, B. (2011) 'A comparison of pixel-based and object-oriented approaches to VHR imagery for mapping saltmarsh plants', *Ecological Informatics*, 6(2), pp. 136-146.

Paleczny, M., Hammill, E., Pauly, D. and Pauly, D. (2015) 'Population Trend of the World's Monitored Seabirds, 1950-2010', *Plos One*, 10(6).

Parrish, C.E., Dijkstra, J.A., O'Neil-Dunne, J.P.M., McKenna, L. and Pe'eri, S. (2016) 'Post-Sandy Benthic Habitat Mapping Using New Topobathymetric Lidar Technology and Object-Based Image Classification', *Journal of Coastal Research*, Special Issue 76, pp. 200-208.

Parry, M.E.V. (2014) *JNCC Marine Habitat Classification for Britain and Ireland: Overview of User Issues*. Peterborough: JNCC.

Paull, C.K., Caress, D.W., Lundsten, E., Gwiazda, R., Anderson, K., McGann, M., Conrad, J., Edwards, B. and Sumner, E.J. (2013) 'Anatomy of the La Jolla Submarine Canyon system; offshore southern California', *Marine Geology*, 335, pp. 16-34.

Perez-Alberti, A. and Trenhaile, A.S. (2014) 'An initial evaluation of drone-based monitoring of boulder beaches in Galicia, north-western Spain', *Earth Surface Processes and Landforms*, 40(1), pp. 105-111.

Peterson, D.L., Brass, J.A., Smith, W.H., Langford, G., Wegener, S., Dunagan, S., Hammer, P. and Snook, K. (2003) 'Platform options of free-flying satellites, UAVs or the International Space Station for remote sensing assessment of the littoral zone', *International Journal of Remote Sensing*, 24(13), pp. 2785-2804.

Pettorelli, N. (2014) 'A new platform to support research at the interface of remote sensing, ecology and conservation', *Remote Sensing in Ecology and Conservation*, 1(1), pp. 1-3.

Pettorelli, N., Laurance, W.F., O'Brien, T.G., Wegmann, M., Nagendra, H. and Turner, W. (2014) 'Satellite remote sensing for applied ecologists: opportunities and challenges', *Journal of Applied Ecology*, 51(4), pp. 839-848.

Phinn, S.R., Hochberg, E.M. and Roelfsema, C.M. (2013) 'Visible and Infrared: An Overview', in Goodman, J.A., Purkis, S.J. and Phinn, S.R. (eds.) *Coral Reef Remote Sensing*. Dordrecht: Springer, pp. 3-28.

Phinn, S.R., Roelfsema, C.M. & Mumby, P.J. (2012) 'Multi-scale, object-based image analysis for mapping geomorphic and ecological zones on coral reefs', *International Journal of Remote Sensing*, 33(12), pp. 3768-3797.

Pittman, S.J. and Brown, K.A. (2011) 'Multi-Scale Approach for Predicting Fish Species Distributions across Coral Reef Seascapes', *PLOS ONE*, 6(5).

Pittman, S.J., Costa, B.M. and Battista, T.A. (2009) 'Using Lidar Bathymetry and Boosted Regression Trees to Predict the Diversity and Abundance of Fish and Corals', *Journal of Coastal Research*, 25(6), pp. 27-38.

Pontius, R.G. and Millones, M. (2011) 'Death to Kappa: birth of quantity disagreement and allocation disagreement for accuracy assessment', *International Journal of Remote Sensing*, 32(15), pp. 4407-4429.

Populus, J. and Perrot, T. (2007) *Recommended operating guidelines (ROG) for single-beam echosounder surveying*. Mapping European Seabed Habitats (MESH). [Online]. Available at: http://www.emodnet-seabedhabitats.eu/Default.aspx?page=1915.

Portman, M.E. (2016) 'Marine Spatial Planning', in Portman, M.E. (ed.) *Environmental Planning for Oceans and Coasts: Methods, Tools and Technologies*. Switzerland: Springer International Publishing, pp. 97-115.

Prenzel, B.G. and Treitz, P. (2006) 'Spectral and spatial filtering for enhanced thematic change analysis of remotely sensed data', *International Journal of Remote Sensing*, 27(5-6), pp. 835-854.

Preston, J. (2009) 'Automated acoustic seabed classification of multibeam images of Stanton Banks', *Applied Acoustics*, 70(10), pp. 1277-1287.

Prigent, C., Aires, F., Bernardo, F., Orlhac, J.C., Goutoule, J.M., Roquet, H. and Donlon, C. (2013) 'Analysis of the potential and limitations of microwave radiometry for the retrieval of sea surface temperature: Definition of MICROWAT, a new mission concept', *Journal of Geophysical Research-Oceans*, 118(6), pp. 3074-3086.

Purkis, S.J. (2018) 'Remote Sensing Tropical Coral Reefs: The View from Above', *Annual Review of Marine Science*, 10(1).

Rapinel, S., Hubert-Moy, L. and Clement, B. (2015) 'Combined use of LiDAR data and multispectral earth observation imagery for wetland habitat mapping', *International Journal of Applied Earth Observation and Geoinformation*, 37, pp. 56-64.

Rattray, A., Ierodiaconou, D., Burq, S. and Reston, M. (2009) 'Hydroacoustic remote sensing of benthic biological communities on the shallow South East Australian continental shelf', *Estuarine Coastal and Shelf Science*, 84, pp. 237-245.

Rattray, A., Ierodiaconou, D., Monk, J., Laurenson, L.J.B. and Kennedy, P. (2014) 'Quantification of Spatial and Thematic Uncertainty in the Application of Underwater Video for Benthic Habitat Mapping', *Marine Geodesy*, 37(3), pp. 315-336.

Rattray, A., Ierodiaconou, D., Monk, J., Versace, V.L. and Laurenson, L.J.B. (2013) 'Detecting patterns of change in benthic habitats by acoustic remote sensing', *Marine Ecology Progress Series*, 477, pp. 1-13.

Rees, M.J., Jordan, A., Price, O.F., Coleman, M.A. and Davis, A.R. (2014) 'Abiotic surrogates for temperate rocky reef biodiversity: implications for marine protected areas', *Diversity and Distributions*, 20, pp. 284-296.

Reid, P.C., Colebrook, J.M., Matthews, J.B.L., Aiken, J. and Team, C.P.R. (2003) 'The Continuous Plankton Recorder: concepts and history, from plankton indicator to undulating recorders', *Progress in Oceanography*, 58(2-4), pp. 117-173.

Reiss, H., Birchenough, S., Borja, A., Buhl-Mortensen, L., Craeymeersch, J., Dannheim, J., Darr, A., Galparsoro, I., Gogina, M., Neumann, H., Populus, J., Rengstorf, A.M., Valle, M., van Hoey, G., Zettler, M.L. and Degraer, S. (2015) 'Benthos distribution modelling and its relevance for marine ecosystem management', *ICES Journal of Marine Science*, 72(2), pp. 297-315.

Reiss, H., Cunze, S., Konig, K., Neumann, H. and Kroncke, I. (2011) 'Species distribution modelling of marine benthos: a North Sea case study', *Marine Ecology Progress Series*, 442, pp. 71-86.

Remondino, F., Del Pizzo, S., Kersten, T.P. and Troisi, S. (2012) 'Low-cost and open-source solutions for automated image orientation - a critical overview', *Lecture Notes in Computer Science*, 7616, pp. 40-54.

Richmond, S., Stevens, T. (2014) 'Classifying benthic biotopes on sub-tropical continental shelf reefs: How useful are abiotic surrogates?', *Estuarine Coastal and Shelf Science*, 138, pp. 79-89.

RICS (2010) *Vertical aerial photography and digital imagery. 5th edition, guidance note GN61/2010*. Coventry, UK: Royal Institution of Chartered Surveyors.

Rinne, H., Kaskela A., Anna-Leena Downie, A-L., Tolvanend, H., von Numersa, M., Mattila, J. (2014) 'Predicting the occurrence of rocky reefs in a heterogeneous archipelago area with limited data', *Estuarine Coastal and Shelf Science*, 138, pp. 90-100.

Rippin, D.M., Pomfret, A. and King, N. (2015) 'High resolution mapping of supra-glacial drainage pathways reveals link between micro-channel drainage density, surface roughness and surface reflectance', *Earth Surface Processes and Landforms*, 40(10), pp. 1279-1290.

Risk, M.J. (1972) 'Fish diversity on a coral reef in the Virgin Islands', *Atoll Reserve Bulletin*, 193, pp. 1-6.

Robertson, L.D. and King, D.J. (2011) 'Comparison of pixel- and object-based classification in land cover change mapping', *International Journal of Remote Sensing*, 32(6), pp. 1505-1529.

Robinson, K.A., Ramsay, K., Lindenbaum, C., Frost, N., Moore, J., Wright, A.P. and Petrey, D. (2011) 'Predicting the distribution of seabed biotopes in the southern Irish Sea', *Continental Shelf Research*, 31(2), pp. S120-S131.

Rodwell, L.D., Fletcher, S., Glegg, G.A., Campbell, M., Rees, S.E., Ashley, M., Linley, E.A., Frost, M., Earll, B., Wynn, R.B., Mee, L., Almada-Villela, P., Lear, D., Stanger, P., Colenutt, A., Davenport, F., Bradshaw, N.J.B. and Covey, R. (2014) 'Marine and coastal policy in the UK: Challenges and opportunities in a new era', *Marine Policy*, 45, pp. 251-258.

Roelfsema, C., Kovacs, E.M., Saunders, M.I., Phinn, S., Lyons, M. and Maxwell, P. (2013a) 'Challenges of remote sensing for quantifying changes in large complex seagrass environments', *Estuarine Coastal and Shelf Science*, 133, pp. 161-171.

Roelfsema, C., Phinn, S., Jupiter, S., Comley, J. and Albert, S. (2013b) 'Mapping coral reefs at reef to reef-system scales, 10s-1000s km(2), using object-based image analysis', *International Journal of Remote Sensing*, 34(18), pp. 6367-6388.

Rush, S. and Solandt, J.L. (2017) 'Challenges on providing conservation advice for a growing network of English Marine Protected Areas', *Marine Policy*, 83, pp. 75-82.

Schlacher, T.A., Schlacher-Hoenlinger, M.A., Williams, A., Althaus, F., Hooper, J.N.A. and Kloser, R. (2007) 'Richness and distribution of sponge megabenthos in continental margin canyons off southeastern Australia', *Marine Ecology Progress Series*, 340, pp. 73-88.

Schneider, A. (2012) 'Monitoring land cover change in urban and peri-urban areas using dense time stacks of Landsat satellite data and a data mining approach', *Remote Sensing of Environment*, 124, pp. 689-704.

Scopelitis, J., Andrefouet, S., Phinn, S., Arroyo, L., Dalleau, M., Cros, A. and Chabanet, P. (2010) 'The next step in shallow coral reef monitoring: Combining remote sensing and in situ approaches', *Marine Pollution Bulletin*, 60(11), pp. 1956-1968.

Serpetti, N., Heath, M., Armstrong, E. and Witte, U. (2011) 'Blending single beam RoxAnn and multi-beam swathe QTC hydro-acoustic discrimination techniques for the Stonehaven area, Scotland, UK', *Journal of Sea Research*, 65(4), pp. 442-455.

Serra, P., Pons, X. and Sauri, D. (2003) 'Post-classification change detection with data from different sensors: some accuracy considerations', *International Journal of Remote Sensing*, 24(16), pp. 3311-3340.

Sexton, J.O., Urban, D.L., Donohue, M.J. and Song, C.H. (2013) 'Long-term land cover dynamics by multi-temporal classification across the Landsat-5 record', *Remote Sensing of Environment*, 128, pp. 246-258.

Shang, X. and Chisholm, L.A. (2014) 'Classification of Australian Native Forest Species Using Hyperspectral Remote Sensing and Machine-Learning Classification Algorithms', *Ieee Journal of Selected Topics in Applied Earth Observations and Remote Sensing*, 7(6), pp. 2481-2489.

Sheehan, E.V., Cousens, S.L., Nancollas, S.J., Stauss, C., Royle, J. and Attrill, M.J. (2013) 'Drawing lines at the sand: evidence for functional vs. visual reef boundaries in temperate Marine Protected Areas', *Mar Pollut Bull*, 76(1-2), pp. 194-202.

Sheehan, E.V., Stevens, T.F. and Attrill, M.J. (2010) 'A quantitative, non-destructive methodology for habitat characterisation and benthic monitoring at offshore renewable energy developments', *PLOS ONE*, 5(12).

Shumchenia, E.J. and King, J.W. (2010) 'Comparison of methods for integrating biological and physical data for marine habitat mapping and classification', *Continental Shelf Research*, 30, pp. 1717-1729.

Siddiqui, M.D. and Zaidi, A.Z. (2015) 'Worldview-2 and Landsat 8 Satellite Data for Seaweed Mapping along Karachi Coast', *Pakistan Journal of Engineering, Technology and Science*, 5(2), pp. 134-151.

Simons, D.G. and Snellen, M. (2009) 'A Bayesian approach to seafloor classification using multi-beam echo-sounder backscatter data', *Applied Acoustics*, 70(10), pp. 1258-1268.

Singh, A. (1989) 'Digital Change Detection Techniques Using Remotely-Sensed Data', *International Journal of Remote Sensing*, 10(6), pp. 989-1003.

Smale, D.A., Burrows, M.T., Moore, P., O'Connor, N. and Hawkins, S.J. (2013) 'Threats and knowledge gaps for ecosystem services provided by kelp forests: a northeast Atlantic perspective', *Ecology and Evolution*, 3(11), pp. 4016-4038.

Smith, C.M. and Alberte, R.S. (1994) 'Characterization of in-Vivo Absorption Features of Chlorophyte, Phaeophyte and Rhodophyte Algal Species', *Marine Biology*, 118(3), pp. 511-521.

Snavely, N., Seitz, S.M. and Szeliski, R. (2008) 'Modeling the world from Internet photo collections', *International Journal of Computer Vision*, 80(2), pp. 189-210.

Son, N.T., Chen, C.F., Chang, N.B., Chen, C.R., Chang, L.Y. and Thanh, B.X. (2015) 'Mangrove Mapping and Change Detection in Ca Mau Peninsula, Vietnam, Using Landsat Data and Object-Based Image Analysis', *IEEE Journal of Selected Topics in Applied Earth Observations and Remote Sensing*, 8(2), pp. 503-510.

Sotheran, I. and Crawford-Avis, O. (2014) *Mapping habitats and biotopes from acoustic datasets to strengthen the information base of Marine Protected Areas in Scottish waters* (Report Number 503). Peterborough: JNCC. [Online]. Available at: http://jncc.defra.gov.uk/pdf/503_web.pdf.

St Pierre, J.I. and Kovalenko, K.E. (2014) 'Effect of habitat complexity attributes on species richness', *Ecosphere*, 5(2).

Stephens, D. and Diesing, M. (2014) 'A Comparison of Supervised Classification Methods for the Prediction of Substrate Type Using Multibeam Acoustic and Legacy Grain-Size Data', *PLOS ONE*, 9(4).

Stevens, T. and Connolly, R.M. (2005) 'Local-scale mapping of benthic habitats to assess representation in a marine protected area', *Marine and Freshwater Research*, 56(1), pp. 111-123.

Stopa, J.E. and Mouche, A. (2017) 'Significant wave heights from Sentinel-1 SAR: Validation and applications', *Journal of Geophysical Research-Oceans*, 122(3), pp. 1827-1848.

Stow, D., Hamada, Y., Coulter, L. and Anguelova, Z. (2008) 'Monitoring shrubland habitat changes through object-based change identification with airborne multispectral imagery', *Remote Sensing of Environment*, 112(3), pp. 1051-1061.

Strasser, T. and Lang, S. (2015) 'Object-based class modelling for multi-scale riparian forest habitat mapping', *International Journal of Applied Earth Observation and Geoinformation*, 37, pp. 29-37.

Strong, J.A. (2015) *Habitat area as an indicator of Good Environmental Status under the Marine Strategy Framework Directive: the identification of suitable habitat mapping methods with recommendations on best-practice for the reduction of uncertainty. Defra Project Code: ME5318*. London: DEFRA DEFRA.

Strong, J.A. and Elliott, M. (2017) 'The value of remote sensing techniques in supporting effective extrapolation across multiple marine spatial scales', *Marine Pollution Bulletin*, 116(1-2), pp. 405-419.

Tang, J., Salem, A. and Huan, L. (2014) 'Feature Selection for Classification: A review', in Aggarwal, C.C. (ed.) *Data Classification: Algorithms and Applications*. Florida, USA: CRC Press.

Tehrany, M.S., Pradhan, B. and Jebuv, M.N. (2014) 'A comparative assessment between object and pixel-based classification approaches for land-use/land-cover mapping using SPOT 5 imagery', *Geocarto International*, 29(4), pp. 351-369.

Tewkesbury, A.P., Comber, A.J., Tate, N.J., Lamb, A. and Fisher, P.F. (2015) 'A critical synthesis of remotely sensed optical image change detection techniques', *Remote Sensing of Environment*, 160, pp. 1-14.

Thompson, R.C., Crowe, T.P. and Hawkins, S.J. (2002) 'Rocky intertidal communities: past environmental changes, present status and predictions for the next 25 years', *Environmental Conservation*, 29(2), pp. 168-191.

Thomson, A.G., Fuller, R.M., Yates, M.G., Brown, S.L., Cox, R. and Wadsworth, R.A. (2003) 'The use of airborne remote sensing for extensive mapping of intertidal sediments and saltmarshes in eastern England', *International Journal of Remote Sensing*, 24(13), pp. 2717-2737.

Thonfeld, F., Hecheltjen, A. and Menz, G. (2015) 'Bi-temporal Change Detection, Change Trajectories and Time Series Analysis for Forest Monitoring', *Photogrammetrie Fernerkundung Geoinformation*, (2), pp. 129-141.

Thorner, J., Kumar, L. and Smith, S.D.A. (2013) 'Fine-Scale Three-Dimensional Habitat Mapping as a Biodiversity Conservation Tool for Intertidal Rocky Reefs', *Journal of Coastal Research*, 29(5), pp. 1184-1190.

Tiede, D., Lang, S., Albrecht, F. and Holbling, D. (2010) 'Object-based Class Modeling for Cadastre-constrained Delineation of Geo-objects', *Photogrammetric Engineering and Remote Sensing*, 76(2), pp. 193-202.

Tillin, H.M., Luff, A., Davison, J.J., Perrett, J., Huvenne, V., Bett, B.J. and Van Rein, H. (2018) *Autonomous Underwater Vehicles for use in marine benthic monitoring*. Peterborough: JNCC.

Tillin, H.M.R., S.I. Frida, C.L.J., Aapala, K. (2008) 'Approaches to classifying benthic habitat quality', *Marine Policy*, 32, pp. 455–464.

Trebilco, R., Dulvy, N.K., Stewart, H. and Salomon, A.K. (2015) 'The role of habitat complexity in shaping the size structure of a temperate reef fish community', *Marine Ecology Progress Series*, 532, pp. 197-211.

Trimble (2014) *eCognition Developer 9.0 User Guide*. Munchen, Germany: Trimble.

Turner, W., Rondinini, C., Pettorelli, N., Mora, B., Leidner, A.K., Szantoi, Z., Buchanan, G., Dech, S., Dwyer, J., Herold, M., Koh, L.P., Leimgruber, P., Taubenboeck, H., Wegmann, M., Wikelski, M. and Woodcock, C. (2015) 'Free and open-access satellite data are key to biodiversity conservation', *Biological Conservation*, 182, pp. 173-176.

Turner, W., Spector, S., Gardiner, N., Fladeland, M., Sterling, E. and Steininger, M. (2003) 'Remote sensing for biodiversity science and conservation', *Trends in Ecology & Evolution*, 18(6), pp. 306-314.

Underwood, A.J. and Chapman, M.G. (1989) 'Experimental Analyses of the Influences of Topography of the Substratum on Movements and Density of an Intertidal Snail, Littorina unifasciata', *Journal of Experimental Marine Biology and Ecology*, 134(3), pp. 175-196.

United Nations (1982) *United Nations Convention on the Law of the Sea (UNCLOS)*. Jamaica: United Nations.

United Nations (1992) *United Nations Convention on Biological Diversity*. Rio de Janeiro, Brazil: United Nations Environment Programme (UNEP). [Online]. Available at: http://www.cbd.int/doc/legal/cbd-en.pdf.

Valentini, E., Taramelli, A., Filipponi, F. and Giulio, S. (2015) 'An effective procedure for EUNIS and Natura 2000 habitat type mapping in estuarine ecosystems integrating ecological knowledge and remote sensing analysis', *Ocean & Coastal Management*, 108, pp. 52-64.

Valle, M., Pala, V., Lafon, V., Dehouck, A., Garmendia, J.M., Borja, A. and Chust, G. (2015) 'Mapping estuarine habitats using airborne hyperspectral imagery, with special focus on seagrass meadows', *Estuarine Coastal and Shelf Science*, 164, pp. 433-442.

van Rein, H., Brown, C.J., Quinn, R., Breen, J. and Schoeman, D. (2011) 'An evaluation of acoustic seabed classification techniques for marine biotope monitoring over broad-scales (> 1 km(2)) and meso-scales (10 m(2)-1 km(2))', *Estuarine Coastal and Shelf Science*, 93(4), pp. 336-349.

van Rein, H.B., Brown, C.J., Quinn, R. and Breen, J. (2009) 'A review of sublittoral monitoring methods in temperate waters: a focus on scale', *International Journal of the Society for Underwater Technology*, 28(3), pp. 1-15.

Varela, R.A.D., Rego, P.R., Iglesias, S.C. and Sobrino, C.M. (2008) 'Automatic habitat classification methods based on satellite images: A practical assessment in the NW Iberia coastal mountains', *Environmental Monitoring and Assessment*, 144(1-3), pp. 229-250.

Vargas, M., Brown, C.W. and Sapiano, M.R.P. (2009) 'Phenology of marine phytoplankton from satellite ocean color measurements', *Geophysical Research Letters*, 36(1).

Vasquez, M., Mata Chacon, D., Tempera, F., O'Keeffe, E., Galparsoro, I., Sanz Alonso, J.L., Goncalves, J.M.S., Luis, B., Amorim, P., Henriques, V., McGrath, F., Monteiro, P., Mendes, B., Freitas, R., Martins, R. and Populus, J. (2014) 'Broad-scale mapping of seafloor habitats in the north-east Atlantic using existing environmental data', *Journal of Sea Research*, 100, pp. 120-132.

Vaz, A.S., Marcos, B., Goncalves, J., Monteiro, A., Alves, P., Civantos, E., Lucas, R., Mairota, P., Garcia-Robles, J., Alonso, J., Blonda, P., Lomba, A. and Honrado, J.P. (2015) 'Can we predict habitat quality from space? A multi-indicator assessment based on an automated knowledge-driven system', *International Journal of Applied Earth Observation and Geoinformation*, 37, pp. 106-113.

Verfaillie, E., Doornenbal, P., Mitchell, A., White, J. and Van Lancker, V. (2007) *The bathymetric position index (BPI) as a support tool for habitat mapping. Worked example for the MESH final guidance.* Mapping European Seabed Habitats (MESH). [Online]. Available at:

http://www.emodnet-seabedhabitats.eu/pdf/gmhm4_bathymetric_position_index_(bpi).pdf.

Visser, F., Buis, K., Verschoren, V. and Schoelynck, J. (2016) 'Mapping of submerged aquatic vegetation in rivers from very high-resolution image data, using object-based image analysis combined with expert knowledge', *Hydrobiologia*.

Visser, F., Wallis, C. and Sinnott, A.M. (2013) 'Optical remote sensing of submerged aquatic vegetation: Opportunities for shallow clearwater streams', *Limnologica*, 43(5), pp. 388-398.

Visser, H. and de Nijs, T. (2006) 'The Map Comparison Kit', *Environmental Modelling and Software*, 21, pp. 346-358.

Wahidin, N., Siregar, V.P., Nababan, B., Jaya, I. and Wouthuyzen, S. (2015) 'Object-based image analysis for coral reef benthic habitat mapping with several classification algorithms', *1st International Symposium on Lapan-Ipb Satellite (Lisat) for Food Security and Environmental Monitoring*, 24, pp. 222-227.

Wang, K., Franklin, S.E., Guo, X.L. and Cattet, M. (2010) 'Remote Sensing of Ecology, Biodiversity and Conservation: A Review from the Perspective of Remote Sensing Specialists', *Sensors*, 10(11), pp. 9647-9667.

Weise, C. (2014) *Documentation Feature Space Optimization*. Trimble. [Online]. Available at: http://community.ecognition.com/home/Feature%20Space%20Optimization.pdf (Accessed: July 2016).

Wells, E. (2007) *A Field Guide to the British Seaweeds: As required for assistance in the classification of water bodies under the Water Framework Directive* Bristol: Environment Agency.

Wells, E., Wilkinson, M., Wood, P. and Scanlan, C. (2007) 'The use of macroalgal species richness and composition on intertidal rocky seashores in the assessment of ecological quality under the European Water Framework Directive', *Marine Pollution Bulletin*, 55(1-6), pp. 151-161.

Westoby, M.J., Brasington, J., Glasser, N.F., Hambrey, M.J. and Reynolds, J.M. (2012) ''Structure-from-Motion' photogrammetry: A low-cost, effective tool for geoscience applications', *Geomorphology*, 179, pp. 300-314.

White, W.H., Harborne, A.R., Sotheran, I.S., Walton, R. and Foster-Smith, R.L. (2003) 'Using an Acoustic Ground Discrimination System to map coral reef benthic classes', *International Journal of Remote Sensing*, 24(13), pp. 2641-2660.

Wilcoxon, F. (1945) 'Individual Comparisons by Ranking Methods', *Biometrics Bulletin*, 1(6), pp. 80-83.

Wilding, T.A., Palmer, E.J.L. and Polunin, N.V.C. (2010) 'Comparison of three methods for quantifying topographic complexity on rocky shores', *Marine Environmental Research*, 69(3), pp. 143-151.

Williams, A., Dowdney, J., Smith, A.D.M., Hobday, A.J. and Fuller, M. (2011) 'Evaluating impacts of fishing on benthic habitats: A risk assessment framework applied to Australian fisheries', *Fisheries Research*, 112(3), pp. 154-167.

Willis, K.S. (2015) 'Remote sensing change detection for ecological monitoring in United States protected areas', *Biological Conservation*, 182, pp. 233-242.

Wilson, M.A., Costanza, R., Boumans, R. and Liu, S. (2005) 'Integrated assessment and valuation of ecosystem goods and services provided by coastal systems', in Wilson, J.G. (ed.) *The Intertidal Ecosystem: The Value of Ireland's Shores*. Dublin: Royal Irish Academy, pp. 1-24.

Wilson, M.F.J., O'Connell, B., Brown, C., Guinan, J.C. and Grehan, A.J. (2007a) 'Multiscale terrain analysis of multibeam bathymetry data for habitat mapping on the continental slope', *Marine Geodesy*, 30(1-2), pp. 3-35.

Wilson, S.K., Graham, N.A.J. and Polunin, N.V.C. (2007b) 'Appraisal of visual assessments of habitat complexity and benthic composition on coral reefs', *Marine Biology*, 151(3), pp. 1069-1076.

Woodget, A.S., Visser, F., Maddock, I.P. and Carbonneau, P.E. (2016) 'The Accuracy and Reliability of Traditional Surface Flow Type Mapping: Is it Time for a New Method of Characterizing Physical River Habitat?', *River Research and Applications*, 32(9), pp. 1902-1914.

Worm, B., Barbier, E.B., Beaumont, N., Duffy, J.E., Folke, C., Halpern, B.S., Jackson, J.B.C., Lotze, H.K., Micheli, F., Palumbi, S.R., Sala, E., Selkoe, K.A., Stachowicz, J.J. and Watso, R. (2006) 'Impacts of Biodiversity Loss on Ocean Ecosystem Services', *Science*, 314, pp. 787-790.

Wright, D. and Heyman, W. (2008) 'Introduction to the Special Issue: Marine and Coastal GIS for Geomorphology, Habitat Mapping, and Marine Reserves', *Marine Geodesy*, 31, pp. 223-230.

Wyn, G., Brazier, P., Birch, K., Bunker, A., Cooke, A., Jones, M., Lough, N., McMath, A. and Roberts, S. (2006) *Handbook for Marine Intertidal Phase 1 Biotope Mapping Survey*. Bangor: Countryside Council for Wales.

Wynn, R.B., Huvenne, V.A.I., Le Bas, T.P., Murton, B.J., Connelly, D.P., Bett, B.J., Ruhl, H.A., Morris, K.J., Peakall, J., Parsons, D.R., Sumner, E.J., Darby, S.E., Dorrell, R.M. and Hunt, J.E. (2014) 'Autonomous Underwater Vehicles (AUVs): Their past, present and future contributions to the advancement of marine geoscience', *Marine Geology*, 352, pp. 451-468.

Xu, J.P., Zhao, J.H., Li, F., Wang, L., Song, D.R., Wen, S.Y., Wang, F. and Gao, N. (2016) 'Object-based image analysis for mapping geomorphic zones of coral reefs in the Xisha Islands, China', *Acta Oceanologica Sinica*, 35(12), pp. 19-27.

Xu, L.L., Li, J. and Brenning, A. (2014) 'A comparative study of different classification techniques for marine oil spill identification using RADARSAT-1 imagery', *Remote Sensing of Environment*, 141, pp. 14-23.

Yesson, C., Bush, L.E., Davies, A.J., Maggs, C.A. and Brodie, J. (2015) 'Large brown seaweeds of the British Isles: Evidence of changes in abundance over four decades', *Estuarine Coastal and Shelf Science*, 155, pp. 167-175.

Yoerger, D.R., Jakuba, M., Bradley, A.M. and Bingham, B. (2007) 'Techniques for deep sea near bottom survey using an autonomous underwater vehicle', *International Journal of Robotics Research*, 26(1), pp. 41-54.

Young, N.E., Anderson, R.S., Chignell, S.M., Vorster, A.G., Lawrence, R. and Evangelista, P.H. (2017) 'A survival guide to Landsat preprocessing', *Ecology*, 98(4), pp. 920-932.

Zacharias, M., Niemann, O. and Borstad, G. (1992) 'An Assessment and Classification of a Multispectral Bandset for the Remote Sensing of Intertidal Seaweeds', *Canadian Journal of Remote Sensing*, 18(4), pp. 263-274.

Zacharias, M.A. and Gregr, E.J. (2005) 'Sensitivity and vulnerability in marine environments: an approach to identifying vulnerable marine areas', *Conservation Biology*, 19(1), pp. 86-97.

Zavalas, R., Ierodiaconou, D., Ryan, D., Rattray, A. and Monk, J. (2014) 'Habitat Classification of Temperate Marine Macroalgal Communities Using Bathymetric LiDAR', *Remote Sensing*, 6(3), pp. 2154-2175.

Zawada, D.G. and Brock, J.C. (2009) 'A Multiscale Analysis of Coral Reef Topographic Complexity Using Lidar-Derived Bathymetry', *Journal of Coastal Research*, 25(6), pp. 6-15.

Zawada, D.G., Piniak, G.A. and Hearn, C.J. (2010) 'Topographic complexity and roughness of a tropical benthic seascape', *Geophysical Research Letters*, 37.

Zhang, C.Y. (2015) 'Applying data fusion techniques for benthic habitat mapping and monitoring in a coral reef ecosystem', *ISPRS Journal of Photogrammetry and Remote Sensing*, 104, pp. 213-223.

Zhang, C.Y., Selch, D., Xie, Z.X., Roberts, C., Cooper, H. and Chen, G. (2013) 'Object-based benthic habitat mapping in the Florida Keys from hyperspectral imagery', *Estuarine Coastal and Shelf Science*, 134, pp. 88-97.

Zhang, Y., Maxwell, T., Tong, H. and Dey, V. (2010) 'Development of a Supervised Software Tool for Automated Determination of Optimal Segmentation Parameters for Ecognition', *100 Years ISPRS Advancing Remote Sensing Science, Pt 2*, 38, pp. 690-696.

Zhen, Z., Quackenbush, L.J., Stehman, S.V. and Zhang, L.J. (2013) 'Impact of training and validation sample selection on classification accuracy and accuracy assessment when using reference polygons in object-based classification', *International Journal of Remote Sensing*, 34(19), pp. 6914-6930.

Appendix 1: Publications, oral and poster presentations during PhD

Lightfoot, P., Polunin, N.V.C., Scott, C.L. and Fitzsimmons, C. Using a UAV to monitor temperate intertidal habitats: an assessment of photogrammetry and object-based image analysis. Department for Environment, Food and Rural Affairs Earth Observations Centre of Excellence, Nobel House, London, UK. October 2017. Oral presentation.

Lightfoot, P., Polunin, N.V.C., Scott, C.L. and Fitzsimmons, C. Using a UAV to monitor temperate intertidal habitats: an assessment of photogrammetry and object-based image analysis. UAS4Enviro2017: Small Unmanned Aerial Systems for Environmental Research, University of Trás-os-Montes e Alto Douro, Portugal. June 2017. Oral presentation.

Lightfoot, P., Polunin, N.V.C., Scott, C.L. and Fitzsimmons, C. Mapping and monitoring temperate intertidal habitats: an object-based approach. GeoHab 2017 Marine Geological and Biological Habitat Mapping, Nova Scotia, Canada. May 2017. Oral presentation.

Lightfoot, P., Stephenson, F. and Tinlin, A. Science in support of MPA management and monitoring. Webinar for Natural England and the Joint Nature Conservation Committee, Newcastle, UK. February 2017. Oral presentation.

Lightfoot, P., Polunin, N.V.C., Scott, C.L. and Fitzsimmons, C. Intertidal habitat mapping from remote sensing data: an object-based approach. Natural England workshop on marine evidence and monitoring, Nottingham, UK. January 2017. Oral presentation.

Lightfoot, P., Polunin, N.V.C., Scott, C.L. and Fitzsimmons, C. Mapping intertidal seaweed communities from remote sensing data: an object-based approach. British Phycological Society Conference, School of Ocean Sciences, Bangor University, Bangor, UK. January 2017. Oral presentation.

Lightfoot, P., Pickles, S., Polunin, N.V.C., Scott, C.L. and Fitzsimmons, C. Building skills in using unmanned aerial vehicles and object-based image analysis for ecological surveys. Chartered Institute of Ecology and Environmental Management Autumn Conference 'Skills for the Future', Nottingham, UK. November 2016. Oral presentation.

Lightfoot, P., Polunin, N.V.C., Scott, C.L. and Fitzsimmons, C. Unmanned aerial vehicles and object-based image analysis offer cost-effective, robust solutions for intertidal habitat survey. Newcastle University Business and Industrial Advisory Board meeting and poster competition 'Real World Research', Newcastle, UK. November 2016. Poster and oral presentation, awarded first prize.

Lightfoot, P., Skerritt, D.J., Stephenson, F., Tinlin, A., Polunin, N.V.C., Scott, C.L. and Fitzsimmons, C. Science in support of management. Northumberland Inshore Fisheries and Conservation Authority Stakeholders Forum, Morpeth, UK. March 2015. Oral presentation.

Fitzsimmons, C., Lightfoot, P. & Stephenson, F. (2015) Coquet to St Mary's rMCZ post-survey site report. Report for the Department for Environment, Food and Rural Affairs as part of the Marine Protected Areas Data and Evidence Co-ordination Programme 2013-14.

Fitzsimmons, C., Lightfoot, P. & Stephenson, F. (2015) Runswick Bay rMCZ post-survey site report. Report for the Department for Environment, Food and Rural Affairs as part of the Marine Protected Areas Data and Evidence Co-ordination Programme 2013-14.

Appendix 2: OBIA workflow for mapping temperate intertidal habitats

Knowledge-based OBIA workflow used in chapter 4 for classifying broadscale habitats at Level 1 and biotopes at Level 2.

Abbreviations:

DEM = Digital Elevation Model

NDVI = Normalised Difference Vegetation Index

RE = imagery collected using Canon Powershot ELPH 110 camera (red edge)

RGB = imagery collected using Canon IXUS 127 camera (red, green, blue)

AG = Approximate Gaussian (curve defining membership function)

Membership function values generated from samples are shown as lower, mid and upper values of the range separated by colons. Membership function values defined using predefined functions are shown as upper and lower values preceded by the type of function (Figure 6.2).

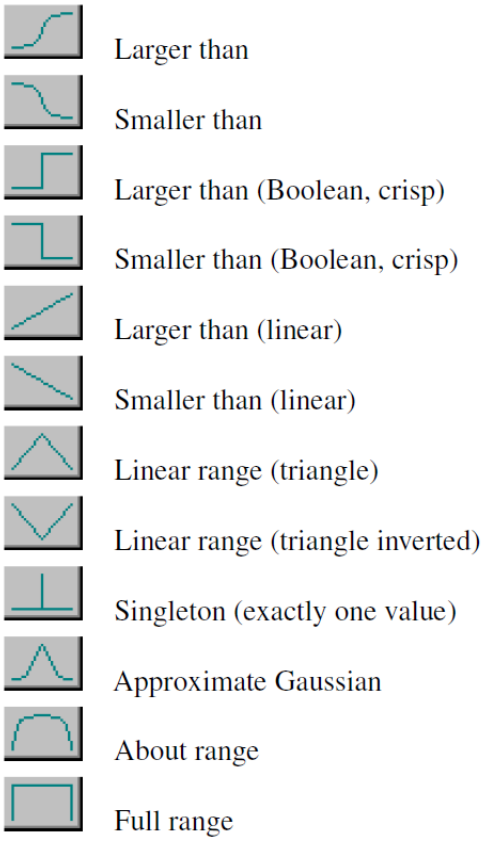

Figure 6.2: Predefined membership function types used in eCognition.

Numbers in brackets are membership function weightings.

At Level 1				
Remove Cliffs	Multiresolution segmentation at pixel level creating Level 1.	Scale: 120, Shape: 0.1, Compactness: 0.5 Use DEM		
	Classification	Mean DEM > 51.2		
	Merge region	Class filter: Cliff		
Remove Sea	Multiresolution segmentation at image object level	Class filter: unclassified Level usage: Use current Scale 90, Shape 0.1, Compactness 0.9 Use DEM, NDVI, RE Blue, RE Green, RE Red, RGB Blue, RGB Green, RGB Red x 1 each.		
	Classification	Class filter: unclassified <u>Sea</u>: Mean DEM < 45.54 and RGB Red/Green <0.9 <u>Grow Sea</u>: Mean DEM <46.02 and Mode[Median] NDVI <-0.4 and RGB Red/Green < 0.865 Assign Class: Grow Sea to Sea		
	Merge region	Class filter: sea		
Remove Shadow	Classification	Class filter: unclassified <u>Boulder shadow</u>: Border contrast slope >0.55 and Mean DEM > 45.53 and mode[median] Blue RGB < 100 and mode[median] NDVI < -0.15 <u>Cliff shadow</u>: Mode[median] Blue RGB < 200 and RGB Red/Blue <0.7 <u>Grow cliff shadow</u>: Border to cliff shadow >= 1 pixel and mode[median] NDVI <-0.15 or Border to Cliffs >= 1 pixel and mean NDVI < 0 Assign Class: boulder shadow, cliff shadow, grow cliff shadow to Shadow		
	Merge region	Class filter: Shadow		
Classify barnacle/rock and algae	Multiresolution segmentation at image object level	Class filter: unclassified Level usage: Use current Scale 10, Shape 0.1, Compactness 0.9 Use DEM, NDVI, RE Blue, RE Green, RE Red, RGB Blue, RGB Green, RGB Red (weighted x 1 each).		
	Classification	Class filter: unclassified		
		Barnacle /rock	Logical operator: And (minimum)	
			Brightness	87.439 : 172.6 : 243.36
			RE Red/Blue	0.408 : 0.855 : 1.412
			Mode Blue RGB	55.189 : 155.83 : 233.67
			Mode Blue RE	84.773 : 180.6 : 254
			Mode Red RGB	67.24: 171.02 : 250.5
			Mode Green RE	63.855 : 155.48 : 228
			Mean Green RE	79.49 : 164.69 : 245.23
			Mean Red RGB	81.39 : 178.44 : 254
		Algae	Logical operator: Mean (arithmetic)	

			Mode NDVI	-0.503 : 0.14 : 0.739
			Mean NDVI	-0.349 : 0.218 : 0.78
			RGB Green/Blue	0.468 : 1.158 : 2.238
			Mean Green RGB	0 : 104.75 : 234.97
				0.613 : 1.165 : 1.529
			RGB Red/Green	0 : 94.867 : 254
			Mode Red RGB	
Classify red, green and brown algae	Classification	Class filter: algae		
		Brown	Logical operator: Mean (arithmetic)	
			Mode NDVI	0 : 0.433 : 0.739
			Mean NDVI	-0.349 : 0.309 : 0.78
		Green	Logical operator: Mean (arithmetic)	
			RGB Green/Blue	0.88 : 1.51 : 2.14 (AG)
			Mean Green RGB	29.59 : 125.62 : 222.42 (AG)
		Red	Logical operator: Mean (arithmetic)	
			RGB Red/Green	0.969 : 1.165 : 1.446
			RGB Green/Blue	0.658 : 1.1 : 1.731
			Mode Red RGB	0 : 126.5 : 254 (AG)
	Assign Class	Class filter: Red Threshold: RGB red/green < 1.1 and mean DEM <=45.83 = Brown		
	Assign Class	Class filter: unclassified Threshold: Brightness <95 = Brown		
	Assign Class	Class filter: unclassified Threshold: Brightness >= 95 = Barnacle/rock		
Classify red algae as *Osmundea*, *Corallina*, *Corallina* (pool), Rhodo/Poly or Red rock	Assign Class	Class filter: Red Threshold: mean DEM > 48 = red rock		
	Assign Class	Class filter: Red Threshold: RGB green/blue < 1.01 and mean DEM < 45.83 = rhodo/poly		
	Classification	Class filter: Red		
		Osmundea	Logical operator: Mean (arithmetic)	
			Mean blue RGB	37.56 : 70.52 : 118.83
			Mean red RE	99.22 : 136.08 : 175.7
			Mode red RE	91.35 : 130.19 : 172.6
			RGB green/blue	0.948 : 1.261 : 1.663
			RGB red/blue	1.055 : 1.54 : 2.203
		Corallina	Logical operator: Mean (arithmetic)	
			Brightness	101.39 : 147.39 : 211.53
			Mean blue RGB	93.14 : 131.15 : 180.782
			Mean green RGB	99.913 : 145.84 : 209.87
			Mode blue RGB	80.09 : 122.55 : 178.889
			Mode green RGB	86.864 : 134.53 : 207.97
		Corallina (pool)	Logical operator: Mean (arithmetic)	
			Mean green RGB	85.569 : 110.45 : 128.59
			RGB green/blue	0.918 : 1.09 : 1.35
			RGB red/blue	1.077 : 1.364 : 1.547
Classify brown algae as *Fucus*	Assign Class	Class filter: Brown Threshold: Mean DEM > 48.5 = *Fucus spiralis*		

***spiralis*, *Fucus vesiculosus*, *Fucus serratus*, *Laminaria* or Rockpool**	Assign Class	Class filter: Brown Threshold: Mean DEM >= 46.58 and Mean DEM < 48.5 = *Fucus vesiculosus*		
	Assign Class	Class filter: Brown Threshold: Brightness <= 55 and Mean DEM >= 45.48 or Brightness <= 45 and Mean DEM >= 45.3 = *Laminaria* (pool)		
	Assign Class	Class filter: Brown Threshold: Mean DEM >=45.75 = *Fucus serratus*		
	Assign Class	Class filter: Brown Threshold: Mean DEM < and Brightness <= *Laminaria* rockpools		
At Level 2				
Create biotope size objects	Multiresolution segmentation	Class filter: UNCLASSIFIED Parameter Level: Level 1 Level Name: Level 2 Level Usage: Create above Scale 120, Shape 0.1, Compactness 0.9 Use DEM, NDVI, RE Blue, RE Green, RE Red, RGB Blue, RGB Green, RGB Red weighted x 1 each.		
Add cliffs to this level	Assign class	Class filter: unclassified Condition: Area of sub objects Cliff >= 1 pixel = Cliff		
Add sea to this level	Assign class	Class filter: unclassified Condition: Area of sub objects Sea >= 1 pixel = Sea		
Add shadow to this level	Assign class	Class filter: unclassified Condition: Relative area of sub objects Shadow >=0.5		
Classify Coff, Cor, Eph.Ent, Sem, FvesR, Fser.R, FvesB, Ldig, FspiB, Rkp.FK and bare rock	Classification	Class filter: unclassified Condition: Rel. area of sub objects Corallina >= 0.5 Logical operator: Mean (arithmetic) for all classes Membership function weighting shown in brackets		
		Bare rock	(2) Mean DEM Rel. area of algae Rel. area of barnacle/rock	About range 48.2 to 52 Smaller than 0 to 0.1 Larger than 0.75 to 1
		Coff	Mean DEM Rel. area of barnacle/rock Rel. area of *Corallina* Rel. area of *Corallina* (pool) Rel. area of *Osmundea*	About range 45.25 to 48 Smaller than 0 to 0.75 Larger than (Boolean, crisp) 0.33 Smaller than 0 to 0.4 Smaller than 0 to 0.5
		Cor	(4) Rel. area *Corallina* (pool) Mean DEM Mean Slope Rel. area *Corallina* Rel. area *Osmundea*	Larger than (Boolean, crisp) 0.5 About range 45.25 to 48.5 Smaller than 0 to 20 Smaller than 0 to 0.5 Smaller than (Boolean, crisp) 0.1

		Eph.ent	(3) Rel. area of Green Mean DEM Rel. area of Barnacle/rock Rel. area of *Fucus spiralis*	Full range 0.02 to 1 About range 49 to 50 About range 0 to 1 Full range 0 to 0.6
		Fser.R	(3) Rel. area *Fucus serratus* Mean DEM Rel. area of *Corallina* Rel. area of *Corallina* (pool) Rel. area of *Laminaria* Rel. area of *Laminaria* (pool) Rel. area of Rhodo/Poly	Larger than (Boolean, crisp) 0.5 Full range 45 to 46.1 Smaller than linear 0 to 0.8 Smaller than linear 0 to 0.6 Smaller than (Boolean, crisp) 0.75 Smaller than 0 to 0.1 Smaller than 0 to 0.2
		FspiB	Mean DEM Rel. area of Barnacle/rock Rel. area of *Fucus spiralis* Rel. area of Green	Full range 48.2 to 51 Full range 0 to 0.7 Full range 0.18 to 1.01 Smaller than 0 to 0.05
		FvesB	(5) Rel. area *F. vesiculosus* Mean DEM Rel. area of Barnacle/rock Rel. area of *Corallina* Rel. area of *Corallina* (pool) Rel. area of *Osmundea*	Larger than 0.1 to 1 About range 47 to 48 Smaller than 0 to 0.11 Smaller than 0 to 0.7 Smaller than 0 to 0.1 Smaller than 0 to 0.1
		FvesR	Algae Mean DEM Rel. area of Barnacle/rock	Smaller than linear 0.02 to 1 About range 46 to 49.5 Smaller then linear 0.06 to 1

		Ldig	(3) Rel. area of *Laminaria* Mean DEM Rel. area of Barnacle/rock Rel. area of *Corallina* Rel. area of *Corallina* (pool) Rel. area of *Fucus serratus* Rel. area of *Laminaria* (pool) Rel. area of Rhodo/Poly	Larger than (Boolean, crisp) 0.36 Full range 45 to 46 Smaller than 0 to 0.25 Smaller than linear 0 to 0.1 Full range 0 to 0.25 Full range 0 to 0.3 Full range -0.01 to 0.15 Full range -0.01 to 0.2
		Osm	(4) Rel. area of *Osmundea* Mean DEM Rel. area of Barnacle/rock Rel. area of *Corallina* Rel. area of *Corallina* (pool) Rel. area of *Fucus serratus* Rel. area of *F. vesiculosus* Rel. area of *Laminaria*	Larger than (Boolean, crisp) 0.09 About range 45.25 to 48.5 Smaller than 0 to 0.08 Smaller than 0 to 0.4 Smaller than linear 0 to 1 Smaller than 0 to 0.71 Smaller than 0 to 0.5 Smaller than 0 to 0.5
		Rkp.FK	Mean DEM Rel. area of *Corallina* Rel. area of *Corallina* (pool) Rel. area of *Fucus serratus* Rel. area of *Laminaria* Rel. area of *Laminaria* (pool)	About range 45 – 46.5 Smaller than 0 – 0.05 Smaller than 0 – 0.4 About range 0 – 0.65 Larger than 0 – 0.5 Full range 0.5 - 1
		Sem	(2) Mean DEM Algae Rel. prop. of barnacle/rock	About range 45 to 49.5 Smaller than 0 to 0.15 Larger than 0 to 1
Merge	Merge region			